

CRANFIELD INSTITUTE OF TECHNOLOGY
SCHOOL OF AUTOMOTIVE STUDIES

Ph.D THESIS

D W PARKINS

STATIC AND DYNAMIC CHARACTERISTICS OF
AN HYDRODYNAMIC JOURNAL BEARING

MAY 1976

ProQuest Number: 10832203

All rights reserved

INFORMATION TO ALL USERS

The quality of this reproduction is dependent upon the quality of the copy submitted.

In the unlikely event that the author did not send a complete manuscript and there are missing pages, these will be noted. Also, if material had to be removed, a note will indicate the deletion.



ProQuest 10832203

Published by ProQuest LLC (2018). Copyright of the Dissertation is held by Cranfield University.

All rights reserved.

This work is protected against unauthorized copying under Title 17, United States Code
Microform Edition © ProQuest LLC.

ProQuest LLC.
789 East Eisenhower Parkway
P.O. Box 1346
Ann Arbor, MI 48106 – 1346

SUMMARY

Hydrodynamic oil film bearings exhibit lateral flexibility which influences the dynamics of rotors they support. This lateral flexibility is specified by coefficients which relate forces generated by the oil film to the instantaneous journal centre velocity and its displacement from an equilibrium position. Previous investigators adopted a linear treatment by taking uniform viscosity with small displacement and velocity increments. Relatively large journal centre velocities are possible in rotating machinery. Therefore, this thesis investigates the non-linear behaviour of these oil film coefficients.

Coefficient calculations allowed viscosity to vary with temperature and pressure rendering the governing Reynolds Equation non-linear. A range of positive and negative displacement and velocity increments were examined. Novel experimental techniques have been developed which allow determination of coefficient variation with respective displacement and velocity. Coefficients were deduced from specially chosen, imposed vibration orbits arising from two mutually perpendicular external oscillating forces of variable relative magnitude and phase. Journal centre displacement and velocity were measured using high speed data logging equipment. A unique feature was the ability to obtain experimental displacement coefficients from the results of both dynamic and incremental loading. It was found necessary to establish the bearing centre separately for each warm-up/load combination.

Journal clearance in the hot rotating condition could not be measured to the precision required by its sensitivity to calculated load. Clearance and cavitation zone pressures were deduced from simultaneous predictions of the measured vertical load and attitude angle. Theoretical oil film tensile forces were necessary, a proposition supported by recently published experimental findings. Theoretical results for an equivalent uniform viscosity combined with experimental data gave a simple static locus design procedure. A temperature profile was assumed for theoretical work but choice thereof was found to be not critical.

Coefficients are defined in terms of a "zero" value and linear gradient. Using realistic criteria, measured coefficient variation was found to be significant at eccentricity ratios greater than 0.78. Theory adequately predicted most "zero" values but not gradients. It is concluded that improvement in the coefficient prediction will depend on the inclusion of some previous history dependent factors.

C O N T E N T S

	Page
1 INTRODUCTION	1
2 REVIEW OF PREVIOUS WORK	
2.1 Experimental Work	4
2.2 Theoretical Work	7
3 EXPERIMENTAL METHODS	
3.1 Survey of possible methods of determining displacement and velocity coefficients	11
3.2 Description of Test Apparatus	
3.2.1 Construction of Test and Slave Bearings	15
3.2.2 Static and Incremental Bearing Loads	17
3.2.3 Dynamic Bearing Loads	19
3.2.4 Construction of Air Bearing Pulley	21
3.2.5 Oil Supply System	22
3.2.6 Measurements	22
3.3 Displacement Transducer Calibration	
3.3.1 Calibration Technique	24
3.3.2 Results	26
3.3.3 Measurement of Clearance Circle (C _r hot)	27
3.4 Experimental procedures	
3.4.1 Static Locus	28
3.4.2 Displacement Coefficients by Incremental Loading	30
3.4.3 Displacement and Velocity Coefficients by Dynamic Loading	32
3.5 Vibration Characteristics of Test Rig	34
4 THEORETICAL METHODS	
4.1 Solution of Reynolds Equation	37
4.2 Journal Centre Location	43
4.3 Velocity and Displacement Coefficients	44
4.4 Program Verification	46
4.5 Short Bearing Theory	
4.5.1 Solution of Reynolds Equation and Journal Centre Location	47
4.5.2 Displacement and Velocity Coefficients	50
4.6 Temperature Profile	50
5 RESULTS	
5.1 Static Characteristics	53
5.2 Dynamic Characteristics	56
6 CONCLUSIONS	63
7 SUGGESTIONS FOR FURTHER WORK	
7.1 Experimental	65
7.2 Theoretical	65
8 ACKNOWLEDGEMENTS	66
9 REFERENCES	67

APPENDICES

A	Sign Conventions, Definition of oil film displacement and velocity coefficients, and determination of oil film forces	73
B	Example of Analysis Sequence	78
C	Effect of Temperature on Radial Clearance	79
D	Coefficients in r,s Co-ordinate System	81

TABLES

1	Summary of good and weak features of Methods A, B & C	
2	Stiffness of Force Gauge Mounting Device	
3	Inductive Displacement Transducer Calibration	
4	Resonant Frequencies of Wire Support Brackets	
5	Test Frequency ranges	
6	Published experimental measurement of Temperature Profiles	
7	Values of $\Delta T^{\circ}\text{C}$ $\frac{\text{SR}}{\text{C2}}$ Rule 1	
8	Values of $\Delta T^{\circ}\text{C}$ $\frac{\text{SR}}{\text{C2}}$ Rule 2	
9	Measured and Calculated Static Properties, variable viscosity theory	
10	Measured and Calculated Static Properties, uniform viscosity.	
11	List of Experimental Investigations	

FIGURES 1 - 79.

F I G U R E S

1. Test and Slave Bearing Construction
2. Test Bearing and Inner Ring Details
3. Photograph of Test and Slave Bearings
4. Displacement Transducer Mounting
5. Rear View Showing Belt Drives for Test Shaft and Sine Wave Generator
6. View of Test Rig and Instrumentation
7. Lubricant Viscosity - Temperature Characteristics
8. Steady and Incremental Loading Arrangement
9. Horizontal Steady Loading Arrangement with Gas Bearing Pulley
10. Vertical Steady and Incremental Loading Arrangement
11. Photograph showing Horizontal, Vertical, Steady and Dynamic Load Arrangements connected.
12. Connection to Vertical Vibrator and Oil Collection
13. Oil Supply Circuit Diagram
14. Horizontal Vibrator Connector
15. Accommodation of Test Bearing Housing Displacement by Vibrator Connectors.
16. Construction of Air Bearing Pulley
17. Oil Supply Unit
18. Instrumentation Block Diagram
19. Mounting of Capacitance Displacement transducers
20. Co-ordinate System for Displacement Transducer Calibration
21. Inductive Displacement Transducer Calibration - Vertical
22. Inductive Displacement Transducer Calibration - Horizontal
23. Measured Clearance Circle - Motor End
24. Measured Clearance Circle - Free End
25. Eccentricity and Location of Bearing Centre - Low Eccentricity
26. Eccentricity and Location of Bearing Centre - Large Eccentricity

27. Effect of Vibrator and Transverse Wire Connection
28. Incremental Loading, Relative Journal Displacement and Forces Applied to Test Housing
29. Flow Chart - Digitised Data Reduction Program
30. Example of Measured Journal Centre Vibration, Test Type 1, Horizontal
31. Example of Measured Journal Centre Vibration, Test Type 1, Vertical
32. Example of Journal Centre Response to Dynamic Loading, Test Type 1
33. Example of Journal Centre Response to Dynamic Loading, Test Type 2
34. Example of Journal Centre Response to Dynamic Loading, Test Type 3, Horizontal
35. Example of Journal Centre Response to Dynamic Loading, Test Type 3, Vertical.
36. Bearing Nomenclature
37. Flow Diagram - Solution of Reynolds' Equation
38. Simplified Flow Diagram - Calculation of Journal Centre Location, Velocity and Displacement Coefficients
39. Journal centre displacement, nomenclature
40. Simpson's Rule Table $m = 49$, $n = 9$.
41. Journal Centre locus
42. Attitude Angle, Load Number and Eccentricity Ratio
43. Vertical Load and Attitude Angle, Calculated and Measured (low ϵ/C_r).
44. Vertical Load and Attitude Angle, Calculated and Measured (high ϵ/C_r).
45. Constant Viscosity Factor
46. Bearing Radial Clearance
47. Measured and Calculated Displacement Coefficients $N = 1180$ rpm, $W_y = 150$ lbf, $PS = 30$ lbf/in².
48. Measured and Calculated Displacement Coefficients $N = 1500$ rpm $W_y = 150$ lbf, $PS = 30$ lbf/in²
49. Measured and Calculated Displacement Coefficients $N = 2200$ rpm $W_y = 150$ lbf, $PS = 30$ lbf/in²
50. Measured and Calculated Displacement Coefficients $N = 1180$ rpm $W_y = 150$ lbf, $PS = 15$ lbf/in²

51. Measured and Calculated Displacement Coefficients $N = 1500$ rpm
 $W_y = 150$ lbf, $PS = 15$ lbf/in²
52. Measured and Calculated Displacement Coefficients $N = 2200$ rpm
 $W_y = 150$ lbf, $PS = 15$ lbf/in²
53. Measured and Calculated Displacement Coefficients $N = 1180$ rpm
 $W_y = 150$ lbf, $PS = 7.5$ lbf/in²
54. Measured and Calculated Displacement Coefficients $N = 1500$ rpm
 $W_y = 150$ lbf, $PS = 7.5$ lbf/in²
55. Measured and Calculated Displacement Coefficients $N = 2200$ rpm
 $W_y = 150$ lbf, $PS = 7.5$ lbf/in²
56. Measured and Calculated Velocity Coefficients $N = 1180$ rpm
 $W_y = 150$ lbf, $PS = 30$ lbf/in²
57. Measured and Calculated Velocity Coefficients $N = 1500$ rpm
 $W_y = 150$ lbf, $PS = 30$ lbf/in²
58. Measured and Calculated Velocity Coefficients $N = 2200$ rpm
 $W_y = 150$ lbf, $PS = 30$ lbf/in²
59. Measured and Calculated Velocity Coefficients $N = 1180$ rpm
 $W_y = 150$ lbf, $PS = 15$ lbf/in²
60. Measured and Calculated Velocity Coefficients $N = 1500$ rpm
 $W_y = 150$ lbf, $PS = 15$ lbf/in²
61. Measured and Calculated Velocity Coefficients $N = 2200$ rpm
 $W_y = 150$ lbf, $PS = 15$ lbf/in²
62. Measured and Calculated Velocity Coefficients $N = 1180$ rpm
 $W_y = 150$ lbf, $PS = 7.5$ lbf/in²
63. Measured and Calculated Velocity Coefficients $N = 1500$ rpm
 $W_y = 150$ lbf, $PS = 7.5$ lbf/in²
64. Measured and Calculated Velocity Coefficients $N = 2200$ rpm
 $W_y = 150$ lbf, $PS = 7.5$ lbf/in²
65. Influence of Vibration \sim Rotational frequency Ω/ω
66. Measured indirect Velocity Coefficients
67. Comparison of Measured and Calculated Displacement Coefficients
68. Comparison of Measured and Calculated Displacement Coefficient Gradients.
69. Comparison of Measured and Calculated Velocity Coefficients
70. Comparison of Measured and Calculated Velocity Coefficient Gradients

71. Comparison of Measured and Calculated Displacement Coefficients and Gradients, $W_y = 300$ and 500 lbf
72. Displacement Coefficients, $W_y = 300$ lbf, $PS = 30$ lbf/in²,
N = 1180, 1500 and 2200 rpm.
73. Velocity Coefficients, $W_y = 300$ lbf, $PS = 30$ lbf/in²,
N = 1180, 1500 and 2200 rpm.
74. Displacement Coefficients $W_y = 500$ lbf, $PS = 30$ lbf/in²,
N = 1500, 2200 and 2900 rpm.
75. Velocity Coefficients $W_y = 500$ lbf, $PS = 30$ lbf/in²,
N = 1500, 2200 and 2900 rpm.
76. Significance of Displacement Coefficient Gradient
77. Significance of Velocity Coefficient Gradient
78. Theoretical Location of Cavitation Zone and Peak Pressure -
small displacement and velocity increments.
79. Theoretical Location of Cavitation Zone and Peak Pressure -
large displacement and velocity increments.

N O T A T I O N

a_{xx} , etc.	displacement coefficient
a_{xx0} , etc	'zero' displacement coefficient
A_{xx} , etc	non-dimensioned displacement coefficient
A_{xx0} , etc	non-dimensioned 'zero' displacement coefficient
A1 - A4 (ch.4.1)	convenient substitution
b	bearing land width
b_{xx} , etc	velocity coefficient
b_{xx0} , etc	'zero' velocity coefficient
B_{xx} , etc	non-dimensioned velocity coefficient
B_{xx0} , etc	non-dimensioned 'zero' velocity coefficient
B6 - B9 (ch.4.1)	constants
B1, B5 (ch.4.1)	Substitutions, functions of (i)
B2, B3, B4 (ch.4.1)	Substitutions, functions of (i,j)
C_r	Radial clearance
C1, C2	Constants specifying temperature profile (see ch.4.6)
CF, CF2	Convergence factors, pressure, viscosity
D	Bearing diameter
FT_i (ch.4.1)	viscosity factor due to temperature
F_x, F_y	oil film forces (see Appendix A)
h	oil film thickness
i,j	grid location
k (ch.4.1)	iteration count
k	stiffness
l_1, l_2, l_3 (Fig 20)	lengths
m (Appendix A)	mass
m,n	grid size
$n = \epsilon/C_r$ (ch.4.5)	Eccentricity ratio
N	rotational speed rpm
N'	rotational speed rev/sec
$NS_{i,j}$	Elements in Simpsons Rule table
ORF	over relaxation factor (pressure)

P_x, P_y	external forces on bearing
$P_{i,j}$	pressure
PS	supply pressure
PC	cavitation zone mean pressure
$P^* = W_y/2bD$	specific load
q	see ϕ
r	journal radius
R (ch.4.1)	Bearing radius
R1 - R4	voltmeter readings, channels 1 - 4.
r,s (Appendix D)	radial, tangential co-ordinates
SR	constant specifying temperature profile (see ch.4.6)
t	time
T	temperature
\bar{T}	temperature corresponding to $\bar{\eta}$
$u_o = r\omega$	journal surface velocity
v	journal centre velocity
VRF	viscosity over-relaxation factor
W_x, W_y, W'_x, W'_y	external forces on journal
w_1, w_2, w_3	weights of components of steady loading system (see Fig 8)
x (ch.4.1)	distance around journal
x,y (see Appendix A)	horizontal, vertical journal centre co-ordinates
x_h, y_h	horizontal, vertical bearing housing co-ordinates
z	distance across bearing
α_{xx} , etc	displacement coefficient gradient
α^*_{xx} , etc	non-dimensioned displacement coefficient gradient
$\alpha_1 - \alpha_4$ (ch.3.3.1)	calibration gradient
α (ch.3.4.2)	angle of steady load
α (ch.4.1)	coefficient of thermal expansion
β_{xx} , etc	velocity coefficient gradient
β^*_{xx} , etc	non-dimensioned velocity coefficient gradient
β (ch.4.1)	coefficient of viscosity variation with pressure
γ_x, γ_y	non-dimensioned displacement

ϵ, ϵ'	journal centre eccentricity
η	absolute viscosity
$\bar{\eta}$	equivalent uniform viscosity
$\theta = 2\pi \frac{(i-1)}{(m-1)}$	angular distance around journal
ν	kinematic viscosity
ξ (Fig 28, ch.3.4.2)	Displacement Angle
ρ	density
$\sigma = \frac{\bar{T}-T_1}{T_1 \{(SR)^{C1} (2)^{C2} -1\}}$	constant viscosity factor
ϕ, ϕ'	attitude angle
$\Phi = ph^q$	transformed variable
ψ	angle of velocity vector
ω	rotational frequency
Ω	vibration frequency

1 INTRODUCTION

Hydrodynamic journal bearings are widely used in all types of machinery. Applications range from the very large rotors of turbo-generators down to those of the smallest instrument. Hydrodynamic journal bearings have the considerable advantage of generating the load-supporting fluid pressure as a result of the relative motion of the two members. They also offer low friction, especially if the fluid is air. They are also able to operate in the higher load/speed combinations and thence find almost universal application in the crankshaft bearings of reciprocating engines. However, hydrodynamic journal bearings also have lateral flexibility. It is now widely recognised that this flexibility exerts a significant influence on the dynamic behaviour of the rotor it supports. References (1) and (2) emphasise the importance of this point.

Economic pressures dictate a continuous trend for bearings to support higher loads and rotational speeds. Social, environmental and reliability considerations require machinery to produce less noise and vibration. Therefore, it is especially important that the lateral flexibility of hydrodynamic bearings is well understood. It is also well known that hydrodynamic bearings may exhibit instability. Indeed, its manifestations necessitated interest in bearing research at an earlier stage. Sternlicht and Reiger (3)[†] thoroughly reviewed this aspect in 1968.

Stodola (4) first described bearing flexibility by eight partial derivatives of the forces exerted by the fluid film when the journal centre was displaced from its equilibrium position with a finite velocity. These are now known as displacement and velocity coefficients. This study considers four of each, with two direct and two indirect coefficients in each case. They are defined in Appendix A. Other workers (5) and (6) have considered a greater number of coefficients. Hence, study of rotor response and stability requires understanding of the bearing coefficients. Although these coefficients were first described as far back as 1925, most work thereon dates from 1956.

Theoretical works are more numerous. To compute coefficients, a pressure field is calculated which is summated to produce forces. Experimental studies, apart from being less numerous, have been recently criticised on the grounds of quality by Lund (7) and Sternlicht and Reiger (3). Lund states:

"Furthermore, it is not always clear if extraneous factors have been totally eliminated from the test apparatus (e.g. external damping and external vibration sources). For these reasons, the results are often contradictory."

Two experimental studies (8) and (9) were reported between the appearance of this criticism and the inception of this investigation. Morton's (8) experimental technique required the solution of two 4×4 matrices, and the measurement of phase between the displacement and unbalanced force. He acknowledged the lack of agreement with theoretical results.

[†] Numbers in parentheses indicate reference numbers.

Woodcock and Holmes (9) reduced the problem to the solution of four 2×2 matrices with the use of two separate test rigs. Woodcock (10) reports the considerable experimental difficulties of phase measurement.

Whilst the necessity of a knowledge of the oil film coefficients is well understood and recognised, there appears a definite need for some new approach to their experimental determination, which would preferably remove some of the disadvantages of those used hitherto. Hence, this thesis describes a new technique for the experimental determination of all eight oil film coefficients, on the same bearing and at one warm-up setting, sufficient data being collected over a few minutes. Phase measurements are not needed, and in principle, only a set of single equations each containing one unknown coefficient is required. It utilises two unique features, the measurement of journal centre velocity using high speed data logging equipment, and the imposition of particular vibration orbits. Their combination offers a significant advance in experimental techniques.

Some earlier workers determined displacement coefficients by a method of incremental loading. This method, with some useful improvements, was incorporated in this work. The apparatus was arranged so that dynamic and incremental loading tests could be performed at the same rig setting. This allowed another new feature, a comparison between displacement coefficients obtained under both loading methods for the same test conditions. Extreme care was taken to eliminate any unknown extraneous forces. Particular attention was paid to the establishment of all bearing geometric details in the hot, rotating condition. Chapter 3 gives full details of all experimental methods.

Most, but not all, theoretical studies assume a uniform viscosity throughout the oil film. In this work, viscosity is allowed to vary with temperature and pressure. Coefficient calculations require oil film forces with either, a small displacement from the equilibrium position with zero squeeze-film component, or, forces with and without squeeze-film components at the equilibrium position. All workers hitherto have used a single small increment of displacement or velocity to justify linearity. It is possible in a real machinery situation for the journal to move through its equilibrium position with a considerable velocity. A novel feature in this work, is that the displacement and velocity increments were allowed to vary over a positive and negative range.

For the velocity range ^(v_{max}) envisaged, the squeeze-film component can give very large pressures. The effect of pressure on viscosity then becomes significant and was therefore incorporated in all calculations (except when deliberately suppressed). It creates considerable complications because the governing equation becomes non-linear. Inclusion of the variation of viscosity with pressure for the calculation of coefficients is a new feature, although Sternlicht (11) recommended its inclusion as far back as 1959.

A single set of boundary conditions were used in all theoretical aspects of this thesis. These were the simplest possible and involved least assumption. Axial pressure boundaries were those of the circumferential groove and atmosphere. Circumferential boundaries required the pressure gradient to be zero and the pressure to take any non-positive value.

All previous workers have made this value zero. However, the admission of negative values allows a useful and unique advantage in the prediction of any combination of attitude angle and load.

Journal clearance changed between the cold and hot rotating conditions. It was found that clearance in the working conditions could not be measured to the necessary precision required for the prediction of load. Therefore, a new system was devised to obtain the requisite value. Chapter 4 describes all theoretical methods.

Chapter 5 discusses all results, both theoretical and experimental under separate subject headings. Conclusions are drawn in Chapter 6.

Hersey and Snapp (12) thoroughly surveyed the design of 31 bearing test rigs published before 1955. They distinguished between those intended for endurance testing and those for reasearch. Until 1955 all "research" test rigs were used to study the static properties, namely journal centre locus, speed load characteristics, friction and oil flow. At that date none had investigated the oil film lateral flexibility. Section 2.1 reviews techniques used since 1955 to experimentally determine the displacement and velocity coefficients which describe this flexibility. Section 2.2 reviews theoretical work of significance to the background to this study. It is not intended to be an exhaustive survey of all publications which discuss fluid film bearings. In both sections reference is only made to parts of papers deemed relevant to this work. It is intended to highlight points of particular interest arising in the literature. Woodcock (10) gives a good survey which covers many other aspects of bearing research.

2.1 Experimental Work

Two contributions from the pre-1956 period are relevant. Buske and Rolli (13), 1937, in pre-war Germany applied oscillating loads through a hydraulic system at ratios $\Omega/\omega = 1.0$ and 2.0 . They found that under dynamic loading, peak pressures moved around the bearing, but were unable to relate these to the journal orbit. Shawki and Freeman (14) 1955, applied steady and oscillating loads through a complicated system of levers and springs. Although their dynamic loads were limited to a maximum frequency of 3 hz, they achieved ratios $\Omega/\omega = 0.4$ to 1.5 . They reported a large increase in journal vibration around $\Omega/\omega = 0.5$.

Hagg and Sankey (15), 1956, were the first to report measurements of displacement and velocity coefficients. However, they restricted their investigations to the four direct coefficients only, thereby simplifying the experimental procedure. All subsequent workers have included the indirect coefficients making a possible total of at least eight.

Two basic test rig arrangements are possible, namely whether the bearing or journal is "free"* to move perpendicular to the longitudinal axis. In the latter case, the journal both rotates and vibrates, whereas in the former, the roles are, in general, separated, one element rotating and the other vibrating. Mitchell *et al* (16), Glienicke (17) and Morton (8) used the "free bearing" arrangement. "Free journal" test rigs were used by Hagg and Sankey (15), Orcutt and Arwas (18), Nakagawa and Aoki (19), and Morton (20). Woodcock and Holmes (9) devised an experimental procedure which utilised both arrangements. Hagg and Sankey (15) chose a vertical journal, all others used the horizontal layout. The "free bearing" arrangement lends itself straightforwardly to the use of a single test bearing. However, in the "free journal" the rotor weight itself conveniently provides the steady load in a two test bearing arrangement. Examples are given by Nakagawa and Aoki and Morton. Two other workers, Hagg and Sankey (15) and Orcutt and Arwas used a single test bearing and applied variable steady loads to the journal through an additional slave bearing.

* see footnote at end of Appendix A

Dynamic loads may be applied by either unbalanced rotation or independent vibrator. The former are limited to $\Omega/\omega = 1.0$ (unless auxiliary shafts are used), whereas the latter may take any frequency but impose the problems of connection without constraint. Examples of the former were used by Hagg and Sankey (15), Nakagawa and Aoki, and Woodcock and Holmes. Independent vibrators were used by Glienicke and Morton (8). Morton's apparatus tested large diameter bearings (20-28 inches) and required large steady loads (50 tons max). Dynamic loads (up to 2 tons) were applied by electro-hydraulic vibrators. Glienicke rotated the steady load through 180° by using three pressurised bellows directly attached to the "free bearing". Whilst such bellows are flexible when unloaded, they can become very much stiffer when pressurised. Under test conditions it seems possible that they could exert a constraint on the bearing. Morton (8) overcame this problem by introducing long rods between his single bellows and bearing. Glienicke applied dynamic loads through an extremely complicated mechanical system, which also appears likely to offer significant constraint.

Morton (20) recently reported a different method of obtaining relative motion between journal and bearing. He displaced the journals of a two-bearing rotor from their equilibrium positions by loading through a very short intermediate slave bearing. The load was released and the eight coefficients deduced from the ensuing decaying transient journal vibration. Coefficients could only be obtained for a limited range of operating conditions. However, it gives data for the operating conditions on that particular machine, a valuable feature in industrial research.

Woodcock and Holmes measured displacement coefficients on one rig and velocity coefficients on another. An incremental loading technique was used with a "free bearing" rig to obtain displacement coefficients in a similar manner to Mitchell *et al.* Velocity coefficients were obtained on a "free journal" rig with two test bearings and unbalanced rotation providing dynamic forces.

Orcutt and Arwas used an indirect approach to coefficient determination. They measured journal orbits produced by a synchronous unbalanced rotation. Displacement and velocity coefficients obtained from theory were used to predict the journal vibration. Validity of the oil film coefficients was inferred from a satisfactory comparison between the experimental and theoretical orbits. Bannister (5) used the same principle. Previous experience (21) has shown this to be a better conditioned process than the direct determination of coefficients from experimental data.

Middleton *et al.* (22) applied steady and dynamic loads to a "free test bearing" through a system of cams, levers and flexural elements. They measured vibration orbits resulting from a variety of loading patterns. Experimental and theoretical orbits were compared. They did not measure displacement or velocity coefficients. Cole and Hughes (23) used a similar principle to apply dynamic loads to a perspex bearing which facilitated photography of the oil film extent.

Eight papers have described direct experimental determination of the displacement and velocity coefficients. Their reference numbers are:

(8), (9), (10), (15), (16), (17), (19) and (20).

Hagg and Sankey (15) neglected the indirect coefficients, assumed the oil film to be linear, and from the resulting harmonic response to unbalanced rotation, expressed each unknown coefficient in terms of measured quantities.

Mitchell *et al* measured the direct and indirect displacement coefficients by successively applying horizontal and vertical incremental loads. Two sets of simultaneous equations, having two in each set, were obtained by combining equations for horizontal and vertical oil film forces in each of the two loadings.

Glienicke, Nakagawa and Aoki and Morton (8) measured the complete eight coefficients and required two sets of simultaneous equations having four in each set. Woodcock and Holmes introduced an improvement by using their two separate rigs to obtain displacement and velocity coefficients. This gave four sets of simultaneous equations each set containing two equations. However, it did mean that displacement coefficients from one rig had to be used with results from another. This necessitated either extreme manufacturing precision so that the bearings could be deemed identical, or the use of some non-dimensional relationships.

In 1956 Hagg and Sankey (15) published direct coefficients for a 150° partial arc, and a pivoted pad bearing. In the former case clearance values did not significantly affect non-dimensional coefficients. However, some experimental scatter was shown with the higher coefficients at larger Sommerfeld Numbers. Mitchell *et al* using a larger than normal clearance, obtained good agreement between measured influence coefficients and theoretical values given by the Short Bearing Approximation. Displacement coefficients were computed from the smoothed influence coefficients. They were also satisfactorily compared with values given by a method due to Morrison (24) using the journal centre static locus. Glienicke obtained good agreement between measured and theoretical static loci for a cylindrical bearing. He gives curves for all eight coefficients as functions of Sommerfeld Number for two non-circular bearings. It is difficult to assess this work because no experimental data points are shown. Nakagawa and Aoki compared coefficients obtained experimentally with those given by two theoretical methods. The latter showed good agreement. However, whilst individual experimental data points are not given, their representative curves diverge from theory at $\epsilon/C_r > 0.7$ for displacement coefficients, and at $\epsilon/C_r > 0.6$ for velocity coefficients.

Kikuchi (25), 1971 refers to displacement and velocity coefficients obtained by Funakawa and Tatara (26), whose paper is currently only available in the original Japanese.

Woodcock and Holmes tested a circumferentially grooved bearing which makes their work particularly relevant to this thesis. They solved a constant viscosity form of Reynolds Equation using an iterative technique with successive over-relaxation, and obtained good agreement between experimental and theoretical results. In his thesis, Woodcock (10) states that the phase (beteen) force and displacement

between

vectors showed a periodic drift even at constant running conditions. A special phase-averaging unit was developed to overcome this difficulty. He also found that the journal response waveforms were not harmonic. Curves for experimental values of the four displacement coefficients are given without individual data points. Woodcock also discusses the importance of a phenomena of oil film "swinging". This refers to the circumferential movement of the positive pressure part of the oil film, and hence cavitation zone and its extent, around the bearing as a result of the journal centre velocity. Woodcock and Holmes expressed non-dimensioned coefficients in terms of the load on one bearing land. Since this is especially suited to the circumferentially grooved bearing, the practice is followed in this thesis.

Morton (8) used the same basic layout for his experimental apparatus as that described in this work, but his journal diameter and loads were immensely larger. Furthermore, the experimental techniques are significantly different. Morton used non-synchronous vibrating forces and removed the residual synchronous signal electronically. Two values of vibration frequency were used, 10 and 15 hz. each applied separately within a brief time interval, to give the requisite set of equations. All eight coefficients were determined in the dynamic experiments, and are compared to iso-viscous theoretical results. Poor agreement was obtained in some cases, particularly a_{yy} and b_{yy} at $\epsilon/C_r = 0.8$.

However, Morton found that measurements of journal vibration response to unbalance for large rotors confirmed that theoretical values were too high, and that those derived experimentally were of the correct order. Morton (20) shows that displacement coefficients obtained by his transient technique compare favourably with those predicted by Smith (27) over a wide range of eccentricity ratio. Experimental velocity coefficients obtained by this method show some scatter.

Woodcock and Holmes, and Morton, made significant advances in the study of oil film dynamic properties. Both workers indicate the difficulties of the experimental aspect.

All hitherto published experimental techniques for the measurement of all eight coefficients assume they are linear and require the measurement of phase. Neither restriction applies to the work described in this thesis.

2.2 Theoretical Work

Reynolds (28) in 1886 developed his well-known equation for the pressure distribution in an oil film. It is a second order partial differential equation which is non-linear if viscosity is allowed to vary with pressure (see Chapter 4).

Sommerfeld (29) in 1904 obtained an analytical solution for the iso-viscous steady load case by neglecting axial pressure variation, thereby rendering his conclusions valid for "long" bearings only. His work achieved historical significance since he introduced the concept of a single non-dimensioned quantity, now known as Sommerfeld Number, which is a function of eccentricity ratio only. Sommerfeld predicted negative pressures in the divergent zone, which many subsequent workers have

neglected to obtain better agreement between observed and calculated behaviour. In a very recent paper, Dyer and Reason (30) reappraised the Sommerfeld pressure distribution in the light of their experimental findings.

Whilst studying the influence of journal bearings on rotor stability, Stodola (4) introduced eight partial derivatives to describe the oil film behaviour. These are now known as the displacement and velocity coefficients. Stodola computed stiffness coefficients using Sommerfeld's steady state solution, and was therefore unable to predict velocity coefficients.

Christopherson (31) introduced numerical solutions to Reynolds Equation using Southwell's relaxation method to produce steady state pressure profiles in a 120° partial arc bearing. He also presented additional techniques which allowed viscosity to vary with both temperature and pressure. Soon after the war, Cameron and Wood (32), and Walther and Sassenfeld (33) both considered the 360° bearing with constant viscosity. The latter authors introduced the transformed pressure variable which has less severe gradients at high pressure. Some years later, 1956, with the availability of digital computers, Raimondi and Boyd (34) used an iterative procedure to give numerical solutions to Reynolds equation. They presented design charts for the 360° and partial arc bearing. Burwell (35) obtained numerical solutions using the Sommerfeld model and was able to predict journal response to various dynamic loading patterns typical of those in reciprocating engines.

Somewhat earlier, Hagg (36), 1946 represented the oil film by a single spring and viscous damper in a study of rotor stability.

A significant step in the field of analytical solutions occurred in 1952 when Dubois and Ocvirk (37), (38) and (39), published their Short Bearing Approximation. They neglected circumferential pressure variation, thereby deleting one of the terms in Reynolds equation, and produced results representative of "narrow" bearings. Their predicted journal static locus showed better agreement with practice than that of Sommerfeld.

In 1960, Holmes (40) extended the Short Bearing Approximation to include the journal centre velocity terms and was able to develop expressions for the eight coefficients in the r, s co-ordinate system (see Appendix D). Smith (27) in 1963, used a combination of methods to evaluate the eight coefficients for "short", "long" and finite length bearings over a range of eccentricity ratio. Smith (27) and Holmes (41) in a later paper recognised that the oil film extent depends also upon the magnitude and direction of the journal centre velocity - found to be a very significant point in this work. Morrison (24) in 1962, used a different approach to develop the same equations as Holmes in 1960.

Three years earlier, Sternlicht (11) using a numerical method and putting sub-zero pressures to zero, obtained expressions for the four displacement and two direct velocity coefficients. He claimed that b_{xy} , b_{yx} were small compared to the direct coefficients and could therefore be neglected. Work described in this thesis shows that this is not necessarily true.

Smalley *et al* (42) in 1965 also computed journal bearing static properties with an iterative numerical solution of Reynolds' equation using a number of different boundary conditions. They also discussed the effect of mesh size and convergence limits on accuracy of solution. In 1967, Lloyd and McCallion (43) reviewed theoretical methods. They described several approaches to the solution of Reynolds' equation and discussed the optimum over-relaxation factor for iterative schemes.

Woodcock and Holmes (9) in 1970 calculated the complete eight displacement and velocity coefficients for a 360° circumferentially grooved bearing from iterative numerical solutions of Reynolds' equation using uniform viscosity. They used these coefficients to predict the behaviour of a real rotor which compared favourably with observed performance. Lundholm (44) specified more complicated boundary conditions which necessitated a second iteration process to obtain their conformity. Cavitation zone pressures were set to zero and viscosity considered constant. He computed displacement and velocity coefficients for a circumferentially grooved bearing.

Since this project was started, a Symposium has discussed Cavitation and Related Phenomena in Lubrication. Dowson and Taylor (45) described the fundamental aspects of cavitation in bearings. Temperley (46) discussed tensile strength of liquids and Floberg (47) considered their effect on cavitation boundary conditions. Milne (48) considered the variation of film extent in dynamically loaded bearings.

Somewhat earlier, Smalley and McCallion (49) in 1967 investigated the effect of viscosity variation on bearing steady state performance. Its effect on coefficients was not studied. They allowed viscosity to vary with temperature, but not pressure. Reynolds and Energy equations were successively solved until the pressure field converged. In that same year Dowson and March (50) published a thermohydrodynamic analysis of journal bearings. Viscosity varied with temperature and pressure, and Reynolds, Energy and Heat Conduction equations were solved. They computed shaft and bearing surface temperatures, and contours throughout the oil film. Experimental findings justified the neglect of axial temperature gradients. Again, coefficients were not studied.

Viscosity was allowed to vary with both temperature and pressure by Hakansson (51) 1964. He assumed an initial viscosity field from which a pressure field was computed. This permitted a revision of the viscosity field from which a further pressure field was obtained. This process was continued until the pressure field converged. Hakansson obtained a temperature, and hence a viscosity field from pressure by solving an Energy equation. Computed temperature profiles differed significantly from his single experimental result (and those in all other published work) in the divergent zone. However, good agreement was obtained between calculated and observed power absorbed. Coefficients were not investigated.

It is clear from this review that oil film coefficients have received greatest attention since 1956. That same period saw, the high speed digital computer become a standard aid, and a significant trend towards environmental considerations which require less noise and

vibration from rotating machinery. These facts may well be related. It is also clear that theoretical determinations of coefficients are more numerous than experimental. This may well reflect the difficulties of the latter approach. Lund (7) thought it necessary to criticise experimental techniques published prior to 1966. Although fewer authors have given both experimental and theoretical coefficients, they deserve credit for clarifying the situation and its difficulties.

3. EXPERIMENTAL METHODS

Section 3.1 surveys possible experimental techniques which avoid the hitherto assumption of harmonic response and measurement of phase. Distinct advantages are shown for a dynamic method in which measurements of journal centre velocity are combined with two particular imposed orbits. Section 3.4 gives the experimental procedure devised to meet these requirements. A full description of the test rig construction and instrumentation is given in section 3.2. Section 3.3 describes the displacement transducer calibration method and results, and the vibration characteristics of the rig are discussed in section 3.5.

3.1 Survey of Possible Methods of Determining Displacement and Velocity Coefficients

This chapter presents brief details of some of the methods considered suitable for the experimental determination of the displacement and velocity coefficients. At the outset, it was considered that a non-harmonic journal displacement response would result from an harmonic force input. It followed that possible benefits might accrue from an avoidance of the assumption of an harmonic response as used by other workers.

Furthermore, previous experience, (21) and comments by Woodcock (10) showed that phase between an input force and response may vary during the vibration cycle. Hence it was decided to concentrate on methods which avoided both the assumption of harmonic displacement response and the introduction of phase. Since it was hoped that the selected experimental method would demonstrate any variation of displacement coefficient with relevant distance, or velocity coefficient with velocity, it was necessary that the method acknowledge these restrictions. Hence it was assumed that:

$$a_{xx}, a_{yx} = \text{Function } (x)$$

$$a_{yy}, a_{xy} = \text{Function } (y)$$

$$b_{xx}, b_{yx} = \text{Function } (\dot{x})$$

$$b_{xy}, b_{yy} = \text{Function } (\dot{y})$$

in addition to being functions of eccentricity and possibly rotational speed (N), vertical load (W_y) and supply pressure (PS).

When considering possible methods it was also assumed that an apparatus would be available which would incorporate the following features:

- (a) Ability to apply horizontal and vertical incremental loads up to 100 lbf.
- (b) Ability to apply horizontal and vertical oscillating forces ± 100 lbf at any chosen frequency with a variable relative phase and magnitude.
- (c) Instrumentation would allow the production of accurate time histories of $x, y, \dot{x}, \dot{y}, \ddot{x}_h, \ddot{y}_h, P_x, P_y$.

It was felt desirable to conduct experiments so that if possible all data required to obtain results (8 coefficients plus journal centre location) could be collected at one W, N, PS combination in the shortest possible time. This obviates using data obtained in one experimental setting in conjunction with that obtained in another, possibly on a different day, thereby eliminating the uncertainties so caused. A novel feature is the use of measurements of velocity to determine velocity coefficients.

Method A

- (a) Adjust the relative phase and magnitude of the vibrating forces P_x and P_y so that at one time during the cycle, say t_1 , $\dot{x} = \dot{y} = 0$.
- (b) Reset relative phase and magnitude so that a similar situation is achieved at some other time during the cycle, say t_2 , $\dot{x} = \dot{y} = 0$.
- Hence in the horizontal direction equations A1 - 11 and 12 become:

$$\text{at } t_1; a_{xx} \dot{x}_1 + a_{xy} \dot{y}_1 = P_{x1} - m_h \ddot{x}_{h1}$$

$$\text{and at } t_2; a_{xx} \dot{x}_2 + a_{xy} \dot{y}_2 = P_{x2} - m_h \ddot{x}_{h2}$$

and in the vertical direction:

$$\text{at } t_1; a_{yy} \dot{y}_1 + a_{yx} \dot{x}_1 = P_{y1} - m_h \ddot{y}_{h1}$$

$$\text{and at } t_2; a_{yy} \dot{y}_2 + a_{yx} \dot{x}_2 = P_{y2} - m_h \ddot{y}_{h2}$$

each pair of simultaneous equations respectively yield a_{xx} , a_{xy} and a_{yy} , a_{yx} .

- (c) Reset the relative phase and magnitude of the vibrating forces P_x , P_y , so that a value of time say t_3 may be selected such that $\dot{x} = 0$ (it may be possible to utilise another time from the setting in either (a) or (b) above.

Hence equations A1 - 11 and 12 become:

$$b_{xy} \dot{y}_3 = -a_{xx} \dot{x}_3 - a_{xy} \dot{y}_3 + P_{x3} - m_h \ddot{x}_{h3}$$

$$b_{yy} \dot{y}_3 = -a_{yy} \dot{y}_3 - a_{yx} \dot{x}_3 + P_{y3} - m_h \ddot{y}_{h3}$$

At this setting there will be some other time say t_4 such that $\dot{y} = 0$

Hence equations A1 - 11 and 12 become:

$$b_{xx} \dot{x}_4 = -a_{xx} \dot{x}_4 - a_{xy} \dot{y}_4 + P_{x4} - m_h \ddot{x}_{h4}$$

$$b_{yx} \dot{x}_4 = -a_{yy} \dot{y}_4 - a_{yx} \dot{x}_4 + P_{y4} - m_h \ddot{y}_{h4}$$

After inserting values for $a_{xx} \dots a_{yy}$, obtained in (a) and (b) above, these equations yield $b_{xx} \dots b_{yy}$. Other settings of relative phase and magnitude of P_x, P_y could permit determination of the variation of b_{xx}, b_{yx} with \dot{x} , and b_{yy}, b_{xy} with \dot{y} .

Method B

Adjust the relative phase and magnitude of vibrating forces P_x, P_y so that:

- (a) $x = \dot{x} = 0$ at all t (i.e. journal locus is a vertical line passing through the origin).

and another setting so that:

- (b) $y = \dot{y} = 0$ at all t (i.e. journal locus is a horizontal line passing through the origin).

From results of setting (a) choose t_1 such that $\dot{y} = 0$ and $y \neq 0$

Equations A1 - 11 and 12 become:

$$\left. \begin{aligned} a_{xy} y_1 &= P_{x1} - m_h \ddot{x}_{h1} \\ a_{yy} y_1 &= P_{y1} - m_h \ddot{y}_{h1} \end{aligned} \right\} \text{these equations yield } a_{xy}, a_{yy}.$$

Then choose another t_2 such that $y = 0, \dot{y} \neq 0$

Equations A1 - 11 and 12 become:

$$\left. \begin{aligned} b_{xy} \dot{y}_2 &= P_{x2} - m_h \ddot{x}_{h2} \\ b_{yy} \dot{y}_2 &= P_{y2} - m_h \ddot{y}_{h2} \end{aligned} \right\} \text{these equations yield } b_{xy}, b_{yy}.$$

From results of setting (b) choose t_3 such that $\dot{x} = 0, x \neq 0$

Equations A1 - 11 and 12 become:

$$\left. \begin{aligned} a_{xx} x_3 &= P_{x3} - m_h \ddot{x}_{h3} \\ a_{yx} x_3 &= P_{y3} - m_h \ddot{y}_{h3} \end{aligned} \right\} \text{these equations yield } a_{xx}, a_{yx}$$

Choose another time t_4 such that $x = 0, \dot{x} \neq 0$

Equations a1 - 11 and 12 become:

$$\left. \begin{aligned} b_{xx} \dot{x}_4 &= P_{x4} - m_h \ddot{x}_{h4} \\ b_{yx} \dot{x}_4 &= P_{y4} - m_h \ddot{y}_{h4} \end{aligned} \right\} \text{these equations yield } b_{xx}, b_{yx}$$

It was anticipated that difficulties may arise in setting the conditions (a) and (b) above. However, useful advantage would be obtained if $\dot{x} = \dot{y} = 0$ were obtained for part of the cycle instead of all time. However, Morton (8) suggested in a footnote that such settings were possible.

Method C

This method utilised a combination of dynamic and incremental loading techniques. Coefficients $a_{xx} \dots a_{yy}$ are determined by the incremental loading technique (described in 3.4.2) with vibrators connected but $P_x = P_y = 0$. Then x and y time histories are obtained under response to a vibrating force. It is possible to conduct this test with only one vibrator. The vibrating test is conducted with incremental loading weights in position. From the respective time histories choose t_1 such that $\dot{x} = 0$, whence equations A1 - 11 and 12 become:

$$b_{xy} \dot{y}_1 = P_{x1} - m_h \ddot{x}_{h1} - a_{xx} x_1 - a_{xy} y_1$$

$$b_{yy} \dot{y}_1 = P_{y1} - m_h \ddot{y}_{h1} - a_{yy} y_1 - a_{yx} x_1$$

and choose t_2 such that $\dot{y} = 0$ whence equations A1 - 11 and 12 become:

$$b_{xx} \dot{x}_2 = P_{x2} - m_h \ddot{x}_{h2} - a_{xx} x_2 - a_{xy} y_2$$

$$b_{yx} \dot{x}_2 = P_{y2} - m_h \ddot{y}_{h2} - a_{yy} y_2 - a_{yx} x_2$$

These four equations yield the coefficients $b_{xx} \dots b_{yy}$ after inserting values for $a_{xx} \dots a_{yy}$ obtained from the incremental load tests.

Consideration in some length was given to the feasibility of obtaining coefficients $b_{xx} \dots b_{yy}$ from velocity readings taken during the application of the incremental loading and using the "before" and "after" journal locations to obtain the displacement coefficients. This has the advantage of obtaining all eight coefficients from the data obtained over a very brief period of time. It was eventually discarded because the magnitude of the available velocity was too low. Velocity could be increased by allowing an oscillatory motion to occur upon application of the incremental load but would, nevertheless remain small relative to that obtained by a vibrating force method. Such a method would have had many similarities to the transient technique described by Morton (20), in a recent publication. The possibility of repeating experiments with varying values of P_x, P_y , all other settings unchanged, was considered. It was discarded due to lack of time.

Table 1 summarises the good and weak features of Methods A, B and C.

Measurement of velocity, and imposition of particular vibration orbits specified in Method B are two novel features which combine to give potential advantages over previously used techniques. They allow study of the extent of non-linearity, utilise only measured quantities thereby eliminating the dependence on other derived coefficients, and avoid measurement of phase.

Coefficients a_{xx} ... a_{yy} may be determined by the incremental load method independently of the above methods. Such values are obtained in the static condition. Section 3.4.2 gives full details of how the established methods were modified for this work.

Notwithstanding its potential advantages Method B suffers, however, from possible setting difficulties. Section 3.4.3 gives full details of the standard sequence used in dynamic testing. Briefly, results were taken at two settings of a relative phase and magnitude of vibrating force P_x , P_y which made the nearest available approach to the requirements of Method B (i.e. horizontal and vertical line loci). Results were also taken at a third setting chosen for its good response which equated to one of the settings required under Method A.

3.2 Description of Test Apparatus

A basic concept of a free[†] test bearing and fixed shaft was chosen in preference to the bearing fixed - shaft free arrangement. Hence dynamic bearing loads could be more readily adjusted and measured, and a simplification was afforded by allowing one element only to rotate and one only to vibrate. Placing the test bearing between two slave bearings meant that the latter only supported approximately half the bearing load. It was considered an important design principle that the various test parameters could be obtained with a minimum of modification.

This chosen experimental arrangement differs from that which commonly occurs in rotating machinery, namely the bearing fixed - shaft free layout. It is important to consider whether dynamic properties established in this test apparatus are valid for the conventional machinery arrangement. Appendix A includes a detailed discussion of this point. Details of loading arrangements, and bearing constraints were arranged so that all forces acting on the bearing would be known. Some care was taken to ensure no extra unaccounted forces were present.

3.2.1 Construction of Test and Slave Bearings

Figure 1 shows the construction of shaft, test and slave bearings. The hydrodynamic test bearing was carried in a housing freely mounted on the rotating shaft. Bearing loads were applied directly to the test bearing housing. Substantial slave bearing housings (1)* containing ball and roller bearings support the shaft, which was belt driven by a variable speed electric motor. A roller bearing located in its outer race was used on the non-driven or free end of shaft. Hence withdrawal of the assembled free end slave bearing housing, outer race and rollers exposed the shaft so that the test bearing could be removed axially without disturbing the driven end. This arrangement also catered for thermal expansion. Small jets delivered oil to the slave bearing and gravity drains returned to the reservoir. Perspex end covers (2) allowed a clear view of the drain space. End covers (3) retained the outer race and acted as shaft oil seals, whilst circlips (10) retained the inner race. An axial key-way (4) transmitted drive to the shaft from the pulley (5). A smaller pulley (6) provided drive for the sine wave generator through an internally toothed belt. Two magnetic pick-ups (7) abutted the end plate (8) at radial positions facing either one or six holes in each

* Numbers in parenthesis refer to circled numbers on the appropriate diagram.

† See footnote at end of Appendix A2

revolution. A radial key (9) retained and locked both small pulley and end plate to the shaft. The complete shaft assembly was balanced by specialist contractor. Axial drillings in the large pulley gave the required balance, and upon completion, the contractor quoted a remaining residual unbalance of 0.0017 Oz - ins at each end. Figure 1 shows the shaft to have a uniform cylindrical surface over the length including test bearing and transducer stations. It is also the largest diameter on the un-assembled shaft. This allowed the complete surface to be accurately ground, thereby giving the best finish, circularity and concentricity between test bearing and transducer measuring stations.

Shaft length between sleeve bearings was made as short as possible consistent with sufficient axial space for the capacitance displacement transducer holders (see section 3.3). Slave bearing housings and supporting structure were made very stiff consistent with reasonable assembly. Both criteria were intended to minimise journal radial motion under dynamic forces (see Appendix A). A support ring (11) is an interference fit into the inner cylindrical surface within the test bearing housing (12). An outer circumferential groove in the ring circulated oil around the bearing and thus to a feed hole, located at the upper most point. Whitemetal was cast directly on to the inner surface of the ring. Its inner surface was subsequently machined to the desired geometry and clearance whilst mounted in the housing (12). This method avoided the use of a split assembly with bearing shells, and gave the best circularity. Also, changes to bearing geometry and clearance are simplified requiring only replacement of the inner ring. Figure 2 details bearing geometry used in this work. Any other bearing width (up to length/diameter ratio = 1.0) can be accommodated by removing or changing the spacers (13). Spacers (14) provide oil drainage space and contain holes in their lower part to allow oil to drain from both sides of the test bearing. Additionally, two brass baffles (15) with relatively small clearance prevent substantial quantities of oil reaching the displacement transducers. End plates (16) retain the inner bearing assembly and carry the displacement transducer mounting cylinders (17). Inductive displacement transducers (18) were fitted into the ends of their mounting cylinders and abutted the shaft. A total of eight transducers were used, operating in the push - pull arrangement, thus giving four displacement readings two each of vertical and horizontal on either side of the bearing. Item (19) clamped the transducer cylinder, whose uniform surface allowed individual adjustment to any clearance. A separate setting jig (not illustrated) enabled the transducer pairs to be set, prior to assembly in the housing. A shoulder on the end plates (16) locates on the housing inner surface, thereby allowing removal and replacement of the end plate without disturbing the transducer origin setting. A single internal cylindrical surface in the housing facilitated machining and assembly. Various longitudinal pins provided accurate circumferential location of all elements. The clearance of all seals was sufficiently large to guarantee no contact with the shaft. Figure 3 shows how circumferential V - grooves around the outer surface provide location for the loading wires. Housing thickness was increased between the loading wire grooves to provide greater ring stiffness and support to the test bearing. Figure 4 shows the assembly of the displacement transducer mounting cylinder. The transducer element was screwed into the one end of the mounting cylinder and secured with Loctite. Tight fitting Silicone rubber sleeves surrounded the wires leading from the transducer

rear to steel pins fitted into the Tufnol end cap. Araldite secured the end cap to the cylinder. To prevent vibration damage to the wires during dynamic testing, the space between sleeves and cylinder was filled with Silicone Rubber Compound.

Using a Talysurf and Talyrond, dimensional checks were taken on the test shaft after manufacture was completed. A C L A value of 0.24 micro-inches was obtained over a sample length of 0.030 inches of the shaft surface in the plane of the test bearing. Circularity readings at two stations of the test journal diameter gave mean zone circles of 100 and 50 micro-inches respectively. Micrometer readings of the shaft diameter indicated 2.4993 inches. With the rig assembled without the test bearing, shaft surface in the plane of the test bearing showed a total run-out of 0.0002 inches, constant at all rotational speeds.

A 5 h.p. D C electric motor provided drive through a 2 inch wide internally toothed belt. Appropriate pulley diameters gave a 3 : 1 speed increase at the test shaft. The belt drives, end plates (8) and one magnetic pick-up (7) can be seen in Figure 5. A variable speed control (left side in Figure 6) allowed any speed to be set in the range 400 to 9000 test shaft r.p.m.

Appendix A gives the equations of motion for the housing, and those from which experimental values of oil film forces were obtained. It also defines the displacement and velocity coefficients and shows that those obtained in the "free bearing" test rig are directly comparable to those used in the normal "fixed" bearing arrangement.

Throughout testing, B.P. Vanellus S.A.E. 30 oil was used. Figure 7 gives the results of an experimental determination of its specific gravity and viscosity-temperature characteristics. These values were used in all theoretical work. It was also found that a linear relationship with negative gradient existed between $\log_{10} (\log_{10} (v + 0.8))$ and $\log (T^{\circ}\text{RANKINE})$.

3.2.2 Static and Incremental Bearing Loads

Steady and incremental loads could be applied separately or together in both horizontal and vertical directions. In each case, steady loads were applied by a turnbuckle arrangement adjusting the tension in the loading wires. Any combination of vertical and horizontal load could be applied. By suitable setting and allowance for the vertical forces due to the weights of the relevant pulleys and test housing, it was possible to apply a constant radial load at any angle. This feature was used to establish the distance between the journal and bearing centres in the operating condition (see section 3.4).

It was important to ensure that the expected test housing displacement did not alter the steady loads. Housing displacement was prevented from altering a mutually perpendicular load by transmitting the forces to the test housing through wires in tension from a fixed point located at a distance many times (approximately 20000:1) greater than the maximum possible housing motion. Figure 8 shows that a spring element was located between the steady force gauge and the fixed point in each system. Inclusion of either one, two or three springs in parallel provided an adjustment of stiffness. Figure 9 shows a three spring arrangement. Stiffness of the spring element was chosen so that it was small compared

to that of the oil film (i.e. $k_x, k_y \ll k_{oil}$). This meant that test housing displacements did not alter a steady force in a parallel direction. Figure 8 shows that the horizontal and vertical steady loading arrangements are similar. Steady forces were measured by pre-calibrated horseshoe dynamometers. These were self contained and gave a direct reading on a dial indicator. Intermediate pulleys were positioned next to the test housing. These comprised wheels supported by low friction bearings (rolling element) which allowed the test housing freedom to rotate around two mutually perpendicular axes whilst under a large steady load. Freedom around these axes allowed the bearing to align itself with the journal longitudinal axis and also eliminated any constraint around the journal centre line. Hence a separate constraint was required to resist torque exerted by the oil film. This was provided by either a separate torque restraining link (see Figure 3), or a spring balance (not illustrated).

This spring balance was included when it was required to measure the power absorbed by the bearing. In this case a re-positioning turnbuckle was provided in conjunction with a position marker, the lines for which are just visible in Figure 3. In all measurements this torque reaction force was found to be small (less than 1 lbf) compared to other vertical forces, and was therefore neglected. Figure 10 shows that all loading wires are looped so that only one junction is required, and the pulleys ensure load equalisation in each length.

Determination of oil film displacement coefficients by the method of incremental loads required the latter to be very much smaller than the steady forces. It was also important that the incremental loads should be known to a reasonable accuracy. If the steady loading system were used for this additional purpose, the relative magnitude of the incremental and steady forces would have placed a prohibitive accuracy requirement upon the steady load measuring device. Therefore, incremental loads were measured and applied by using commercial "weights" acting under gravity. In the vertical direction, this was straightforward but in the horizontal direction it was necessary to rotate the gravitational force through a right angle without the introduction of any additional forces. This was achieved by the use of a gas bearing pulley which is fully described in section 3.2.4.

Consider a state 1 before, and a state 2 after the application of an incremental load, then Figure 8 shows that:

$$P_{x1} - F_{x1} = 0$$

$$P_{x2} - \Delta P_x - F_{x2} = 0$$

$$P_{x2} - P_{x1} = k_x (x_2 - x_1)$$

Hence
$$\Delta P_x = - (F_{x2} - F_{x1}) - k_x (x_2 - x_1)$$

also
$$W_1 + W_2 + W_3 + F_{y1} - P_{y1} = 0$$

$$W_1 + W_2 + W_3 + F_{y2} - P_{y2} + \Delta P_y = 0$$

$$k_y (y_2 - y_1) = P_{y2} - P_{y1}$$

$$\text{Hence} \quad \Delta P_y = - (F_{y2} - F_{y1}) + k_y (y_2 - y_1)$$

Stiffnesses k_x and k_y were arranged to be very much less than the oil film stiffness s (about 1:1000). Hence, if the loading wires remain of constant length between the test bearing and end of the spring element, the terms involving k_x and k_y in the above equations can be neglected.

$$\text{Then:} \quad \Delta P_x = - (F_{x2} - F_{x1})$$

$$\Delta P_y = - (F_{y2} - F_{y1})$$

Hence the added incremental loads measure the change in oil film force to an accuracy better than 1%. In practice, the above mentioned constant wire length requirement necessitated continual observation. Addition of either incremental load altered the tension in the wires between their point of attachment and the test housing. This change in tension altered the length of the loops in the wire at their connectors, and therefore made a very small change to the steady force. This was most significant in the horizontal case with lowest steady load when the wire tension was least. As a precautionary measure throughout all incremental load tests, the change in steady force was recorded and in all cases found to be an insignificant fraction of the incremental load. Figure 9 also shows how all elements in the horizontal loading arrangement were prevented from sagging under their own weight by vertical strings suspended from the horizontal arm.

3.2.3 Dynamic Bearing Loads

Oscillating bearing loads could be applied either vertically or horizontally or together with any relative phase and magnitude. Figure 6 shows the two electromagnetic vibrators. In principle, the forces could take any frequency, but only certain fixed values were used for reasons given in chapter 5. Vibrating forces were measured by Dynamic Force Gauges. These gauges were very stiff in their normal force direction, but it was necessary to protect them from large forces in other directions. Figure 12 shows the mounting device (1) surrounding the gauge (2). The stiffness of this gauge mounting device was determined prior to installation, and Table 2 gives results for both horizontal and vertical units. A thickness of 0.015 inch was used for the spring steel webs. Table 2 also shows, that the device was very much less stiff than the force gauge ($0.83 \cdot 10^3$ and $0.72 \cdot 10^3 : 5.0 \cdot 10^6$) in the load direction. Hence, any force transmitted through the device could be neglected. The devices were significantly stiffer in the other two directions. Experience obtained when a dynamic load was inadvertently misaligned showed the device to be effective.

Figure 12 also shows how the test bearing drain oil was collected and returned to the reservoir when the vertical vibrator was in use. Oil drains under gravity from the housing on to a cap (3) from which it drips into the funnel (4). Cap dimensions are such that it completely clears and overlaps the chimney (5) through which the vibrator connector passes. Hence, providing the funnel did not fill above the chimney top, oil did not escape down the vibrator connector. This arrangement was

effective even at very high supply pressures. When the vertical vibrator was not required, the chimney was capped as shown in Figure 13.

Figure 12 also shows the connector between vertical vibrator and test bearing housing. The horizontal vibrator (partly shown in Figure 14) was connected by a similar arrangement. It was vitally important to ensure that the vibrator connectors imposed negligible constraint on the test bearing housing. It was necessary to design the apparatus to meet this objective and then demonstrate that it had been achieved. This section explains that design principle and assembly sequence, and section 3.4 describes how the attainment of the objective was demonstrated. Identical vibrators were used for both horizontal and vertical forces. In each case, the vibrator plunger exhibited freedom to rotate through a small angle about any axis perpendicular to its own longitudinal axis. Each plunger could also move axially through at least 0.1 inch without imposing additional spring force. Each vibrator plunger was located at least 12 inches from its point of attachment to the housing. Each connector comprised a pivot (6), a rod (7), a spacer (8), and a clamp arrangement (9). Figure 15 shows both connectors and their components labelled with identical numbers. Figure 15 shows how the connectors permit a horizontal displacement of the test bearing housing. The horizontal connector simply moves along its axis. A small rotation of the vertical plunger allows its connector rod to move laterally at the pivot, which item allows the required angular change. A vertical displacement of the test bearing housing is accommodated in a similar manner with the functions of vertical and horizontal elements transposed. Since the possible maximum housing displacement was 0.002 inch and the connector length at least 12 inches, the angular change is very small. Pivots (6) were manufactured from EN 24 steel and their thinnest section designed to transmit the required dynamic forces in tension and compression consistent with the greatest flexibility.

It was also very important to ensure that the process of connecting the vibrators did not alter the position of the journal relative to the bearing. In this context it was necessary to ensure that any consequential relative motion between journal and bearing was very small compared to the operating eccentricity of approximately 0.0015 inch. Since the vibrators were extremely difficult to move, it was decided to locate them in approximately the correct position and make fine adjustments within the connectors. The following procedure was adopted:

38.1(μm)

1. Allow the test rig to reach a stable temperature whilst operating at the required speed and steady vertical load. Vibrators disconnected.
2. Observe journal centre locus at both measuring planes on separate oscilloscopes. Note displacement transducer readings (D.V.M.). At least 3 successive readings were required to show negligible change. This usually required about 1½ hours.
3. Adjust tension in the transverse locating wires (see separate discussion on their development below) until all wires were tight and locknuts set. This process had to be completed without significant change to D.V.M. readings, and therefore no significant change in journal centre position or alignment. Experience showed that this was quite easy to achieve even if somewhat time consuming.

4. Connect vertical vibrator. Rod (7) is threaded on to the pivot (6) so that ample clearance remains for spacer (8). Abut spacer (8) to plunger and unthread rod (7) from pivot until firm even contact is made with spacer, and then tighten clamp nuts. Tighten locknut on pivot thread. Repeat for horizontal vibrator. With both vibrators connected a final check was made on the D.V.M. readings. If necessary further adjustments could be made, but experience showed these were not necessary.

Section 3.4 details the precision which was attained using this procedure. Small lateral misalignments between vibrator and housing were accommodated by using flat end faces on the spacer, rod end, and plunger combined with adequate clearance for the rod within the clamp. Small angular misalignments were accommodated by the pivot.

With the steady load only applied to the test bearing, plus the torque reaction arm, the housing remains free to move axially along the shaft through a small distance. This feature was used as a convenient check on whether the oil film was correctly functioning and supporting the load with low friction. However, when dynamic loads were applied, it was found that only a microscopic misalignment thereof was sufficient to cause an unacceptably large longitudinal vibration and torsional oscillation about an axis perpendicular to the journal centre line. To obviate this, various arrangements of adjusting the connector alignment were tried without success. Hence, transverse locating wires were introduced for the dynamic tests. Figure 3 shows these wires, six in number, parallel to the journal axis with their ends fixed to a base. They allow the bearing to move transversely, and remain parallel, to the shaft, whilst preventing any misalignment or axial motion. Hence, the journal remains aligned to the bearing. Wire length, at least 8 inches is long compared to the maximum possible housing displacement of 0.002 inches. Hence these wires transmit no static transverse forces to the housing. Dynamic behaviour is separately discussed in section 3.5.

Figure 11 shows all four loading arrangements simultaneously connected.

3.2.4 Construction of Air Bearing Pulley

Figure 16 shows the construction of the air bearing pulley. Compressed air is fed into a hollow steel cylinder (1) which is firmly secured by two clamps (2). End caps (3) with O-ring seals (4) enclose the cylinder. Air exhausts from the cylinder from two rows of eight jets, 0.020 inch diameter, located under the free pulley (5). This gives the pulley both axial and rotational freedom. It was found that axial movement to either clamp did not seriously reduce the load capacity even though this made the jets displaced from the plane of the load. Tests showed that an air supply of 100 p.s.i. would support a load of 144 lbf with negligible friction. The axial freedom also provided an indication of perpendicularity to the load line. Spacers (6), and fore-aft movement of the clamp rods (7) along slots in the base, provided the necessary adjustments. The axial freedom also provided an indication of correct functioning when in normal use. Clearance between pulley and shaft was 0.00193 inch. Filters, and an oil mist unit incorporated in the compressed air supply, prevented jet blockage and corrosion. The pulley wheel (5) was made in aluminium.

3.2.5 Oil Supply System

A separate framework supported the oil supply unit. Flexible pipes delivered oil to, and collected from, the main apparatus, thereby preventing the transmission of any vibration generated by the oil pump, its electric motor and fluid circulation to the test rig. Figure 13 shows the oil supply circuit. Flexible pipe was also used immediately prior to the test bearing housing so that the supply pipe did not impede housing motion. This flexibility was verified by observing the housing axial freedom at working temperature when the pipe was especially flexible.

Drain oil from the test bearing was collected under gravity in a funnel, and thence returned to the reservoir. Figure 13 shows the funnel chimney capped when the vibrator was not required. Figure 12 shows the arrangement with vibrator connected (see 3.2.3). This arrangement prevented the oil supply and collection exerting any force on the test bearing.

Oil was delivered to the ball and roller slave bearings through two small jets and returned under gravity to the reservoir. Perspex end covers gave a clear view of the oil level remaining in the slave bearing housing. This allowed instant remedial measures if the level became too high, thus preventing a condition which could result in overheating.

Oil supply pressure to the test bearing could be set to any value within the range 5 to 70 p.s.i. by suitable combined adjustment of the bypass valve and that supplying the test bearing. This allowed the pump to operate on a favourable characteristic and the bypass flow helped maintain a uniform reservoir temperature. A filter protected the oil supplied to both slave and test bearings. A facility for measuring oil flow to the test bearing was incorporated. An immersion heater pre-heated the reservoir oil, thereby allowing oil of suitable viscosity through the pump. It was standard starting practice to operate the oil pump when the reservoir temperature reached 30°C and then allow oil to circulate through the test and slave bearings before rotating the shaft. Figure 17 shows the oil supply unit.

Circulating pump:	Worthington Simpson Gear Pump type 2GAUF 6.45 g.p.m. max Pressure 100 p.s.i.
Filter:	Purolator
Flowmeter:	Meter-Flow Ltd Turbine Flowmeter type M2/0500/B3
Pressure Gauges:	Bourdon type
Immersion Heater:	Heatrae 2.5 kW.

3.2.6 Measurements

Figure 18 shows a block diagram of the instrumentation. Relative displacement between test bearing and journal was measured by four pairs of inductive transducers operating in push-pull, located on each side of the bearing in the horizontal and vertical directions. Figure 1 shows their mounting and location. This arrangement permitted calculation of displacement at either bearing end or centre plane.

Section 3.3 gives full details of the inductive transducer calibration. It was also necessary to insert low pass filters into their output channels. Oscilloscopes displayed the journal locus path for each end. Steady state values of output voltage were measured on a Digital Voltmeter (D.V.M.), and dynamic values recorded on an F.M. tape recorder. Section 3.4 describes the subsequent analysis.

One magnetic pickup abutting the disc (see Figures 1 and 5) was arranged to face one hole in each shaft revolution. This generated a signal with a positive and negative discursion, when the shaft was moved through a given position. A pulse shaper modified this signal into a rectangular pulse with positive discursion only, and of adjustable duration. Pulse duration was set to be the minimum necessary to guarantee detection by the digitizer unit, thereby minimising the length of disturbed signal. Figure 18 also shows a summing amplifier used to add the "phase locating pulse" onto each displacement signal. Checks were made to ensure that the remainder of the signal was not changed. Signals from the force transducers were also fed separately through the summing amplifier so that their oscilloscope trace incorporated the phase locating pulse.

Another magnetic pickup faced six holes in each shaft revolution. This signal was fed into a digital counter, whose output indicated r.p.m. directly, and gave four significant digits when counting over a ten second period. This was used for accurate speed setting. This signal was also supplied to a unit which gave an analogue output proportional to speed. This was more convenient for "driving" the rig and provided useful check readings. Another speed check was given by a hand held tachometer pressed onto the disc centre, or the sine wave generator pulley wheel.

Large steady forces were measured by horse-shoe dynamometers, which were calibrated on a Dennison Tensile Testing Machine. Incremental loads were known by the value of the added mass (see section 3.2.2). Vibrating forces were measured by two dynamic force gauges attached to the test bearing housing. Their output signals were taken through Charge Amplifiers, into which a sensitivity could be dialled, to oscilloscopes and photographed. The phase locating pulse was added to at least one force signal.

Signals for the electro-magnetic vibrators and their power amplifiers were created by the sine wave generator driven by an internally toothed belt from the test shaft. Initially, signals were provided by a separate generator whose frequency could be adjusted to any value. However, in order to impose a steady journal centre orbit it was found necessary to lock the vibration and rotational frequencies to an integer ratio. This was achieved by selecting the number of teeth on the sine wave generator pulley to be an integer ratio of those on the test shaft pulley. Ratios of 1.0 and 2.0 were used. A phase adaptor adjusted the relative phase between the two forces, and the individual gain controls on each power amplifier allowed adjustment of relative magnitude.

Housing acceleration was measured by two piezzo-electric accelerometers in conjunction with charge amplifiers. It was necessary to pass these signals through a tracking filter to remove excessive noise, prior to photographing the oscilloscope traces. Sine wave generator output also provided the tracking filter reference signal.

Chromel-Alumel thermocouples measured the reservoir, test bearing inlet, and outlet oil temperatures in conjunction with a Comark dial indicator.

3.3 Displacement Transducer Calibration

Non-contacting displacement transducers were chosen to avoid friction and the consequential introduction of unknown forces. Inductive transducers were selected for their ability to operate when their target interspace may contain oil. However, this type require independent calibration. This chapter describes the calibration technique, the results obtained, the method of determining displacements under test conditions, and the measurement of bearing clearance circle in the non-testing condition.

3.3.1 Calibration Technique

Chapter 3.2 describes how the inductive transducers are mounted outboard of the bearing. Relative displacements of the journal centre, rather than the surface are given by operation in the push-pull arrangement. Transducer sensitivity varies inversely with the mean initial gap between transducer and target. Therefore, gap dimensions were chosen as the smallest which would guarantee no physical contact with the shaft under any aligned or misaligned state, thereby providing the largest useable sensitivity.

Direct reading, Wayne-Kerr capacitance transducers with 0 - 0.02 inch range, were chosen for the absolute standard. These were mounted in special holders on the outside face of the plates carrying the inductive displacement transducers. Figure 19 shows a pair of capacitance transducers mounted in the vertical direction. Provision was made for four separate units, but in practice it was found more convenient to treat vertical and horizontal axes separately. Prior to calibration all traces of oil were removed from the shaft in the vicinity of the capacitance transducers. These measured the relative displacement between bearing and shaft surface, while the inductive transducers that between housing and shaft centre. With the non-rotating shaft these relative displacements are equal. In the revolving shaft case, assuming rotation about its centre, non-circularity could alter both inductive transducer sensitivity and capacitance transducer reading, cyclically during a shaft revolution. However, shaft non-circularity was very small compared to the initial gap setting of 0.025 inch and the capacitance transducer readings. Therefore these effects were neglected. Calibration data were taken in the cold non-rotating condition and at the normal operating temperature and speed.

500 (μm)625 (μm)

A series of relative horizontal displacements were readily obtained by applying a suitable vertical load, and then rotating the housing through a set of small angles around the vertical axis. The vertical load ensured that the housing remained stationary whilst readings were taken. A series of vertical displacements were obtained by a similar procedure. Figure 20 shows the relative positions of journal and both sets of transducers, and defines the various displacements (applicable for this chapter only). It shows the journal centre line in two arbitrary positions. It was assumed that in all journal positions the angle between the line joining the origins of the capacitance transducers was parallel to the journal centre line. Maximum possible deviation was 0.01 inch over 4.95 inch. It was also assumed that the axis of the capacitance transducers was perpendicular to the journal centre line.

0.254 mm

125.7 mm

Objective of the calibration was to establish values of α_1 , α_2 , α_3 and α_4 such that:

$$\alpha_1 = \frac{\Delta R_1}{\Delta x_2}, \quad \alpha_2 = \frac{\Delta R_2}{\Delta y_2}, \quad \alpha_3 = \frac{\Delta R_3}{\Delta x_2'}, \quad \alpha_4 = \frac{\Delta R_4}{\Delta y_2'}$$

where $\Delta x_2 \dots \Delta y_2'$ represent displacement of journal centre line at the inductive transducer station.

$\Delta R_1 \dots \Delta R_4$ represent the corresponding voltage change from the inductive transducers.

This implies a linear relationship between voltage R and the relative displacement at the same axial station. Capacitance transducers are at different axial stations. From Figure 20 it follows that corresponding displacements at inductive transducer stations can be obtained from capacitance transducer readings by:

$$\begin{aligned} \Delta x_2 &= \frac{(\ell_3 + \ell_2)}{2\ell_3} \Delta x_3 + \frac{(\ell_3 - \ell_2)}{2\ell_3} \Delta x_3' \\ \Delta x_2' &= \frac{(\ell_3 + \ell_2)}{2\ell_3} \Delta x_3' + \frac{(\ell_3 - \ell_2)}{2\ell_3} \Delta x_3 \\ \Delta y_2 &= \frac{(\ell_3 + \ell_2)}{2\ell_3} \Delta y_3 + \frac{(\ell_3 - \ell_2)}{2\ell_3} \Delta y_3' & \ell_1 &= 0.466 \text{ inch} \\ & & \ell_2 &= 1.6875 \text{ inch} \\ \Delta y_2' &= \frac{(\ell_3 + \ell_2)}{2\ell_3} \Delta y_3' + \frac{(\ell_3 - \ell_2)}{2\ell_3} \Delta y_3 & \ell_3 &= 2.475 \text{ inch} \end{aligned}$$

Capacitance transducer readings gave Δx_3 , $\Delta x_3'$, Δy_3 and $\Delta y_3'$ which were used with the above equations to compute Δx_2 , Δy_2 , $\Delta x_2'$ and $\Delta y_2'$. Values of ℓ_1 , ℓ_2 and ℓ_3 are given. Inductive transducer readings were taken from the Digital Volt Meter.

For the calibration in the hot rotating condition, it was endeavoured to set the rig so that the absolute value, and difference in temperature, between oil entering and leaving the bearing, and between opposite elements of a transducer pair, were as severe as any to be met during testing. Oil temperatures into and leaving the bearing were measured by the normal thermocouples described in chapter 3.2. A special hand held thermocouple was constructed so that its tip could be placed on the inductive transducer head. Oil and transducer head temperatures were noted, having stabilised with the journal rotating at 3130 rpm. A small load adjustment was made to facilitate test bearing housing rotation around the vertical axis. Capacitance transducers were then inserted into their holders in the horizontal direction. Great care was taken to ensure that no oil was in the vicinity of the capacitance transducers throughout the experiment. A temporary arrangement of wires held the housing in a series of fixed positions whilst readings were taken. A similar arrangement was used for calibration in the vertical direction. Typical temperatures in $^{\circ}\text{C}$ were:

	Oil Temperatures		Transducer Head Temperatures	
	in	out	upper	lower
Temperatures during vertical calibration	51.85	62.7	upper 56.5	lower 60.0
Temperatures during horizontal calibration	51.0	62.0	left 55.5	right 57.1

Oil outlet temperatures did not exceed 65.0°C at any time during testing. Transducer head temperatures and their differences measured during this calibration were shown to be equal to the maximum met during testing. Temperatures were very sensitive to speed. Suitable temperatures for this calibration were obtained by using a higher speed than any used in testing.

3.3.2 Results

Figures 21 and 22 show data points from which values of $\alpha_1 \dots \alpha_4$ were obtained. Different capacitance transducer origin settings in the several tests cause the lateral displacement of the three curves. This is immaterial since gradients only are required. Table 3 lists the values of α and the established extent of the linear relationship. One set was taken in the cold stationary condition some days before testing started. As a precautionary measure this was repeated mid-way through testing (April 1975). A further set was taken in the hot rotating condition to determine whether $\alpha_1 \dots \alpha_4$ were influenced by the change from cold starting, to the hot rotating condition. Results for this 'hot' calibration (3.3.1 gives experimental technique) of necessity cover a lesser displacement range but incorporate that mostly used during testing. Table 3 shows that α varies considerably between channels. However, for a given channel there is negligible variation between values obtained in the cold condition at widely separated times, and those for the hot rotating condition. Consequently, one value of α was used for each channel in all subsequent calculations.

During normal testing, values of $R_1 \dots R_4$ were converted into displacement readings at the bearing edges and centre respectively by:

$$\Delta x_1 = \frac{(\ell_2 + \ell_1) \Delta R_1}{2\ell_2 \alpha_1} + \frac{(\ell_2 - \ell_1) \Delta R_3}{2\ell_2 \alpha_3}$$

$$\Delta x'_1 = \frac{(\ell_2 - \ell_1) \Delta R_1}{2\ell_2 \alpha_1} + \frac{(\ell_2 + \ell_1) \Delta R_3}{2\ell_2 \alpha_3}$$

$$\Delta y_1 = \frac{(\ell_2 + \ell_1) \Delta R_2}{2\ell_2 \alpha_2} + \frac{(\ell_2 - \ell_1) \Delta R_4}{2\ell_2 \alpha_4}$$

$$\Delta y_1' = \frac{(\ell_2 - \ell_1) \Delta R_2}{2\ell_2 \alpha_2} + \frac{(\ell_2 + \ell_1) \Delta R_4}{2\ell_2 \alpha_4}$$

$$\Delta x_o = \frac{(\Delta x_1 + \Delta x_1')}{2}, \quad \Delta y_o = \frac{(\Delta y_1 + \Delta y_1')}{2}$$

It is important to note that these equations utilise calibrated gradients α only, and therefore yield changes in the distance between bearing and journal. Furthermore, gradients α were shown to be valid for the operational conditions over most of their required range. The origin for these displacements is such that $R_1 \dots R_4$ are zero, i.e. the so called electrical origin. Section 3.4 details how the bearing and journal centres were located within this co-ordinate system. Moreover, no changes whatsoever were made to the measuring system or rig between calibration and test (apart from the withdrawal of the capacitance transducer heads). This is a very important and valuable feature.

3.3.3 Measurement of Clearance Circle

Two methods were devised whereby the journal clearance circle was measured in the cold non-rotating condition using the installed loading system with the inductive transducers and their calibration.

(i) Parallel Method

Combinations of horizontal and vertical loads were applied to the test bearing so that the journal contacted the bearing surface at a number of positions around the circumference. Displacement transducer readings were taken at each point and converted to values applicable to the bearing ends. Figures 23 and 24 show the results. It was intended that the bearing and journal centre lines should remain parallel throughout the experiment, although in practice, it was found difficult to verify this point. A method of "lifting off" one side and allowing the journal to return confirmed that the surfaces touched. However, the bearing could easily rotate through a small angle around the axis of the load direction, and parallelism in this sense could not be verified. In some instances, it was clearly not obtained. Difficulties were also experienced in producing points near the top of the clearance circle at the free end. This was because the required vertically downwards load was difficult to apply. Since the normal loading system applied vertically upwards forces, it was necessary to construct a temporary arrangement for downwards forces. Additionally, space restrictions made it difficult to align the temporary load. Furthermore, difficulty was experienced in finding and verifying a stable position with this loading arrangement. Consequently, the upper section of the circle at the free end is rather devoid of points. However, points were obtained over a sufficient arc to enable a good circle to be drawn and a diameter established.

difficult

(ii) Inclined Method

Vertically upwards load was adjusted so that it completely balanced the weight of the test bearing housing. Then the housing was rotated so that the journal was contacted by opposite edges of the bearing. A temporary arrangement of thin wires held it in position whilst readings were taken. Very few points were taken with this method. However, some are included in Figure 24 over an arc where none were obtained by the parallel method. Extreme care was necessary to avoid excessive force when effecting the rotation, due to the high risk of damage to the bearing edges. In this method, correctness of location was less readily verified and stability inferior to that exhibited by the parallel method. Hence, the parallel method was preferred.

These experiments provided the clearance circle in the cold non-rotating condition. Radial clearance in the hot rotating condition is discussed in section 3.4.1 and Chapter 5.

3.4 Experimental Procedures

Chapter 3.3 describes how relative journal centre displacements were measured in the operating condition. The first section of this chapter describes the procedure used to find how these displacements related to the bearing. Later sections describe the methods used to determine displacement and velocity coefficients.

3.4.1 Static Locus

Chapter 3.3 shows that the origin for the journal centre displacement measurements is at the electrical centre. It was found that the transition between cold stationary and hot rotating conditions caused significant drift in the displacement readings. This could be due to either or both, a shift in the origin itself relative to the transducers, or a relative displacement of bearing and transducers during the warm-up period. Thermal gradients within the housing could cause either of these effects. It is important to note that the chosen method relies only on the gradients $\alpha_1 \dots \alpha_4$ which were shown to be invariant between cold and operating conditions.

Three separate quantities are required to establish the static locus. It is necessary to locate (i) journal centre, (ii) bearing centre and (iii) bearing surface, all in the operating condition. This latter proviso is vitally important.

- (i) Journal centre is given by the D.V.M. readings and appropriate choice from equations given in 3.3.2.
- (ii) Bearing centre, and hence eccentricity and attitude angle were located in the following manner:

Vertical load, supply pressure and speed were set to the desired test values, and oil temperatures allowed to stabilise. Temperature stability was deemed to have been reached when three identical, consecutive readings were obtained over a 15 minute period. This warm-up procedure

took about 1 hour. Journal centre readings were then taken with various combinations of horizontal and vertical loads arranged so that the bearing experienced the same load at a series of different, known angles. It was normal practice to move the load from 0 to 80° to the vertical in 10° intervals. It was found that a plot of these journal centre locations formed a part of the circumference of a circle. This result was possible because the test bearing had circumferential symmetry. Figures 25 and 26 give typical examples of large and small eccentricity respectively. The centre of this circle is the bearing centre, and its radius is the eccentricity. Given the bearing centre, attitude angle could be obtained from any of the nine points for which the load direction was known. It was normal practise to use a mean of values given by all the available points. Bearing centre, eccentricity and attitude angle were established by the above methods for each individual test. Oil inlet and outlet temperatures were recorded whilst the series of radial loads were applied. They showed negligible variation. Whilst Figures 25 and 26 show results for the bearing centre plane, any misalignment may be indicated by repeating this procedure with data applicable to the bearing edges. Cases so treated showed small misalignment.

- (iii) Location of the bearing surface and centre yields the radial clearance. Appendix C shows that some change in the radial clearance will occur during the transition from cold to hot conditions. It is most important that the clearance should be evaluated for the working condition, but this presents experimental difficulties. It was found that oil inlet and outlet temperatures were extremely sensitive to rotational speed. Temperatures were changed significantly whilst the speed was reduced to zero, even if the reduction was performed as quickly as safety conditions would permit. (N.B. It was necessary to reduce speed and load together to avoid either, instability if the load alone was reduced, or, damage due to stopping with full test load applied). The following procedure was adopted:

Oil inlet and outlet temperatures were noted throughout testing. Having completed a test, speed (and load) were reduced as quickly as possible. Readings of all four displacement channels and both oil temperatures were taken immediately after stopping. Then a series of radial loads were applied in various directions so that in each case the journal was held against the bearing surface. Again journal displacement channels and temperatures were recorded. Sufficient points were taken to cover a reasonable arc, as quickly as possible to minimise the temperature change. This sequence required about 3 minutes. It was assumed that the bearing centre obtained under test conditions was applicable to the single point obtained immediately after stopping, thereby providing a value of radial clearance. A separate bearing centre was obtained from the second series of points, thus providing a second value of radial clearance. Figures

25 and 26 illustrate results from both procedures. Each of these values of radial clearance were plotted against their respective temperatures. Extrapolation to the test condition temperature gave an approximate value of the required radial clearance. Figure 46 contains the results.

Figure 25 shows typical data points from which eccentricity and attitude angle were deduced, obtained before and after the vibrating load tests (two vibrators and transverse wires connected in each case). It also shows the journal centre location between individual tests. These results demonstrate the negligible change in bearing centre, eccentricity and attitude angle throughout.

Figure 27 shows data points from which eccentricity was deduced, (a) without and (b) with the two vibrators and transverse wires connected. These show that the small load changes required for each 10° rotation, produce similar displacements in each case. Repeatability is indicated by the small difference in eccentricity obtained in the two tests over a 3 months interval. Points taken before and after (Fig 27(b) $\alpha = 30^\circ$) illustrate the negligible journal centre movement arising from the connection process. Furthermore, examination of the displacement arising from incremental loadings during determination of displacement coefficients, show no effect due to transverse wires and vibrator connections.

Hence, it was concluded that:

- (a) the transverse wires and vibrator connection did not impose any significant lateral constraint.
- (b) their assembly did not significantly move the journal centre

3.4.2 Displacement Coefficients by Incremental Loading

Section 3.2.2 describes how the incremental loads were applied and measured. Two separate sets of displacement increments with their associated loads are required to provide a data for two equations requiring simultaneous solution to yield the four displacement coefficients. It was convenient to apply one horizontal and one vertical incremental load thereby giving the two required sets of displacements. If the incremental loading sequence was performed with a vertical steady force, it was found that an unreasonably large horizontal displacement was necessary to ensure that the vertical displacement was sufficiently above the value to which the instrumentation could discriminate. This feature arose because the four displacement coefficients have considerably different values (in extreme cases 10 : 1).

It was important that the entire sequence was performed as quickly as possible to minimise the effect of any possible changes in the nominally identical conditions. It was also desirable to apply incremental loads in both positive and negative directions in the same sequence. Section 3.2.2 also describes how the horizontal incremental loads were applied through the gas bearing pulley. Hence, in order to apply both positive and negative horizontal incremental loads, without a lengthy re-arrangement, it was necessary for the incremental load to adjust the tension in the main horizontal loading wires. This required the application of the horizontal incremental load whilst some steady horizontal force was also applied. It was, therefore, decided to perform the incremental loading sequence whilst the direction of the large steady load was rotated to some

angle (30 or 40°) to the vertical. This load rotation was achieved by setting a suitable combination of horizontal and vertical steady loads as described in section 3.4.1. It follows that the incremental displacements were similarly rotated, took more nearly equal values and were vastly greater than the instrumentation discrimination, when modest incremental loads were applied. Hence the above mentioned difficulty was removed and a significant advantage gained over previous methods. It was usual practise to apply a sequence of positive and negative sets of horizontal and vertical incremental loads with zero values in between each loading. Adjacent zeros were used in each subsequent calculation.

Figure 28 shows a typical journal displacement from x_1, y_1 to x_2, y_2 . Steady load is at an angle α to the vertical. Its magnitude and direction are known from its horizontal and vertical components. Section 3.3 shows how $x_1, x_2, y_1,$ and y_2 were determined from voltage readings. From Figure 28 it follows that:

$$l = \left[(x_2 - x_1)^2 + (y_2 - y_1)^2 \right]^{\frac{1}{2}} \quad \Delta x = l \cos \xi$$

$$\xi = \tan^{-1} \left(\frac{y_2 - y_1}{x_2 - x_1} \right) - \alpha \quad \Delta y = l \sin \xi$$

$\Delta P_x, \Delta P_y$ are the incremental loads applied to the housing

$\Delta F_x, \Delta F_y$ are the components of incremental loads applied to bearing perpendicular and parallel to the direction of the main steady load.

Two incremental loadings, $+\Delta P_x, +\Delta P_y$ each give positive $\Delta x, \Delta y$ and hence an increase in ϕ .

Figure 28 also shows that for $+\Delta P_x, \Delta F_{xa} = +\Delta P_x \cos \alpha$

$$\Delta F_{ya} = -\Delta P_x \sin \alpha$$

and for $+\Delta P_y, \Delta F_{xb} = +\Delta P_y \sin \alpha$

$$\Delta F_{yb} = +\Delta P_y \cos \alpha$$

Signs are reversed for the negative increments.

Put $\Delta x = x_2 - x_1,$ and $\Delta y = y_2 - y_1.$

Velocities \dot{x}, \dot{y} are zero at both states 1 and 2. Furthermore $\Delta F_x, \Delta F_y$ are also equal to the forces exerted by the journal on to the oil film. Hence, equations numbers A1 - 4 and 5 given in Appendix A become:

$$\Delta F_{xa} = a_{xx} \Delta x_a + a_{xy} \Delta y_a$$

$$-\Delta F_{ya} = a_{yx} \Delta x_a + a_{yy} \Delta y_a$$

$$\Delta F_{xb} = a_{xx} \Delta x_b + a_{xy} \Delta y_b$$

$$\Delta F_{yb} = a_{yx} \Delta x_b + a_{yy} \Delta y_b$$

Putting $D = (\Delta x_a \cdot \Delta y_b) - (\Delta y_a \cdot \Delta x_b)$

yields $a_{xx} = (\Delta y_b \cdot \Delta F_{xa} - \Delta y_a \cdot \Delta F_{xb}) / D$

$$a_{xy} = (\Delta x_a \cdot \Delta F_{xb} - \Delta x_b \cdot \Delta F_{xa}) / D$$

$$a_{yx} = (\Delta y_b \cdot \Delta F_{ya} - \Delta y_a \cdot \Delta F_{yb}) / D$$

$$a_{yy} = (\Delta x_a \cdot \Delta F_{yb} - \Delta x_b \cdot \Delta F_{ya}) / D$$

The above four equations were used to calculate the displacement coefficients for positive and negative increments.

3.4.3 Displacement and Velocity Coefficients by Dynamic Loading

Chapter 3.1 describes several methods of deducing both displacement and velocity coefficients from the response to various dynamic forces. Method B imparts useful advantages if the specified loci can be obtained. Since this doubt could only be resolved by attempting the experiment, the following procedure was adopted.

Rig temperatures were stabilised and data obtained for the determination of attitude angle and eccentricity. Then relative phase and magnitude of P_x , P_y were adjusted so that:

1. $y = \dot{y} = 0$ at all t , i.e. journal centre locus is a horizontal line
2. $x = \dot{x} = 0$ at all t i.e. locus is a vertical line
3. Reasonable response was obtained in both x and y directions. This gave a line or thin loop locus at approximately 45° to the vertical.

Each of the above tests were set and data recorded. Immediately after each test (within 20 seconds) P_x , P_y were smoothly reduced to zero and an "origin" recorded. Journal^x centre location was then checked. Experience showed that tests type 1 and 2 could not always be precisely set. Frequently it was necessary to compromise between a line locus in a slightly wrong direction and an elliptical locus with major axis in the correct direction. After dynamic tests, a series of incremental loading tests were completed at the same temperatures, and without disconnecting the vibrators. This permitted a comparison between displacement coefficients obtained from dynamic and incremental loading techniques. In some cases, data for a complete check on the bearing centre was taken after the dynamic tests. Figure 25 shows the microscopic variation in bearing centre location throughout the vibrating test and that eccentricity remained constant.

A MAC 16 computer digitised data for all displacement channels. This magnetic data tape was used as input for a FORTRAN program using the ICL computer. Figure 29 shows the flow chart for this data reduction program. Digitiser frequency was selected to give at least 100 and 200 data points during each shaft revolution for vibration frequency ratios $\Omega/\omega = 1.0$ and 2.0 respectively. 'Blip' duration was adjusted to the minimum necessary to guarantee inclusion in the digitised data, thereby minimising the disturbed time. Record and playback required different signal ranges on the Racal tape recorder. Consequently, a "playback" calibration was necessary. Known voltages were recorded, digitised and processed. These yielded slight modifications to the range factors and a DC shift for each channel. Range factors were incorporated in the data reduction program.

Displacements due to vibration alone were subsequently obtained by subtracting the "origin" ordinates from those at corresponding times in the immediately preceding dynamically loaded test. Hence the playback DC shift (shown to be invariant along the tape length) was common to both values and no action was needed. Times scales on all data were fixed to a common event by the "blip". However, it was necessary to allow for the "playback shift" when comparing DVM and digitised voltages.

The data reduction program also incorporated equations given in 3.3.2 thereby producing $x_1, x'_1, y_1, y'_1, x_0$ and y_0 . Each digitised data tape contained many Conditions, which in turn included several different tests. A few seconds recording contained a large number of cycles. The program was arranged to process three consecutive cycles, and then calculate a mean value at each time. It then performed the same sequence of data for the next test. Figure 29, Flow Chart, shows how the data reduction program effected these processes.

Figures 30 and 31 show data points for three consecutive cycles with the mean value superimposed. "Origin" data is also shown for the same condition. These figures indicate small variation between the three cycles. Figures 32 to 35 show, for each of the three test types, the response to vibrating force alone derived by the aforementioned subtraction. Figures 30 and 31 show that the "origin" curve displays a significant oscillation at rotational frequency. This is especially significant when attempting to adjust forces so that zero response occurs in one direction (tests 1 and 2). Only the "total" curve was available when making the force adjustment. Indeed, the forces were set to give zero response on the "total" curve. Subsequent subtraction of the "origin" ordinates could possibly produce a "vibration only" response which differed further from the desired curve.

The resultant displacement time histories did not take the precise form specified above. It was found, for example, that $\dot{x} = 0$ could be obtained for a part of the cycle, but it was more difficult to make this occur over long sections and at $x = 0$. Hence, some modifications were necessary to the idealised analysis procedure suggested in Chapter 3.1. Appendix B gives an example of an analysis sequence.

Equations A1 - 11 and 12 are valid at all times. Firstly, equations were applied at times when 3 of the 4 variables x, y, \dot{x}, \dot{y} were zero. Hence, 2 equations were solved each involving one unknown coefficient. Further coefficient values were deduced using these equations at times

when at least one, and preferably two of the four variables were zero. Times and equations were selected using the following guide lines.

- (a) Only coefficients established in the same set of tests (1, 2, or 3) were invoked to evaluate other coefficients.
- (b) Coefficients invoked to evaluate other coefficients, were themselves derived from a similar value of the appropriate variable.
- (c) Well conditioned equations were chosen. Forces evaluated from established coefficients and non-zero variables were much smaller than measured forces (e.g. Appendix B Test 1, $t = 18$). If computed forces of significant magnitude were unavoidable, equations were chosen to avoid having the difference of two relatively large numbers. Preferably the force due to the unknown coefficient was the largest individual force in the equation.

Velocities were obtained from the gradient of the smoothed curve drawn through the data points. Forces P_x , P_y , and housing acceleration \ddot{x}_h , \ddot{y}_h , were obtained from enlarged oscilloscope photographs.

3.5 Vibration Characteristics of Test Rig

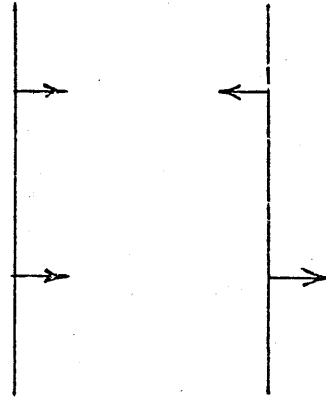
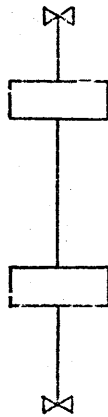
It is particularly important that experimental data analysis considers all significant forces acting on the bearing. In the static loading case this is relatively straightforward and is discussed in section 3.2.2. In dynamic testing, particular care is necessary to ensure that vibration of any other part of the rig does not introduce forces of significant magnitude which have not been included in the analysis. It is necessary to consider possible vibration of all items which can transmit forces to the bearing. These are:

- (a) Steady loading wires (vertical only, in dynamic testing).
- (b) The journal via the oil film
- (c) Vibrator connectors
- (d) Transverse wires

(a) Vertical Steady Loading Wires

Figures 8 and 10 show that two pulley blocks are mounted in the vertical steady loading system, between relatively mass-less wires. Oscillating horizontal forces could be transmitted to the test bearing housing by transverse vibration of these two pulleys. An arrangement of wires at the lower spring ends prevented both their rotation as the load varied, and lateral motion at that point. Hence, the vibrating system possessed two degrees of freedom and comprised two masses joined by mass-less wires. Normal modes and their frequencies were measured in separate tests using correct load and rotational frequency.

Measurements in a direction perpendicular to the journal gave:



1st mode
4.0 hz

2nd mode
7.25 hz

These frequencies were found to be independent of rotation speed, and are well removed from any used in vibration testing. Normal mode frequencies of transverse vibration of these pulleys in a direction parallel to the journal would be very similar to those above because of the near symmetry in the two directions, and could also be neglected. Nonetheless, any such forces are reacted by tension in the transverse wires. Tension existed in the wires due to the steady vertical load and it was assumed that the longitudinal wire stiffness was sufficiently large that the pulley vertical motion could be deemed equal to that of the test bearing housing. Consequently for the purposes of data analysis in the vertical direction the pulley masses were added to that of the test bearing. Nevertheless, pulley masses were considerably less than that of the test bearing housing. Torsional vibration of the pulleys around the wire axis was reacted by the transverse wires.

(b) Journal and Oil Film Vibration is fully discussed in Appendix A2.

(c) Vibrator Connectors

These connectors were extremely stiff and did not exhibit any flexural vibration. Their mass was small compared to the test bearing housing to which they were deemed attached for data analysis purposes.

(d) Transverse Wires

Section 3.2.3 describes how the transverse wires are attached to the test bearing housing. There was no observable transverse vibration by the wires as continuous media. These wires are long compared to both the displacement of the housing, and the observed vibration of their support brackets. Since wires can only transmit tension, they are only able to exert a force on the housing if their support bracket is displaced horizontally, vertically, or in the direction of the wire. Negligible vibration of the support brackets was observed at any

frequency, whilst test data was collected. Nevertheless, it is valuable to know the actual resonant frequencies and hence their proximity to test frequencies. Resonant frequencies of both support brackets were determined experimentally, whilst the rig was rotating in the normal test situation, with transverse wires tensioned.

Results listed in Table 4 showed that all resonances of the motor end could be neglected. The only significant frequency appeared at 2258 c/min. at the free end. This was so sharply tuned and located that it did not interfere with any of the test frequencies, whose ranges are given in Table 5.

4 THEORETICAL METHODS

Section 4.1 describes the solution of the governing differential equations. The method of solution allows viscosity (η) to vary with both temperature and pressure. Hence viscosity varies both around and across the journal and the equations are non-linear. Section 4.2 describes the computation of the journal centre location, and this is extended in Section 4.3 to calculation of the displacement and velocity coefficients. A parallel study using constant viscosity and the short bearing approximation is given in Section 4.5

4.1 Solution of Reynolds Equation

Figure 36 shows the instantaneous journal centre (JC) at an eccentricity ϵ from the bearing centre (BC). The journal is rotating at ω rads/sec around its centre JC and which is moving with velocity v in a general direction ψ . Hence the journal surface velocity relative to the bearing varies with distance around surface x .

Journal surface velocities, parallel and perpendicular to the bearing surface are:

$$v_{\parallel} = r\omega + v \sin(\theta + \phi - \psi) \quad \text{----- 1}$$

$$v_{\perp} = v \cos(\theta + \phi - \psi) \quad \text{----- 2}$$

In all experiments $v < 0.2$ inch/sec and $r\omega > 1.54 \cdot 10^{+2}$ inch/sec

Hence the second item in the expression for v_{\parallel} was neglected.

Since also $x = r\theta$, equations (1) and (2) become

$$v_{\parallel} = r\omega \quad \text{----- 3}$$

$$v_{\perp} = v \cos\left(\frac{x}{r} + \phi - \psi\right) \quad \text{----- 4}$$

Figure 36 also shows that

$$h + r = \epsilon \cos \theta + R \left(1 - \frac{\epsilon^2}{R^2} \sin^2 \theta\right)^{\frac{1}{2}} \quad \text{----- 5}$$

Since $\frac{\epsilon}{R} \ll 1$, and $R-r = C_r$, equation 5 becomes

$$h = C_r + \epsilon \cos \frac{x}{r} \quad \text{----- 6}$$

Cameron (52) derives Reynolds equation from first principles. He gives

$$\frac{\partial}{\partial x} \left(\frac{h^3}{\eta} \frac{\partial p}{\partial x} \right) + \frac{\partial}{\partial z} \left(\frac{h^3}{\eta} \frac{\partial p}{\partial z} \right) = 6u_0 \frac{\partial h}{\partial x} + 12 \frac{\partial h}{\partial t} \quad \text{----- 7}$$

in which $u_0 = v_{\parallel} = r\omega$

$$\frac{\partial h}{\partial t} = v_{\perp} = v \cos \left(\frac{x}{r} + \phi - \psi \right)$$

$$\frac{\partial h}{\partial x} = -\frac{\epsilon}{r} \sin \left(\frac{x}{r} \right) \text{ and } \frac{\partial^2 h}{\partial x^2} = -\frac{\epsilon}{r^2} \cos \frac{x}{r}$$

from eq (3)

Assumptions necessary for the derivation of Reynolds equation are also applicable to this theory.

For convenience put $B1 = \frac{-3 \epsilon \sin \frac{x}{r}}{rh}$

$$B5 = \frac{-6 \omega \epsilon \sin \frac{x}{r} + 12 v \cos \left(\frac{x}{r} + \phi - \psi \right)}{h^3}$$

Since the journal is considered aligned, $\frac{\partial h}{\partial z} = \frac{\partial^2 h}{\partial z^2} = 0$

and allowing $\eta = \eta(x, z)$, equation 7 becomes:

$$B1 \frac{\partial p}{\partial x} - \frac{1}{\eta} \frac{\partial \eta}{\partial x} \frac{\partial p}{\partial x} + \frac{\partial^2 p}{\partial x^2} - \frac{1}{\eta} \frac{\partial \eta}{\partial z} \frac{\partial p}{\partial z} + \frac{\partial^2 p}{\partial z^2} = \eta B5 \quad \text{--- 8}$$

A large pressure gradient is likely in the region of large pressures, and to facilitate convergence it is convenient to solve the equation using a transformed variable ϕ , which has less severe gradients

put $\phi = ph^q$ ----- 9

If viscosity is regarded as constant throughout the film, the equations simplify so that putting $q = 1.5$ affords some further benefit.

Since no particular value appeared to present an advantage, q was retained in general form. Subsequent programming was arranged so that q could be entered as data. As expected, solutions were shown to be independent of q .

Hence $\frac{\partial p}{\partial x} = \frac{\partial}{\partial x} (\phi \cdot h^{-q})$ where ϕ and h are both functions of x

$$\frac{\partial p}{\partial z} = \frac{\partial}{\partial z} (\phi \cdot h^{-q}) = h^{-q} \frac{\partial \phi}{\partial z} \text{ since } h \text{ is not a function of } z.$$

For convenience put

$$B2 = \left[- \left(B1 - \frac{1}{\eta} \frac{\partial \eta}{\partial x} \right) q \cdot h^{-(q+1)} \frac{\partial h}{\partial x} + (q^2 + q) \cdot h^{-(q+2)} \left(\frac{\partial h}{\partial x} \right)^2 - q h^{-(q+1)} \frac{\partial^2 h}{\partial x^2} \right]$$

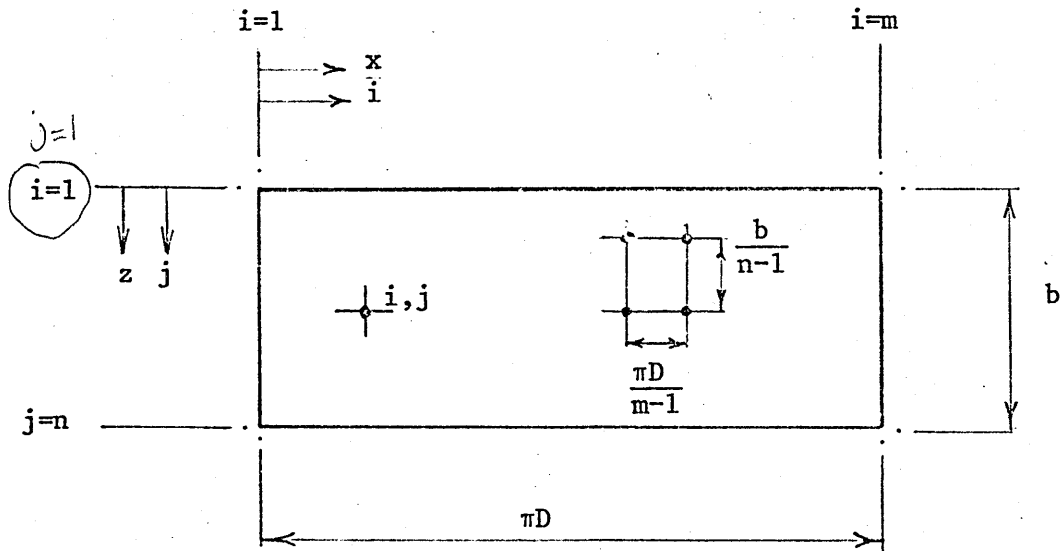
$$B3 = \left[(B1 - \frac{1}{\eta} \frac{\partial \eta}{\partial x}) h^{-q} - 2qh^{-(q+1)} \frac{\partial h}{\partial x} \right]$$

$$B4 = \frac{1}{\eta} \frac{\partial \eta}{\partial z} h^{-q}$$

Hence equation 8 becomes

$$B2 \cdot \phi + B3 \frac{\partial \phi}{\partial x} + h^{-q} \frac{\partial^2 \phi}{\partial x^2} - B4 \frac{\partial \phi}{\partial z} + h^{-q} \frac{\partial^2 \phi}{\partial z^2} = \eta \cdot B5 \text{ ----- 10}$$

To solve equation 10 by an iterative finite difference technique, the bearing surface is divided in a grid with m and n elements around and across respectively.



This shows the developed surface of one bearing land with the circumferential groove adjoining the $j = 1$ ($z = 0$) edge for its entire length.

A general point is denoted by i, j with the grid intervals $\frac{\pi D}{m-1}$ and $\frac{b}{n-1}$ respectively.

Mesh size was arranged so that the pressure gradient may be assumed constant over two grid intervals. This allows finite difference forms of the derivatives thus:

$$\frac{\partial \phi}{\partial x}_{i,j} = \left[\phi_{i+1,j} - \phi_{i-1,j} \right] \frac{(m-1)}{2\pi D}$$

$$\frac{\partial^2 \phi}{\partial x^2}_{i,j} = \left[\phi_{i+1,j} + \phi_{i-1,j} - 2 \phi_{i,j} \right] \frac{(m-1)^2}{\pi^2 D^2}$$

$$\frac{\partial \phi}{\partial z}_{i,j} = \left[\phi_{i,j+1} - \phi_{i,j-1} \right] \frac{(n-1)}{2b}$$

$$\frac{\partial^2 \phi}{\partial z^2}_{i,j} = \left[\phi_{i,j+1} + \phi_{i,j-1} - 2\phi_{i,j} \right] \frac{(n-1)^2}{b^2}$$

viscosity gradients are similarly expressed

$$\frac{\partial \eta}{\partial x}_{i,j} = \left[\eta_{i+1,j} - \eta_{i-1,j} \right] \frac{(m-1)}{2\pi D}$$

$$\frac{\partial \eta}{\partial z}_{i,j} = \left[\eta_{i,j+1} - \eta_{i,j-1} \right] \frac{(n-1)}{2b}$$

For convenience put

$$B6 = \frac{m-1}{2\pi D}$$

$$B7 = \frac{(m-1)^2}{\pi^2 D^2}$$

$$B8 = \frac{(n-1)}{2b}$$

$$B9 = \frac{(n-1)^2}{b^2}$$

B6 to B9 are constant for all i, j . B2, B3, and B4 are functions of (i, j) . B1 and B5 are functions of x only.

It is convenient to write:

$$(B6 \cdot B3_{i,j}) + (B7 \cdot h_i^{-q}) = A1$$

$$(B7 \cdot h_i^{-q}) - (B6 \cdot B3_{i,j}) = A2$$

$$(B8 \cdot B4_{i,j}) - (B9 \cdot h_i^{-q}) = A3$$

$$(B8 \cdot B4_{i,j}) + (B9 \cdot h_i^{-q}) = A4$$

Hence equation 10 becomes:

$$\phi_{i,j} = \frac{\eta_{i,j} B5_i - \phi_{i+1,j} \cdot A1 - \phi_{i-1,j} \cdot A2 + \phi_{i,j+1} \cdot A3 - \phi_{i,j-1} \cdot A4}{B2_{i,j} - 2 \cdot h_i^{-q} (B7 + B8)} \quad - - - 11$$

Equation 11 was solved by the Gauss-Seidel iterative technique in which each calculation uses updated values.

Thus for the k th iteration, at i, j

$$\phi_{i,j}^k = \phi_{i,j}^{k-1} + \text{ORF} (\phi_{i,j}^{k*} - \phi_{i,j}^{k-1})$$

Where ORF = over relaxation factor

$\phi_{i,j}^{k*}$ is the value given by equation 11

A value of ORF was chosen which, according to Lloyd and McCallion (43), gave the quickest convergence for the selected mesh size.

Convergence was satisfied when, for all grid points, results from the k th iteration were such that

$$\left| \phi_{i,j}^k - \phi_{i,j}^{k-1} \right| \leq 0.001 \left| \phi_{i,j}^k \right|$$

Heppenstall (53) shows that various different boundary conditions had little influence on the predicted bearing behaviour. Consequently, the simplest boundary conditions and those most likely to accord with reality were chosen for this work.

Axial boundary condition: $p = PS$ at $z = 0$ for all x
 $p = 0$ at $z = b$ for all x

Support for these conditions was given by the oil inlet hole area being much larger than the outlet, and the bearing edges open to atmospheric pressure.

Circumferential boundary conditions:

$$p = PC$$

$$\frac{\partial p}{\partial x} = 0$$

This condition was achieved by converting any value calculated at less than PC, to PC, as it arose.

Many workers put $PC = 0$. In this work PC was allowed to take zero or any negative value (i.e. $PC \neq 0$).

Solutions were obtained for $\theta = 0$ and $\theta = 2\pi$. Their equality provided a useful check.

The above procedure calculates a pressure field for a given viscosity map. Since viscosity is allowed to vary with pressure, in addition to temperature, the following procedure was adopted.

1. Assume an initial pressure field
2. A temperature profile was assumed. Section 4.6. details how this was related to the desired load-speed combination.
3. A viscosity field was calculated using the temperature profile in 2 and the initial pressure map.
4. A pressure field was calculated using equation 11 and the viscosity map in 3 above.
5. Viscosity field was updated using pressures calculated in 4 and an established relationship between viscosity and pressure.
6. A pressure field was calculated using the viscosity field in 5.
7. Items 5 and 6 were repeated until the viscosity converged over the entire field.

$$\text{i.e. for } k\text{th iteration } \left| \eta_{i,j}^k - \eta_{i,j}^{k-1} \right| < 0.01 \left| \eta_{i,j}^k \right|$$

for all i,j

Figure 37, flow chart describes this procedure.

Criteria for convergence were 0.001 and 0.01 for pressure and viscosity respectively. Provision was made for a viscosity relaxation factor.

Viscosity at any point (i,j) was calculated in the following manner. Let (1) denote the inlet condition and (2) that at any point (i,j) . All calculations used measured inlet temperatures, T_1 . Corresponding kinematic viscosity ν_1 was obtained from the measured lubricant data.

Temperature was allowed to vary around, but not across, the bearing (see 4.6). Thus T_2 varied with i only and was computed from T_1 and the specified temperature profile. Section 4.6 also describes how a temperature profile was defined and selected. Temperature profiles were assumed to be independent of journal centre velocity and displacement.

Define a viscosity factor due to temperature FT_i such that

$$FT_i = \frac{\eta_{2,i}}{\eta_1} = \left(\frac{\nu_{2,i}}{\nu_1} \frac{\rho_{2,i}}{\rho_1} \right)$$

The relationship $\log_{10} \{ \log_{10} (\nu + a_1) \} = a_2 + a_3 \log_{10} T$

was verified experimentally, for the lubricant used throughout testing, where T = Temperature (Rankine). This experiment gave $a_1 = 0.8$ and $a_3 = 3.5$.

Hence for states (1) and (2)

$$v_{2,i} = -a_1 + \text{antilog} \left[\left(\frac{T_{2,i}}{T_1} \right)^{a_3} \log_{10} (v_1 + a_1) \right]$$

for a given mass

$$\frac{\rho_{2,i}}{\rho_1} = \frac{1}{1 + \alpha (T_{2,i} - T_1)}$$

where α = coefficient of thermal expansion

$$\text{Hence } FT_i = \frac{v_{2,i}}{v_1 [1 + \alpha (T_{2,i} - T_1)]}$$

Cameron (52) states that the variation of viscosity with pressure is given by

$$\eta_p = \eta_{p=\text{atmos}} \left[1 + \beta p \right]^{16}$$

A value of β for a lubricant having the same viscosity variation with temperature was selected to represent the test lubricant.

Hence viscosity at any point (i,j) is given by:

$$\eta_{i,j} = \eta_1 \cdot FT_i \cdot (1 + \beta p_{i,j})^{16}$$

Putting $\beta = 0$ suppresses viscosity variation with pressure. This was facilitated by making β an input variable.

4.2 Journal Centre Location

Solution of Reynolds equation yields values of pressure at each grid point. Summation of these pressures gives the forces exerted by the oil film on the journal.

Oil film forces, perpendicular and parallel to the line joining the journal and bearing centres are given by:

$$F_{\perp} = \frac{b \cdot \pi \cdot D}{9.0 (n-1) (m-1)} \sum_{i=1}^{i=m} \sum_{j=1}^{j=n} p_{i,j} \cdot NS_{i,j} \sin \theta$$

$$F_{\parallel} = \frac{b \cdot \pi \cdot D}{9.0 (n-1) (m-1)} \sum_{i=1}^{i=m} \sum_{j=1}^{j=n} p_{i,j} \cdot NS_{i,j} \cos \theta$$

Where $NS_{i,j}$ is the appropriate factor in the Simpson's Rule table given in Figure 40. The above equations apply to all calculations of pressure fields.

Velocity $v = 0$ for calculation of steady journal centre.

The other external force on the journal is W_y acting vertically downwards. At the equilibrium position $W_x = 0$,

Resolving horizontally and vertically gives:

$$\tan \phi = \frac{-F_i}{F_{//}}$$

$$-W_y = 2 (F \sin \phi - F \cos \phi)$$

A Fortran program was written to calculate the pressure and viscosity fields as described in Section 4.1 and then evaluate ϕ and W_y as above.

Input data were:

$m, n, itmax, v, \epsilon, C_r, D, PS, q, N, T_1, SR, C_1, C_2, \nu, \alpha, b.$

$CF = 0.001, ORF = 1.5, \eta_1, \beta, CF2 = 0.01, VRF = 1.0, PC.$

Smalley, Lloyd, Horsnell and McCallion (42) studied the effect of mesh size on accuracy of load calculation and suggest 8 points across the bearing is adequate. An uneven number is required to accommodate the Simpson Rule Table, so $n = 9$ was selected. These authors also show that circumferential mesh size depends on eccentricity ratio to achieve a given accuracy. For an average eccentricity used in this work (say 0.8) they suggest $n = 48$ for a 1% error in load. At the greatest $\epsilon/C_r = 0.92$, load and attitude angle computed using $m = 49$ and 97 differed by 2.5 and 2% respectively. To simplify and compromise between accuracy and computing cost and time, $m = 49$ was used throughout.

4.3 Velocity and Displacement Coefficients

Firstly, steady load W_y and attitude angle ϕ are calculated as in 4.2 with velocity $v = 0$. Then velocity v and angle ψ successively take a series of pre-set values and a new solution of Reynolds equation and resultant external forces W'_x, W'_y obtained for each set, at the same journal location.

Four values of ψ are selected in turn, each giving a velocity in either vertical, horizontal, positive or negative directions. Each set yields two velocity coefficients. Equation A1-4 and A1-5 from Appendix A with $x = y = 0$ become:

$$\psi = \frac{+\pi}{2}, \quad \dot{x} = v \\ \dot{y} = 0$$

$$W'_x - W_x = b_{xx} \dot{x}$$

$$W'_y - W_y = b_{yx} \dot{x}$$

$$\psi = \pi, \dot{y} = v, \dot{x} = 0$$

$$W'_x - W_x = b_{xy} \dot{y}$$

$$W'_y - W_y = b_{yy} \dot{y}$$

$$\psi = \frac{3\pi}{2}, \dot{x} = -v, \dot{y} = 0$$

$$W'_x - W_x = b_{xx} \dot{x}$$

$$W'_y - W_y = b_{yx} \dot{x}$$

$$\psi = 0, \dot{y} = -v, \dot{x} = 0$$

$$W'_x - W_x = b_{xy} \dot{y}$$

$$W'_y - W_y = b_{yy} \dot{y}$$

To compute the displacement coefficients, velocity $v = 0$, and external forces are considered which displace the journal successively in the horizontal and vertical directions. At each new location, eccentricity, attitude angle, film thickness, and its derivatives are revised.

Using the nomenclature of Figure 39 it follows:

$$\gamma_x = \Delta x / \epsilon \quad \gamma_y = \Delta y / \epsilon \quad \epsilon', \phi', \text{ is the new location}$$

$$(a) \quad \begin{array}{l} \text{for } \Delta x + ve \\ \Delta y = 0 \end{array} \quad \tan \Delta \phi = \frac{\gamma_x \cos \phi}{1 + \gamma_x \sin \phi}, \quad \phi' = \phi + \Delta \phi$$

$$\epsilon' = \epsilon [\cos \Delta \phi + \gamma_x \sin \phi']$$

$$(b) \quad \begin{array}{l} \text{for } \Delta y + ve \\ \Delta x = 0 \end{array} \quad \tan \Delta \phi = \frac{\gamma_y \sin \phi}{1 - \gamma_y \cos \phi}, \quad \phi' = \phi + \Delta \phi$$

$$\epsilon' = \epsilon \frac{(1 - \gamma_y \cos \phi)}{\cos \Delta \phi}$$

Similar expressions apply for negative displacements. Reynolds equation was solved and external forces W'_x, W'_y computed at each new location.

Thus

$$\text{for (a)} \quad \frac{W'_x - W_x}{\gamma_x \epsilon} = a_{xx} \quad \frac{W'_y - W_y}{\gamma_x \epsilon} = a_{yx}$$

$$\text{and (b)} \quad \frac{W'_x - W_x}{\gamma_y \epsilon} = a_{xy} \quad \frac{W'_y - W_y}{\gamma_y \epsilon} = a_{yy}$$

Figure 38, a simplified flow diagram, illustrates this procedure.

A Fortran program was written to execute this entire sequence including positive and negative velocities and displacements.

4.4 Program Verification

It is vitally important that computer programs execute the intended processes. Hence the program output was subject to a series of checks. Several programs were written and in each case output from a new program was compared to that of one previously verified. This section gives brief details of comparisons of program output with hand calculation and published data.

(a) Check by hand calculation

- (1) all B1 to 9
- (2) $\Phi_{14,5}$ after 1 iteration
- (3) $\Phi_{14,5}$ after 24 iterations
- (4) $\Phi_{2,5}$ after 1 iteration
- (5) all values of h_i , $\partial h_i / \partial x$, $\partial^2 h_i / \partial x^2$

(b) Peak pressures were compared to those published by Raimondi and Boyd (34).

ϵ / C_r	P_{\max} lbf/inch ²		% difference
	R and B	DWPA	
0.6	157.4	156.4	0.63
0.8	897.9	865.9	3.5
0.9	4245.9	4162.0	1.97

(c) Intermediate pressures were compared to those given by Short Bearing Theory, for cases where the boundary pressures were almost identical. Pressures for similar relative locations were compared thus:

ϵ / C_r	p lbf/inch ²	
	S· π	DWPA
0.8	65.85	65.38
0.9	75.6	75.2

(d) Values of specific load were compared to those given by Raimondi and Boyd for comparable conditions

ϵ/c_r	$W_{y/bD}$ lbf/inch ²		% difference
	R and B	DWPA	
0.6	52.57	52.44	- 0.25
0.8	215.5	214.13	- 0.63
0.9	764.26	769.4	+ 0.66

Similarity of axial boundary pressures between Raimondi and Boyd and DWPA were achieved by taking the results from the latter for one bearing land with zero supply pressure. Circumferential boundary conditions were almost identical in both works.

(e) Velocity based pressure component was verified by comparing the pressure profiles obtained in two cases:

- (1) $v = 0$, eccentricity ϵ , journal rotation ω stationary journal centre
- (2) journal centre rotating around a circular orbit radius ϵ , $v = \epsilon\omega$, ψ perpendicular to ϵ .

Each case produced an identical set of pressure values with appropriately different orientation.

4.5 Short Bearing Theory

Short Bearing Theory was introduced by Dubois and Ocvirk in a series of papers dating from 1954. Its essential feature requires that the bearing axial length (b) is sufficiently small that it is reasonable to neglect circumferential variation. If, additionally, viscosity is considered constant, Reynolds equation (see section 4.1 equation 7) becomes:

$$\frac{\partial}{\partial z} \left[h^3 \frac{\partial p}{\partial z} \right] = 6\eta u_o \frac{\partial h}{\partial x} + 12\eta \frac{\partial h}{\partial t} \quad \text{-----} \quad 15$$

which may be integrated

4.5.1 Solution of Reynolds Equation and Journal Centre Location

Since the journal and bearing longitudinal axes are considered parallel at all times,

$$\frac{\partial h}{\partial t}, \frac{\partial h}{\partial x} \text{ are functions of } x \text{ only}$$

Axial boundary conditions only, are required thus

$$\left. \begin{array}{l} z = 0 \quad p = PS \\ z = b \quad p = 0 \end{array} \right\} \text{ for all } x$$

Integration of equation 15 and insertion of boundary conditions yields:

$$p = \left(z^2 - bz + ab \right) 3\eta u_o \frac{\partial h}{\partial x} + \frac{PS(b-z)}{b} + \left(z^2 - bz + ab \right) \frac{6\eta}{h^3} \frac{\partial h}{\partial t} \quad \text{---16}$$

Assume that only the oil film due to hydrodynamic action in the range $0 \leq \theta \leq \pi$ supports the external load.

If W_y is the external force acting vertically downwards on the journal, and the bearing comprises two lands of axial length b , then resolving forces perpendicular and parallel to the line of centres (see Figure 36) gives:

$$\frac{W_y}{2} \sin \phi - \int_0^\pi \int_0^b \text{p.r.} \sin \theta \, dz \, d\theta = 0 \quad \text{--- 17}$$

$$\frac{W_y}{2} \cos \phi + \int_0^\pi \int_0^b \text{p.r.} \cos \theta \, dz \, d\theta = 0 \quad \text{--- 18}$$

the term $\frac{PS(b-z)}{b}$ is constant for all $0 < \theta < 2\pi$ and therefore makes no contribution to the support of the external load. Accordingly it was omitted in the integration of equations 17 and 18.

$$\text{put } \epsilon/C_r = n, \quad x = r\theta$$

$$\text{Equation 6 gives } h = C_r (1 + n \cos \theta)$$

$$\frac{\partial h}{\partial x} = - \frac{C_r n \sin \theta}{r}$$

$$\text{From section 4.1 } \frac{\partial h}{\partial t} = + v \cos (\theta + \phi - \psi)$$

Given the following integrals:

$$\int_0^\pi \cos \theta \, d\theta = 0$$

$$\int_0^\pi \frac{\sin \theta \cos \theta \, d\theta}{(1 + n \cos \theta)^3} = \frac{-2n}{(1 - n^2)^2}$$

$$\int_0^{\pi} \sin \theta \, d\theta = +2$$

$$\int_0^{\pi} \frac{\sin^2 \theta}{(1 + n \cos \theta)^3} \, d\theta = \frac{\pi}{2(1-n^2)^{3/2}}$$

$$\int_0^{\pi} \frac{\cos \theta \cos (\theta + \phi - \psi)}{(1 + n \cos \theta)^3} \, d\theta = \frac{\pi \cdot \cos (\phi - \psi) + 2n(1-n^2)^{1/2} \sin(\phi-\psi)}{2(1-n^2)^{5/2}}$$

Equations 17 and 18 become:

$$\frac{W_y}{2} \sin \phi = \frac{\eta u_o n b^3 \pi}{4 C_r^2 (1-n^2)^{3/2}} + \frac{b^3 \eta r v}{C_r^3} \left[\frac{2 n \cos (\phi - \psi)}{(1 - n^2)^2} - \frac{\pi \sin (\phi - \psi)}{2(1 - n^2)^{3/2}} \right] \text{----- 19}$$

$$\frac{W_y}{2} \cos \phi = \frac{\eta u_o n^2 b^3}{C_r^2 (1 - n^2)^2} + \frac{b^3 \eta r v}{2 C_r^3 (1 - n^2)^{5/2}} \left[\pi \cos (\phi - \psi) + 2n (1 - n^2)^{1/2} \sin (\phi - \psi) \right] \text{----- 20}$$

To establish the steady journal centre location, put $v = 0$ then equations 19, 20 yield:

$$\tan \phi = \frac{\pi (1 - n^2)^{1/2}}{4n} \text{----- 21}$$

$$W_y = \frac{\eta u_o b^3}{C_r^2} \cdot \frac{n [16n^2 + \pi^2 (1 - n^2)]^{1/2}}{2(1 - n^2)^2} \text{----- 22}$$

Putting $P^* = \frac{W_y}{2bD}$, $u_o = \pi DN'$, $r = \frac{D}{2}$ gives:

$$\frac{P^*}{\eta N'} \left(\frac{C_r}{r} \right)^2 \left(\frac{D}{2b} \right)^2 = \frac{\pi n [16 n^2 + (1-n^2)]^{1/2}}{4 (1 - n^2)^2} \text{----- 23}$$

Equations 21 and 22 were used to compute ϕ , and W_y . Equation 23 gives the relationship between a non-dimensional load number and eccentricity ratio.

4.5.2 Displacement and Velocity Coefficients

Displacement coefficients were calculated by setting $v = 0$, equations 19, 20 and allowing the journal to be successively displaced either horizontally or vertically to some new equilibrium position, n' .

Equation 22 gave a load W_y^* acting in some non-vertical direction for the eccentricity ratio n' . Knowing the geometry, W_y^* was resolved into horizontal and vertical components, thereby allowing displacement coefficients to be obtained by the method and equations of Section 4.3

To compute velocity coefficients, the journal remains at its equilibrium position and loads are computed with zero and finite velocity v in equations 19, and 20. With finite velocity a non-vertical resultant force W_y^{**} is given by

$$W_y^{**} = \left[W_y^2 \cos^2 \phi + W_y^2 \sin^2 \phi \right]^{\frac{1}{2}} \quad ?$$

This force is resolved into its horizontal and vertical components. Thence, angle ψ is given a series of values and velocity coefficients are computed by the procedure described in section 4.3.

4.6 Temperature Profile

Table 6 gives results of a study of published experimental measurements of oil film temperature profiles. If the journal peripheral velocity is less than 417 inch/sec., all workers agree that the circumferential temperature distribution is of the form:

*السرعة المحورية
تأثيرها*

$$T_{\theta} = A \left(1 + \sin \frac{\theta}{2} \right)^B$$

where A, and B are constant for a particular case. All workers indicate negligible variation of temperature in the axial direction.

Journal surface peripheral velocity did not exceed 380 inch/sec in any of the cases reported in this Thesis. Hence, for this theoretical study it was assumed that:

$$(1) \quad T_i = T_1 (SR)^{C1} \left[1 + \sin \frac{\pi (i-1)}{(m-1)} \right]^{C2}$$

$$\text{where } \theta = \frac{2 \pi (i-1)}{m-1}$$

(2) Temperature was independent of axial length z .

Constant C2 controls the temperature profile curvature and $(SR)^{C1}$ the absolute level. For convenience, constant C1 = 1.0 was used throughout.

Hence, it became necessary to establish appropriate values of C2, SR for all N, W_y , PS combinations. It was considered that SR, C2 would be related to the difference between inlet and outlet oil temperatures.

Examination of the experimental values of $\Delta T = T_{out} - T_{in}$ showed significant relationships with N, Wy, PS superimposed upon a small variation between repeated tests. Assuming linear relationships, presented considerable simplification without undue inaccuracy. *مفروضه*

Variation of ΔT with PS, Wy and N was found to be:

N	$\frac{\partial(\Delta T)}{\partial(\text{PS})} \text{ N, Wy}$ C ^o /lbf/inch ²	PS	$\frac{\partial(\Delta T)}{\partial \text{N}} \text{ PS, Wy}$ C ^o /RPM
1180	- 0.084		
1500	- 0.098	7.5	+ 0.005
2200	- 0.142	15.0	+ 0.0036
2900	- 0.125	30.0	+ 0.0035

$$\frac{\partial(\Delta T)}{\partial \text{Wy}} = 2.9 \cdot 10^{-3} \text{ C}^{\circ} / \text{lbf}$$

Using

$$d(\Delta T) = \frac{\partial(\Delta T)}{\partial \text{N}} \text{ PS, Wy} \cdot d\text{N} + \frac{\partial(\Delta T)}{\partial(\text{PS})} \text{ N, Wy} \cdot d(\text{PS}) + \frac{\partial(\Delta T)}{\partial \text{Wy}} \cdot d\text{Wy}$$

with the value $\Delta T = 7.5$ at PS = 30.0 lbf/inch²

$$\text{N} = 2200 \text{ RPM}$$

$$\text{Wy} = 700 \text{ lbf}$$

gave values of ΔT as shown in Table 7.

A combination of N = 2200 rpm, Wy = 700 lbf, and PS = 30 lbf/in² was nearest the corresponding values of published data, which gave mean values of C2 = 0.371 and SR = 1.37. To calculate SR, C2 at any other N, Wy, PS combination, the following arbitrary rule was assumed:

- Rule 1
- (a) C2 \propto N only, independent of PS, Wy
 - (b) SR is independent of N.
 - (c) SR varies with Wy and PS in proportion to ΔT at N = 2200 rpm

Table 7 also shows values of SR, C2

Chapter 5 shows that clearance C_r obtained from experimental data was

insufficiently precise for use as input for predictions of load W_y . Therefore SR, C2 were set to the values given in Table 7, and C_r adjusted until the predicted W_y equalled the experiment value. Then PC was altered until the predicted attitude angle equalled the observed value. Thus the observed W_y and ϕ were simultaneously predicted.

Chapter 5 gives full details of how SR, C2 largely influence W_y , and PC affects attitude angle ϕ only. Only $PC \leq 0$ was allowed. It was found that in only two cases were $W_y \sim \phi$ not predicted using Rule 1, because positive PC was required. Hence Rule 2 was devised, and used to predict these two cases in a similar manner.

Rule 2 (a) At PS = 30, adjust C2 and SR so that:

(i) $W_y \sim \phi$ are correctly predicted with PC approaching zero.

(ii) SR not greater than that for adjacent conditions with larger ΔT .

(b) At PS = 15,

(i) Use C2 given by (a) (i) above

(ii) Adjust SR such that, if at PS = 30 $SR = 1 + X$,

$$\text{at PS} = 15, SR = 1 + \left(\frac{\Delta T_{PS=15}}{\Delta T_{PS=30}} \right) X$$

Table 8 gives values of C2 and SR

This rule was also applied to some cases in which Rule 1 was effective. Chapter 5 discusses the results.

Setting C2 = 0 suppressed the circumferential temperature variation to a constant value of T_1 (SR).

Suppressing both temperature and pressure variation gave a uniform viscosity field equal to η_1 .

Load \sim attitude angle predictions using uniform viscosity took C_r from the corresponding variable viscosity case and adjusted η_1 and PC until the observed W_y and ϕ were predicted. These values of η_1 and PC were used in any subsequent coefficient calculations using constant viscosity.

The above methods utilise published experimental data for the axial and circumferential temperature profiles, with constants for one test condition, and measured values of ΔT . Only the relationship between ΔT , W_y , N, PS and the profile constants was assumed. Two widely differing options have been considered.

5 RESULTS

Theoretical and experimental results are discussed together under the separate headings of static (5.1) and dynamic characteristics (5.2).

5.1 Static Characteristics

Fig 46 shows radial clearance derived by both the experimental method described in 3.4.1 (iii) and the iterative theoretical procedure utilising measured eccentricity and inlet temperature (given in 4.6).

Fig 43, for a lower ϵ/Cr , shows that a change of $10.0 \cdot 10^{-6}$ inch (0.57%) in radial clearance predicts a change of 10 lbf (6.6%) in vertical load. For the larger eccentricity, Fig 44 gives corresponding figures of a change of $4.0 \cdot 10^{-6}$ inch (0.22%) in radial clearance producing a 27 lbf (5.4%) change. In each case the load change is within the range easily measured experimentally, but the corresponding clearance change is very much less than that to which any measurement technique could discriminate. Indeed, the dimensions are so small that the most precise optical techniques would be required, which are completely impractical for the hot rotating journal bearing environment. Moreover, even if some completely new measurement technique became available, a dimension of less than $4.0 \cdot 10^{-6}$ inch is such as to question the concept of a single number to represent the difference between the bearing and journal radius. The dimension is significantly less than the shaft and bearing non-circularity and error in surface finish. Surface distortion due to thermal and pressure gradients become significant when considering small dimensions. An examination of the vertical scale and results on Fig 46 reveals how high this necessary precision is in terms of the accuracy obtained by the extensive experimental procedure used in this work.

Therefore, there appears little prospect of verifying the theoretical model by inserting experimental clearance values and a successful comparison of observed and predicted external vertical load. A more promising approach to model verification would be to compare observed and calculated temperature and pressure profiles. Nonetheless, these measurements present considerable experimental difficulties if they are to be effected without disturbing the oil film.

Due to this extreme sensitivity to load, the completely different temperature profiles specified by Rules 1 and 2 did not require very different clearance values (7.0%, 5.4% and 4.3% for $N = 1180, 1500$ and 2200 rpm, $PS = 15$ lbf/in², $Wy = 150$ lbf). Examination of the pressure profiles obtained with the various clearance values showed negligible circumferential movement of the cavitation zone, but significant change in absolute pressure. Temperature profiles were obtained by utilising published experimental data with the single assumption of the relationship between ΔT , Wy , N , PS and the profile constants.

Figs 43 and 44 show that radial clearance strongly influences the predicted load W_y , but has little effect on attitude angle ϕ .

Conversely, cavitation zone pressure PC has a marked effect on attitude angle with negligible influence on load. Hence, for a given temperature profile, prediction of the experimental combination of $W_y \sim \phi$ requires unique values of C_r and PC.

Table 9 shows that because the conventional PC = 0 setting gave (with 2 exceptions only) smaller ϕ than that observed, a negative value of PC was necessary to predict the experimental result. All experimental combinations of $W_y \sim \phi$ were simultaneously predicted to within 1% of both quantities. Table 9 shows that some PC values are considerably less than atmospheric pressure, thereby specifying a fluid 'tensile stress'. Various papers at the Leeds Symposium (Refs 45-48) indicate that this is a reasonable concept. Very recently, Dyer and Reason (30) reported experimental measurements of oil film tensile stresses of 100 lbf/in² which are considerably larger than any found necessary in this work. Hence PC values giving fluid tensions as shown in Table 9 are perfectly feasible. Figs 43 and 44 show that the sensitivity to cavitation zone pressure is 2.38 and 10.4 lbf/deg for lower and high eccentricity ratios respectively. Accepting that experimental attitude angle may be up to 1° in error, it follows that a possible error in PC is of the order of 10 lbf. Nonetheless, simultaneous prediction of $W_y \sim \phi$ gives results which further demonstrate the presence of fluid tensile stresses.

Additional data points on Figs 43 and 44 show the consequence of excluding the effect of pressure on viscosity. Suppression of this effect produces changes in vertical load of 2 lbf (1.33%) and 40 lbf (8%) at 0.789 and 0.917 eccentricity ratio values respectively. In each case the load change is experimentally measurable, and significant. A greater effect is noted at the larger eccentricity ratios because oil film pressures are higher in that case. It follows that for static load calculation at eccentricity ratios less than say 0.7, little error would be introduced by neglecting the effect of pressure in viscosity.

Figs 43 and 44 also show data for various C_r and PC using a uniform viscosity, which was chosen to predict the experimental $W_y \sim \phi$ combination with the C_r specified by the fully variable viscosity case. Uniform and variable viscosity data display similar effects due to C_r and PC. Separate data points indicate that a change in the uniform viscosity of $0.1 \cdot 10^{-6}$ lbf.sec/in² (3.0% and 6.9%) at low and high eccentricity ratio produces load changes, W_y of 5.5 lbf and 32 lbf (3.7% and 6.4% respectively). Percentage figures indicate the system linearity in the static case when viscosity is deemed uniform (if viscosity were allowed to vary with temperature the system would remain linear in the static case, but become non-linear if the pressure effect on viscosity is included).

The effect of a change in temperature profile, due to SR, C2, or both produces the same results as a viscosity change, and is not illustrated.

Fig 41 compares the measured static loci and that given by the Short Bearing Approximation which is independent of viscosity. At a given attitude angle the experimental points appear at a greater eccentricity. Similar trends have been published by both Morton (8) and Mitchell *et al* (16). Fig 41 shows that larger changes in eccentricity ratio can only be simply effected by a change in vertical load.

Each experimental data point in Fig 41 was obtained from a separate warm-up setting by the procedure described in Chapter 3. It was found that a completely different (and incorrect) journal centre locus was obtained if the vertical load W_y was varied without a separate determination of the bearing centre at each load setting. This implied that the bearing centre, relative to the electrical centre, varied with vertical load and it was therefore necessary to adjust the experimental procedure to recognise the fact.

Vertical load ranged from 150 to 700 lbf giving corresponding eccentricity ratios from 0.78 to 0.94. Table 11 lists all conditions investigated. Limitations were imposed by the risks of instability and bearing damage. Values of oil supply pressure ratio

$$\frac{W_y}{2bD.PS}$$

were restricted to within the likely practical range of 2 to 10.

Fig 42 lower part, shows experimental values of:

$$\text{Load No} = \frac{P^*}{\bar{\eta}N'} \left(\frac{C_r}{r} \right)^2 \left(\frac{D}{2b} \right)^2$$

plotted against measured eccentricity ratio.

Necessarily, these data points are available for cases for which the uniform viscosity was obtained. Although these cases number less than the total, they were arranged to cover the full range of eccentricity ratio.

For a given eccentricity ratio the experimental points exhibit a lower Load No than the Short Bearing Approximation. Middleton *et al.* (22) published a similar finding. It was found that the empirical relationship

$$\left(\frac{\pi n (16n^2 + \pi^2 (1-n^2))^{\frac{1}{2}}}{4(1-n^2)^2} \right)^{0.96} = \frac{P^*}{\bar{\eta}N'} \left(\frac{C_r}{r} \right)^2 \left(\frac{D}{2b} \right)^2 \quad \text{--- (30)}$$

$$\text{where } n = \epsilon/C_r$$

described all experimental points.

Fig 42 upper part shows that the experimental attitude angle, is reasonably described over the range $0.78 < \epsilon/C_r < 0.94$ by:

$$\tan \phi = \frac{\pi(1-n^2)^{\frac{1}{2}}(2-n^2)}{4n} \quad \text{where } n = \epsilon/C_r \quad \text{--- (31)}$$

At a given eccentricity ratio the Short Bearing Approximation slightly under estimates the attitude angle. Factor σ defines, in terms of the temperature profile control, the temperature at which the test lubricant takes the uniform viscosity $\bar{\eta}$. Fig 45 shows viscosity factor σ for the range of vertical loads and rotational speeds. An error of less than 9% is introduced by treating σ as a function of speed only as shown by the accompanying curve.

These empirical relationships suggest a simple design procedure.

1. Select r , C_r , b , lubricant properties, N , W_y , PS , T_1
2. Obtain SR and $C2$ from table 7 - or by interpolation if necessary
3. Obtain σ from Fig 45, and hence $\bar{\eta}$ from lubricant properties
4. Compute load No = $\frac{P^*}{\bar{\eta}N} \left(\frac{C_r}{r}\right)^2 \left(\frac{D}{2b}\right)^2$
5. Obtain $n = \epsilon/C_r$ and ϕ from equation (30) and (31).
6. Check that $h_{\min} = C_r (1 - \epsilon/C_r)$ is satisfactory

Bearings designed within the given range of parameters according to this procedure, have been shown experimentally to operate at satisfactory temperatures.

5.2 Dynamic Characteristics

Figures 47 to 55 show displacement coefficients and their variation with distance moved from the equilibrium position in both normal and non-dimensioned form for all tests at $W_y = 150$ lbf. Each graph shows calculated data given by the fully variable ($\eta = \eta(T, p)$) theory with corresponding experimental data obtained by both the incremental and dynamic loading. Experimental results given by dynamic loading show more scatter but cover a wider range of displacement, than those from the incremental method. No significant difference appears between coefficients obtained by the two methods. Data given by the Short Bearing Approximation (Fig 49) shows similar trends to that of the full theory. For this Approximation, with uniform viscosity, Reynolds Equation becomes linear, but external forces are non-linear functions of eccentricity thereby giving the indicated variation. Figures 72 and 74 show theoretical non-dimensioned displacement coefficients for various rotational speeds at $W_y = 300$ and 500 lbf complete with experimental data from incremental loading tests. Theoretical data obtained with the fully variable theory ($\eta = \eta(T, p)$) are given for all speeds and show consistent behaviour. The effect of viscosity variation with pressure is shown by comparing the fully variable theory at $N = 2200$ rpm with that given by $\eta = \eta(T)$ only and uniform viscosity. Viscosity variation with pressure alters the absolute value of the coefficient but not its variation with displacement. Its effect on coefficients is less significant than that on the static locus. Figures 72 and 74 show that coefficients exhibited very small variation with speed at a given load and higher, almost uniform, eccentricity ratio. Theoretical data given by the Short Bearing Approximation on Figure 74 for $W_y = 700$ lbf show similar behaviour to the full theory except for A_{xy} at large negative displacements. Particularly good agreement between measured and calculated coefficients is shown on Figure 74 by A_{xx} , A_{yx} and A_{xy} at negative

displacements. At the lower load, $W_y = 300$ lbf, Figure 72, shows good agreement for A_{xx} and A_{yy} at negative, and for A_{xy} at both, signs of displacement.

In all cases, theoretical coefficients A_{xx} , A_{xy} increase, and A_{yy} , A_{yx} decrease, with x/C_r , y/C_r .

Theoretical coefficients A_{yy} and A_{xy} exhibit a discontinuity at $y = 0$. Comparison of results on figures 72 and 74 show that significant variation with eccentricity ratio is exhibited by only A_{yy} at positive y and A_{xx} at larger positive x . Experimental data on figures 72 and 74 show negligible variation with rotational speed.

A simple and convenient method of specifying coefficients and their variation is to assume a linear gradient α thus:

$$\begin{aligned} a_{xx} &= a_{xxo} + \alpha_{xx} x & a_{yy} &= a_{yyo} + \alpha_{yy} y \\ a_{yx} &= a_{yxo} + \alpha_{yx} x & a_{xy} &= a_{xyo} + \alpha_{xy} y \end{aligned}$$

where a_{xxo} etc. is the intercept with the zero displacement axis and will be called the "zero" displacement coefficient.

In non-dimensioned form these become:

$$\begin{aligned} A_{xx} &= A_{xxo} + \alpha_{xx}^* (x/C_r) & A_{yy} &= A_{yyo} + \alpha_{yy}^* (y/C_r) \\ A_{yx} &= A_{yxo} + \alpha_{yx}^* (x/C_r) & A_{xy} &= A_{xyo} + \alpha_{xy}^* (y/C_r) \end{aligned}$$

$$\text{where } A_{xxo} = a_{xxo} \frac{2C_r}{W_y}, \quad \alpha_{xx}^* = \alpha_{xx} \frac{2C_r^2}{W_y} \quad \text{etc.}$$

Agreement between theoretical and experimental results will be examined for both "zero" coefficient and gradient. For $W_y = 150$ lbf, Figure 67 shows reasonable agreement between measured and calculated "zero" coefficients. Since they exhibited less scatter, experimental values are deduced from those given by incremental loading. For higher W_y and ϵ/C_r , Figure 71 (lower part) shows that all measured "zero" coefficients were accurately predicted, except for very high ($\approx 4.0 \cdot 10^{+6}$ lbf/inch) values of a_{yyo} .

A linear gradient corresponding to the theoretical curve was obtained by taking a straight line between the values at

$$\frac{x}{C_r}, \frac{y}{C_r} = \pm 0.05 \text{ for } W_y = 150 \text{ lbf}$$

$$\text{and } \frac{x}{C_r}, \frac{y}{C_r} = \pm 0.03 \text{ for all larger } W_y$$

Relative displacements in each case being reasonably typical of those used in experiments. Figure 68 shows that for $W_y = 150$ lbf, gradients α are not well predicted. However, notable exceptions are some values of α_{yy} for which the basic data are given in

Figures 47, 49, 50 and 51. Figure 71 (upper part) compares calculated and measured gradients for $W_y = 300$ and 500 lbf, and shows a similar lack of agreement. It is interesting that experimental gradient α_{yy} appears to change sign with eccentricity ratio having negative, near zero and positive values at $W_y = 150, 300$ and 500 lbf respectively. Furthermore, this observed change of sign for α_{yy} was predicted. Figure 72 illustrates the good agreement between measured and calculated α_{xy} although both halves of the curve have a positive gradient. However, negative theoretical α_{xy} emerges because the corresponding linear gradient is evaluated at $y/C_r = \pm 0.03$. The effect of the discontinuity in theoretical α_{yy} on the corresponding linear gradient, is shown by the fact that α is positive if assessed between $-0.035 < y/C_r < +0.035$, and becomes negative if evaluated over greater y/C_r .

Figures 56 to 64 show velocity coefficients as functions of respective velocity in conventional and non-dimensioned form obtained with $W_y = 150$ lbf. Fully variable theory ($\eta = \eta(T, p)$) was used in all cases. Figure 58 additionally illustrates data given by the Short Bearing Approximation using uniform viscosity. Since both forces required to establish a velocity coefficient are computed at the same eccentricity, and for uniform viscosity Reynolds Equation is linear, then this Approximation yields velocity coefficients invariant with journal centre velocity. Hence horizontal lines are drawn on Figure 58. Nonetheless, several values were calculated to provide a valuable check. Experimental results are given for $\Omega/\omega = 1.0$ and 2.0 . Only integer vibration/rotational frequency ratios could be used because the technique required the imposition of a fixed vibration orbit which could be maintained invariant for at least a few minutes. An alternative method using very low frequencies was discarded because the velocity related forces would have been too low. Higher frequency non-synchronous vibration could not be used due to the resulting "beat" motion arising from interaction with the residual synchronous oscillation, and the non-availability of multiple tracking filters. Experimental points are well grouped on all curves on Figures 56 to 64. In all cases, theoretical curves show that coefficients b_{xx} , b_{xy} increase, and b_{yx} , b_{yy} decrease with x , y .

Choice of either Rule 1 or Rule 2 temperature profile has negligible effect on the coefficient variation and only a small influence on the absolute level.

Velocity coefficients and their variation may also be simply defined by a linear gradient β thus:

$$\begin{aligned} b_{xx} &= b_{xx0} + \beta_{xx} \dot{x} & b_{yy} &= b_{yy0} + \beta_{yy} \dot{y} \\ b_{yx} &= b_{yx0} + \beta_{yx} \dot{x} & b_{xy} &= b_{xy0} + \beta_{xy} \dot{y} \end{aligned}$$

where b_{xx0} etc. is the intersection with the zero velocity axis and will be called the "zero" velocity coefficient. In non-dimensioned form these equations become:

$$\begin{aligned}
 B_{xx} &= B_{xxo} + \beta_{xx}^* \left(\frac{\dot{x}}{r\omega} \right) & B_{yy} &= B_{yyo} + \beta_{yy}^* \left(\frac{\dot{y}}{r\omega} \right) \\
 B_{yx} &= B_{yxo} + \beta_{yx}^* \left(\frac{\dot{x}}{r\omega} \right) & B_{xy} &= B_{xyo} + \beta_{xy}^* \left(\frac{\dot{y}}{r\omega} \right)
 \end{aligned}$$

where

$$B_{xxo} = b_{xxo} \frac{2 C_r \omega}{W_y}, \quad \beta_{xx}^* = \beta_{xx} \frac{2 C_r r \omega^2}{W_y} \quad \text{etc}$$

Figure 65 shows the influence of vibration/rotational frequency ratio Ω/ω upon the measured "zero" velocity coefficient. Direct coefficients b_{xxo} , b_{yyo} determined at $\Omega/\omega = 1.0$ are greater than those evaluated at 2.0. Indirect coefficients b_{xyo} , b_{yxo} deduced at $\Omega/\omega = 1.0$ are less than those obtained at 2.0 although both are negative. Taking the modulus gives

$$0.8 \left| b_{\Omega/\omega = 1.0} \right| = \left| b_{\Omega/\omega = 2.0} \right|$$

Appendix D shows that according to the Short Bearing Approximation, $b_{xy} = b_{yx}$. Figure 66 shows the two measured indirect "zero" velocity coefficients plotted against each other. They all appeared within a band -30 to +40% of each other.

Figures 73 and 75 show velocity coefficients calculated with the fully variable theory ($\eta = \eta(T, p)$) for several speeds at $W_y = 300$ and 500 lbf. respectively. All coefficients exhibited the same form of variation with velocity. Curves are also calculated using $\eta = \eta(T)$ only and uniform viscosity. It follows that the effect of pressure upon viscosity becomes important for the numerically larger coefficients, i.e. B_{xy} , B_{yy} at negative vertical velocities and $\epsilon/C_r > 0.9$. Figure 75 also shows the linear results given by the Short Bearing Approximation at the same level as data from the full theory only for coefficient b_{xxo} . Curves given by the fully variable theory suppressed to uniform viscosity do not display linearity, because that theory allows the cavitation zone to move around the bearing. Non-dimensioning of velocity coefficients involves the rotational speed. It is interesting to observe the closeness of the non-dimensional curves obtained from quite different speeds, thereby indicating the effectiveness of the method.

Agreement between measured and calculated velocity coefficients was examined for both gradient and "zero" values. Figure 69 shows reasonable agreement between the "zero" velocity coefficients obtained from the two sources, except for the largest b_{yyo} where theory over estimates the measured value. Figure 70 illustrates that, in general, velocity coefficients gradients β were not accurately predicted.† Hence, good agreement was obtained between theoretical and measured values of both "zero" displacement and velocity coefficients, but few of the gradients were accurately calculated.

Comparison of experimental results with those of previous workers is complicated by their use of differing bearing geometries. However, Woodcock (10) tested a circumferentially grooved bearing, albeit with different b/D ratio. Comparison is further complicated by other workers use of linear coefficients. Nonetheless, comparison between

† *linear gradient corresponding to theoretical curve established between*

$$\frac{\dot{x}}{r\omega}, \frac{\dot{y}}{r\omega} = \pm 0.5 \cdot 10^{-3}$$

experimental velocity coefficients given by Woodcock (10) and corresponding "zero" values obtained in this work, suggest that (not illustrated) B_{xxo} and B_{xyo} may be independent of ϵ/C_r and b/D .

It is important to establish whether coefficient variation is significant. A suitable criterion was considered to be that variation would be deemed significant if the coefficient changed by 50% over a reasonable and likely velocity/displacement.

Expressing:

$$\frac{A_{xx}}{A_{xxo}} = 1 + \frac{\alpha_{xx}^*}{A_{xxo}} \left(\frac{x}{C_r} \right) \quad \text{and} \quad \frac{B_{xx}}{B_{xxo}} = 1 + \frac{\beta_{xx}^*}{B_{xxo}} \left(\frac{\dot{x}}{r\omega} \right) \quad \text{etc.}$$

then exceeding a 50% variation means that

$$\frac{\alpha_{xx}^*}{A_{xxo}} \left(\frac{x}{C_r} \right) > 0.5 \quad \text{and} \quad \frac{\beta_{xx}^*}{B_{xxo}} \left(\frac{\dot{x}}{r\omega} \right) > 0.5 \quad \text{etc.}$$

A reasonable relative displacement and velocity were considered to be:

$\frac{x}{C_r} = 0.1$ and $\frac{\dot{x}}{r\omega} = 0.5 \cdot 10^{-3}$, and similarly in the vertical direction.

Therefore coefficient variation is significant if:

$$\left| \frac{\alpha_{xx}^*}{A_{xxo}} \right| > 5 \quad \text{and} \quad \left| \frac{\beta_{xx}^*}{B_{xxo}} \right| > 10^{+3} \quad \text{etc.}$$

These are called the 50% ~ 0.1 and 50% $\sim 0.5 \cdot 10^{-3}$ criteria respectively and were applied to all experimental data. Figure 76 shows that variation of displacement coefficient A_{xy} was significant above $\epsilon/C_r = 0.78$. Above $\epsilon/C_r = 0.9$ variation of all displacement coefficients is significant particularly A_{xy} and A_{yy} . Figure 77 confirms that variation of velocity coefficient B_{xy} is significant above $\epsilon/C_r = 0.78$. Variation of all four velocity coefficients is significant at $\epsilon/C_r > 0.86$. Displacement coefficients were obtained over a higher range of ϵ/C_r than velocity coefficients. Any other criterion, which defined a significance boundary at a lesser gradient would recognise coefficient variation above a lower ϵ/C_r . For clarity, only the one specified criterion is marked on Figs 76 and 77.

Theoretical maximum oil film pressure and cavitation zone location obtained with small displacement and velocity increments for a typical condition ($N = 1180$ rpm, $W_y = 150$ lbf, $PS = 30$ lbf/in²) are shown on Figure 78. Figure 79 illustrates their counterparts given by large increments. Each diagram thereon represents a completely separate and independent calculation. Circumferential boundary conditions are governed by the pressure profile itself and not fixed

to any geometrical position. Therefore the cavitation zone is free to move around the oil film. Woodcock (10) described this phenomena as oil film "swinging". Comparison of corresponding diagrams of Figures 78 and 79 reveal considerable theoretical circumferential movement of the cavitation zone at the larger increments. Theory considers that oil film pressures, forces and thence coefficients are solely functions of the journal "state" i.e. its current position and velocity. It takes no account of any preceding position or velocity. Therefore, existing theory treats the dynamic as a succession of independent situations. Thus the current theoretical dynamic treatment may be termed "quasi static". Individual diagrams on Figures 78 and 79 are arranged in the sequence in which they occur during the experimental tests. Figure 78, for small increments, shows little theoretical circumferential movement of the cavitation zone and small variation in peak pressures throughout the cycle. Moreover, theory has been shown to accurately predict coefficients measured for small increments (i.e. "zero" displacement and velocity coefficients). Figure 79, for large increments, shows considerable theoretical cavitation zone movement and extreme variation in peak pressures. Furthermore, theory did not predict coefficients measured with higher increments (i.e. α , β not predicted). This is particularly true for the velocity coefficients. This suggests that in practice, under the specified oscillation the cavitation zone cannot re-locate as theory allows.* If this is so, it means that the oil film pressures depend on a preceding location and velocity in addition to the current values.** This implies that for larger increments, the so-called "quasi-static" theory is inadequate.

It is interesting that the incremental loading methods of determining displacement coefficients allow sufficient time during the experiment for any cavitation zone re-location. Therefore, in this case, both theory and experiment behave as "quasi-static", and give the better agreement between coefficient gradients.

It is important to recall that coefficients are required input data to rotor dynamic calculations, in which truly dynamic situations arise. Therefore, it is essential that oil film coefficients are valid for the dynamic and not the "quasi-static" condition. Furthermore, quite large velocities, comparable to the increments chosen for the significance criteria, are possible in the real machinery situation, thereby necessitating a more complex theory. Since oil film theories can only be verified by successful comparison with experimental results, it follows that more reliable theoretical coefficients of greater value to the rotor dynamicist, will only be obtained by taking some preceding journal state into account. This concept offers the complicating prospect of producing coefficients whose values may vary with choice of previous history.

All experimental techniques were successful. Journal centre measurements and discriminations were excellent, and the "part circle" determination of the bearing found (but not illustrated) to be accurate

* Cole and Hughes (22) visualised different conditions to those in this work.

** The possible alternative of a geometrically fixed boundary condition was discarded because the bearing has circumferential symmetry and the normal static situation does not occur at any time during the vibration cycle.

to better than 5%. Consistent results from the incremental loading technique were encouraging. Suitably steady wave forms were obtained with dynamic loads and the digitisation, phase location pulse and origin subtraction were successful. It is encouraging to note the similarity between the experimental horizontal wave form shown in Fig 32 and that calculated by Holmes (60). Both curves exhibit greater negative discursion, lesser positive velocity, with a pointed minimum and rounded maximum. The measured curves are clearly non-harmonic, thereby justifying an assumption made at the outset of this work (see Chapter 3.1). Journal centre velocities were adequately measured. It was found possible to set the required "line" vibration orbits over a significant part of the cycle in nearly all cases. However, a difficulty subsequently arose due to the necessary of setting the loci by observation of the "total" curves. Each locus specified zero displacement and velocity in one direction over the complete cycle. The residual synchronous vibration, albeit small, was nonetheless quite large in terms of the smallness required of the zeroed displacement. Hence, as seen in the example quoted, it was possible for the deduced "vibration only" curve to depart further from the desired setting than the "total". This problem arises because the "origin" and "total" curves occur at different times. Some complex storage and retrieval system would be necessary for on-line setting to the "vibration only" curve. This would appear to be the only aspect where a significant improvement could be effected. It was also found that, whilst it was possible to set zero velocity for a large part of the cycle, it was more difficult to obtain this curve at zero displacement. This problem arose due to the influence of the indirect displacement coefficients.

calculated!

CONCLUSIONS

1. The main experimental objective, a study of the non-linearity of the eight dynamic oil film coefficients, was attained because all novel experimental features were successful. Further significant improvement can only be achieved by introducing an on-line subtraction of the "origin" journal centre co-ordinates, thereby allowing the specified vibration orbit to be set by reference to the "vibration only" curve. Measurement of journal and bearing centres, displacement coefficients by incremental loading, and journal centre velocity combined with large velocity-based oil film forces were successful. Experimental determination of bearing centre location was found to be necessary at each warm-up/load setting.

2. Sensitivity of vertical load W_y to radial clearance C_r is such that oil film models cannot be verified by comparison of experimental and calculated loads. Radial clearance cannot be measured in the hot rotating condition to the necessary precision, which is sufficiently minute to question the concept of its representation by a single dimension. A more promising approach to model validation may be to compare calculated and measured pressure and temperature fields despite the formidable experimental difficulties of taking measurements in the working condition without disturbing the oil film. Vertical load sensitivity to clearance is sufficiently high that the clearance required by the extremely different temperature profiles specified under Rules 1 and 2, do not differ appreciably. This lessens the significance of choice of temperature profile.

3. For a given temperature profile, simultaneous prediction of W_y and attitude angle ϕ require a unique combination of the almost uncoupled radial clearance C_r and cavitation zone pressure P_C . Fluid film tensile stresses τ in the cavitation zone were found necessary to predict the measured attitude angle, thereby supporting recently published experimental findings.

4. Over the full experimental range of ϵ/C_r and using the equivalent uniform viscosity $\bar{\eta}$, it was found that:

$$\frac{P^*}{\bar{\eta}N} \left(\frac{C_r}{r} \right)^2 \left(\frac{D}{2b} \right)^2 = \left\{ \frac{\pi n (16n^2 + \pi^2 (1-n^2))^{\frac{1}{2}}}{(1-n^2)^2} \right\}^{0.96}$$

$$\tan \phi = \frac{\pi (1-n^2)^{\frac{1}{2}} (2-n^2)}{4n}$$

$$\text{where } n = \epsilon/C_r$$

This leads to the simple design procedures given in 5.1.

5. Variation of viscosity with pressure should be included at $\epsilon/C_r > 0.7$ when computing static loci. It has a less marked influence on coefficients and their sensitivity, but theory suggests it is necessary for those based on the vertical velocity, B_{xy} , B_{yy} at $\epsilon/C_r > 0.9$.

6. Theory reasonably well predicted both the displacement and velocity "zero" coefficients. Apart from a few notable exceptions, coefficient gradients were not accurately predicted, although judgement on this point is partly influenced by the selection of interval over which the equivalent theoretical gradient is taken. Experimental gradients α_{yy} changed sign with eccentricity ratio. Whilst the sign change was predicted, absolute levels were not.

7. No significant difference was observed between displacement coefficients obtained by incremental and dynamic loading, although the latter showed more scatter. Choice of Rule 1 or 2 showed no influence on the theoretical coefficient variation but a small change in absolute level. This further reduces the importance of temperature profile in addition to that in Conclusion 2. Vibration \sim rotation frequency ratio was found to affect velocity coefficients thus

$$0.8 \left| b_{\Omega/\omega} = 1.0 \right| \approx \left| b_{\Omega/\omega} = 2.0 \right|$$

8. Adjudged by the 50% \sim 0.1 criterion, observed variation of A_{xy} is significant at $\epsilon/C_r > 0.78$. According to the 50% \sim $0.5 \cdot 10^{-3}$ criterion, variation of B_{xy} is also significant at $\epsilon/C_r > 0.78$. Measured variation of all velocity and displacement coefficients is significant at $\epsilon/C_r > 0.86$ and 0.90 respectively. Less generous criteria would recognise coefficient variation at lower ϵ/C_r .

9. Significant improvement in coefficient prediction will be obtained by abandoning the so called "quasi-static" theoretical approach in favour of one which takes some account of the preceding journal centre position and velocity. This non-linear effect is important because journal centre velocities of the quoted magnitude occur in rotating machinery.

7 SUGGESTIONS FOR FURTHER WORK

7.1 Experimental

Incorporate some means of setting the specified journal centre loci to the "vibration only" curve. This requires an on-line subtraction of the "origin" from the "total" curves despite their manifestation at different times.

Obtain velocity coefficients at higher ϵ/C_r and possibly higher velocities.

7.2 Theoretical

Some factors relating to the immediately preceding journal centre position and velocity must be added to improve coefficient calculation especially at high velocity increments, for which data is needed by the rotor dynamicist.

8 ACKNOWLEDGEMENTS

The author gratefully acknowledges the support and encouragement given by Professor J R Ellis, Director, School of Automotive Studies throughout this project

I thank Drs D Hodgetts and R Holmes and Mr T Heppenstall for their helpful conversations and acknowledge the support given by the staffs of the Instrumentation, Workshop and Computing Sections.

Thanks are also due to Mrs J Parker and Mrs A Duval for their typing and drawing and to many other friends who have assisted.

9 REFERENCES

1. STERNLICHT B. LEWIS P Vibration problems with high speed turbo machinery
Trans ASME Jnl. of Eng. for Industry Feb 1968
2. HAGG A C. SANKEY G D Elastic and Damping Properties of oil film journal bearings for application to unbalance vibration calculations.
J.Appl.Mech 25 Trans ASME 1958 80 141
3. STERNLICHT B. RIEGER N F Rotor Stability
Proc.Instn Mech Engr. 1967-68 Vol 182 Pt 3A
4. STODOLA A Kritishe Wellenstörung Infolge der Nachgiebigkeit des Oelpolster im lager
Schweizerische Bauzeitung 1925 85 265
- * 5. BANNISTER R H Non-linear oil film force coefficients for a journal bearing operating under aligned and misaligned conditions.
Ph.D. thesis University of Aston
6. SMITH D Journal Bearing Dynamic Characteristics - Effect of Inertia of Lubricant
Proc.I.Mech.E. 1965, 179 (Pt 3J) 37
7. LUND J W Self Excited Stationary Whirl Orbits of a journal in a sleeve bearing
Ph.D. thesis, Rensselaer Polytech Inst New York 1966
8. MORTON P G Measurement of the Dynamic Characteristics of a Large Sleeve Bearing
Trans ASME, Jnl.Lub Tech Jan 1971
9. WOODCOCK J S. HOLMES R Determination and Application of the Dynamic Properties of a Turbo-Rotor Bearing oil film
Proc.Instn Mech Engrs 1969-70 Vol 184 Pt 3L
10. WOODCOCK J S Dynamic Characteristics of a Journal Bearing Oil Film
Ph.D. Thesis University of Sussex 1971
11. STERNLICHT B. Elastic and Damping Properties of Cylindrical Journal Bearings
Trans ASME Jnl. Basic Eng. June 1959
12. HERSEY M D. SNAPP R B. Testing Dynamically Loaded Bearings -
1. A Short History of Bearing Test Machines
Trans ASME Vol 79 (1957) P1247

13. BUSKE A. ROLLI W. Measurement of oil film pressures in Journal Bearings under constant and variable load. Translation from German. NACA Tech Memo 1200
14. SHAWKI G S A. FREEMAN P. Journal Bearing Performance under sinusoidally alternating and fluctuating loads.
Proc. Instn Mech Engrs Vol 169 1955
pp 689-698
15. HAGG A C. SANKEY G O. Some Dynamic properties of oil film journal bearings and reference to the U/B vibration of rotors.
Jnl Appl Mech June 1956
16. MITCHELL J R. HOLMES R
VAN BALLYGOOYEN H. Experimental Determination of a Bearing Oil Film Stiffness.
Proc Instn Mech Engrs 1966 180 (Pt 3K)
90.
17. GLIENICKE J. Experimental Investigation of the Stiffness and Damping Coefficients of Turbine Bearings and their application to Instability Prediction.
Proc Inst Mech Engrs 1967 181 (Pt 3B) 116.
18. ORCUTT F K. ARWAS E B. The Steady State and Dynamic Characteristics of a Full Circular Bearing and a Partial Arc Bearing in the Laminar and Turbulent Flow Regimes.
Trans ASME Jnl Lub Tech April 1967
19. NAKAGAWA E. AOKI H. Approximate Solution of Elastic and Damping Properties of Oil Film in Journal Bearings.
Bull JSME Vol 9, No 34, 1966
20. MORTON P G Dynamic Characteristics of Bearings, Measurement under operating conditions.
GEC Journal of Science & Technology
Vol 42 No 1 1975
21. HOLMES R. PARKINS D W. Assessing Unbalance Effects in a Small turbo-rotor.
ASME 1969 paper 69-DE-9.
22. MIDDLETON V. DUDLEY B P.
McCALLION H. An Investigation into the performance of Dynamically loaded journal bearings: Experiment
Proc Instn Mech Engrs 1966-7 Vol 181 Pt 3B
23. COLE J A. HUGHES C J. Visual Study of film extent in Dynamically loaded complete journal bearings.
Proc Conf Lub and Wear (Instn Mech Engrs)
London 1957, 147.

24. MORRISON D. Influence of plain journal bearings on the whirling action of an elastic rotor
Proc Instn Mech Engrs Vol 176 No 22 1962
25. KIKUCHI K. Analysis of unbalance vibration of rotating shaft system with many bearings and discs.
Bull JSME Vol 13 No 61 1970
26. FUNAKAWA M. TATARA A. Stability Criterion of an Elastic Rotor in journal bearings
Trans Japan Soc Mech Engrs Vol 30 Part 218 1964
27. SMITH D M Dynamic Characteristics of Turbine Journal Bearings
Proc Lub & Wear Conv. 1963 paper 8, 72 (I Mech E).
28. REYNOLDS O. On the Theory of Lubrication and its Application to Mr Beauchamp Tower's Experiments.
Phil Trans 1886 177 (Pt 1) 157
29. SOMMERFELD A. Zur Hydrodynamische Theorie der Schmiermittelreibung
Z Math Phys., 1904, 50, 97
30. DYER D. REASON B R. A study of Tensile Stresses in a journal bearing oil film
Jnl Mech Eng Sci Vol 18, No 1 1976
31. CHRISTOPHERSON D G. A new Mathematical method for the solution of film lubrication problems.
Proc Instn Mech Engrs 1941 146, 126
32. CAMERON A. WOOD Mrs W L. The full journal bearing
Proc Inst Mech Engrs 1949, 161, 59.
33. WALTHER A. SASSENFELD H. Pressure distribution and load in a 360° journal bearing.
DSIR Sponsored Research (Germany)
Report No 11. 1950
34. RAIMONDI A.A. BOYD J. A Solution for the Finite Journal Bearing and its application to Analysis Design I, II and III.
Trans ASLE Vol 1, No 1 April 1958
35. BURWELL J T. The calculated performance of Dynamically loaded sleeve bearings.
Jnl Applied Mech Trans ASME Vol 69 1947.

Part II Jnl Applied Mech Trans ASME Vol 71 1949

Part III Jnl Applied Mech Trans ASME Vol 73 1951

36. HAGG A.C. The influence of oil film journal bearings on the stability of rotating machines.
Jnl Applied Mech Trans ASME Vol 68
Sept 1946.
37. OCVIRK F W. Short Bearing Approximation for full journal bearings
NACA Tech Note 2808, 1952.
38. DUBOIS G.B. OCVIRK F W. Analytical Derivation and Experimental evaluation of short bearing approximation for full journal bearings.
NACA Tech Report 1157, 1953.
39. DUBOIS G B. OCVIRK F W. The Short Bearing Approximation for Plain Journal Bearings
Trans ASME Nov 1955
40. HOLMES R The vibration of a rigid shaft on short sleeve bearings
Jnl Mech Eng Sci 1960 2 337
41. HOLMES R. Oil whirl characteristics of a rigid rotor in 360° journal bearings.
Proc I Mech E 1963 177 (No 11) 291
42. SMALLEY A J. LLOYD T. HORSNELL R. McCALLION H. A comparison of performance predictions for steadily loaded journal bearings.
Proc I Mech E 1965-6 Vol 180 Pt 3K
43. LLOYD T. McCALLION H. Recent developments in fluid film lubrication theory.
Proc I Mech E 1968 182 (Pt 3A) 36.
44. LUNDHOLM G. The Circumferential Groove Journal Bearing Considering Cavitation and Dynamic stability
ACTA POLYTECHNICA SCANDINAVICA
Mechanical Engineering Series No 42
Stockholm 1969
45. DOWSON D. TAYLOR C M. Fundamental aspects of cavitation in bearings.
Paper 1 (iii)
46. TEMPERLEY H N V. The Tensile strengths of liquid
Paper 1 (ii)
47. FLOBERG L. Cavitation boundary conditions with regard to the number of streamers and tensile strength of the liquid
Paper 11(i)

48. MILNE A A. Variations of film extent in dynamically loaded bearing
Paper 1V (i)

References 45 - 48 Proceedings of the 1st Leeds-Lyon Symposium in Tribology
Cavitation and Related Phenomena in Lubrication
University of Leeds - September 1974

- X
49. SMALLEY A J. McCALLION H. The Influence of viscosity variation with Temperature on journal bearing performance.
Proc I Mech E 1966-7 Vol 181 Pt 3B
50. DOWSON D. MARCH C N. A Thermohydrodynamic analysis of journal bearings
Proc I Mech E 1966-7 Vol 181 Pt 30
- X
51. HAKANSSON B. The Journal Bearing Considering Variable Viscosity
Report No 25 Institute of Machine Elements. Chalmers University of Technology. Sweden 1964
52. CAMERON A. Principles of Lubrication - Longmans
53. HEPPENSTALL T. A Theoretical and Experimental Study of a Misaligned Journal Bearing
MSc Thesis Cranfield Institute of Technology 1974
54. HSU Y C. BURTON R.A. Exact Thermoelastic solutions for clearance variation in a short cylindrical bearing configuration with unsymmetrical friction heating
Trans ASME Jnl Lub Tech April 1967
55. AL NICA. Thermal behaviour and friction in journal bearings.
Jnl Lub Tech July 1970 p 373
56. CLAYTON D. WILKIE M J. Temperature distribution in the bush of a journal bearing.
Engineering 1948, 166, 49.
57. WOOLACOTT R G. The Performance at high speeds of complete plain journal bearings with a single hole oil inlet
N.E.L. Report No 194, August 1965
58. COLE J A. An Experimental Investigation of Temperature effects in journal bearings.
Proc Conf Lub and Wear 1957, 111 (I Mech E, London).

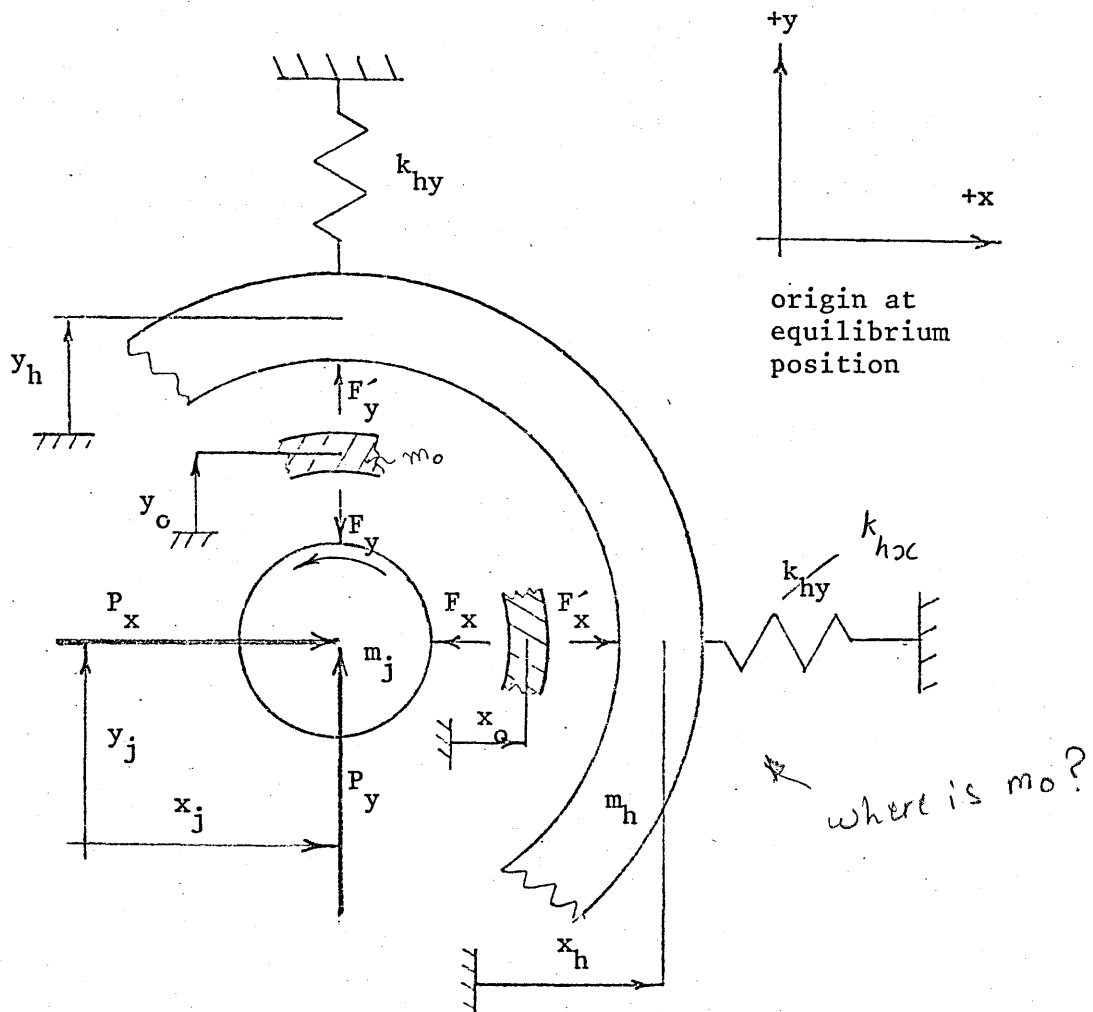
59. DOWSON D.
HUDSON J.D.
HUNTER B.
MARCH C N. An experimental investigation of the
 thermal equilibrium of steadily loaded
 journal bearings
 Proc Instn Mech Engrs 1966-67
 Vol 181 Pt 3B
60. HOLMES R. Non-Linear Performance of Turbine
 Bearings
 Jnl Mech Eng Sci Vol 12 No 6 1970.

* *Reference 5 could not be borrowed before this work was completed.
Any comments upon its contents appearing herein are based upon
information given by private communication.*

APPENDIX A. SIGN CONVENTIONS, DEFINITION OF OIL FILM DISPLACEMENT AND VELOCITY COEFFICIENTS, AND DETERMINATION OF OIL FILM FORCES

A.1 "Normal Machinery" Situation

In this situation the bearing is deemed 'fixed'* and the journal 'free'. Theory also considers this arrangement



Firstly, consider the journal, oil film and bearing to be in equilibrium under a steady vertical force and constant rotational speed. Allow the journal, oil film and bearing to be displaced in positive directions as shown above, by forces having instantaneous values P_x, P_y .

In the above diagram:

k_{hx}, k_{hy} stiffness of springs representing bearing support

m_j, m_o, m_h mass of journal, oil film, housing

x_j, x_o, x_h instantaneous position of journal, oil film and housing mass centres

y_j, y_o, y_h

* see footnote at end of Appendix A2

P_x, P_y	External forces on journal
F_x, F_y	Forces exerted by oil film on journal
F'_x, F'_y	Forces exerted by oil film on bearing

Equations of motion are:

$$\text{journal} \quad P_x - F_x = m_j \ddot{x}_j \quad P_y - F_y = m_j \ddot{y}_j \quad - - - \text{A1-1}$$

$$\text{oil film} \quad F_x - F'_x = m_o \ddot{x}_o \quad F_y - F'_y = m_o \ddot{y}_o \quad - - - \text{A1-2}$$

$$\text{bearing housing} \quad F'_x - k_{hx} x_h = m_h \ddot{x}_h \quad F'_y - k_{hy} y_h = m_h \ddot{y}_h \quad - - - \text{A1-3}$$

Theory in Chapter 4 makes the simplifying assumption that k_{hx} , k_{hy} are sufficiently large that x_h , y_h can be neglected, and further simplifies by putting:

$$x = y_j \quad y = y_j$$

Hence, x , y represent the relative displacement between journal and housing.

Note, however, that this does not mean that the forces $k_{hx} x_h$, $k_{hy} y_h$ may be neglected.

Oil film forces may be expressed in terms of displacement and velocity coefficients thus: $a_{xy} y$

$$F_x = a_{xx} x + a_{xy} y + b_{xx} \dot{x} + b_{xy} \dot{y} \quad - - - - \text{A1-4}$$

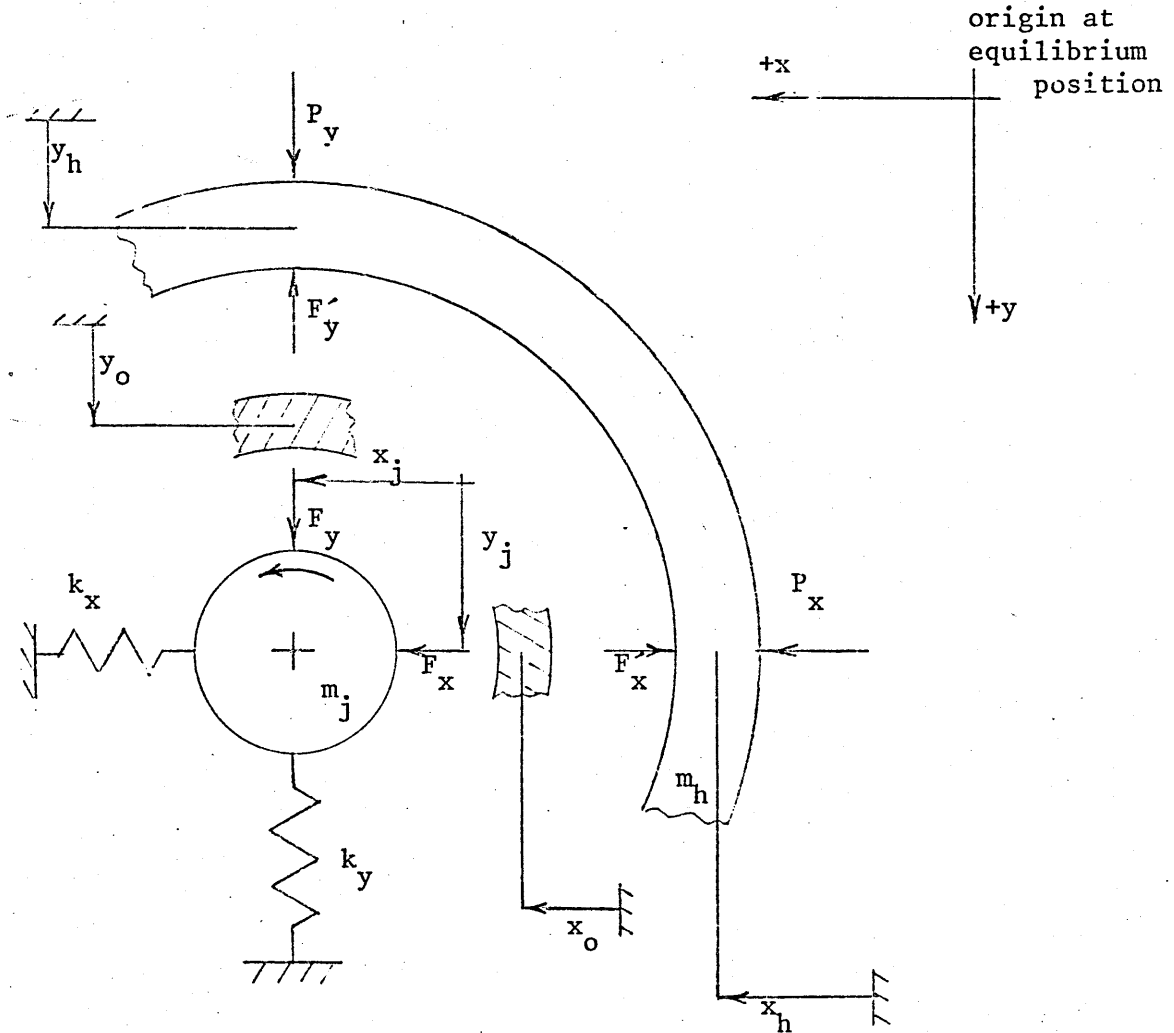
$$F_y = a_{yx} x + a_{yy} y + b_{yx} \dot{x} + b_{yy} \dot{y} \quad - - - - \text{A1-5}$$

In this definition, forces F_x , F_y are those exerted by the journal on the oil film.

Smith (6) found that extra 'acceleration' coefficients related to \ddot{x} and \ddot{y} could be neglected for typical length bearings and rotors.

A.2 Test Rig Situation

In this situation the bearing housing is regarded as 'free'* and the journal 'fixed'*.



This sign convention is opposite to that used in the "normal machinery" arrangement.

In the above diagram:

k_x, k_y stiffness of springs representing journal, slave bearings, their housings and supporting structure

P_x, P_y External forces acting on housing.

All other symbols have the meaning given in A.1.

Allow the journal, oil film and housing mass centres to be displaced from the equilibrium position to the positions shown, by external forces P_x, P_y .

* see footnote at end of Appendix A2.

Equation of motion are:

$$\text{housing} \quad P_x - F'_x = m_h \ddot{x}_h \quad P_y - F'_y = m_h \ddot{y}_h \quad \text{--- A1-6}$$

$$\text{oil film} \quad F'_x - F_x = m_o \ddot{x}_o \quad F'_y - F_y = m_o \ddot{y}_o \quad \text{--- A1-7}$$

$$\text{journal} \quad F_x - k_x x_j = m_j \ddot{x}_j \quad F_y - k_y y_j = m_j \ddot{y}_j \quad \text{--- A1-8}$$

In the test rig, displacement transducers measured the relative displacement between housing and journal.

$$\text{i.e.} \quad x_h - x_j = x$$

$$y_h - y_j = y$$

where x , y have the same meaning as in A.1.

Hence equations A1-4 and A1-5 may be used for this situation where forces F'_x , F'_y are those exerted by the journal on the oil film and given in equation A1-7 or A1-8 above.

Therefore, coefficients determined experimentally on the test rig may be readily compared to those given by theory, and used in the "normal machinery" situation with the sign convention of A.1.

It follows from equations A1-6 and 7 that:

$$F_x = P_x - (m_h \ddot{x}_h + m_o \ddot{x}_o) \quad \text{--- A1-9}$$

$$F_y = P_y - (m_h \ddot{y}_h + m_o \ddot{y}_o) \quad \text{--- A1-10}$$

Accelerometers attached to the bearing housing measured \ddot{x}_h , \ddot{y}_h , their combination with the inductive transducer readings yielded x_j , y_j

It was shown that if

$$-3 < \frac{\ddot{x}_j}{\ddot{x}_h} < +3 \quad \text{then} \quad m_o \ddot{x}_o \leq 0.01 m_h \ddot{x}_h$$

and similarly in the y direction.

All experimental data were found to meet this condition. Morton (8) also states that the oil film transverse inertial forces may be neglected. Therefore oil film forces were calculated from:

$$F_x = P_x - m_h \ddot{x}_h \quad \text{--- A1-11}$$

$$F_y = P_y - m_h \ddot{y}_h \quad \text{--- A1-12}$$

At each experimental test, the maximum values of $m_h \ddot{x}_h$, $m_h \ddot{y}_h$ were calculated from the original photographs of oscilloscope traces. These terms were neglected in equations A1-11 and 12 if:

- (a) max. $m_h \ddot{x}_h$, $m_h \ddot{y}_h$ were less than 2.0 lbf
 or
 (b) max. $m_h \ddot{x}_h$, $m_h \ddot{y}_h$ were less than $0.03 \left[\begin{matrix} \text{unknown} \\ \text{coefficient} \end{matrix} \right] \times \left[\begin{matrix} \text{appropriate} \\ \text{force or} \\ \text{displacement} \end{matrix} \right]$

In case (a) forces $m_h \ddot{x}_h$, $m_h \ddot{y}_h$ did not exceed the typical error due to reading the enlarged photograph of the dynamic force trace.

In case (b) forces $m_h \ddot{x}_h$, $m_h \ddot{y}_h$ were insignificant compared to the forces appearing in the equation from which the required coefficient was obtained.

If neither (a) nor (b) were met then \ddot{x}_h , \ddot{y}_h were obtained at the required times within the cycle from enlarged photographs of the oscilloscope traces.

A majority of tests did meet (a) or (b) above.

This procedure minimised the number and cost of photographic enlargements without significant loss of accuracy.

* In each of the two situations, the bearing housing and journal experience constraining forces from:

	Normal machinery	Test Rig
Bearing housing	(i) supporting structure (ii) oil film	(i) external force (ii) oil film
Journal	(i) oil film (ii) external force	(i) oil film (ii) supporting structure
Simplified terminology	Bearing 'fixed' Journal 'free'	Bearing 'free' journal 'fixed'

In the non-rotating condition, with no oil film or external forces, stiffness of the supporting structure creates the only remaining force. In such circumstances, elements supported by the structure appear relatively fixed. Although the relative terms 'fixed' and 'free' have no significance in the dynamic situation, they are used at the start of Appendices A1 and 2 to give a concise text.

APPENDIX B. EXAMPLE OF ANALYSIS SEQUENCE

Part of analysis of condition 8 $\Omega/\omega = 1.0$ Figs 32 to 35 show relevant curves

Test No	time	x		y		$P_x - m_h \ddot{x}_h$		$P_y - m_h \ddot{y}_h$		output
		10^{-3}	inch units	10^{-3}	inch units/sec	lbf	lbf	lbf	lbf	
1	119.5	0.0	0.0	-30.56	0.0	-54.2	+32.7	b_{xx}	b_{yx}	
2	132.5	0.0	0.0	0.0	+14.78	-38.8	+73.17	b_{xy}	b_{yy}	
2	103	0.0	-0.120	0.0	0.0	+2.89	-52.7	a_{xy}	a_{yy}	
1	18	-0.378	-0.040	0.0	0.0	-62.4	+93.97	a_{xx}	a_{yx}	
1	55.5	0.0	-0.020	+34.6	+16.57	+62.53	-55.5	b_{xx}	b_{yx}	

Equations A1-4, A1-5, A1-11 and A1-12 combine to give:

$$a_{xx} x + a_{xy} y + b_{xx} \dot{x} + b_{yx} \dot{y} = P_x - m_h \ddot{x}_h$$

$$a_{yx} x + a_{yy} y + b_{yx} \dot{x} + b_{yy} \dot{y} = P_y - m_h \ddot{y}_h$$

Using above data gives:

Test No	time	units	10^{-3}	inch	$\frac{\text{lbf. sec}}{10^{-3} \text{ inch}}$
1	119.5	-30.56	$b_{xx} = -54.2 \Rightarrow$	$b_{xx} = +1.774$	
1	119.5	-30.56	$b_{yx} = +32.7 \Rightarrow$	$b_{yx} = -1.070$	
2	132.5	+14.78	$b_{xy} = -38.8 \Rightarrow$	$b_{xy} = -2.625$	
2	132.5	+14.78	$b_{yy} = +73.17 \Rightarrow$	$b_{yy} = +4.951$	
2	103	-0.12	$a_{xy} = +2.89 \Rightarrow$	$a_{xy} = -24.1$	
2	103	-0.12	$a_{xy} = -52.7 \Rightarrow$	$a_{yy} = +439.2$	
1	18	-0.378	$a_{xx} = -62.4 - (0.04)(-24.08) \Rightarrow$	$a_{xx} = +167.6$	
1	18	-0.378	$a_{yx} = +93.97 + (0.04)(439.2) \Rightarrow$	$a_{yx} = -295.1$	
1	55	+34.6	$b_{xx} = +62.53 + (0.02)(-24.08) - (16.57)(-2.625) \Rightarrow$	$b_{xx} = +3.048$	
1	53	+34.6	$b_{yx} = -55.5 + (0.02)(439.2) - (16.57)(4.951) \Rightarrow$	$b_{yx} = -3.721$	

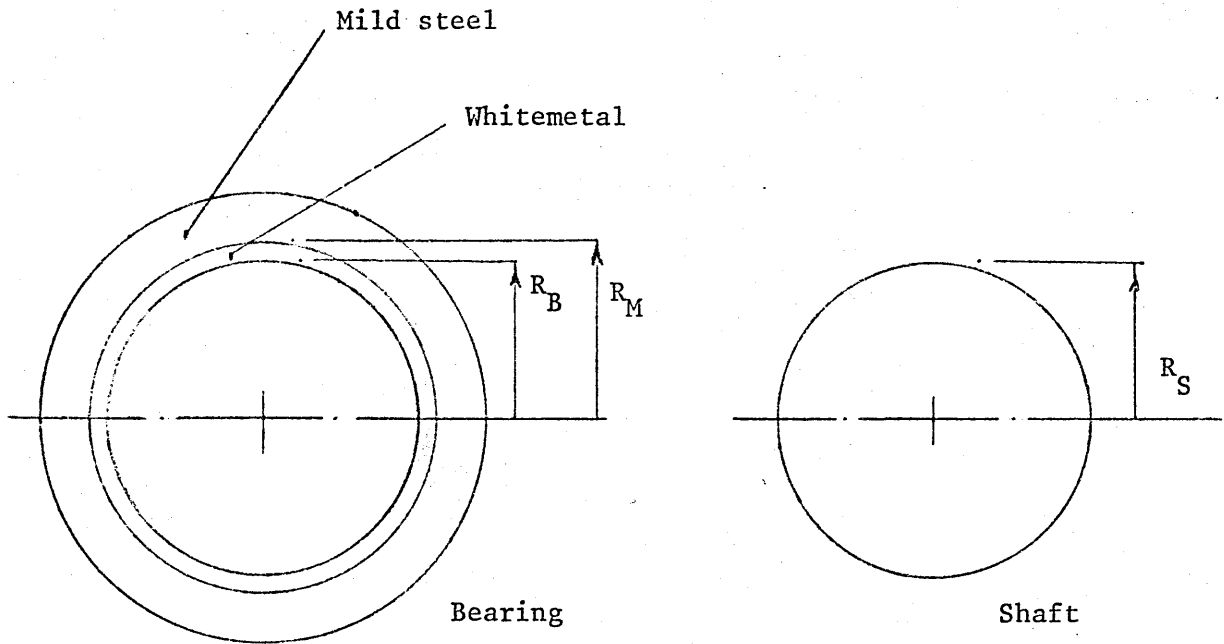
At test 2 - 103, $P_x - m_h \ddot{x}_h$ is small and liable to greater error than usual. The consequent value of a_{xy} should be treated with reserve. However, notice that where this value of a_{xy} is subsequently invoked, i.e. in equations at 1-18 and at 1-55, it produces a microscopic force compared with others in the equation.

Hence, even if a_{xy} from 2 - 103 were, say in 200% error, it would have negligible effect on the a_{xx} and b_{xx} derived from equations at 1-18 and 1-55.

Analyses were arranged to observe this principle whenever possible.

APPENDIX C. EFFECT OF TEMPERATURE ON RADIAL CLEARANCE

The test bearing comprises a large cylinder with a thin inner ring of white metal.



R_M = inner radius of steel housing

R_B = radius of bearing surface

R_S = shaft radius

C_r = radial clearance

α_m = coefficient of linear thermal expansion for mild steel, and shaft

α_w = coefficient of linear thermal expansion for whitemetal

ΔT_m = representative temperature change during warm-up for steel housing.

ΔT_s = representative temperature change during warm-up for shaft

ΔT_w = representative temperature change during warm-up for whitemetal

signifies operating condition

$$C_r = R_B - R_S \quad \text{at room temperature}$$

$$C'_r = R'_B - R'_S \quad \text{at operating temperature}$$

$$\text{put } R'_M = R_M (1 + \alpha_m \Delta T_m)$$

$$R'_S = R_S (1 + \alpha_m \Delta T_s)$$

Allow the whitmetal to change dimension so that

$$(R'_M - R'_B) = (R_M - R_B) (1 + \alpha_w \Delta T_w)$$

It can be shown that the change in radial clearance between cold and working condition is given by:

$$C'_r - C_r = \alpha_m \Delta T_s \left(\frac{R_M \Delta T_M}{\Delta T_S} - R_S \right) - \frac{\alpha_w \Delta T_w}{w} (R_M - R_B)$$

typical values

$$\alpha_w = 23.0 \cdot 10^{-6} \quad \text{C}^{-1}$$

$$\alpha_m = 11.0 \cdot 10^{-6} \quad \text{C}^{-1}$$

Since $R_M > R_B$, the second term makes a negative contribution to $C'_r - C_r$. Moreover, the thermal expansion coefficient associated with the second is twice that with the first term.

Because R_M and R_S differ by only 0.1 in 1.25 inch and ΔT_M is likely to be less than T_S , it is probable that the bracket of the first term will also make a negative contribution. It follows that $C'_r - C_r$ will be negative and that radial clearance will decrease with warm-up. Experimental results (see 5.1) confirmed this finding.

Hsu and Burton (54) give a more complex analysis of clearance change due to temperature for short cylindrical dry bearings. They also generally conclude that clearance is reduced in the operating condition.

APPENDIX D. COEFFICIENTS IN r, s CO-ORDINATE SYSTEM

$$r = x \sin \phi - y \cos \phi$$

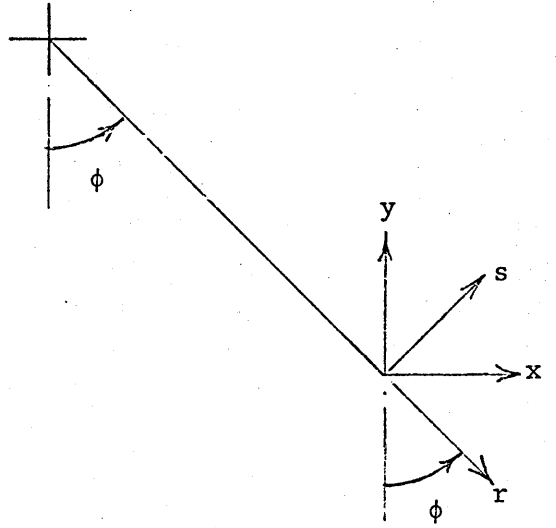
$$s = y \sin \phi + x \cos \phi$$

$$F_x = a_{xx} \dot{x} + a_{xy} \dot{y} + b_{xx} \ddot{x} + b_{xy} \ddot{y}$$

$$F_y = a_{yx} \dot{x} + a_{yy} \dot{y} + b_{yx} \ddot{x} + b_{yy} \ddot{y}$$

$$F_r = a_{rr} \dot{r} + a_{rs} \dot{s} + b_{rr} \ddot{r} + b_{rs} \ddot{s}$$

$$F_s = a_{ss} \dot{s} + a_{sr} \dot{r} + b_{ss} \ddot{s} + b_{sr} \ddot{r}$$



$$a_{rr} = a_{xx} \sin^2 \phi - (a_{xy} + a_{yx}) \sin \phi \cos \phi + a_{yy} \cos^2 \phi$$

$$a_{rs} = a_{xy} \sin^2 \phi + (a_{xx} - a_{yy}) \sin \phi \cos \phi - a_{yx} \cos^2 \phi$$

$$a_{ss} = a_{yy} \sin^2 \phi + (a_{yx} + a_{xy}) \sin \phi \cos \phi + a_{xx} \cos^2 \phi$$

$$a_{sr} = a_{yx} \sin^2 \phi + (a_{xx} - a_{yy}) \sin \phi \cos \phi - a_{xy} \cos^2 \phi$$

$$b_{rr} = b_{xx} \sin^2 \phi - (b_{yx} + b_{xy}) \sin \phi \cos \phi + b_{yy} \cos^2 \phi$$

$$b_{rs} = b_{xy} \sin^2 \phi + (b_{xx} - b_{yy}) \sin \phi \cos \phi - b_{yx} \cos^2 \phi$$

$$b_{ss} = b_{yy} \sin^2 \phi + (b_{yx} + b_{xy}) \cos \phi \sin \phi + b_{xx} \cos^2 \phi$$

$$b_{sr} = b_{yx} \sin^2 \phi + (b_{xx} - b_{yy}) \sin \phi \cos \phi - b_{xy} \cos^2 \phi$$

Holmes (40) showed that $b_{rs} = b_{sr}$

Substituting from the above equations gives:

$$\begin{aligned} b_{xy} \sin^2 \phi + (b_{xx} - b_{yy}) \sin \phi \cos \phi - b_{yx} \cos^2 \phi \\ = b_{yx} \sin^2 \phi + (b_{xx} - b_{yy}) \sin \phi \cos \phi - b_{xy} \cos^2 \phi \end{aligned}$$

manipulation yields $b_{xy} = b_{yx}$

METHOD	GOOD FEATURES	WEAK FEATURES
A	<p>(1) Obtains displacement coefficients under dynamic conditions</p> <p>(2) Extra settings could allow determination of variation of</p> <p>b_{xx}, b_{xy} with \dot{x}</p> <p>b_{yy}, b_{xy} with \dot{y}</p>	<p>(1) Difficulty in setting both $\ddot{x} = 0$ and $\ddot{y} = 0$ at same time</p> <p>(2) Difficulty in detecting whether settings have been achieved whilst test is in progress</p> <p>(3) Does not allow a_{xx}, a_{yx} to vary with x or a_{yy}, a_{xy} to vary with y.</p>
B	<p>(1) Obtains displacement coefficients under dynamic conditions</p> <p>(2) Only two settings required</p> <p>(3) Allows determination of variation of</p> <p>b_{xx}, b_{yx} with \dot{x}</p> <p>b_{yy}, b_{xy} with \dot{y}</p> <p>a_{xx}, a_{yx} with x</p> <p>a_{yy}, a_{xy} with y</p> <p>(4) Less dependence on values of other coefficients</p>	<p>(1) Specified settings may be difficult or impossible to obtain</p> <p>(2) Difficulty in detecting whether settings have been obtained whilst test is in progress</p>
C	<p>(1) Only one vibrator necessary</p> <p>(2) Only one vibration experiment required</p> <p>(3) No setting problems</p> <p>(4) Extra vibrator and settings could allow determination of a variation of:</p> <p>b_{xx}, b_{yx} with \dot{x}</p> <p>b_{yy}, b_{xy} with \dot{y}</p>	<p>(1) Does not obtain displacement coefficients under dynamic conditions</p> <p>(2) Dependence on coefficients obtained in separate experiments.</p>

TABLE 1. SUMMARY OF GOOD AND WEAK FEATURES OF METHODS A, B & C

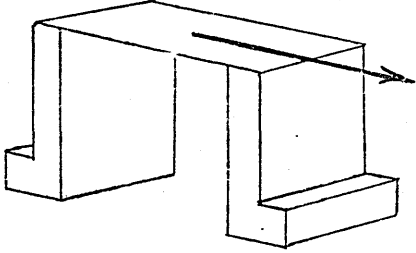
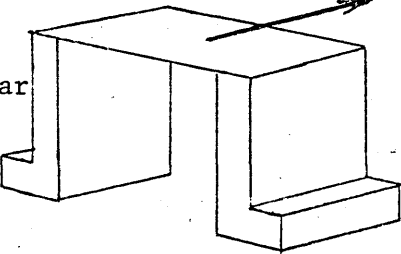
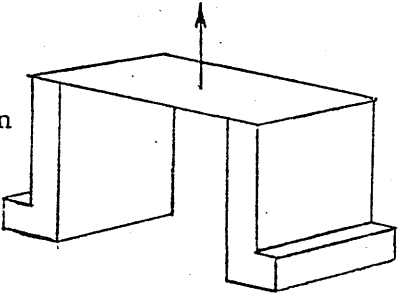
		Stiffness lbf/inch	
		Device A	Device B
Parallel to Figure		$5.76 \cdot 10^3$	$6.0 \cdot 10^3$
Perpendicular to Figure		$19.4 \cdot 10^3$	$22.2 \cdot 10^3$
In direction of dynamic load		$0.83 \cdot 10^3$	$0.72 \cdot 10^3$
Stiffness of force gauge in load direction (manufacturers value)		$5.0 \cdot 10^6$	

TABLE 2. STIFFNESS OF FORCE GAUGE MOUNTING DEVICE

	Channel No			
	1	2	3	4
Values of α obtained before testing (room temperature) 23-31 Oct 74 Volts/10 ⁻³ inch	0.630	0.358	0.578	0.456
Values of α obtained at operating temperatures 30 Dec 74 - 2 Jan 75 Volts/10 ⁻³ inch	0.636	0.352	0.562	0.465
Values of α obtained mid-way through testing 7 Apr 75 Volts/10 ⁻³ inch	0.637	0.357	0.572	0.455
established extent of linear relationships Volts	(Cold)			
	(Hot)			
	+ 2.0 - 1.2	- 0.2 - 2.4	+ 0.3 - 3.0	+ 1.5 - 1.0
	+ 1.35 0.0	- 0.6 - 1.9	- 1.01 - 1.4	+ 1.1 - 0.7
Values of α used to compute experimental data	0.630	0.358	0.578	0.456
Maximum and minimum R values used throughout testing Volts	+ 1.3 - 1.1	- 0.64 - 1.68	- 0.4 - 1.67	+ 0.89 - 0.56

TABLE 3. INDUCTIVE DISPLACEMENT TRANSDUCER CALIBRATION

Resonant Frequencies, cycles/min.		
	Motor End	Free End
Horizontal, perpendicular to wires	1154	2258*
Horizontal, parallel to wires	1176	greater than 5000 (outside test frequency range)
Vertical	2095	4285 (outside test frequency range)
	All the above showed negligible response	* significant peak, sharply tuned with negligible response at N = 2240 c/min. and N = 2318 c/min.

TABLE 4. RESONANT FREQUENCIES OF WIRE SUPPORT BRACKETS

N cycles/min	Test Frequency Range, cycles/min	
	$\Omega/\omega = 1.0$	$\Omega/\omega = 2.0$
1180	1190 - 1170	2380 - 2340
1500	1505 - 1495	3010 - 2990
2200	2210 - 2190	Not used

TABLE 5. TEST FREQUENCY RANGES

Source (Ref No)	N rpm	P* lbf inch ²	D inch	L/D	C _r inch	Geometry and oil supply pressure lbf/inch ²	Peripheral velocity r _ω inch/sec	Circumferential Temperature distribution (experimental)	Axial Temperature Variation
AL NICA (55)								1.0 $\left[1 + \sin \frac{\theta}{2} \right]^{0.406}$	Theory and Experiment) Nil
HAKANSSON (51)			3.9	1.0		plain bearing axial groove	< 198	$\left[1 + \sin \frac{\theta}{2} \right]$	Theory Nil
CLAYTON & WILKIE (56)	3,000	1500	2.0	0.875	0.0025	plain bearing single oil hole 40	313	1.2 $\left[1 + \sin \frac{\theta}{2} \right]^{0.365}$ [T ₁ = 70°C] 1.8 $\left[1 + \sin \frac{\theta}{2} \right]^{0.5}$ [T ₁ = 40°C]	Experiment. shows constant temperature contours across bearings
	4,000					40	313	$\left[1 + \sin \frac{\theta}{2} \right]$	
	3,000					180° circumferential groove	417	$\left[1 + \sin \frac{\theta}{2} \right]$	
WOOLACOTT (57)	29,000	200	2.0	0.5	0.0082	plain bearing single oil hole	2090	$\left[1 + \cos \theta \right]$	small
COLE (58)	2,700	633	2.0	0.5	0.004		282	1.0 $\left[1 + \sin \frac{\theta}{2} \right]^{0.378}$	insignificant
	5,465	157	2.0				560	$\left[1 + \cos \theta \right]$	
DOWSON (59)	1,500	156	4.0	1.0	0.005	axial groove 40	314	1.0 $\left[1 + \sin \frac{\theta}{2} \right]^{0.49}$ 0 < θ < 180 $\left[1 + \cos \theta \right]$ θ > 180	negligible

TABLE 6. PUBLISHED EXPERIMENTAL MEASUREMENT OF TEMPERATURE PROFILES

PS = 30.0

N rpm	Wy lbf									
	150		200		300		500		700	
1180	2.33	1.077 0.199	2.47	1.104 0.199	2.77	1.157 0.199				
1500	3.45	1.077 0.253	3.59	1.104 0.253	3.88	1.157 0.253	4.47	1.26 0.253	5.05	1.37 0.253
2200	5.9	1.077 0.371	6.04	1.104 0.371	6.34	1.157 0.371	6.92	1.26 0.371	7.5	1.37 0.371
2900			8.49	1.104 0.489	8.78	1.157 0.489	9.37	1.26 0.489	9.95	1.37 0.489

PS = 15.0

N rpm	Wy lbf			
	150		300	
1180	3.59	1.46 0.199	4.03	1.545 0.199
1500	4.92	1.46 0.253	5.36	1.545 0.253
2200	8.03	1.46 0.371	8.47	1.545 0.371
2900			10.66	1.545 0.489

PS = 7.5

N rpm	Wy 150 lbf
1180	4.22 1.66 0.199
1500	5.65 1.66 0.253
2200	9.09 1.66 0.371

TABLE 7. VALUES OF ΔT ($^{\circ}C$) SR C2 - RULE 1

N rpm	$W_y = 150 \text{ lbf/inch}^2$	
	$PS = 30 \text{ lbf/inch}^2$	$PS = 15 \text{ lbf/inch}^2$
1180	1.100	1.150
	0.28	0.28
1500	1.100	1.142
	0.28	0.28
2200		1.105
		0.371

TABLE 8. VALUES OF $\frac{SR}{C2}$ - RULE 2

N rpm	PS lbf/in ²	measured			calculated					
		W _y lbf	ε 10 ⁻³ inch	φ deg	W _y lbf	φ deg	C _r 10 ⁻³ inch	PC lbf/in ²	Rule No	ε/C _r
1180	7.5	150	1.415	35.9	150.4	35.8	1.646	- 25.4	1	0.859
1180	15.0	150	1.420	37.1	149.1	37.36	1.730	- 11.0	1	0.821
1180	15.0	150	1.420	37.1	150.1	37.30	1.809	- 2.0	2	0.785
1180	30	150	1.415	38.5	151.8	38.85	1.790	0.0	2	0.790
1500	7.5	150	1.445	36.71	149.8	36.7	1.659	- 35.0	1	0.871
1500	15.0	150	1.405	38.38	149.5	38.27	1.685	- 17.9	1	0.834
1500	15.0	150	1.405	38.38	150.4	38.4	1.782	- 5.0	2	0.788
1500	30.0	150	1.3975	39.85	149.6	39.92	1.792	0.0	2	0.779
2200	7.5	150	1.395	37.15	149.8	36.83	1.614	- 30.3	1	0.864
2200	15.0	150	1.365	39.7	149.9	39.41	1.644	- 19.0	1	0.830
2200	15.0	150	1.365	39.7	150.4	39.6	1.769	- 3.5	2	0.771
2200	30.0	150	1.3725	41.27	150.3	41.25	1.7375	- 4.5	1	0.789
1180	30.0	200	1.43	36.23	201.4	36.4	1.748	- 6.2	1	0.818
1500	30.0	200	1.425	37.3	200.3	37.3	1.740	- 7.8	1	0.819
2200	30.0	200	1.380	38.03	200.0	38.0	1.708	- 6.2	1	0.808
2900	30.0	200	1.342	38.91	200.1	39.2	1.657	- 9.5	1	0.810
1180	15.0	300	1.600	29.02	301.1	29.05	1.775	- 49.7	1	0.902
1500	15.0	300	1.500	29.5	302.7	29.40	1.674	- 43.7	1	0.896
2200	15.0	300	1.570	29.9	299.9	29.8	1.734	- 60.0	1	0.905
2900	15.0	300	1.520	30.67	299.4	30.6	1.676	- 68.0	1	0.907
1180	30.0	300	1.60	30.75	297.9	30.7	1.852	- 13.5	1	0.864
1500	30.0	300	1.55	31.55	298.3	31.5	1.808	- 13.0	1	0.857
2200	30.0	300	1.54	31.96	303.0	31.9	1.771	- 24.0	1	0.869
2900	30.0	300	1.50	29.27	300.3	29.33	1.723	- 6.3	1	0.870
1500	30.0	500	1.69	24.04	500.1	24.0	1.8736	- 14.0	1	0.902
2200	30.0	500	1.70	23.78	502.9	23.72	1.868	- 22.0	1	0.910
2900	30.0	500	1.69	23.51	498.1	23.50	1.842	- 31.4	1	0.917
1500	30.0	700	1.765	19.4	701.0	19.42	1.905	- 10.0	1	0.926
2200	30.0	700	1.80	18.4	698.6	18.4	1.9355	- 1.0	1	0.930
2900	30.0	700	1.86	17.95	704.0	17.93	1.975	- 23.0	1	0.942

TABLE 9. MEASURED AND CALCULATED STATIC PROPERTIES, VARIABLE VISCOSITY THEORY

N	PS	W_y	ϕ	W_y	ϕ	PC	$\bar{\eta}$
rpm	lbf/in ²	lbf	deg	lbf	deg	lbf/in ²	lbf sec/in ²
measured				calculated			
1180	30.0	150	38.5	150.6	38.7	- 1.0	$6.48 \cdot 10^{-6}$
1500	30.0	150	39.85	149.8	39.94	- 1.5	$5.6 \cdot 10^{-6}$
2200	30.0	150	41.27	149.9	41.38	- 7.5	$3.3 \cdot 10^{-6}$
1180	30.0	300	30.75	301.4	30.6	- 14.0	$6.0 \cdot 10^{-6}$
1500	30.0	300	31.55	298.3	31.45	- 14.0	$4.88 \cdot 10^{-6}$
2200	30.0	300	31.96	288.8	31.84	- 26.0	$2.73 \cdot 10^{-6}$
1500	30.0	500	24.04	498.7	24.0	- 13.0	$4.2 \cdot 10^{-6}$
2200	30.0	500	23.78	500.9	23.7	- 22.0	$2.45 \cdot 10^{-6}$
2900	30.0	500	23.51	501.2	23.3	- 31.0	$1.55 \cdot 10^{-6}$
1500	30.0	700	19.4	701.2	19.6	- 6.0	$3.5 \cdot 10^{-6}$
2200	30.0	700	18.4	704.5	18.7	0.0	$2.25 \cdot 10^{-6}$
2900	30.0	700	17.95	699.6	18.0	- 17.0	$1.275 \cdot 10^{-6}$

TABLE 10. MEASURED AND CALCULATED STATIC PROPERTIES, UNIFORM VISCOSITY.

		W_y lbf
PS = 7.5 lbf/in ²		150
N rpm =	1180	L,L,V1,V2,Δ
	1500	L,L,V1,V2,Δ
	2200	L,L,V1, Δ

L = measurement of ϵ , ϕ .

Δ = displacement coefficients by incremental loading

V1 = Dynamic loading Ω/ω
= 1.0

V2 = Dynamic loading Ω/ω
= 2.0

		W_y lbf	
PS = 15 lbf/in ²		150	300
N rpm =	1180	L,L,V1,V2,Δ	L, Δ
	1500	L,L,V1,V2 Δ	L, Δ
	2200	L,L,V1,V2,Δ	L, Δ
	2900		L, Δ

		W_y lbf				
PS = 30 lbf/in ²		150	200	300	500	700
N rpm =	1180	L,L,V1,V2,Δ	L,L,V1,Δ	L, Δ		
	1500	L,L,V1,V2 Δ	L,	L,L Δ	L,L Δ	L,L,Δ
	2200	L,L,V1, Δ	L,L, Δ	L, Δ	L,L,Δ	L,L,Δ
	2900		L,L, Δ	L, Δ	L, Δ	L, Δ

TABLE 11. LIST OF EXPERIMENTAL INVESTIGATIONS

TEST BEARING
OIL SUPPLY

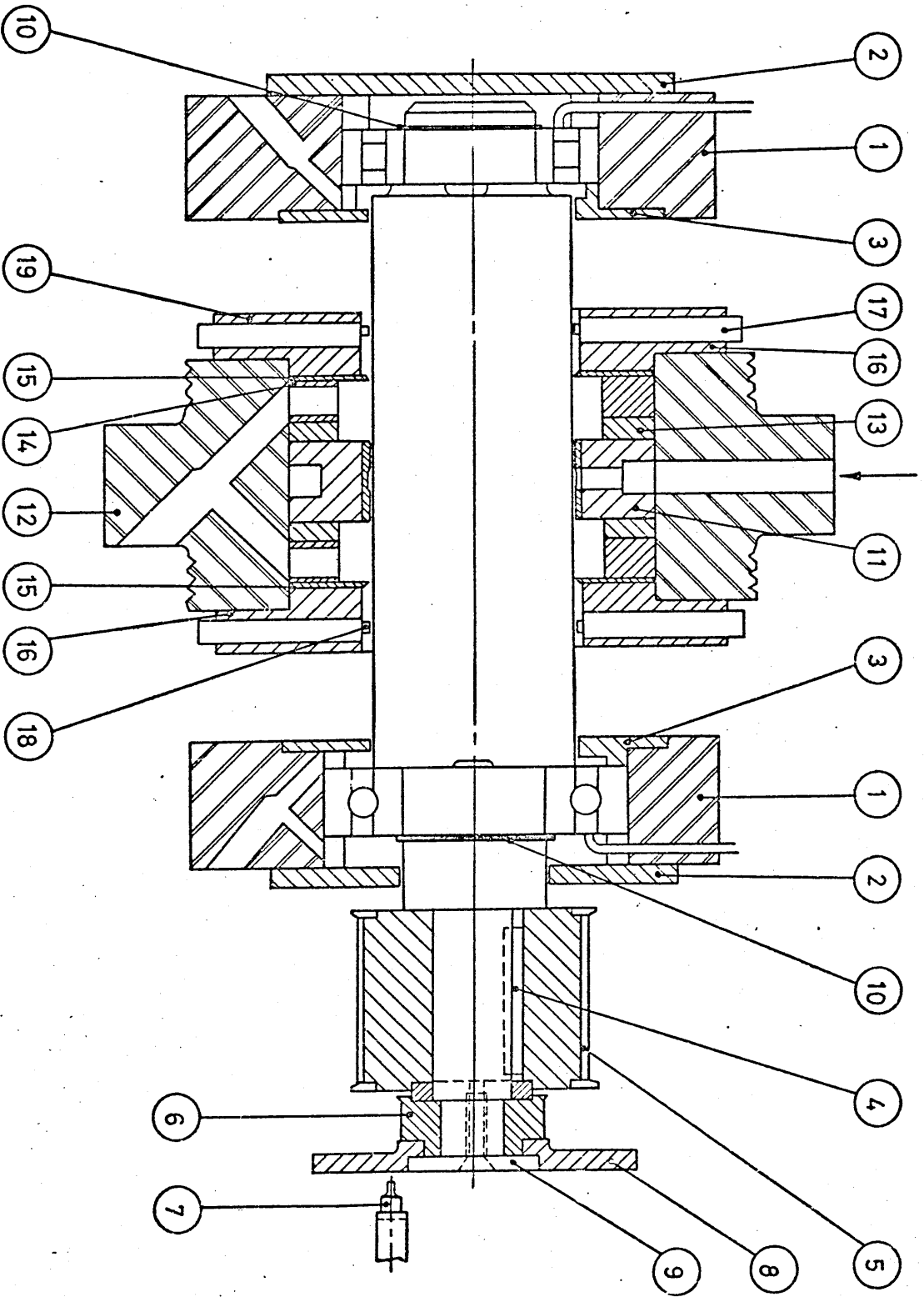


FIGURE 1. TEST AND SLAVE BEARING CONSTRUCTION.

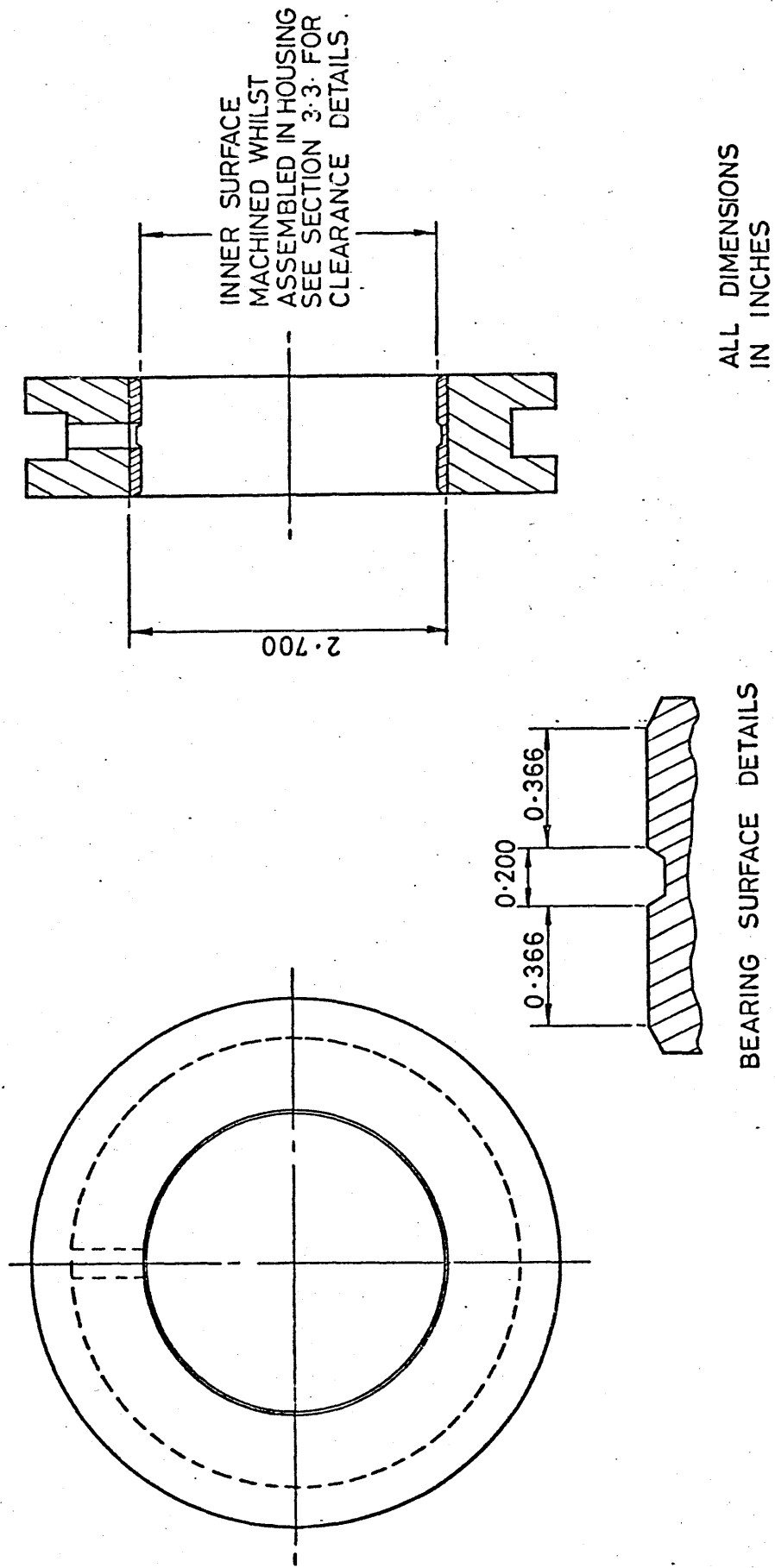


FIGURE 2. TEST BEARING AND INNER RING DETAILS.

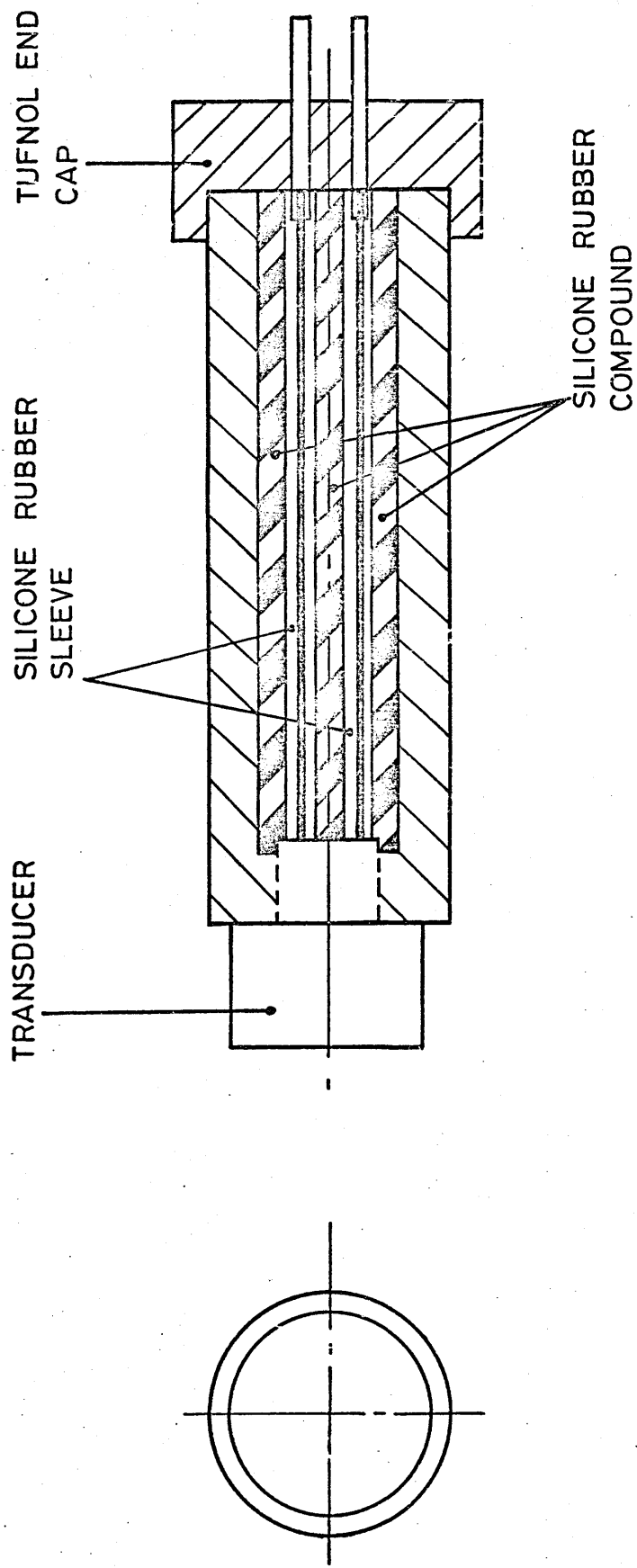


FIGURE 4. DISPLACEMENT TRANSDUCER MOUNTING.

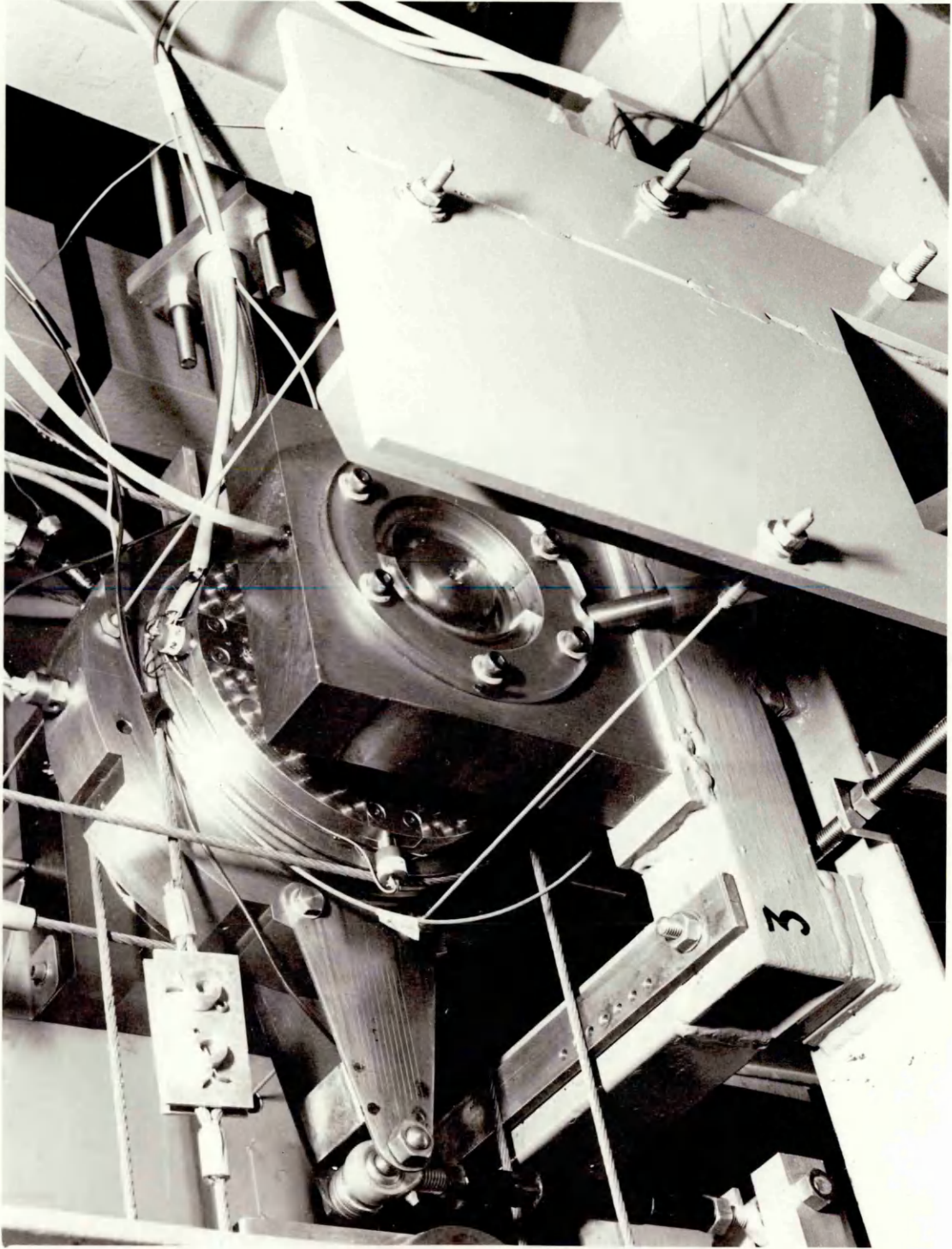


FIGURE 3. PHOTOGRAPH OF TEST AND SLAVE BEARINGS

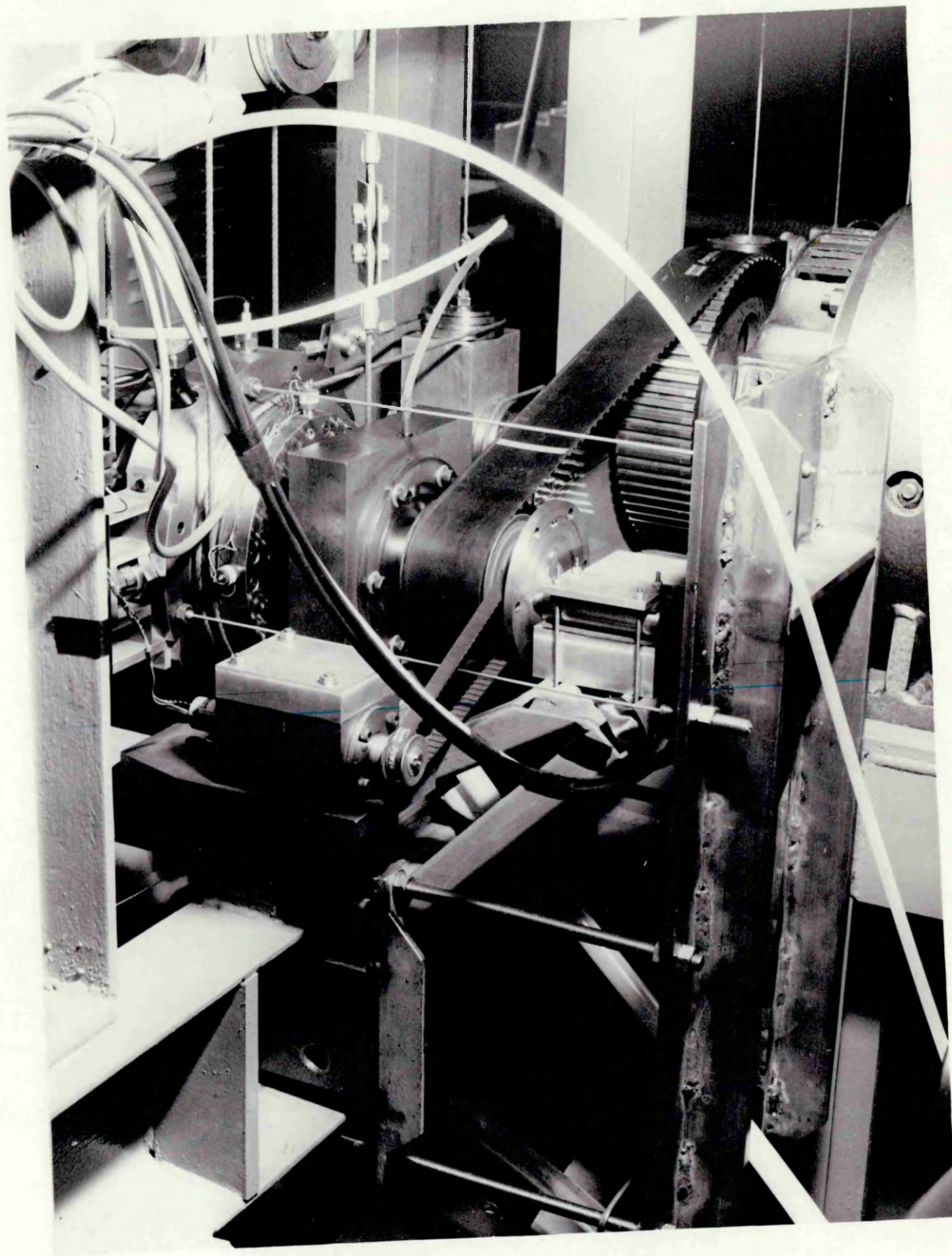


FIGURE 5. REAR VIEW SHOWING BELT DRIVES FOR TEST SHAFT AND SINE WAVE GENERATOR

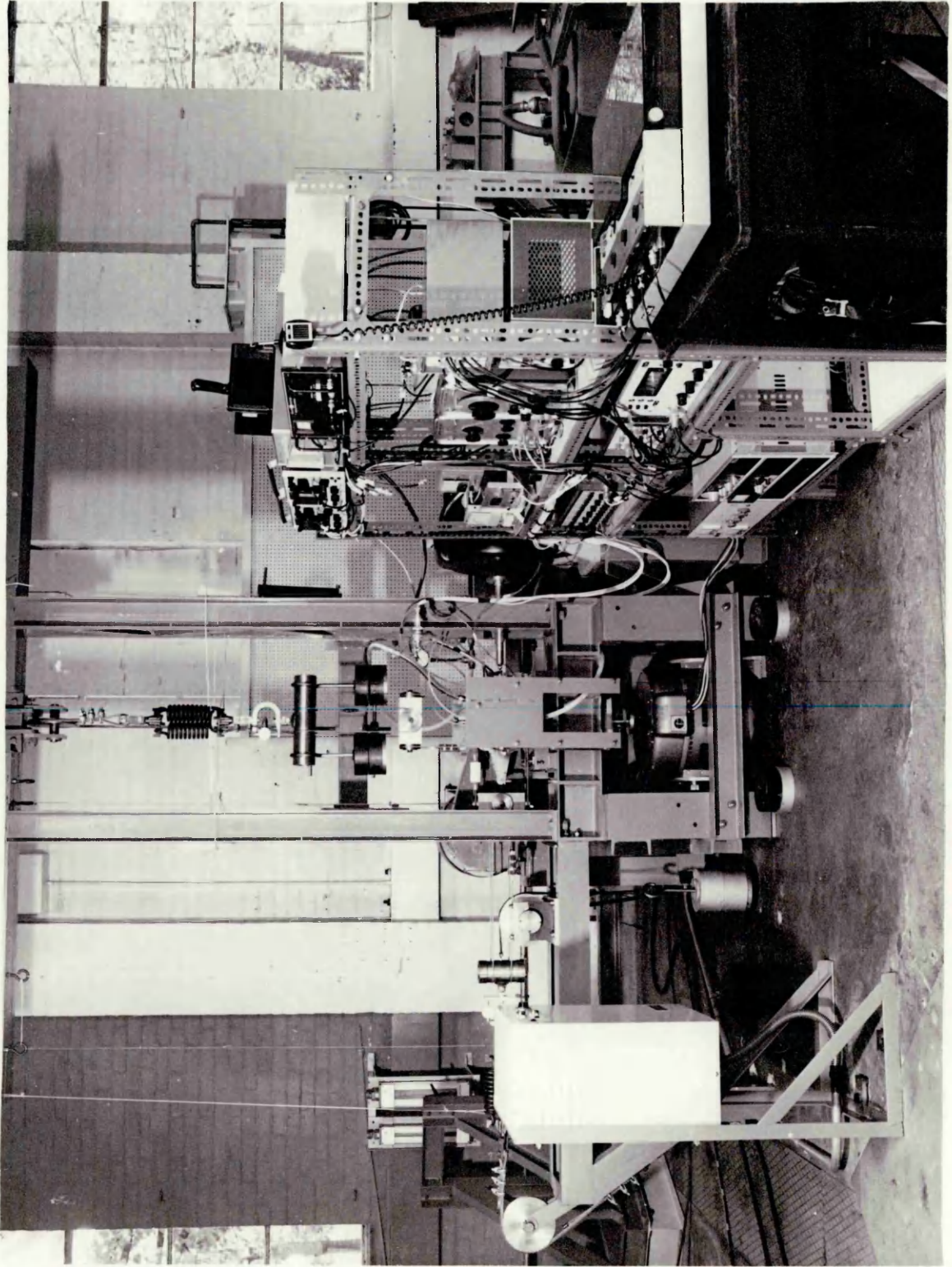


FIGURE 6. VIEW OF TEST RIG AND INSTRUMENTATION

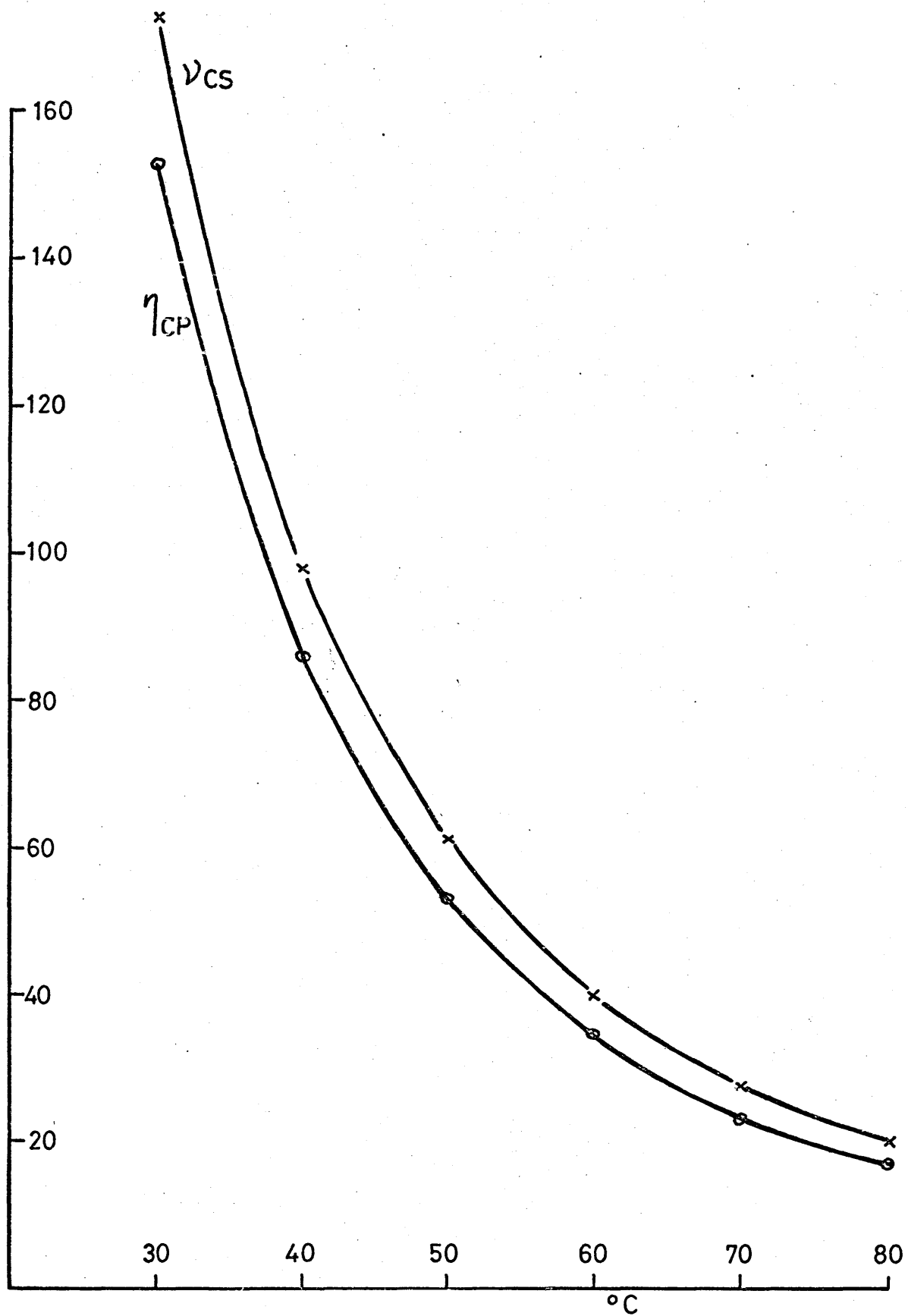


FIGURE 7. LUBRICANT VISCOSITY - TEMPERATURE CHARACTERISTICS

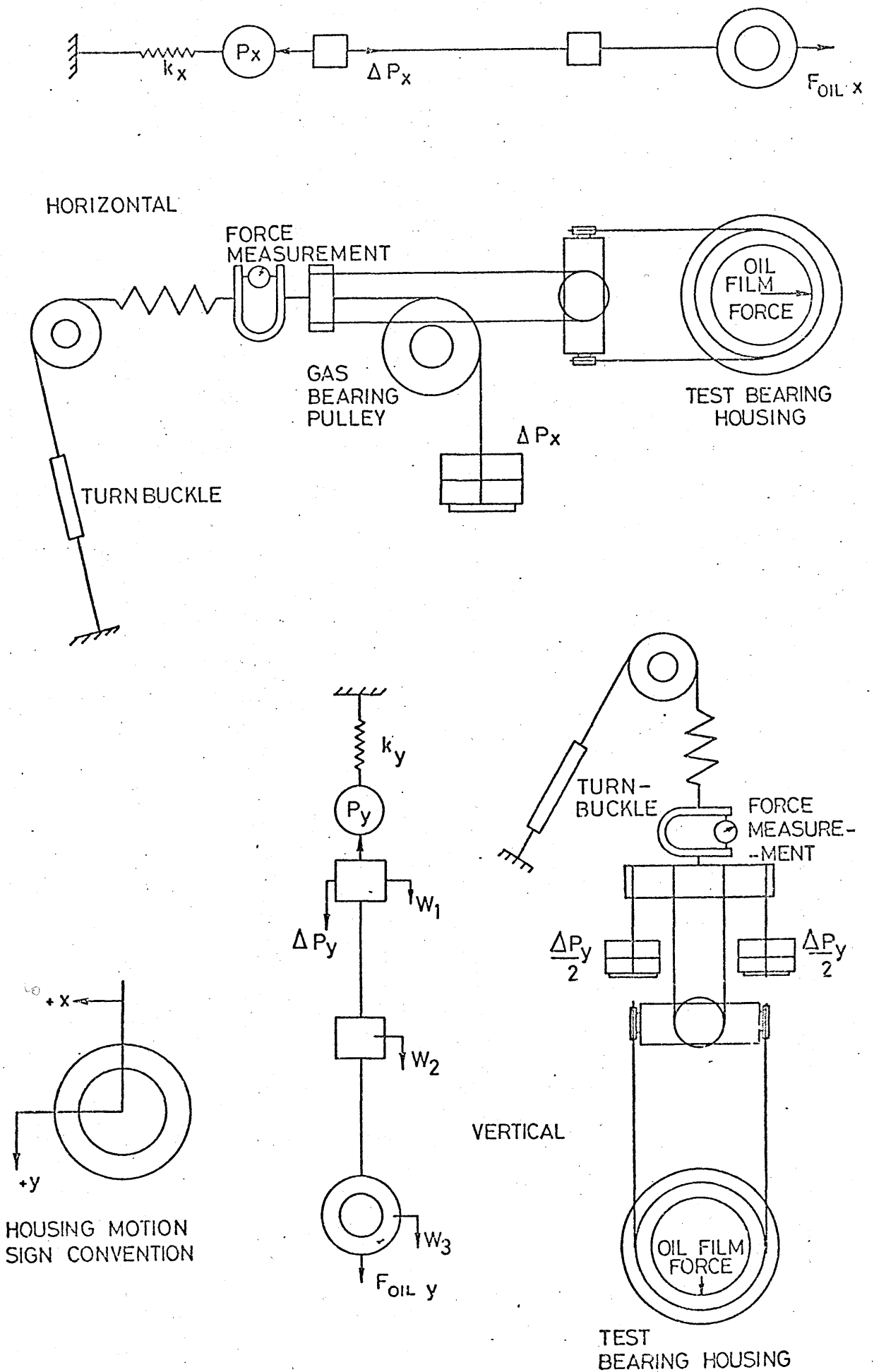


FIGURE 8 STEADY & INCREMENTAL LOADING ARRANGEMENT

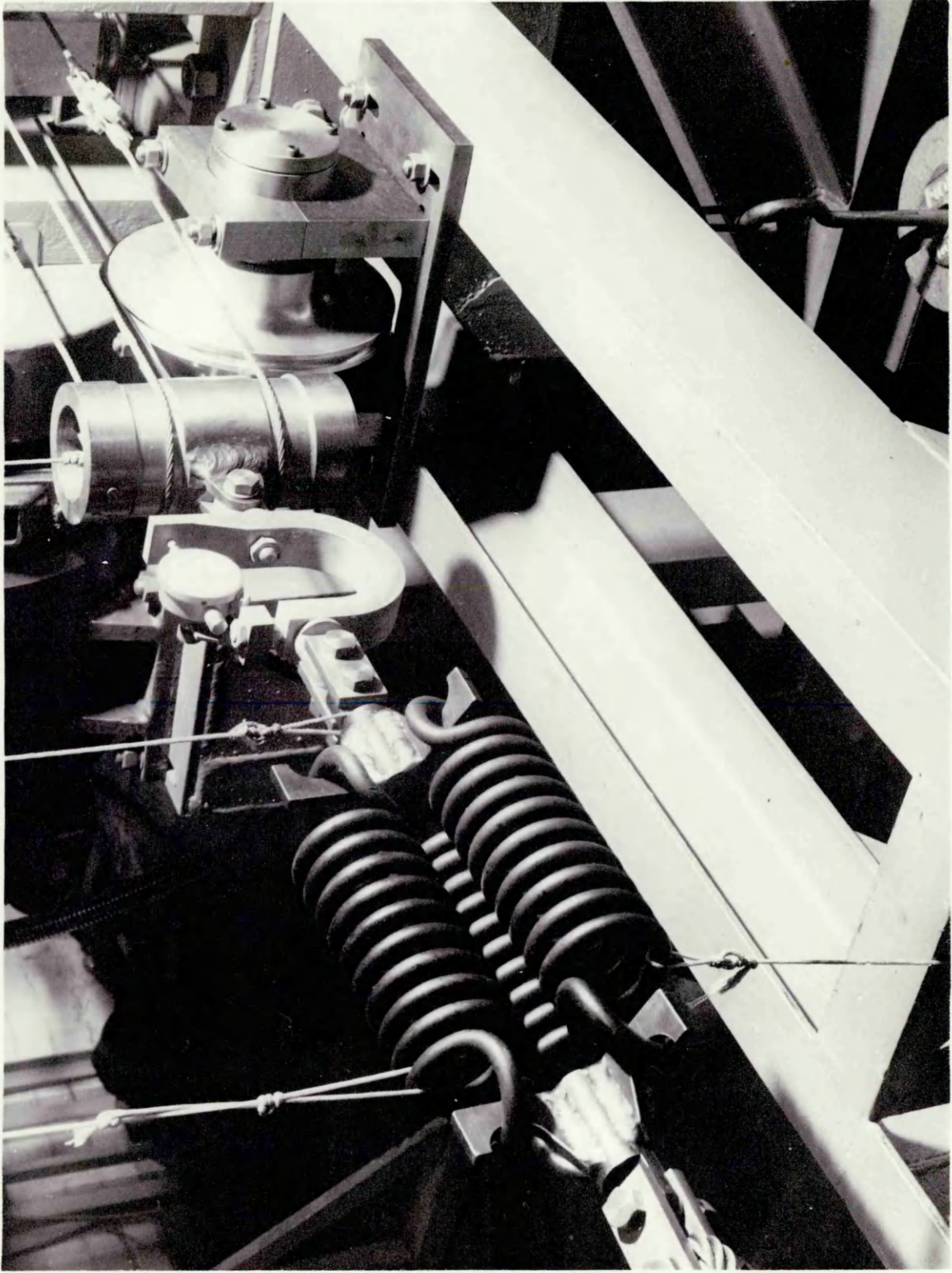


FIGURE 9. HORIZONTAL STEADY LOADING ARRANGEMENT WITH GAS BEARING PULLEY

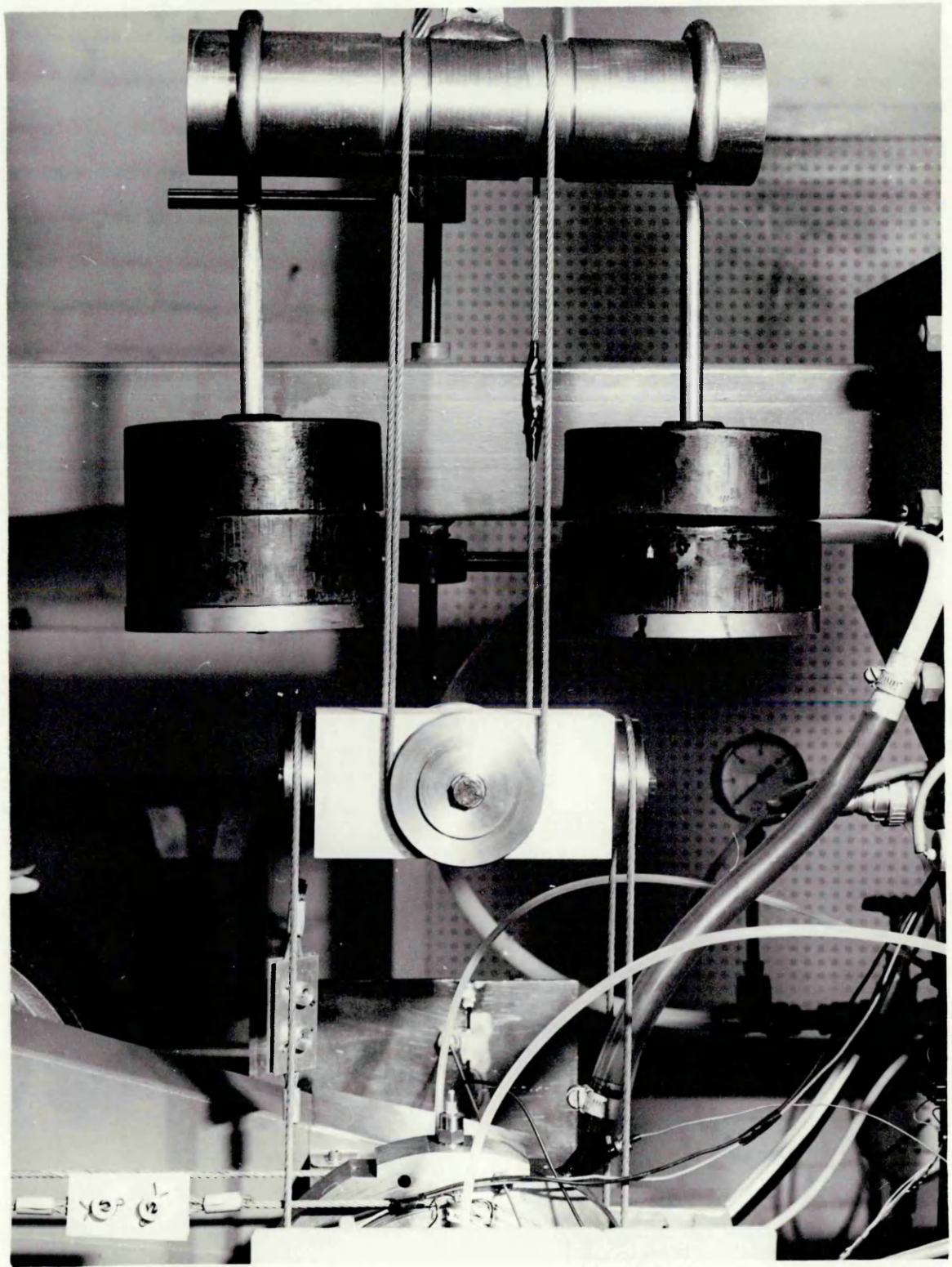


FIGURE 10. VERTICAL STEADY AND INCREMENTAL LOADING ARRANGEMENTS

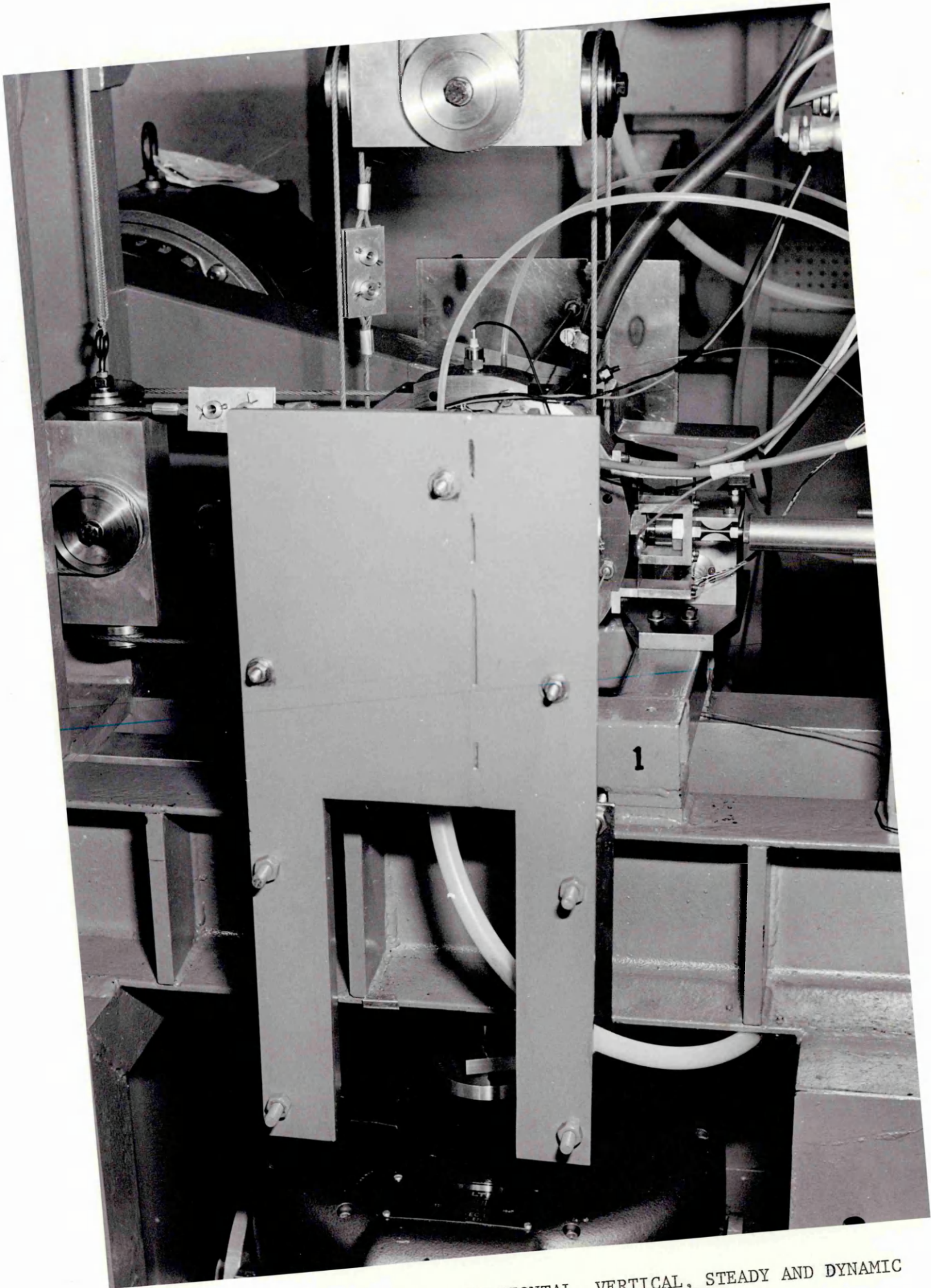


FIGURE 11. PHOTOGRAPH SHOWING HORIZONTAL, VERTICAL, STEADY AND DYNAMIC LOAD ARRANGEMENTS CONNECTED

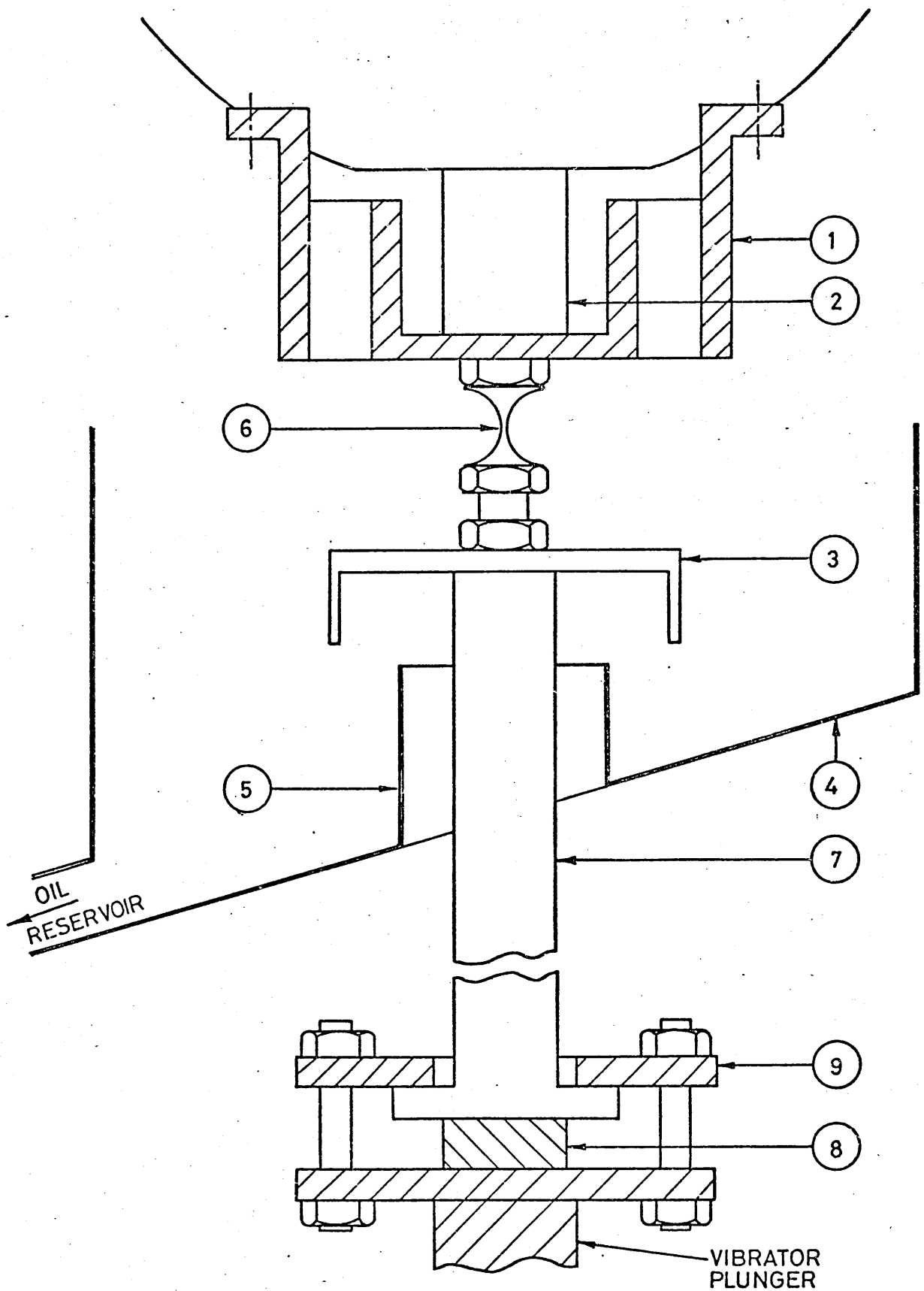


FIGURE 12 CONNECTION TO VERTICAL VIBRATOR AND OIL COLLECTION.

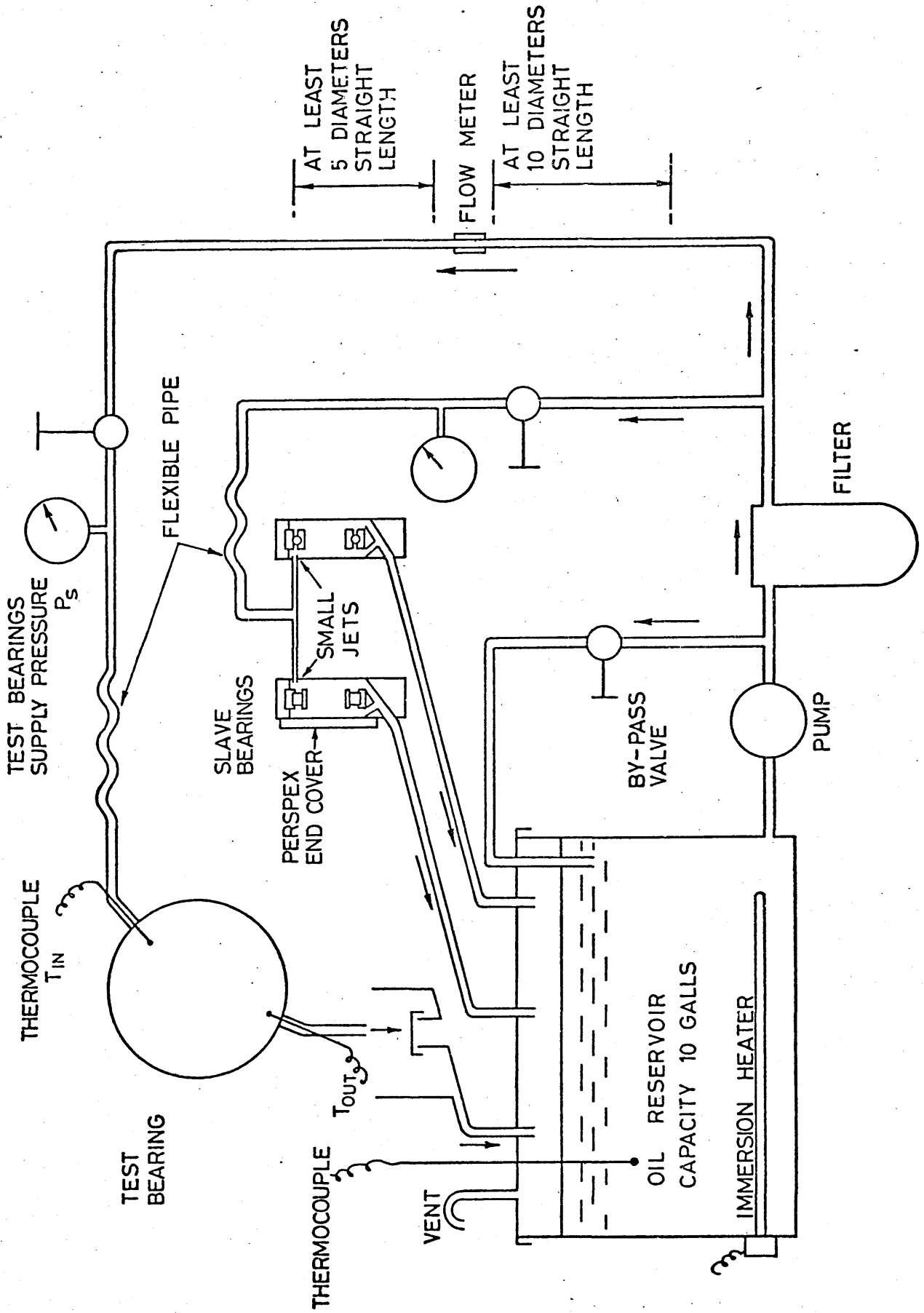


FIGURE 13. OIL SUPPLY CIRCUIT DIAGRAM.

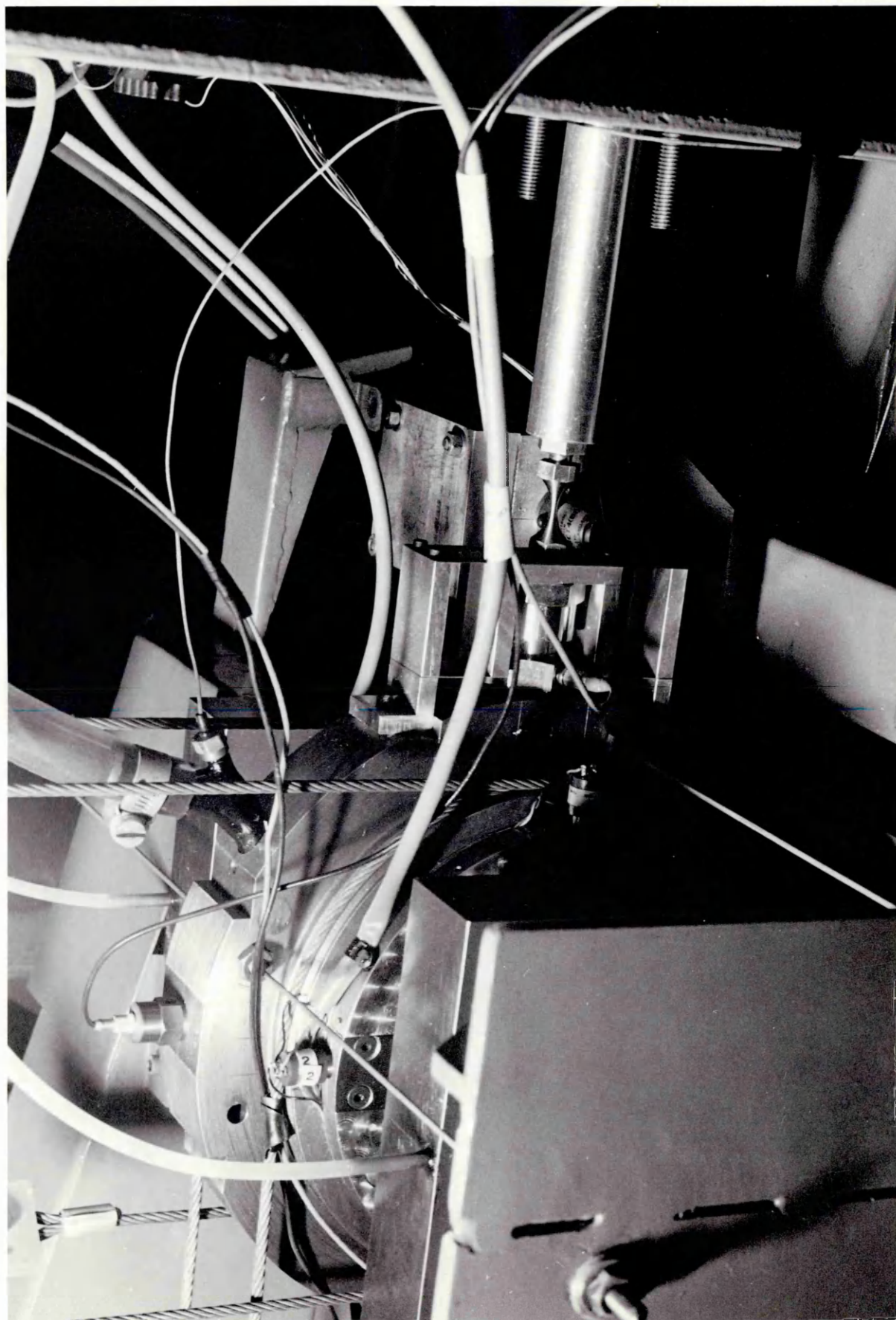


FIGURE 14. HORIZONTAL VIBRATOR CONNECTOR

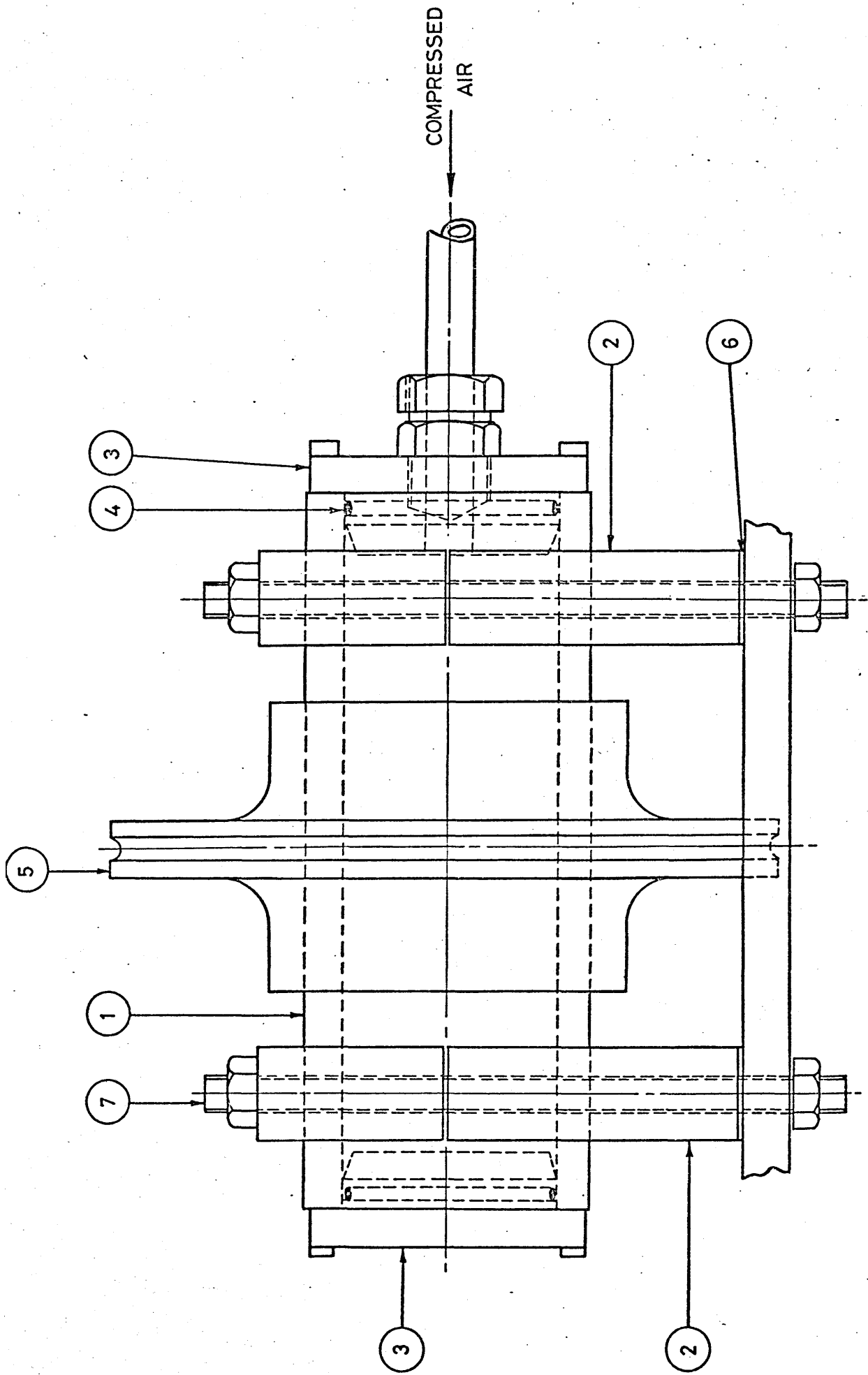


FIGURE 16 CONSTRUCTION OF AIR BEARING PULLEY.

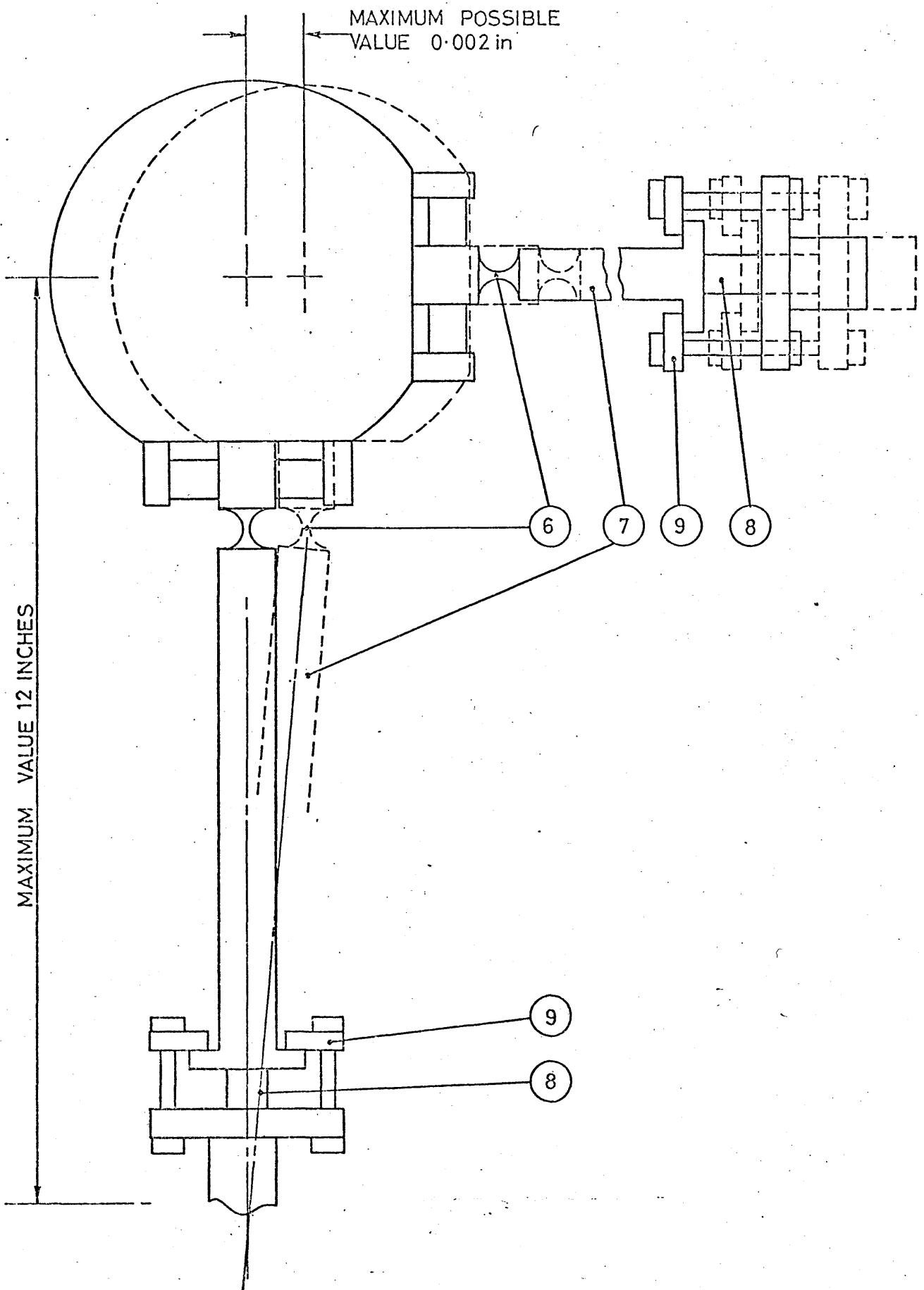


FIGURE 15 ACCOMMODATION OF TEST BEARING HOUSING DISPLACEMENT BY VIBRATOR CONNECTORS.

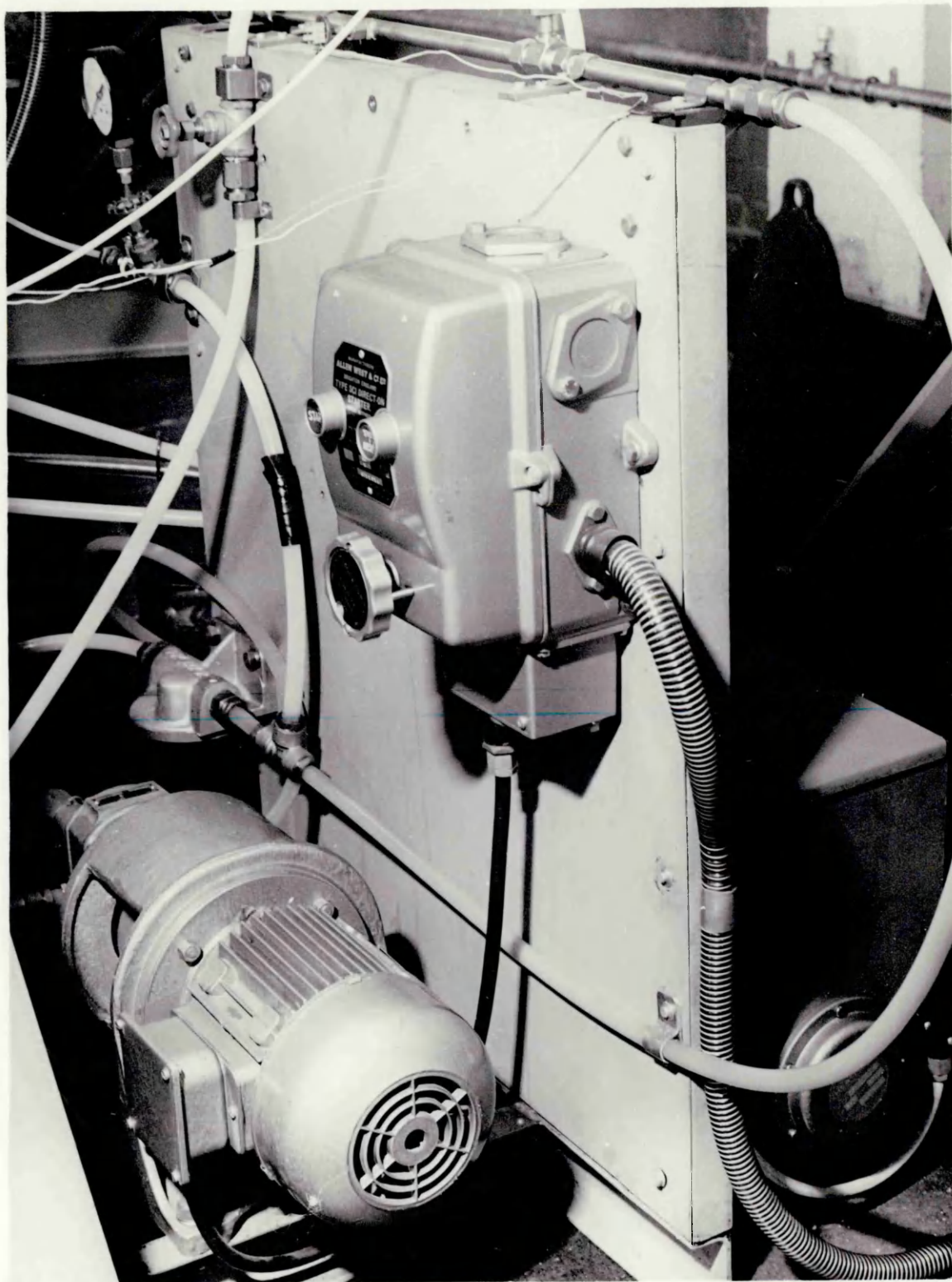


FIGURE 17. OIL SUPPLY UNIT

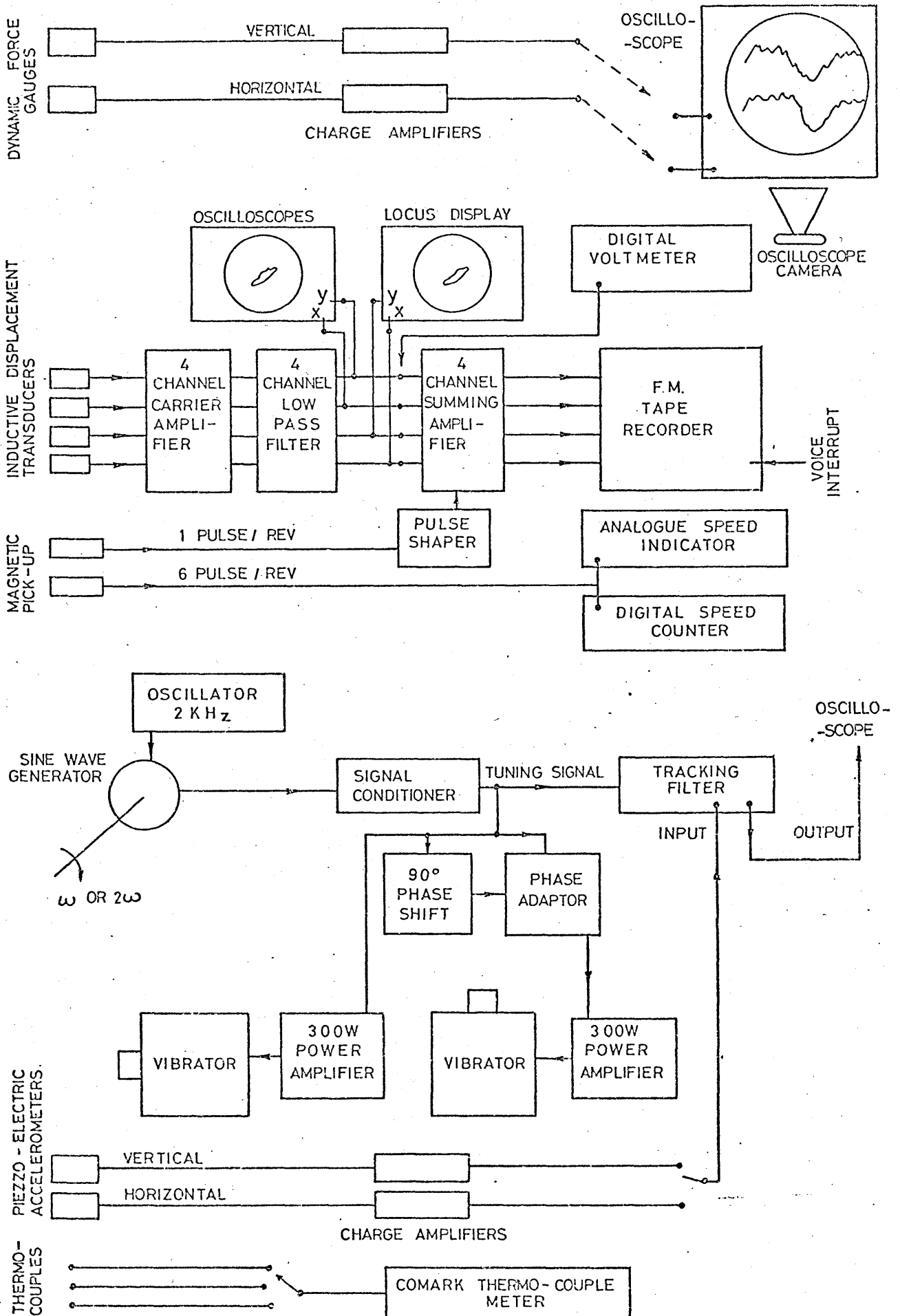


FIGURE 18 INSTRUMENTATION BLOCK DIAGRAM.

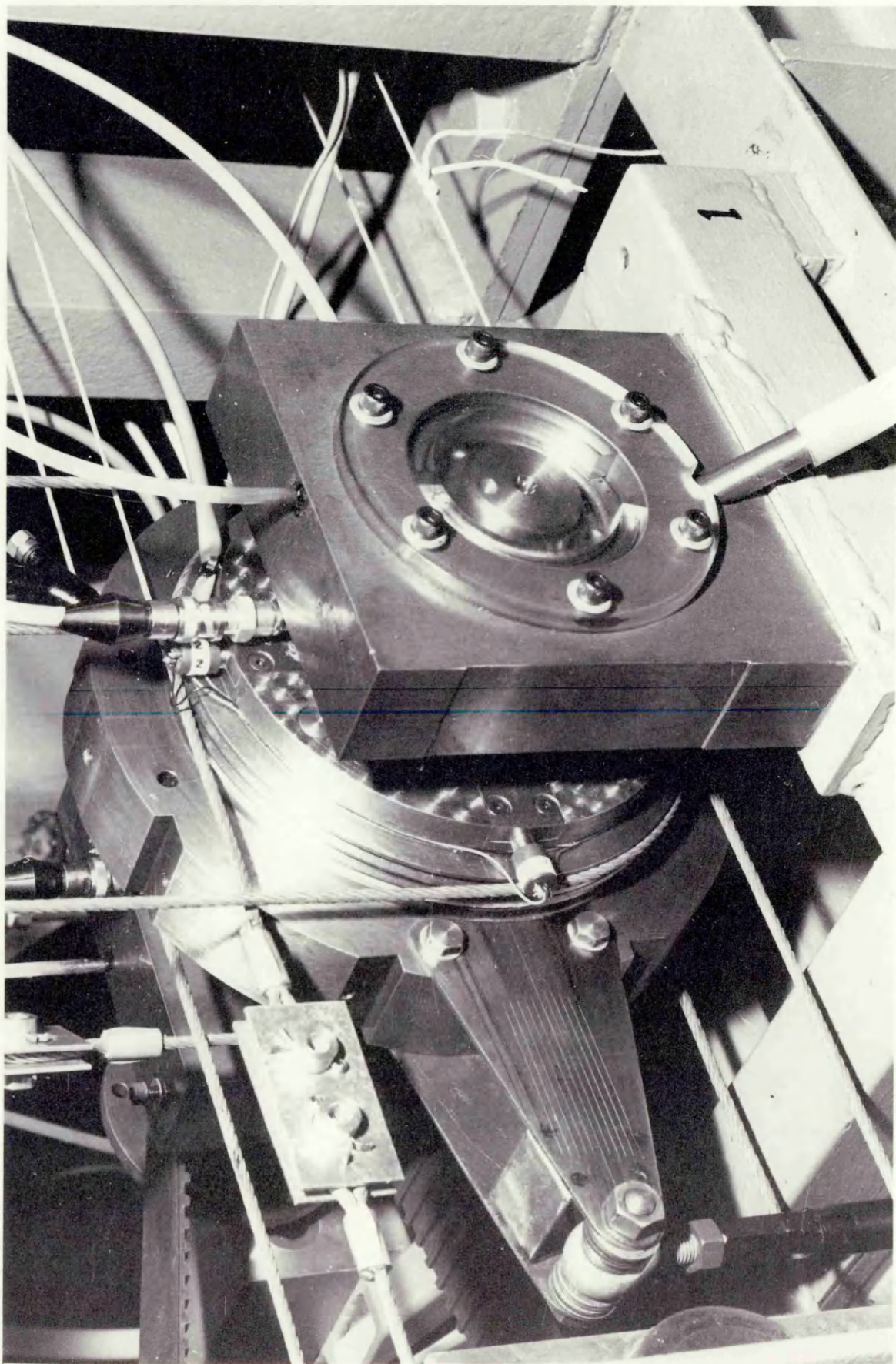


FIGURE 19. MOUNTING OF CAPACITANCE DISPLACEMENT TRANSDUCERS

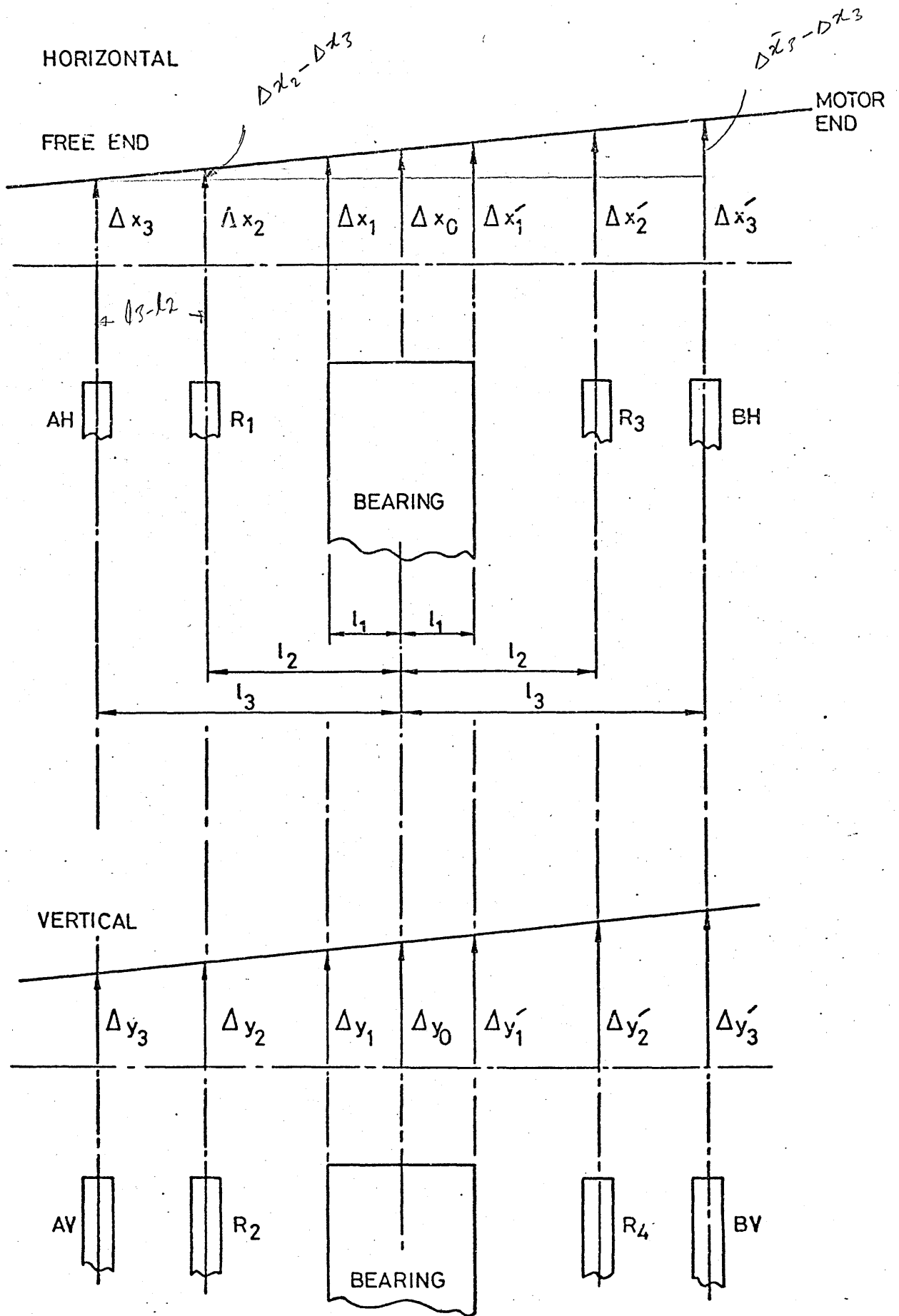


FIGURE 20 CO ORDINATE SYSTEM FOR DISPLACEMENT TRANSDUCER CALIBRATION

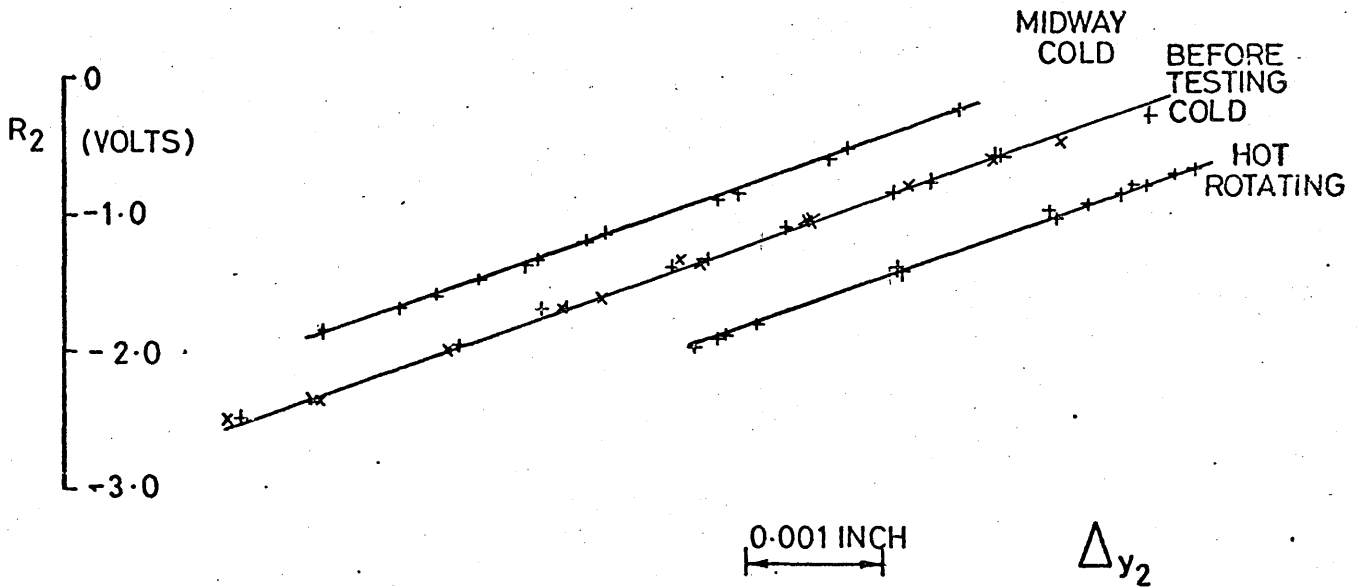
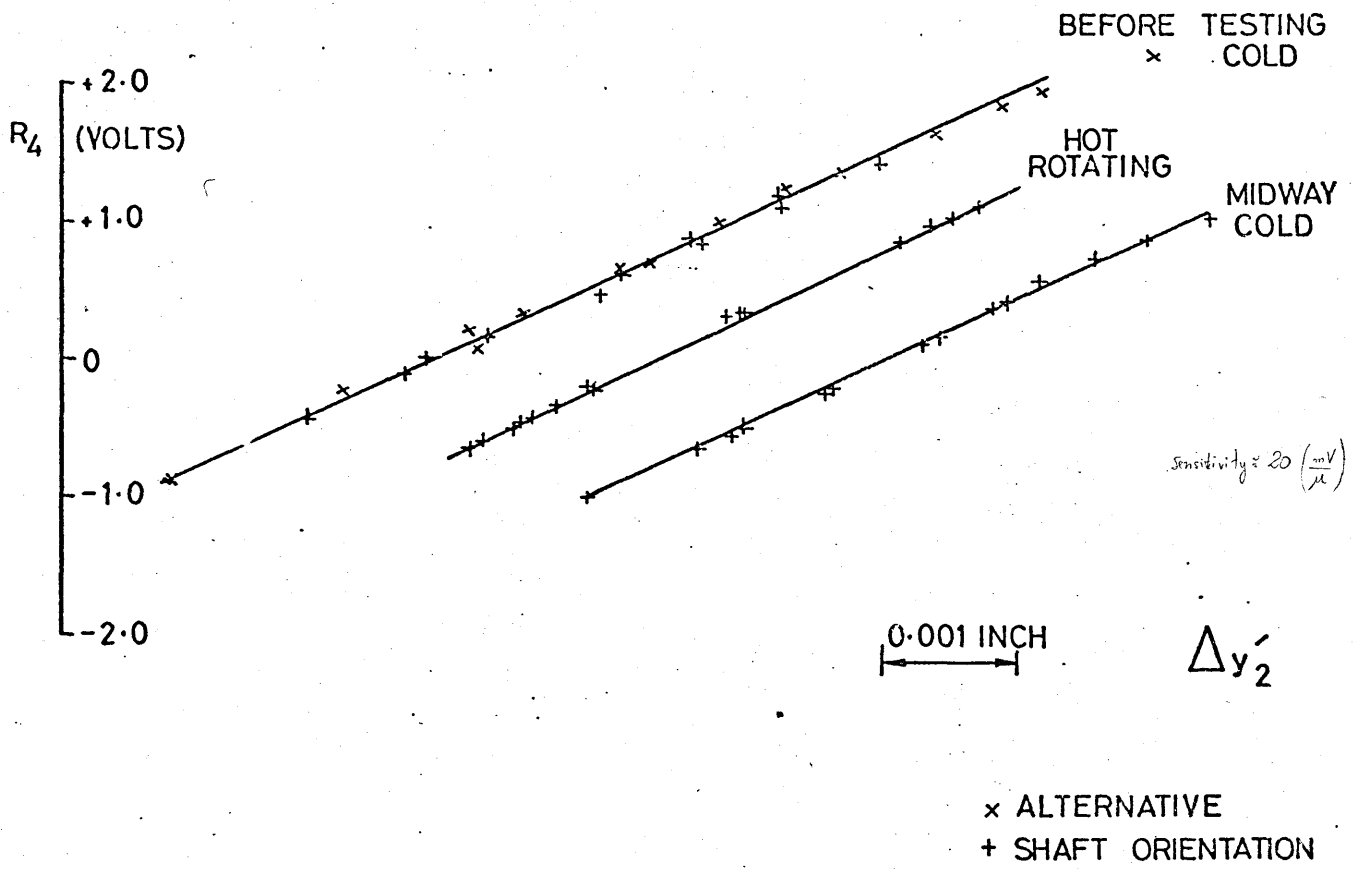


FIGURE 21 INDUCTIVE DISPLACEMENT TRANSDUCER CALIBRATION - VERTICAL.

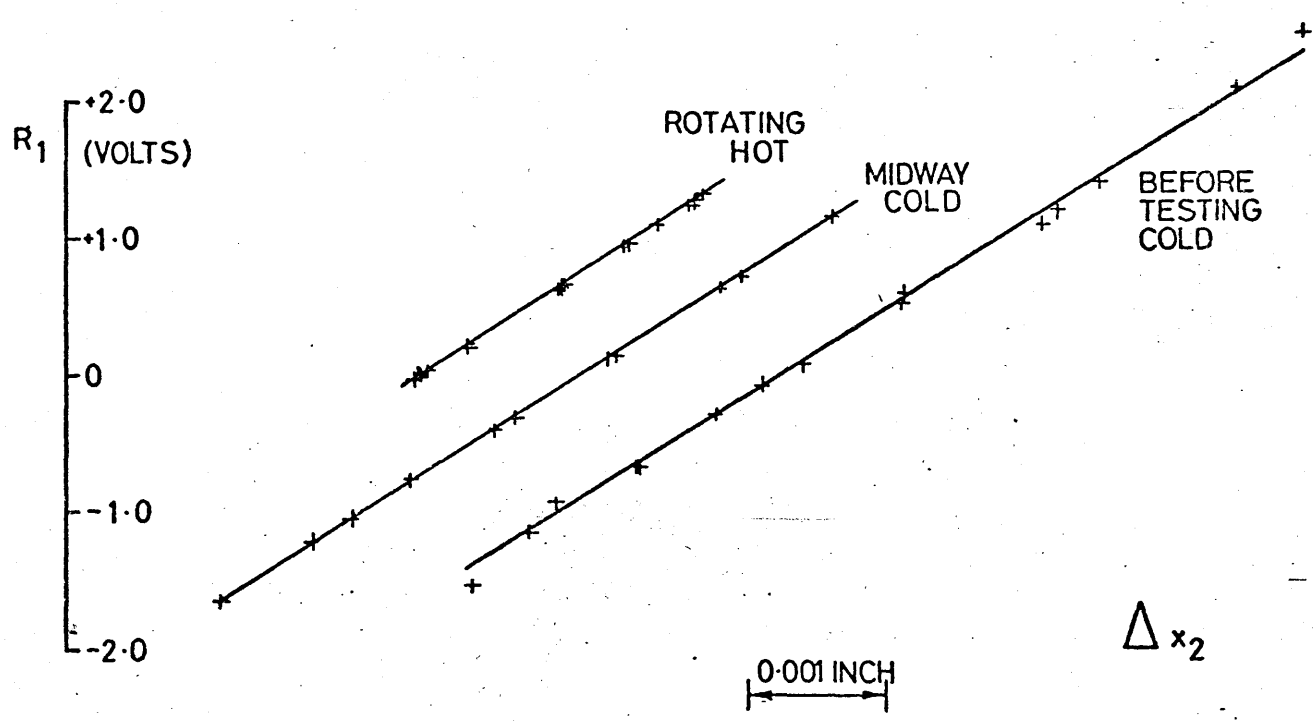
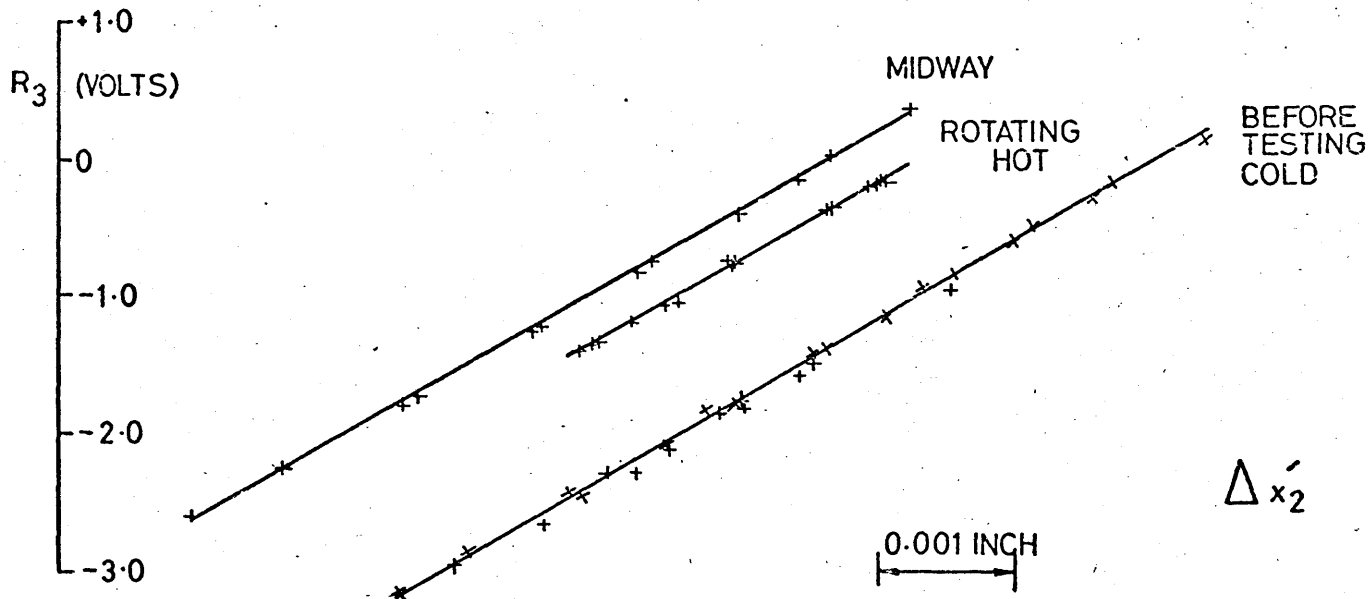


FIGURE 22 INDUCTIVE DISPLACEMENT TRANSDUCER CALIBRATION - HORIZONTAL

+ PARALLEL METHOD

x INCLINED METHOD

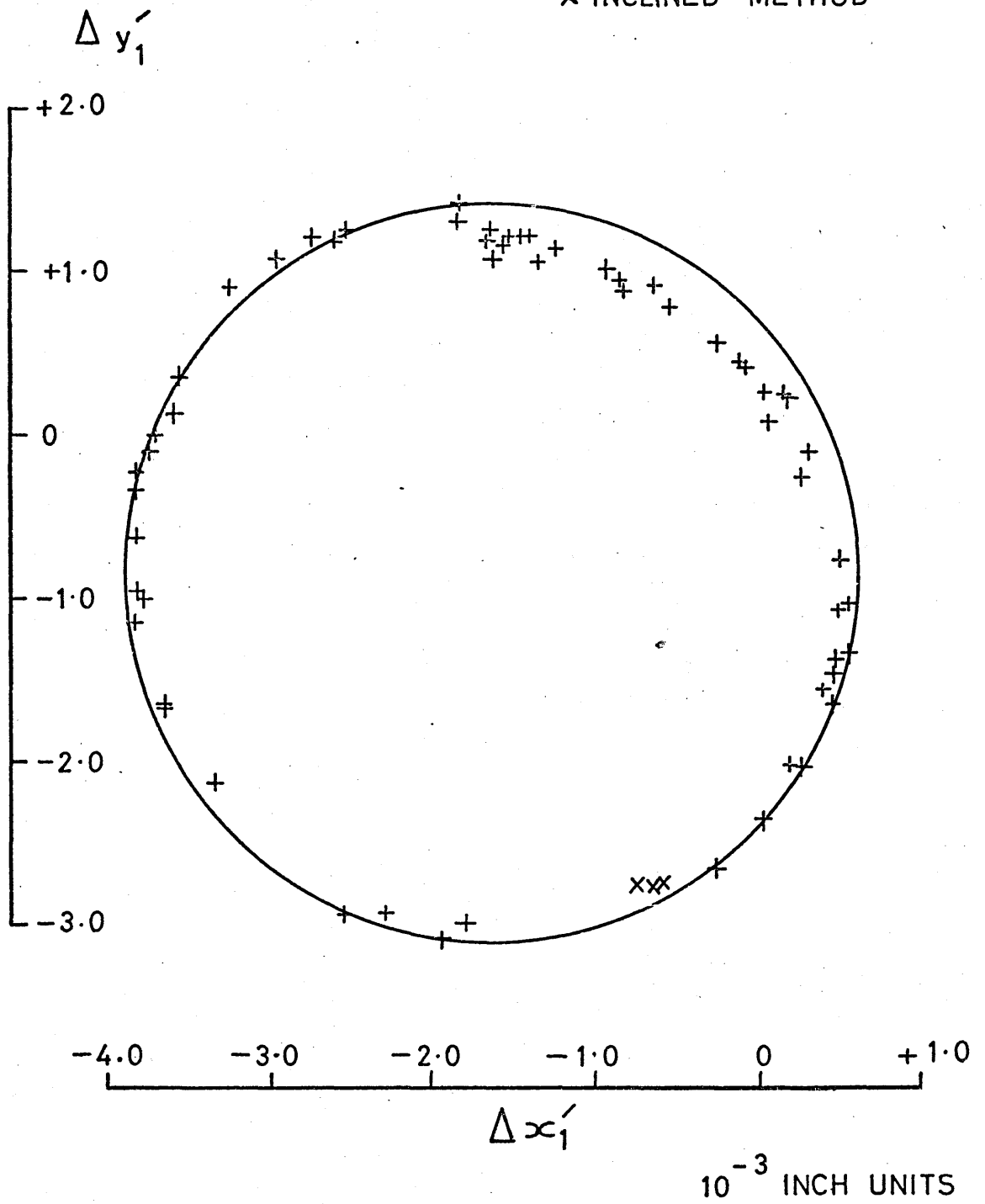
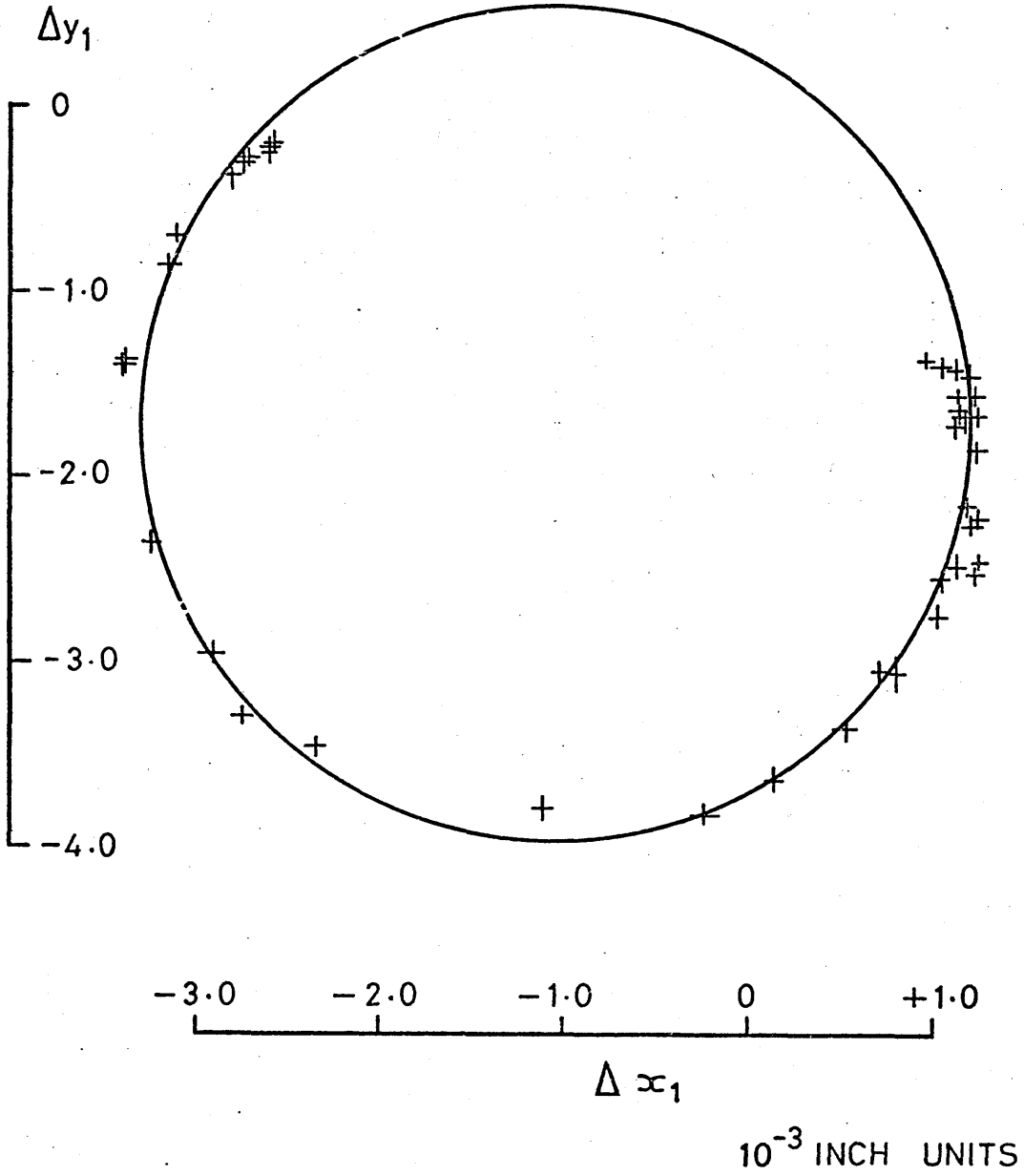


FIGURE 23 MEASURED CLEARANCE CIRCLE - MOTOR END.

+ PARALLEL METHODS
x INCLINED METHOD

xxx



$$C_r = 2.25 \cdot 10^{-3} \text{ INCH}$$

FIGURE 24 MEASURED CLEARANCE CIRCLE - FREE END.

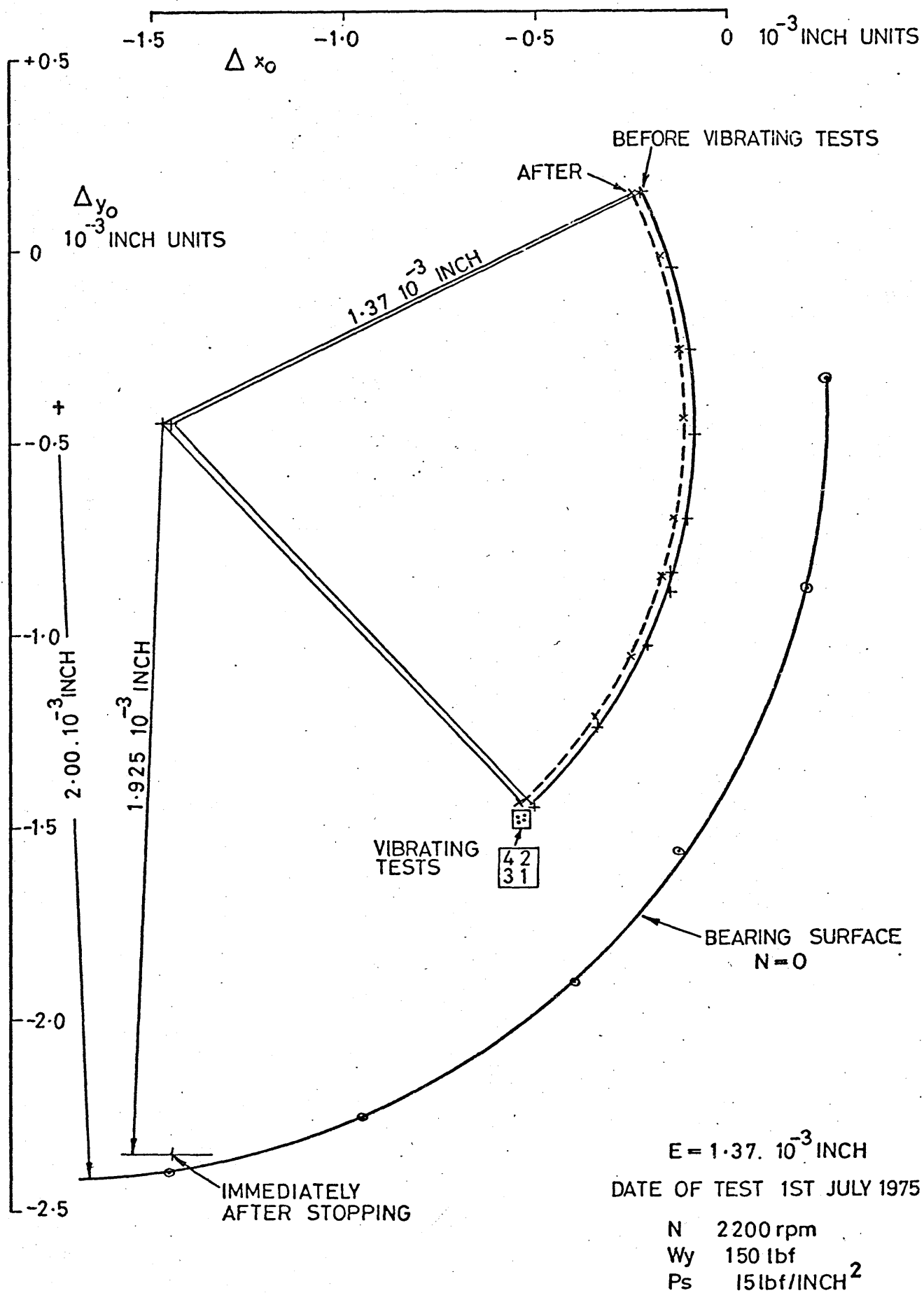


FIGURE 25 ECCENTRICITY AND LOCATION OF BEARING CENTRE - LOW ECCENTRICITY.

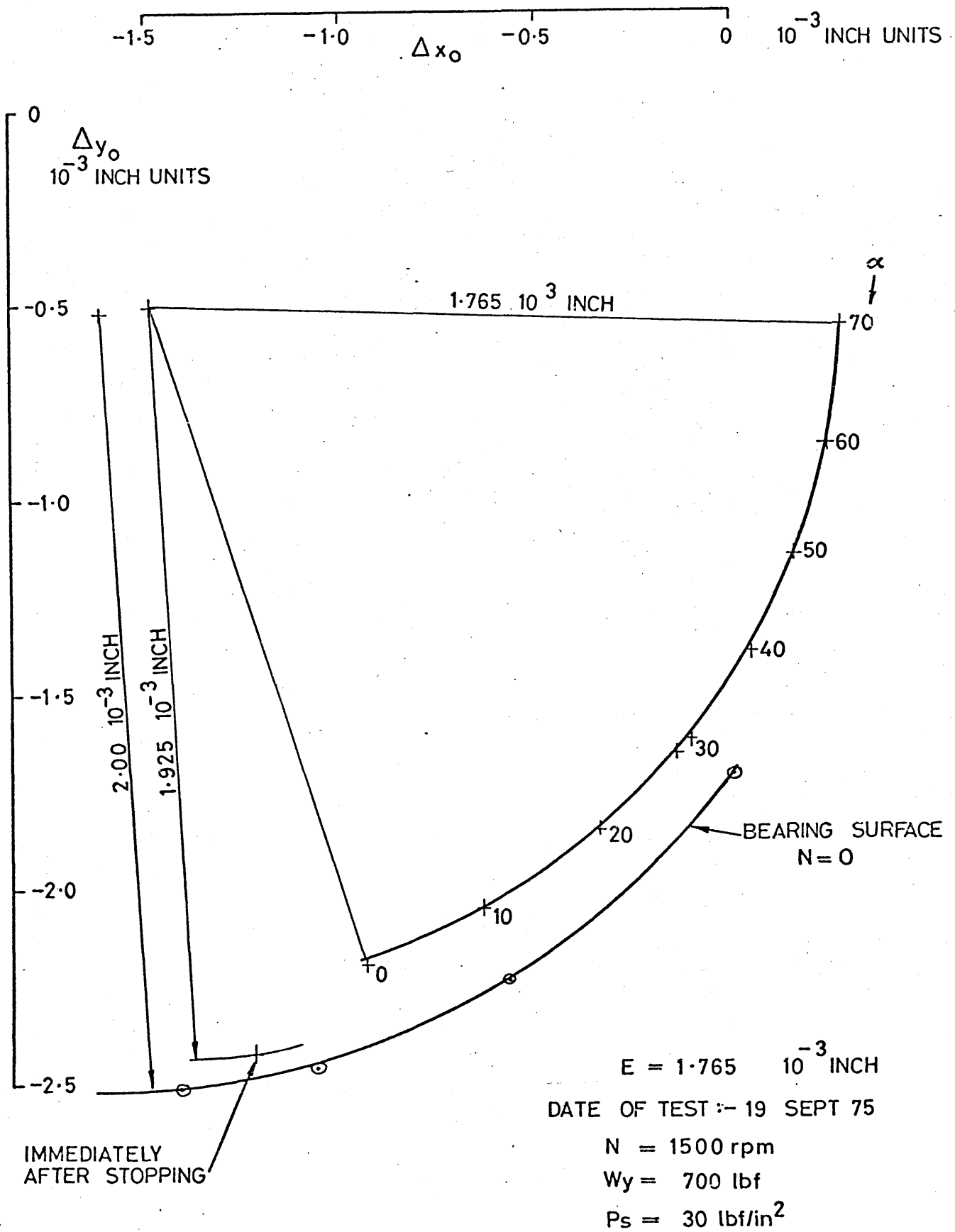
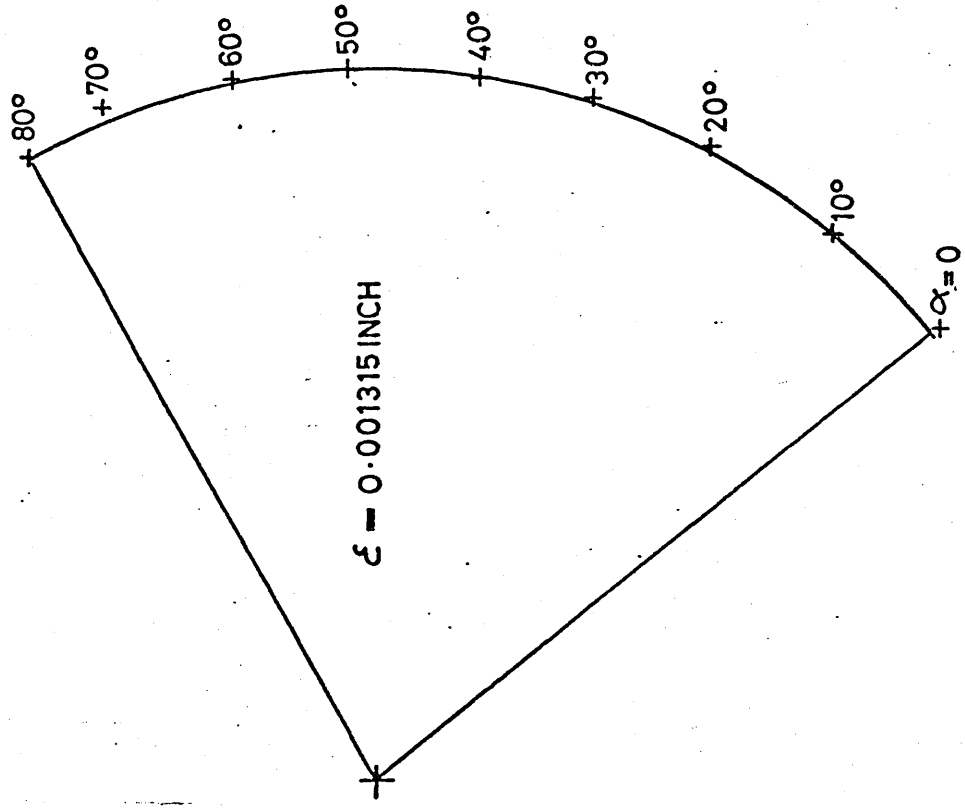
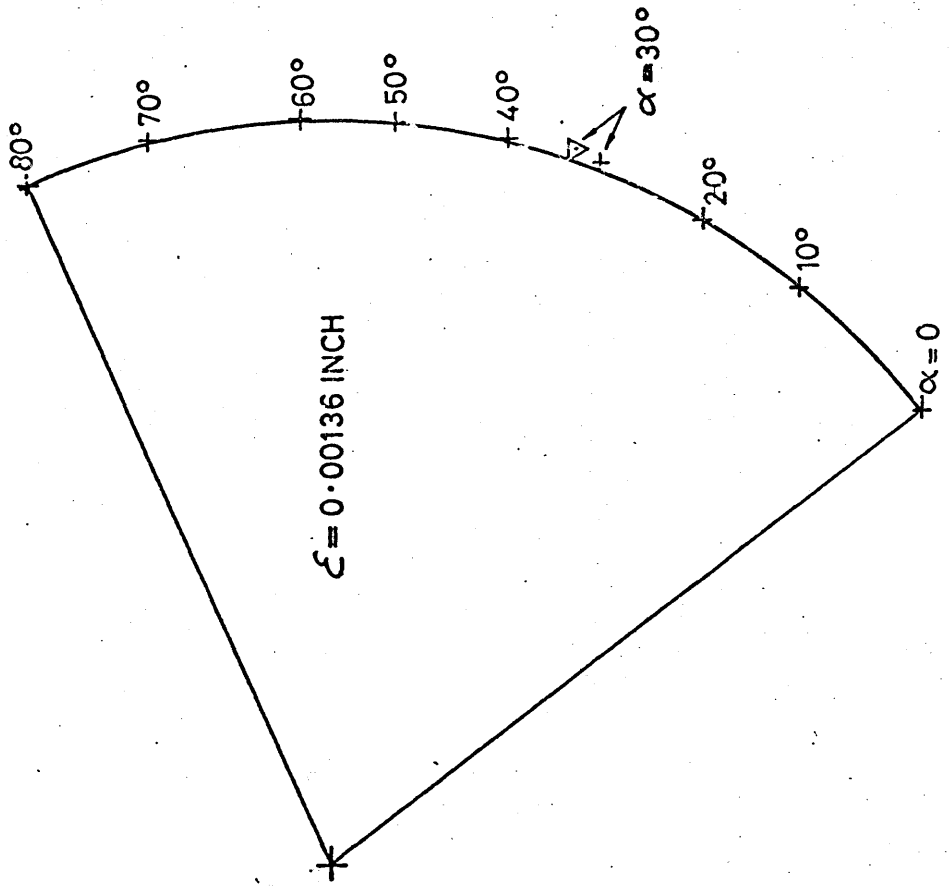


FIGURE 26 ECCENTRICITY AND LOCATION OF BEARING CENTRE — LARGE ECCENTRICITY.

$N = 2900 \text{ rpm}$
 $W_y = 200 \text{ lb/f}$
 $PS = 30 \text{ lb/f}$



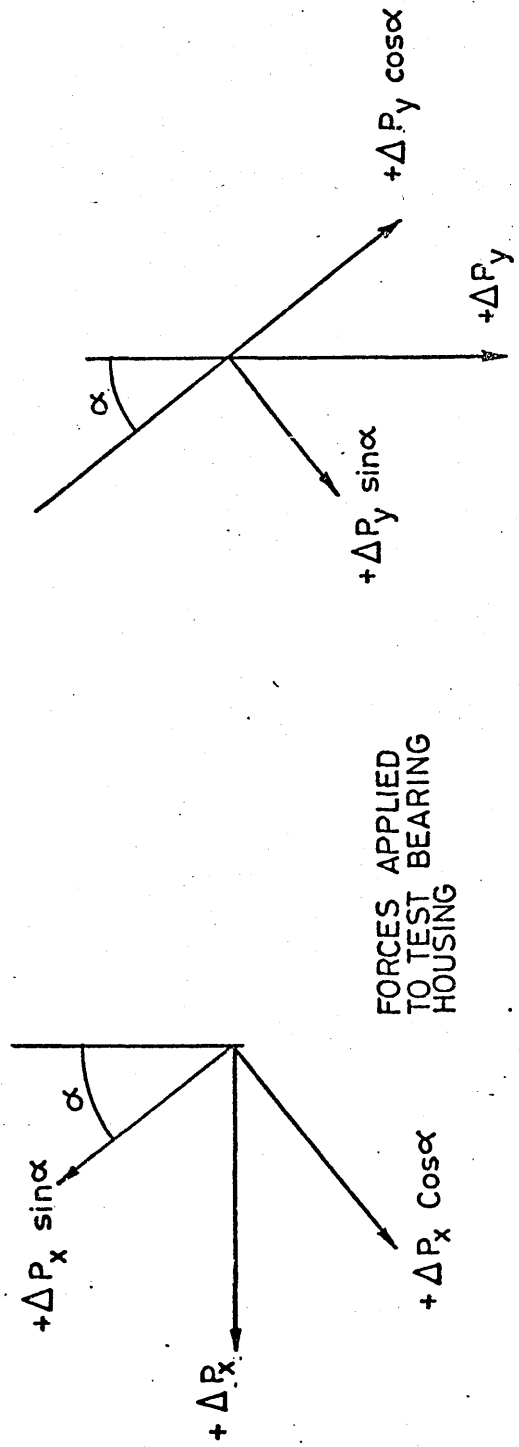
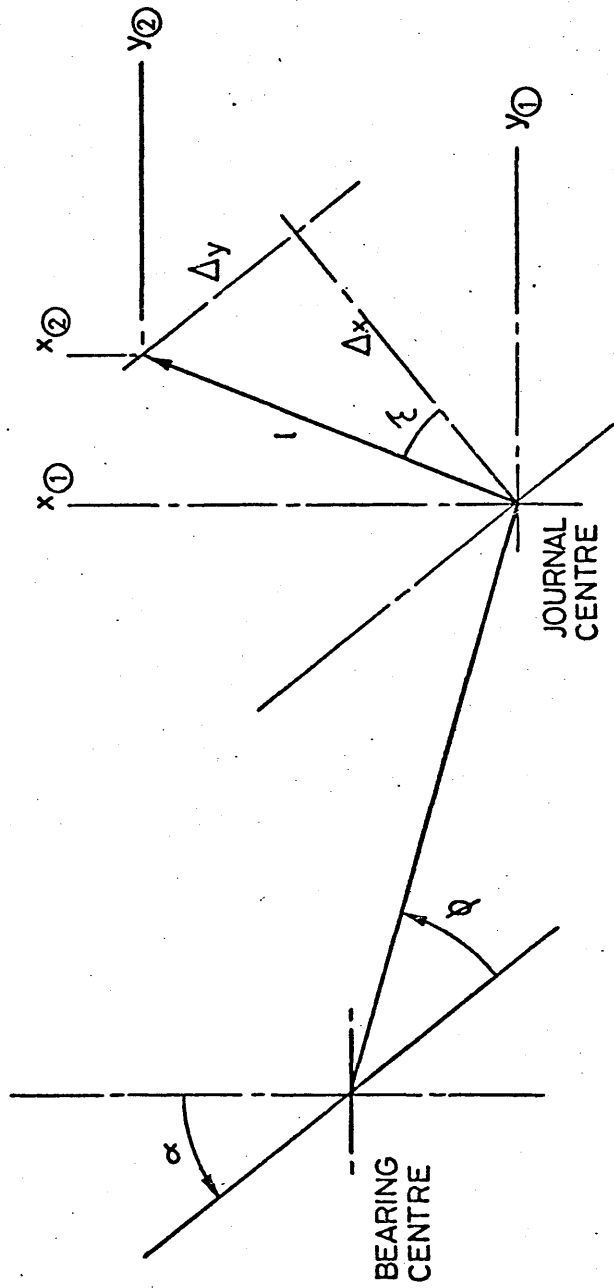
a) VIBRATORS AND TRANSVERSE
 WIRES NOT CONNECTED
 5th FEB 1975



b) TWO VIBRATORS & TRANSVERSE
 WIRES CONNECTED 5th MAY 1975
 ▽ BEFORE CONNECTION $\alpha = 30$

FIGURE 27 EFFECT OF VIBRATOR AND TRANSVERSE WIRE CONNECTION

RELATIVE JOURNAL DISPLACEMENT



FORCES APPLIED TO TEST BEARING HOUSING

FIGURE 28 INCREMENTAL LOADING — RELATIVE JOURNAL DISPLACEMENT & FORCES APPLIED TO TEST BEARING HOUSING.

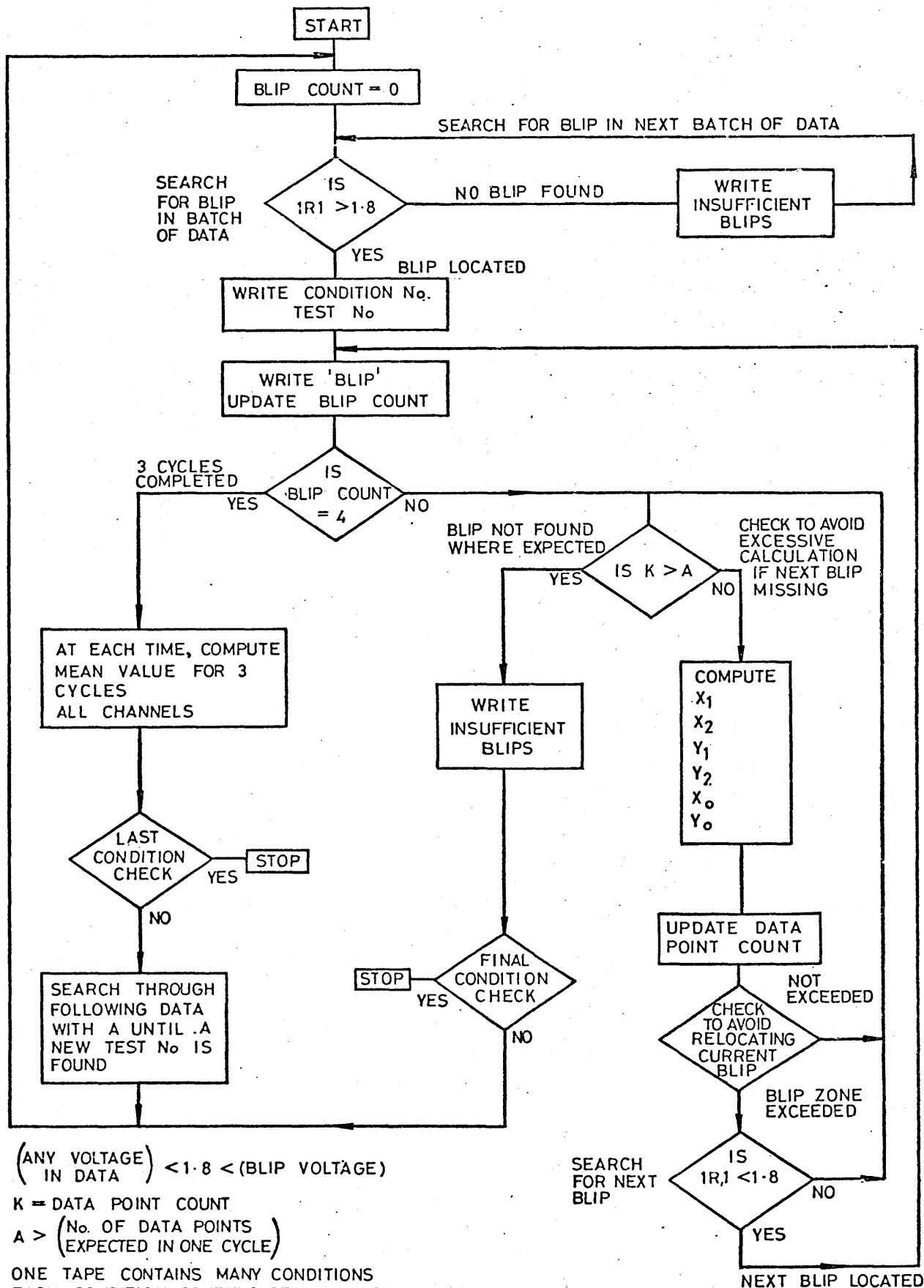


FIGURE 29 FLOW CHART — DIGITISED DATA REDUCTION PROGRAM

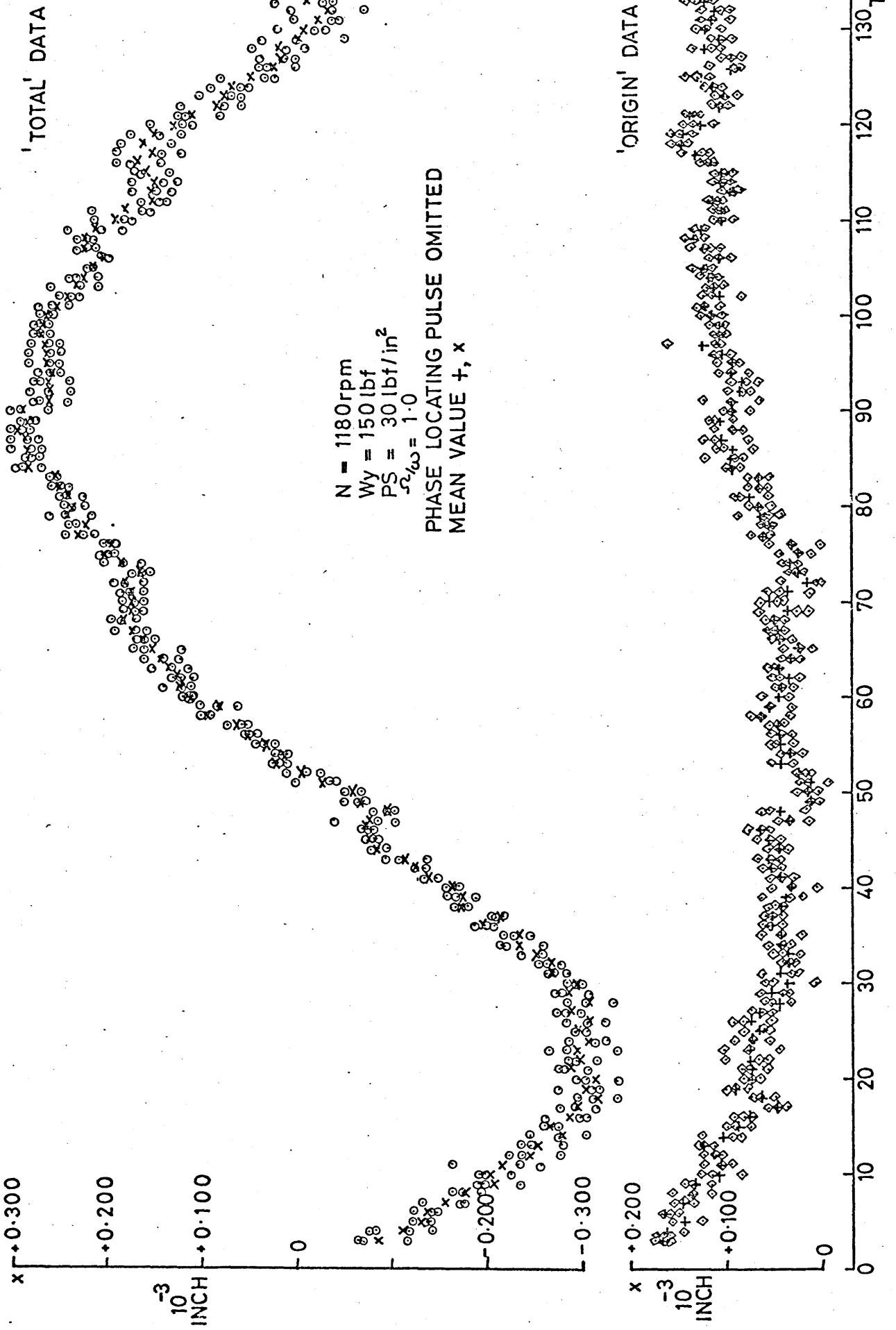


FIGURE 30 EXAMPLE OF MEASURED JOURNAL CENTRE VIBRATION, TEST TYPE 1, HORIZONTAL.

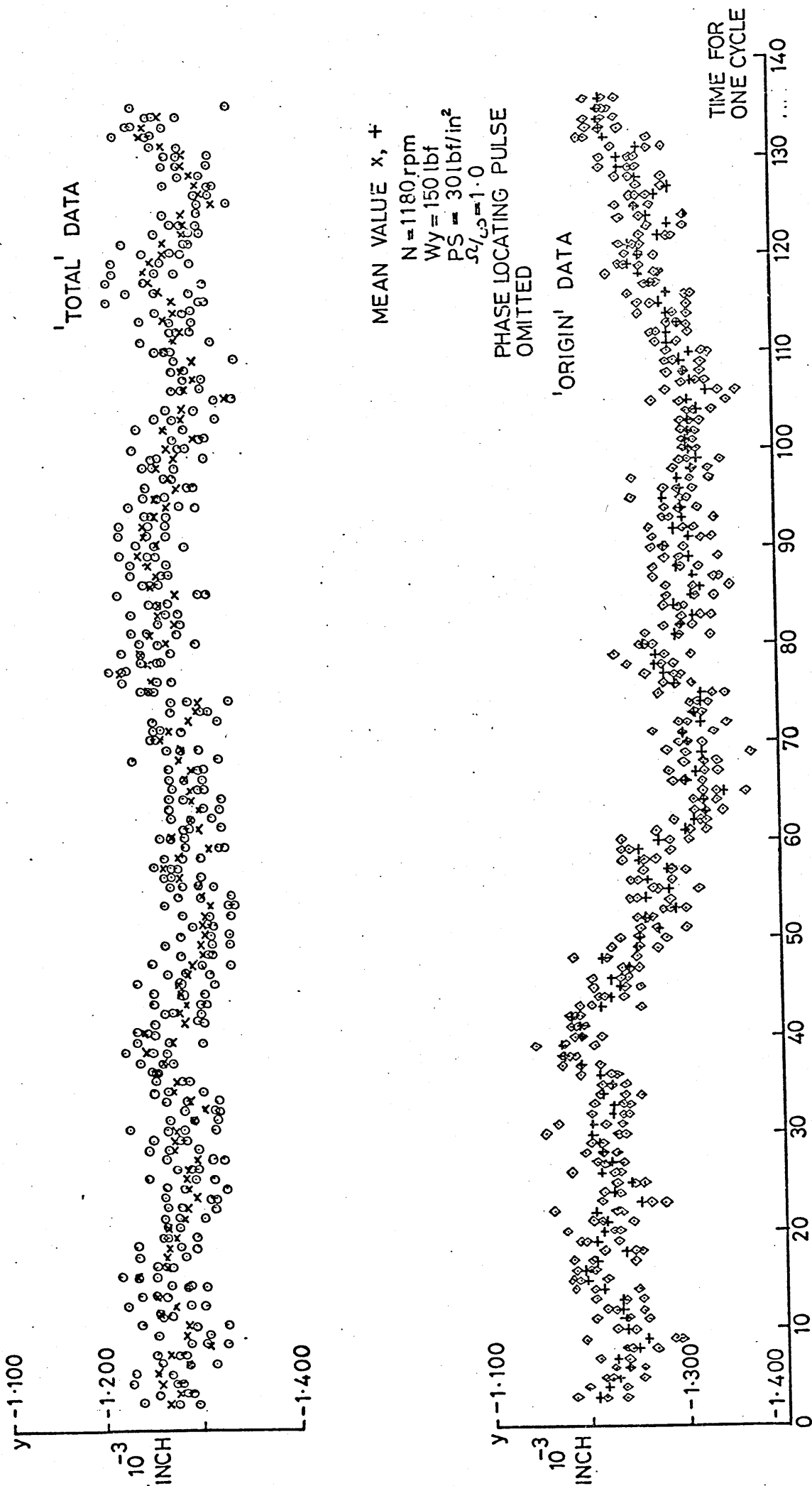


FIGURE 31 EXAMPLE OF MEASURED JOURNAL CENTRE VIBRATION TEST TYPE 1. VERTICAL

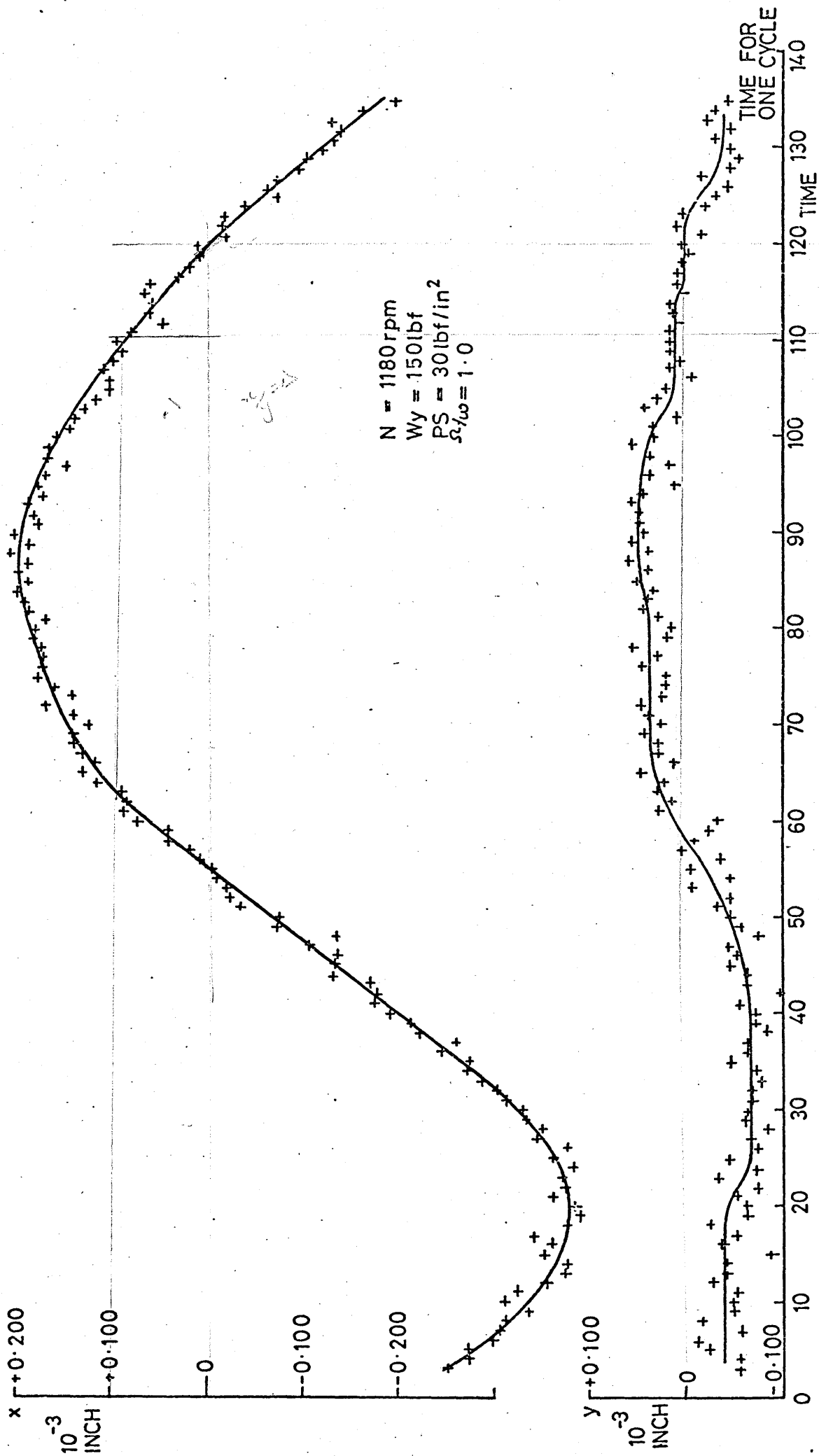


FIGURE 32 EXAMPLE OF JOURNAL CENTRE RESPONSE TO DYNAMIC LOADING TEST TYPE 1

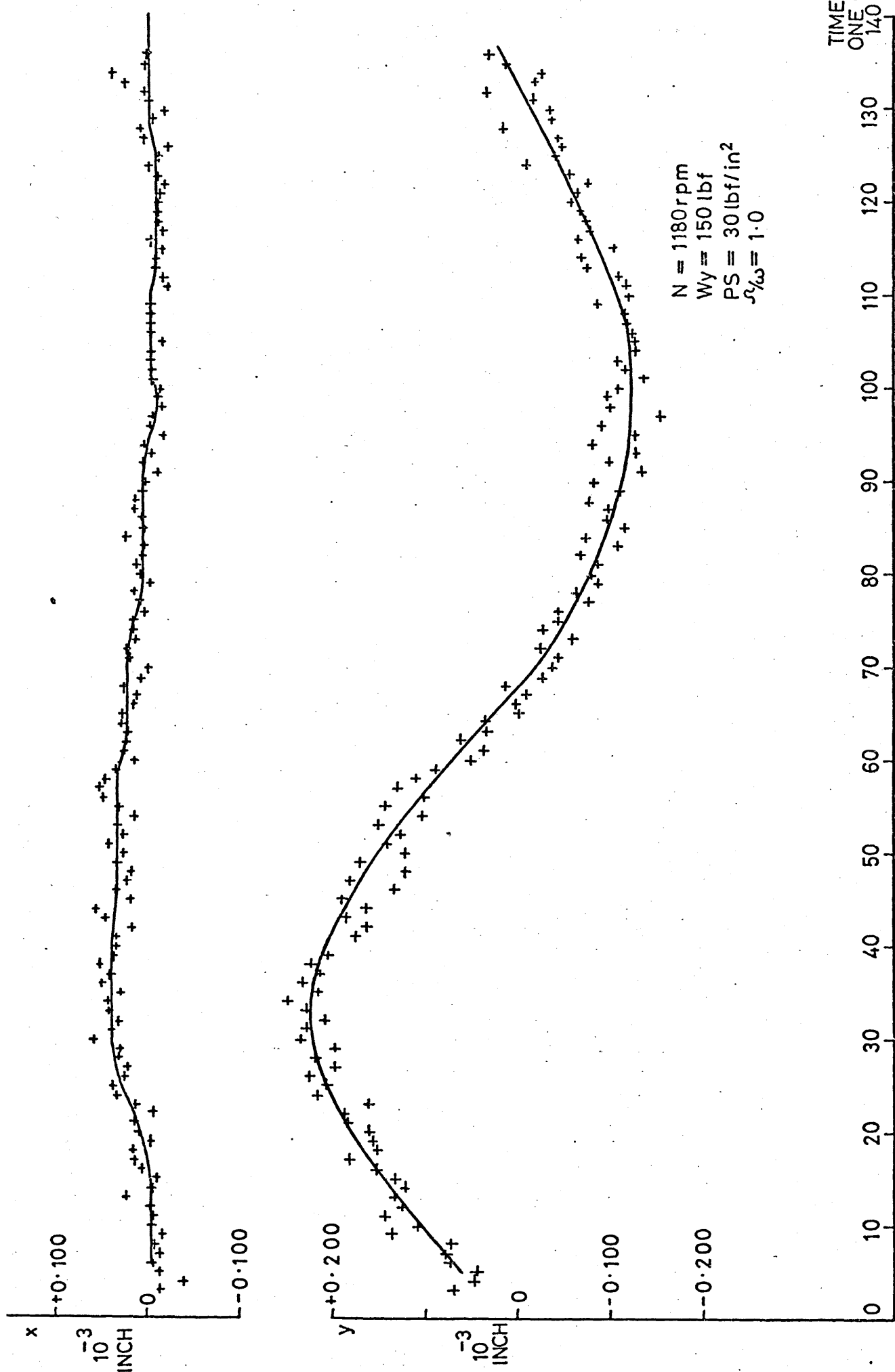


FIGURE 33 EXAMPLE OF JOURNAL CENTRE RESPONSE TO DYNAMIC LOADING, TEST TYPE 2

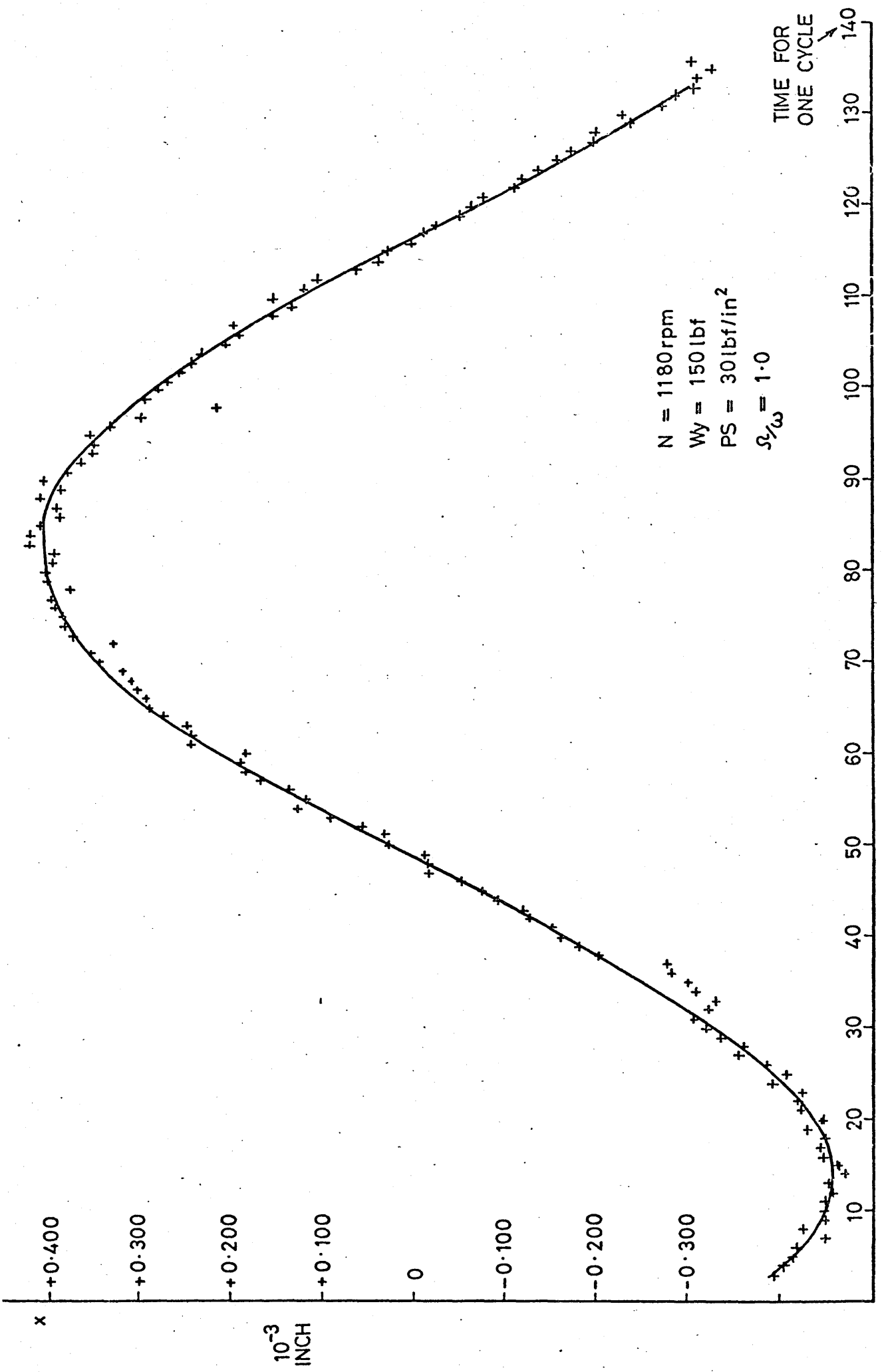


FIGURE 34 EXAMPLE OF JOURNAL CENTRE RESPONSE TO DYNAMIC LOADING, TEST TYPE 3. HORIZONTAL

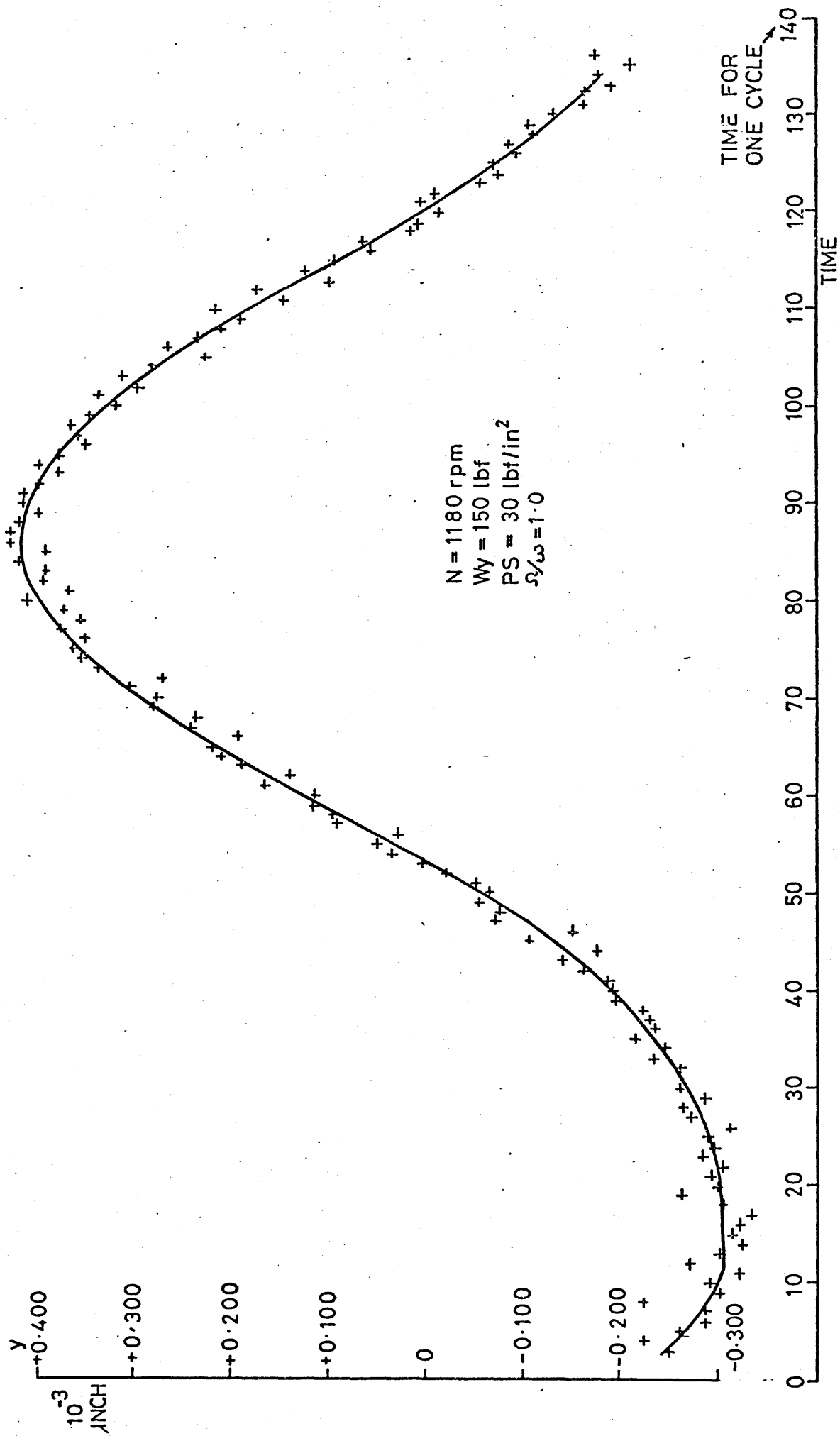
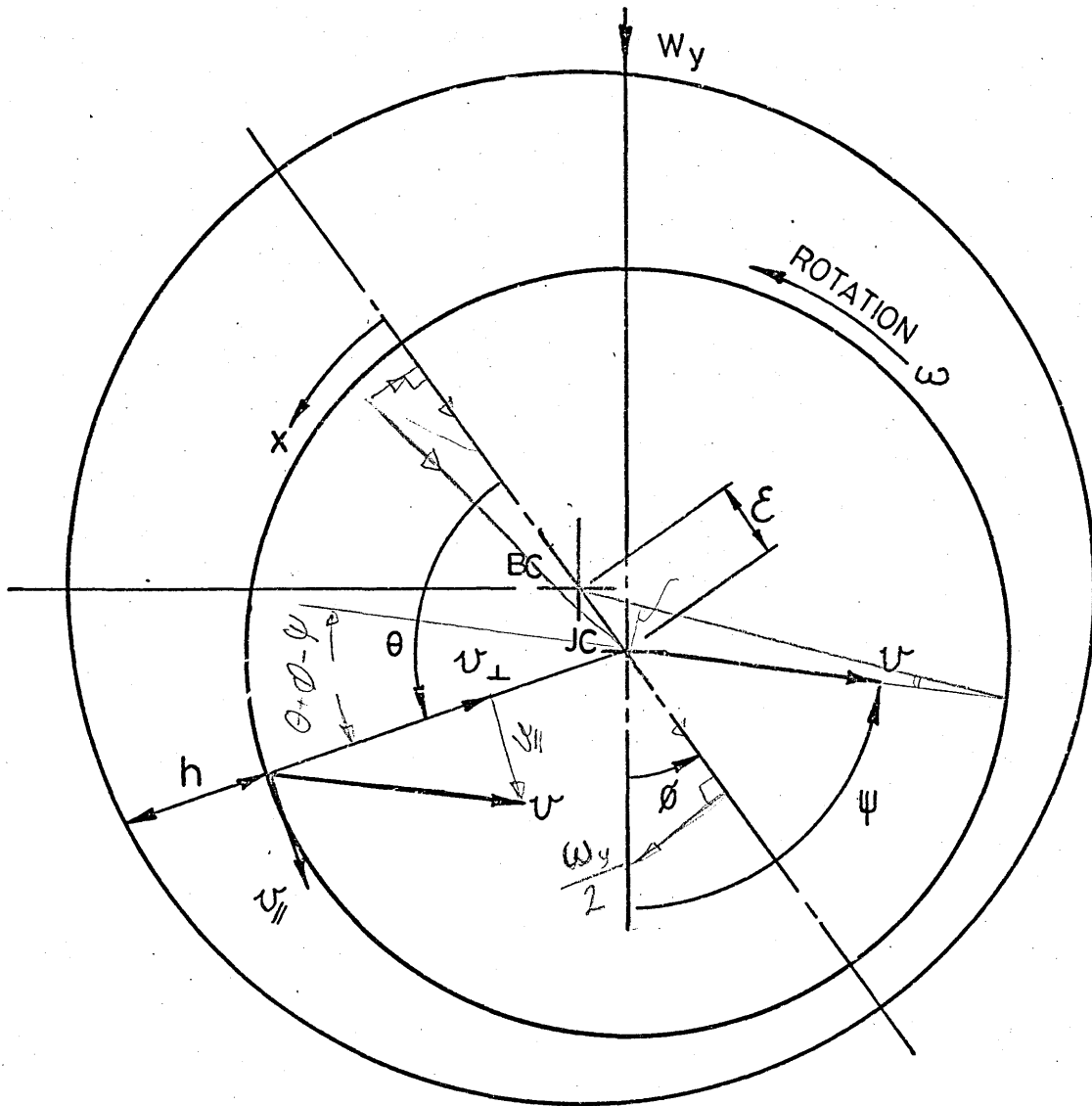


FIGURE 35. EXAMPLE OF JOURNAL CENTRE RESPONSE TO DYNAMIC LOADING TEST TYPE 3, VERTICAL



- BC BEARING CENTRE.
- JC JOURNAL CENTRE
- τ JOURNAL RADIUS
- R BEARING RADIUS

FIGURE 36. BEARING NOMENCLATURE.

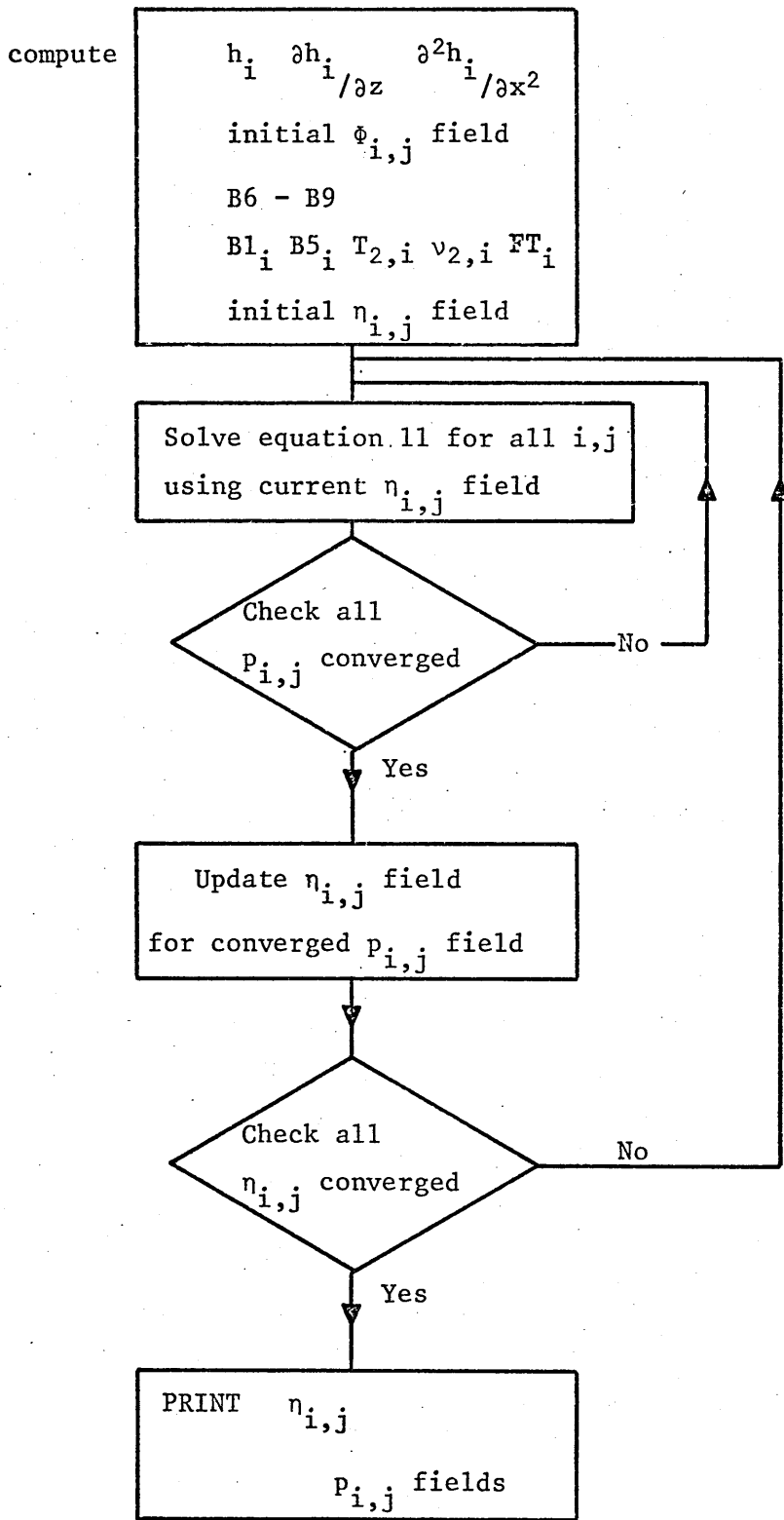


FIGURE 37. FLOW DIAGRAM - SOLUTION OF REYNOLD'S EQUATION

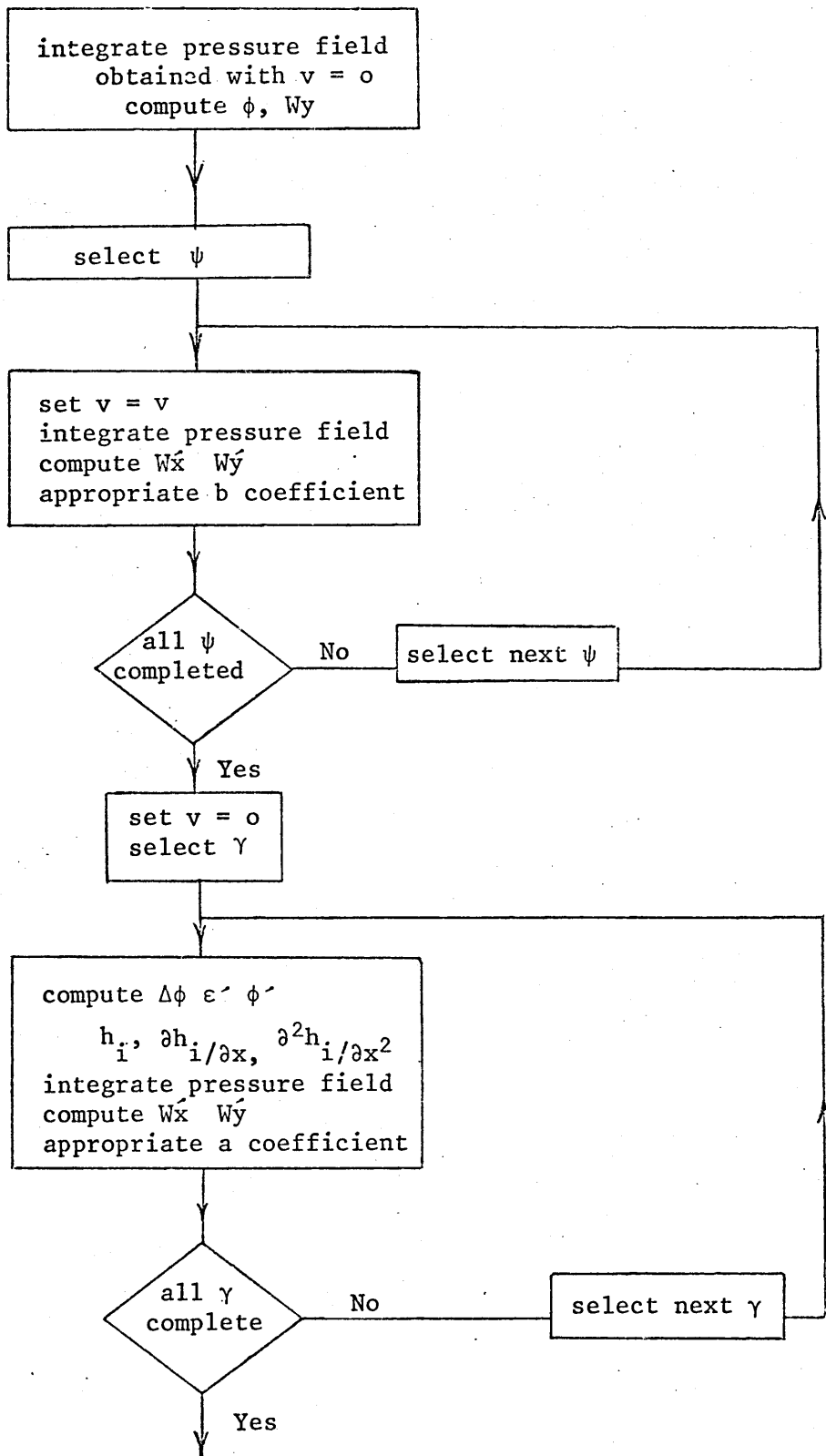


FIGURE 38. SIMPLIFIED FLOW DIAGRAM. CALCULATION OF JOURNAL CENTRE LOCATION, VELOCITY AND DISPLACEMENT COEFFICIENTS

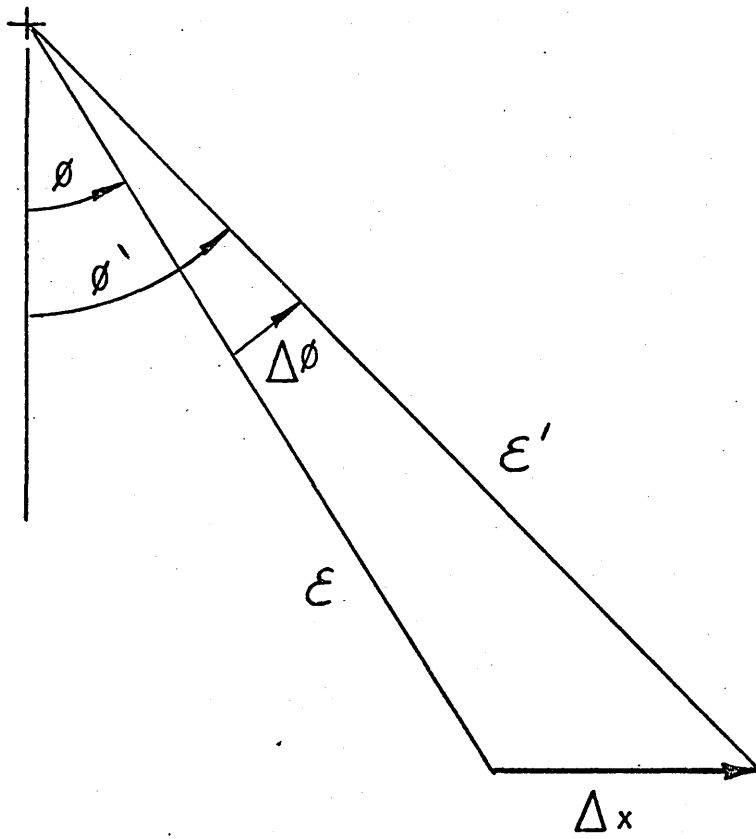
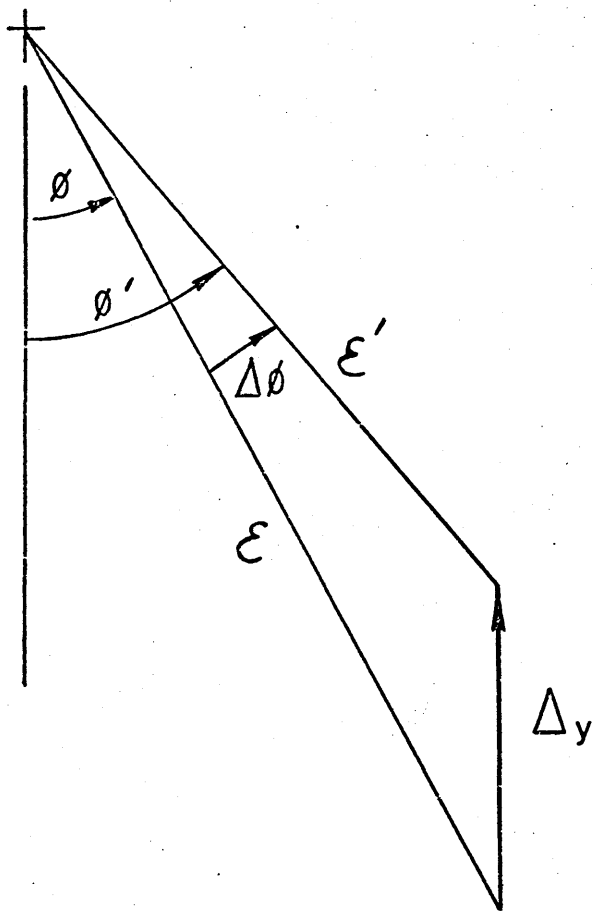
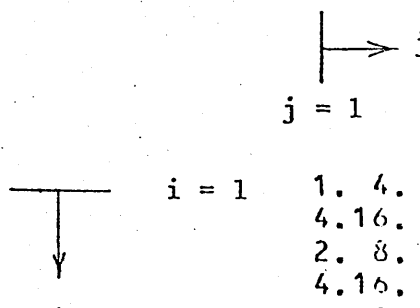


FIGURE. 39. JOURNAL CENTRE DISPLACEMENT, NOMENCLATURE.



	$j = 1$					$j = n$
$i = 1$	1. 4.	2. 4.	2. 4.	2. 4.	2. 4.	1.
	4. 16.	8. 16.	3. 16.	3. 16.	3. 16.	4.
	2. 8.	4. 3.	4. 3.	4. 3.	4. 3.	2.
	4. 16.	3. 16.	3. 16.	3. 16.	3. 16.	4.
	2. 8.	4. 3.	4. 3.	4. 3.	4. 3.	2.
	4. 16.	3. 16.	3. 16.	3. 16.	3. 16.	4.
	2. 8.	4. 3.	4. 3.	4. 3.	4. 3.	2.
	4. 16.	3. 16.	3. 16.	3. 16.	3. 16.	4.
	2. 8.	4. 3.	4. 3.	4. 3.	4. 3.	2.
	4. 16.	3. 16.	3. 16.	3. 16.	3. 16.	4.
	2. 8.	4. 3.	4. 3.	4. 3.	4. 3.	2.
	4. 16.	3. 16.	3. 16.	3. 16.	3. 16.	4.
	2. 8.	4. 3.	4. 3.	4. 3.	4. 3.	2.
	4. 16.	3. 16.	3. 16.	3. 16.	3. 16.	4.
	2. 8.	4. 3.	4. 3.	4. 3.	4. 3.	2.
	4. 16.	3. 16.	3. 16.	3. 16.	3. 16.	4.
	2. 8.	4. 3.	4. 3.	4. 3.	4. 3.	2.
	4. 16.	3. 16.	3. 16.	3. 16.	3. 16.	4.
	2. 8.	4. 3.	4. 3.	4. 3.	4. 3.	2.
	4. 16.	3. 16.	3. 16.	3. 16.	3. 16.	4.
	2. 8.	4. 3.	4. 3.	4. 3.	4. 3.	2.
	4. 16.	3. 16.	3. 16.	3. 16.	3. 16.	4.
	2. 8.	4. 3.	4. 3.	4. 3.	4. 3.	2.
	4. 16.	3. 16.	3. 16.	3. 16.	3. 16.	4.
	2. 8.	4. 3.	4. 3.	4. 3.	4. 3.	2.
	4. 16.	3. 16.	3. 16.	3. 16.	3. 16.	4.
	2. 8.	4. 3.	4. 3.	4. 3.	4. 3.	2.
	4. 16.	3. 16.	3. 16.	3. 16.	3. 16.	4.
	2. 8.	4. 3.	4. 3.	4. 3.	4. 3.	2.
	4. 16.	3. 16.	3. 16.	3. 16.	3. 16.	4.
	2. 8.	4. 3.	4. 3.	4. 3.	4. 3.	2.
	4. 16.	3. 16.	3. 16.	3. 16.	3. 16.	4.
	2. 8.	4. 3.	4. 3.	4. 3.	4. 3.	2.
	4. 16.	3. 16.	3. 16.	3. 16.	3. 16.	4.
	2. 8.	4. 3.	4. 3.	4. 3.	4. 3.	2.
	4. 16.	3. 16.	3. 16.	3. 16.	3. 16.	4.
	2. 8.	4. 3.	4. 3.	4. 3.	4. 3.	2.
	4. 16.	3. 16.	3. 16.	3. 16.	3. 16.	4.
	2. 8.	4. 3.	4. 3.	4. 3.	4. 3.	2.
	4. 16.	3. 16.	3. 16.	3. 16.	3. 16.	4.
	2. 8.	4. 3.	4. 3.	4. 3.	4. 3.	2.
	4. 16.	3. 16.	3. 16.	3. 16.	3. 16.	4.
	2. 8.	4. 3.	4. 3.	4. 3.	4. 3.	2.
	4. 16.	3. 16.	3. 16.	3. 16.	3. 16.	4.
$i = m$	1. 4.	2. 4.	2. 4.	2. 4.	2. 4.	1.

VALUES OF $NS_{i,j}$

FIGURE 40. SIMPSONS RULE TABLE, $m = 49$, $n = 9$

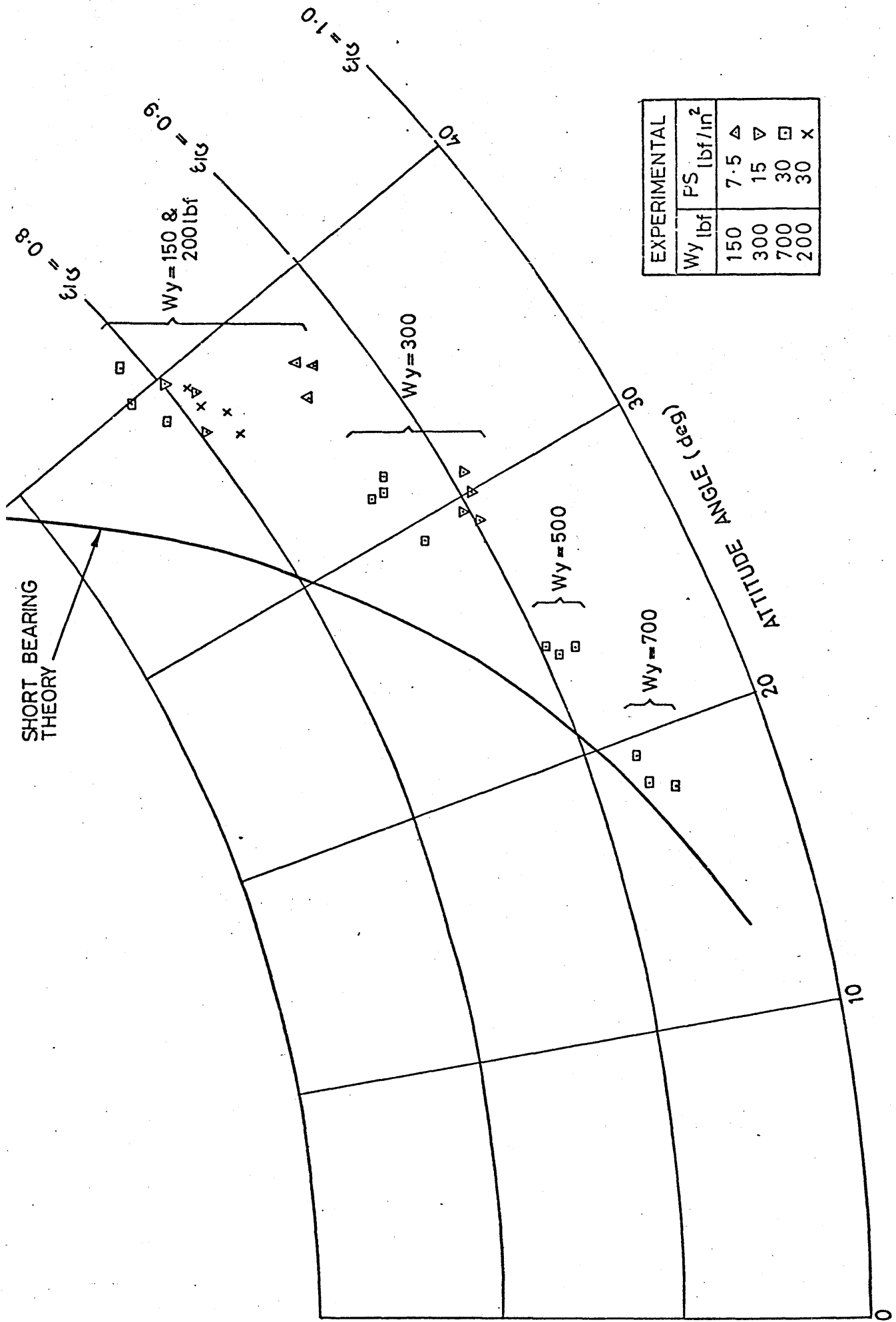


FIGURE 41 JOURNAL CENTRE LOCUS.

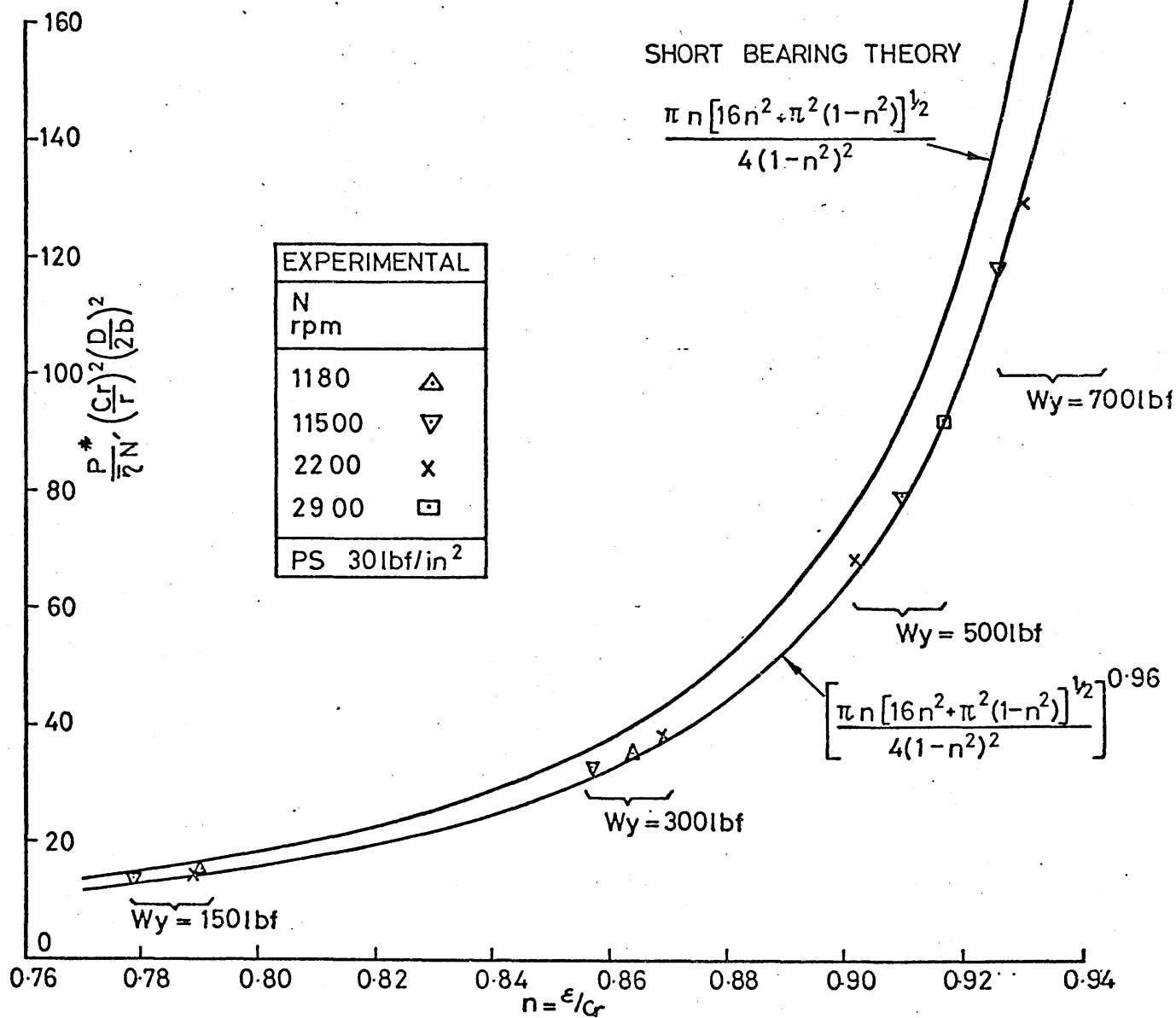
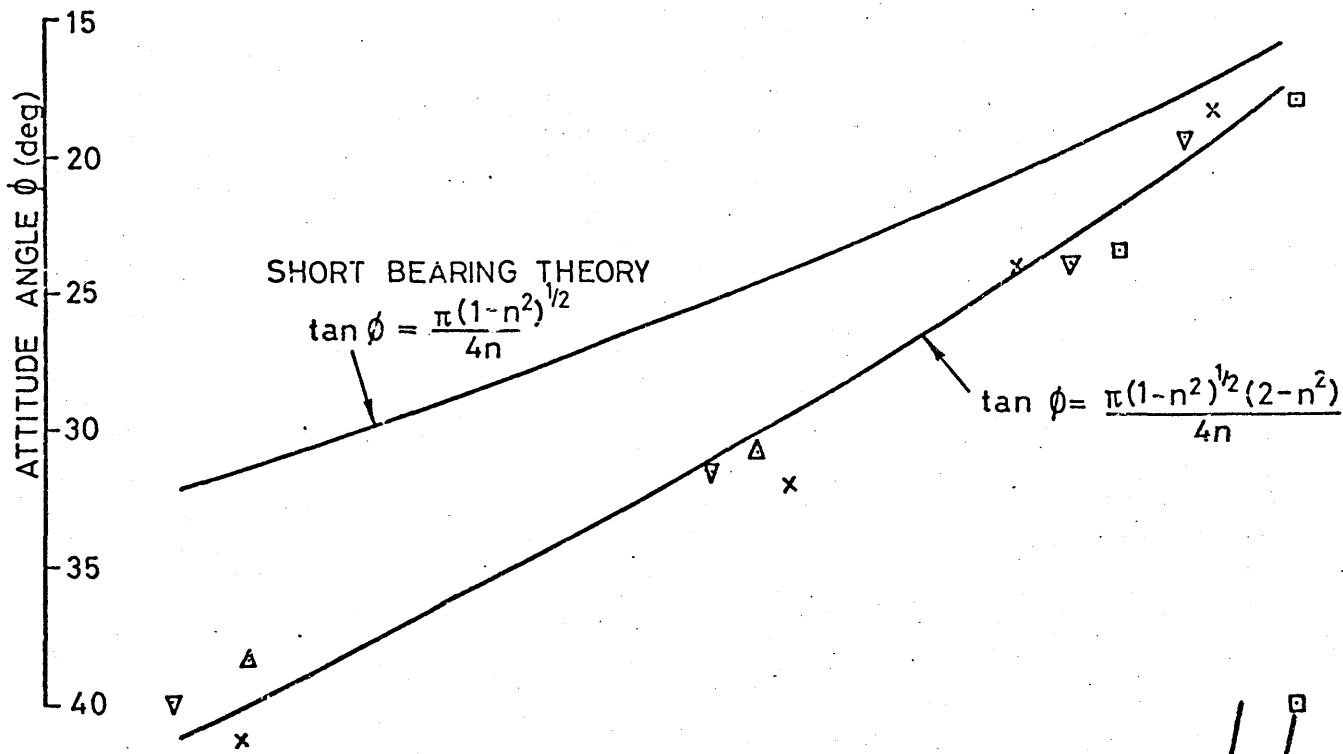


FIGURE 4.2 ATTITUDE ANGLE LOAD NUMBER & ECCENTRICITY RATIO

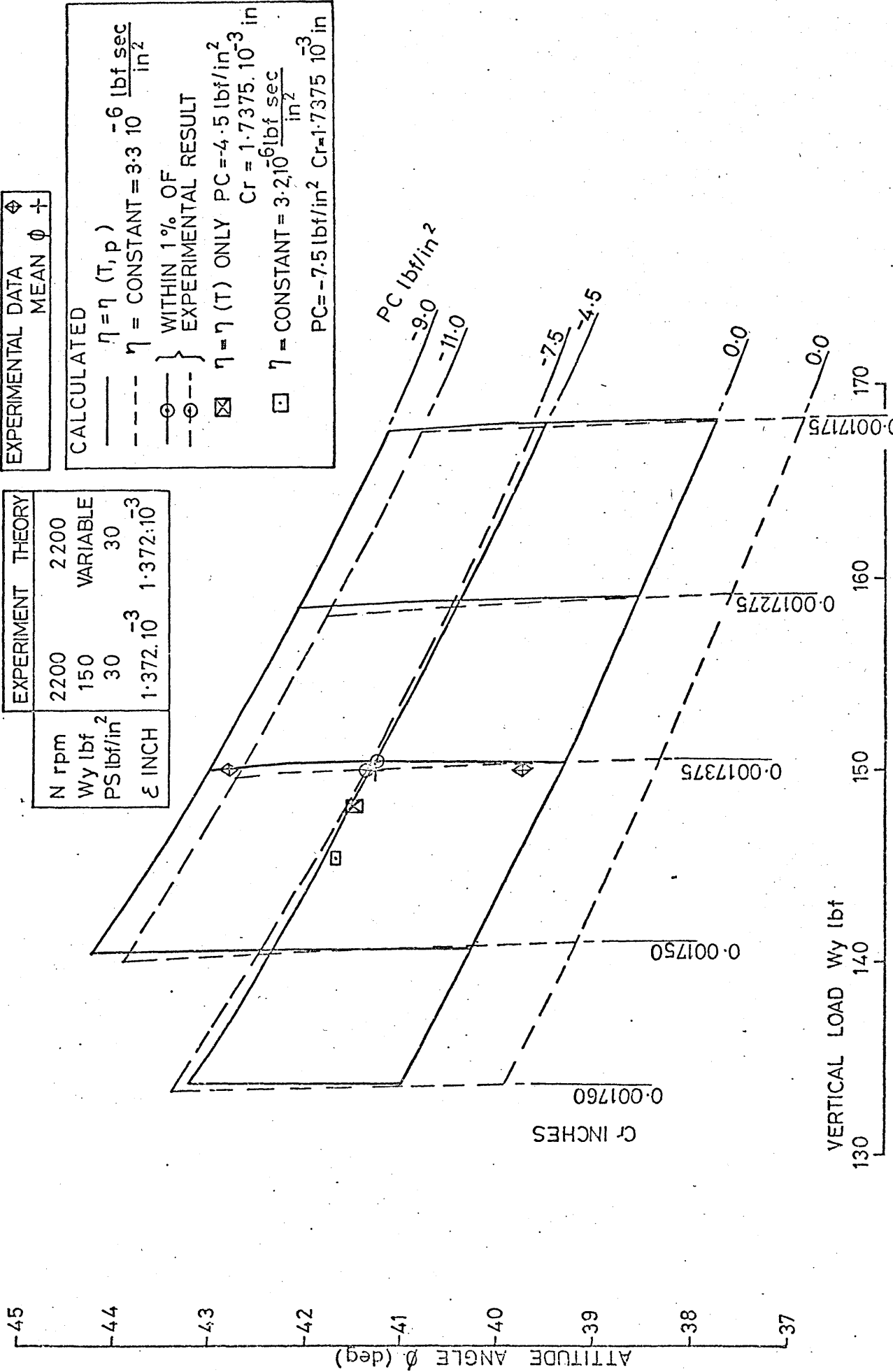


FIGURE 43 VERTICAL LOAD & ATTITUDE ANGLE, CALCULATED & MEASURED (LOW ϵ (Cr))

EXPERIMENTAL DATA

CALCULATED DATA

$\eta = \eta(\tau, p)$
 $\eta = \text{CONSTANT} = 1.55 \cdot 10^{-6} \frac{\text{lb}_f \text{ sec}}{\text{in}^2}$

WITHIN 1% OF
 EXPERIMENTAL RESULT

$\eta = \eta(\tau)$ ONLY $PC = -31.4 \text{ lb}_f/\text{in}^2$
 $Cr = 0.001842 \text{ in}$

$\eta = \text{CONSTANT} = 1.65 \cdot 10^{-6} \frac{\text{lb}_f \text{ sec}}{\text{in}^2}$ } $PC = -31.0 \text{ lb}_f/\text{in}^2$
 $\eta = \text{CONSTANT} = 1.45 \cdot 10^{-6} \frac{\text{lb}_f \text{ sec}}{\text{in}^2}$ } $Cr = 0.001842 \text{ in}$

EXPERIMENT THEORY

N rpm	2900	2900
Wy lbf	500	VARIABLE
PS lbf/in ²	30.0	30.0
ε INCH	0.00169	0.00169

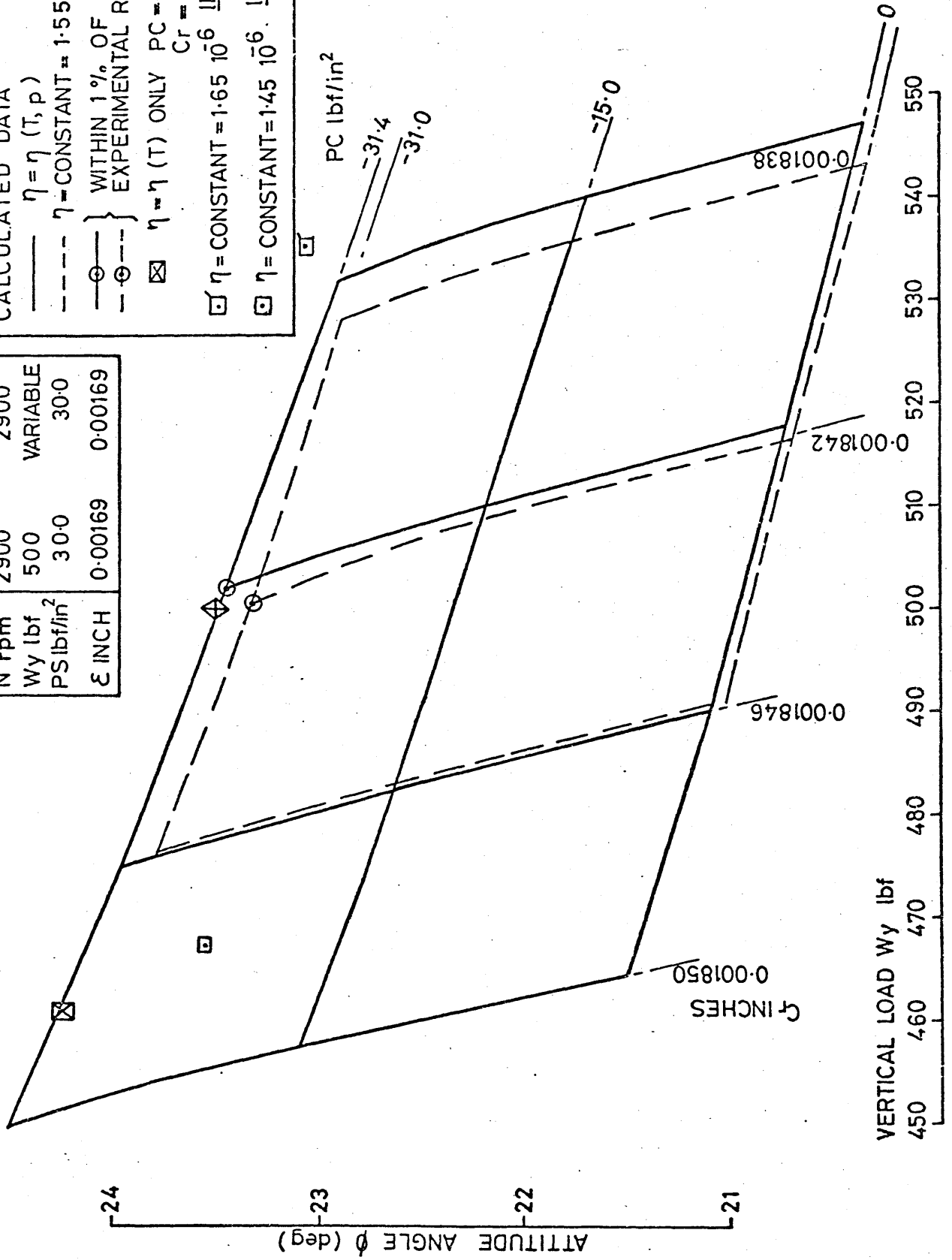


FIG. 44. VERTICAL LOAD, ATTITUDE ANGLE, CALCULATED & MEASURED (HIGH ϵ/Cr)

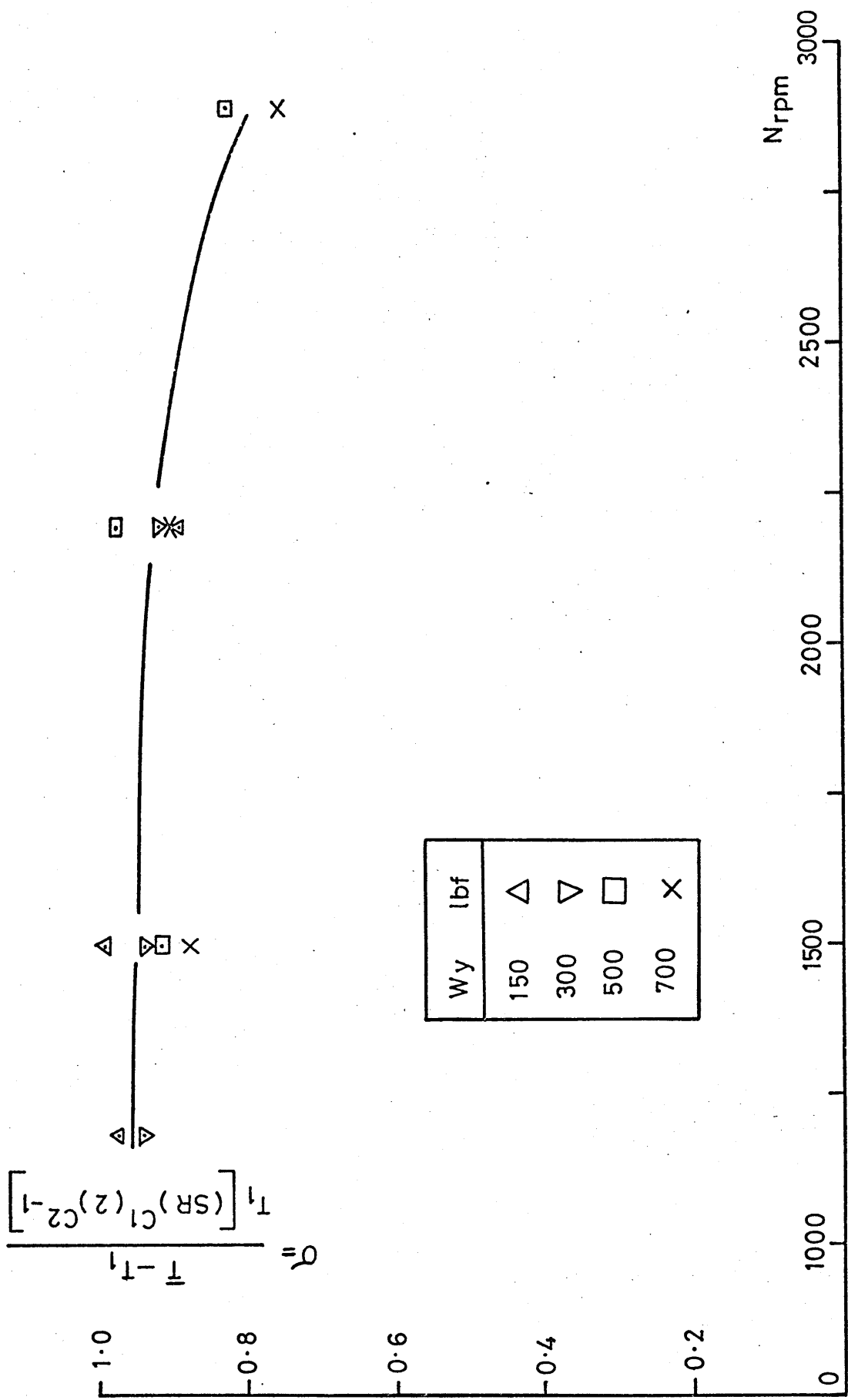


FIGURE 45 CONSTANT VISCOSITY FACTOR.

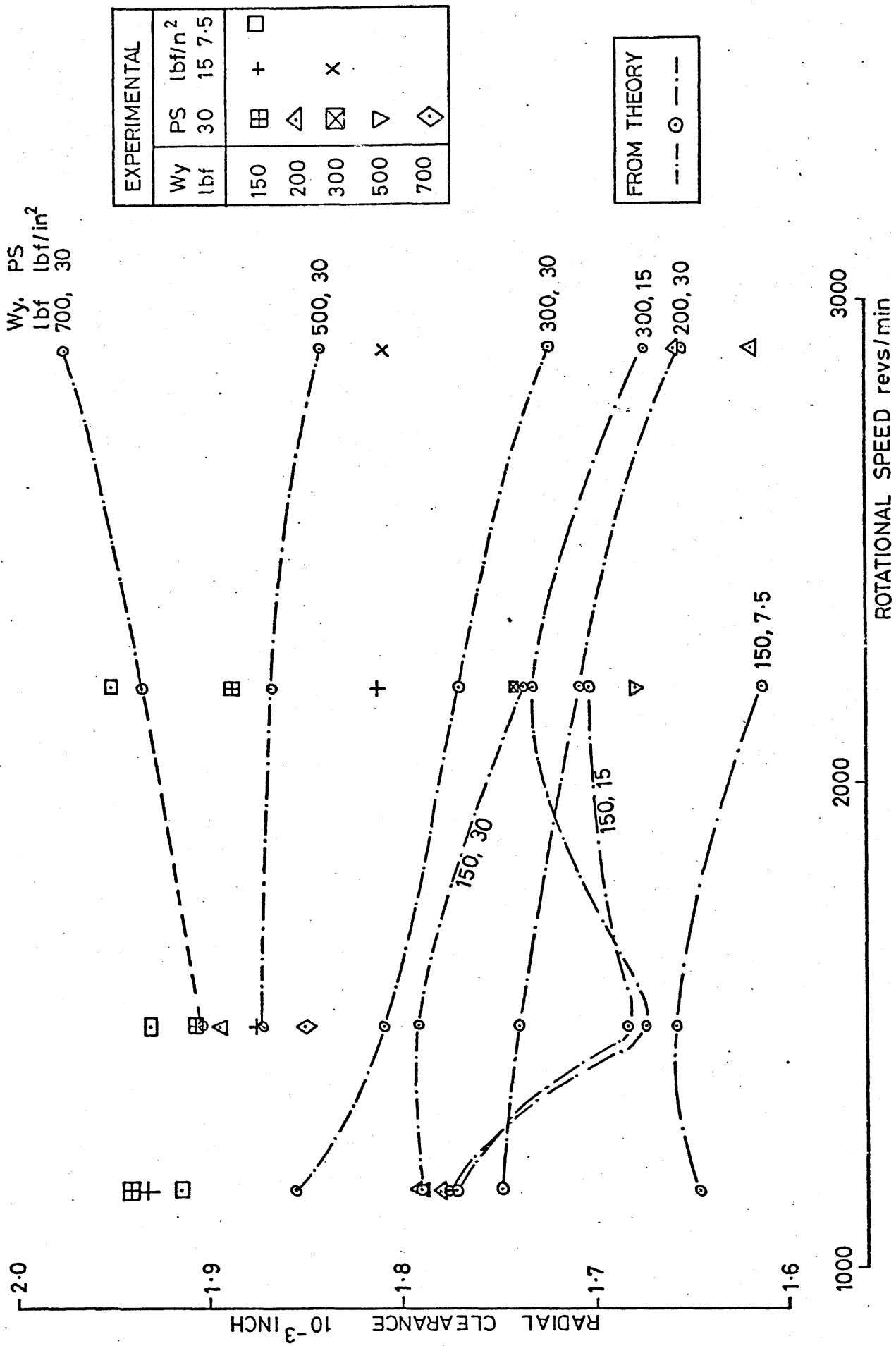


FIGURE 46 BEARING RADIAL CLEARANCE

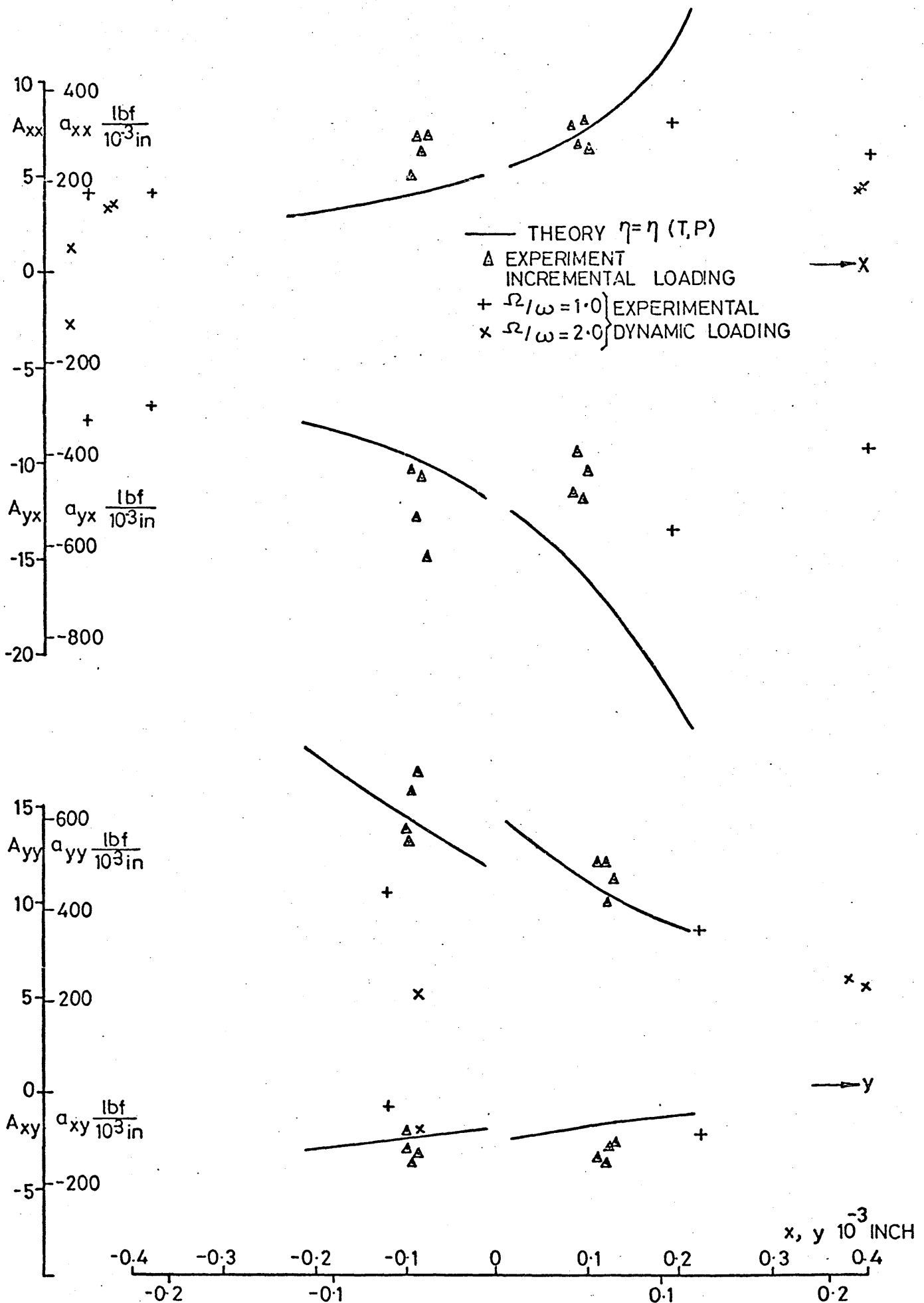


FIGURE 47 MEASURED AND CALCULATED DISPLACEMENT COEFFICIENTS $\frac{x}{Cr}, \frac{y}{Cr}$
 $N = 1180 \text{rpm}, W_y = 150 \text{lbf}, PS = 30 \text{lbf/in}^2$

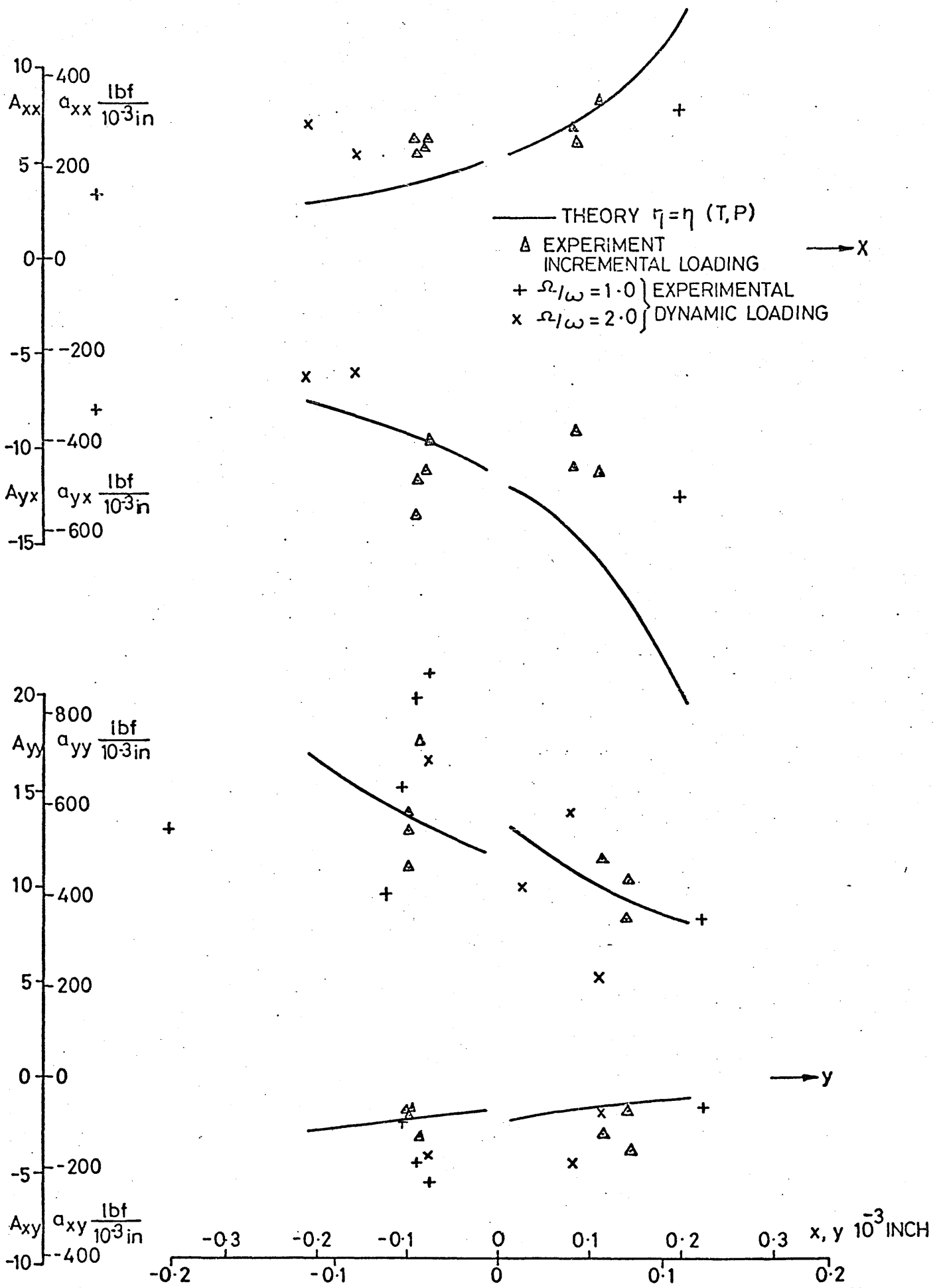


FIGURE 48 MEASURED AND CALCULATED DISPLACEMENT COEFFICIENTS
 $N = 1500 \text{ rpm}$, $W_y = 150 \text{ lbf}$, $PS = 30 \text{ lbf/in}^2$

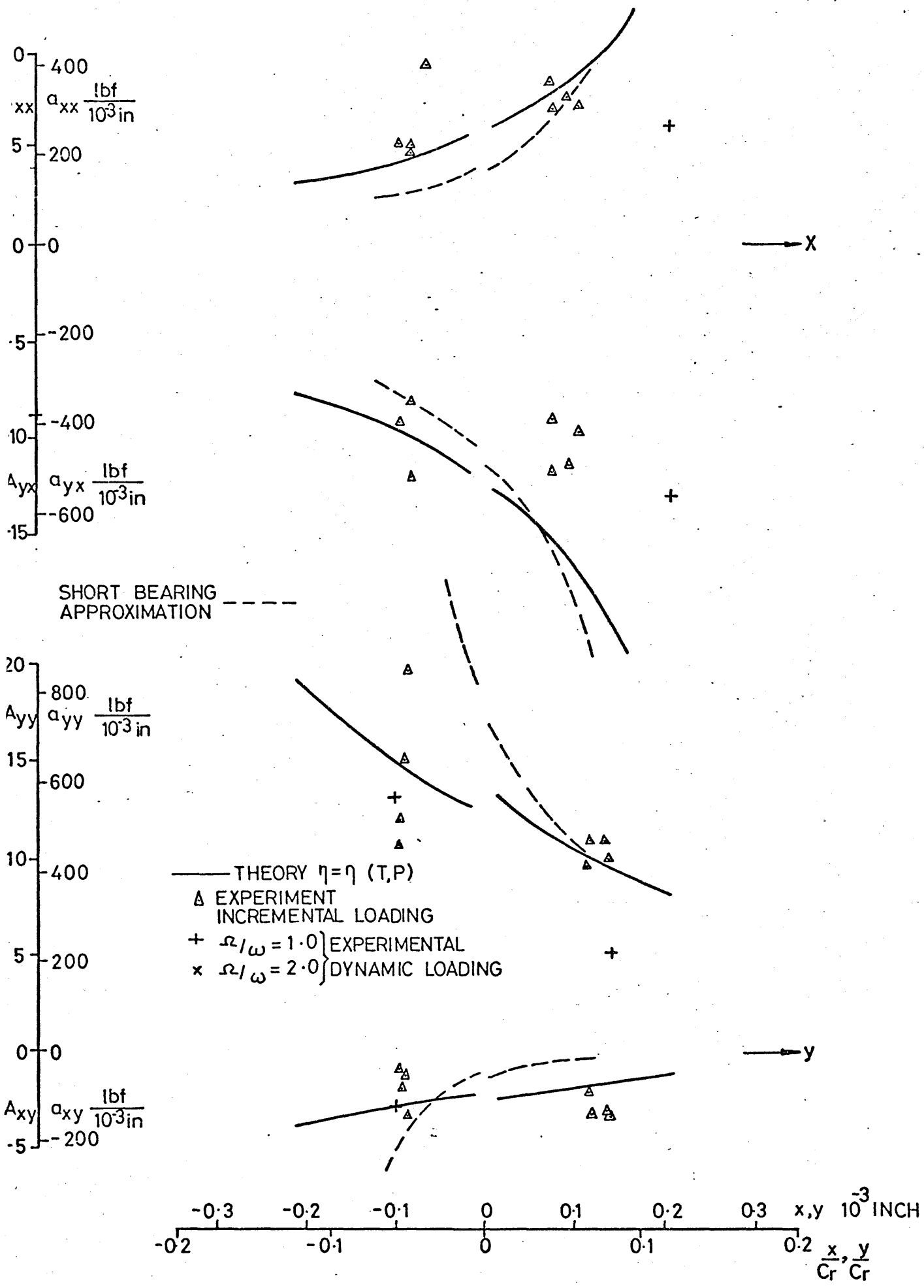


FIGURE 49 MEASURED AND CALCULATED DISPLACEMENT COEFFICIENTS
 $N = 2200 \text{rpm}$, $W_y = 150 \text{lbf}$, $PS = 30 \text{lbf/in}^2$

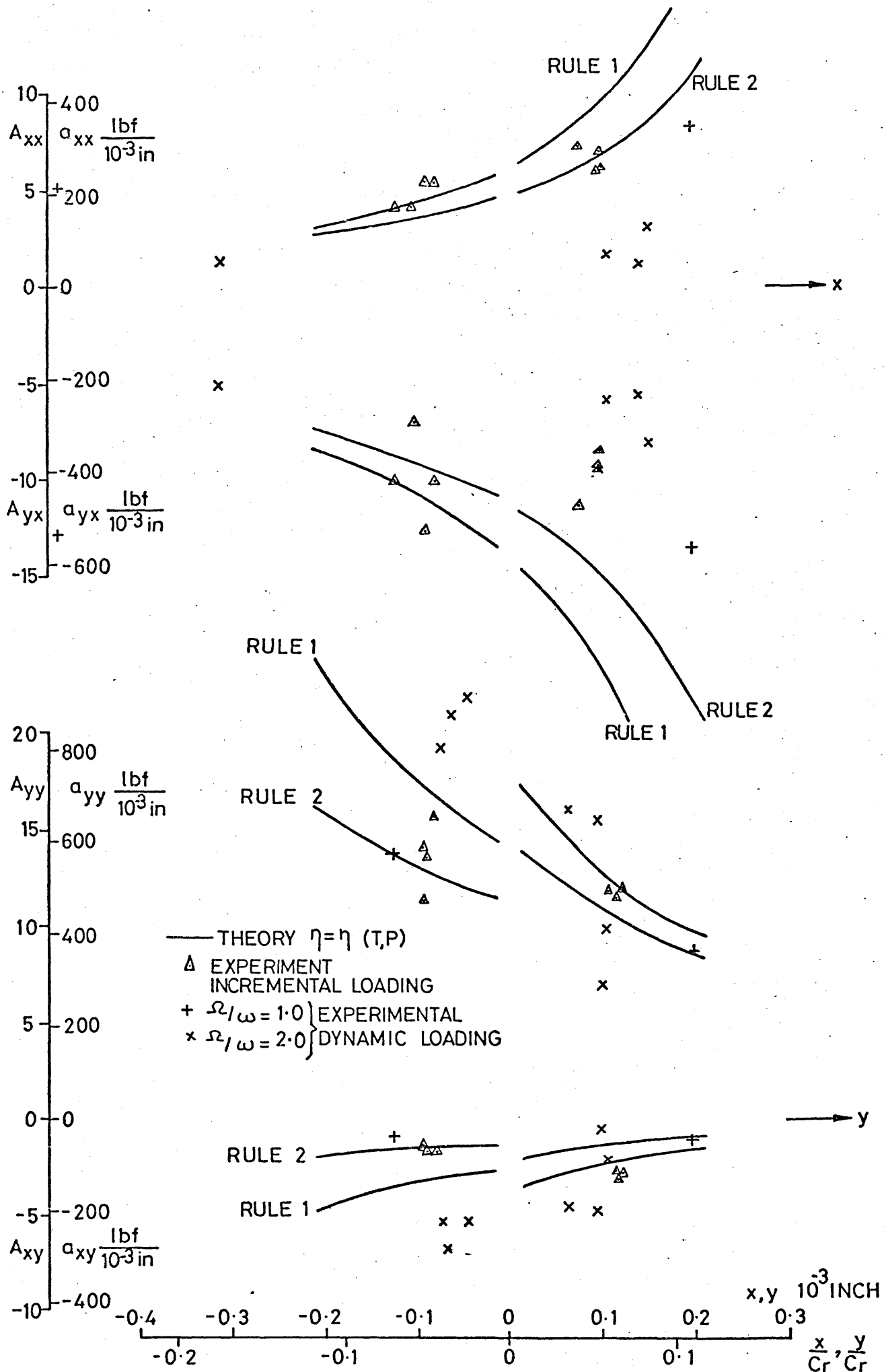


FIGURE 50 MEASURED AND CALCULATED DISPLACEMENT COEFFICIENTS
 $N = 1180 \text{ rpm}$, $W_y = 150 \text{ lbf}$, $PS = 15 \text{ lbf/in}^2$

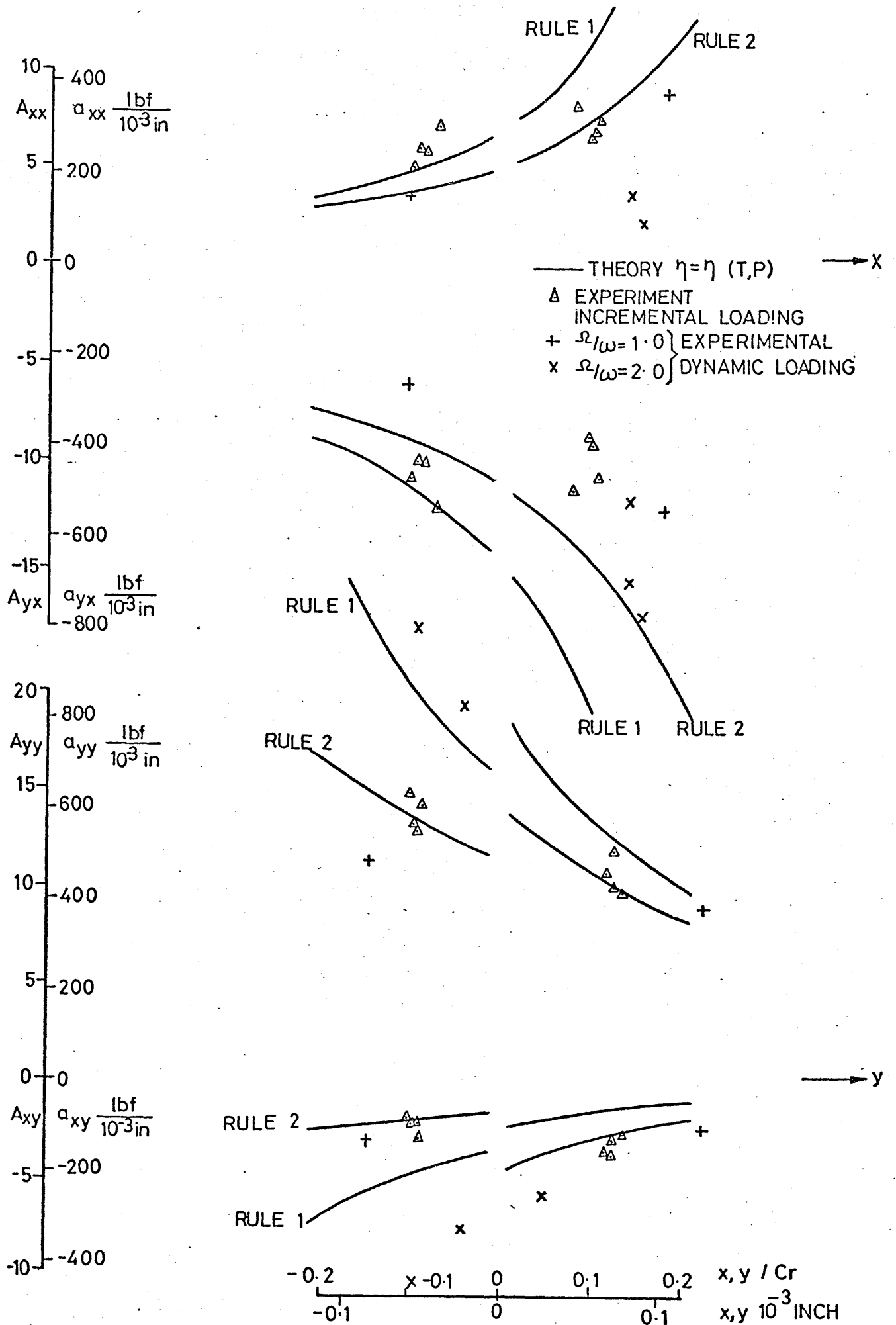


FIGURE 51 MEASURED AND CALCULATED DISPLACEMENT COEFFICIENTS
 $N = 1500$ rpm, $W_y = 150$ lbf, $PS = 15$ lbf/in²

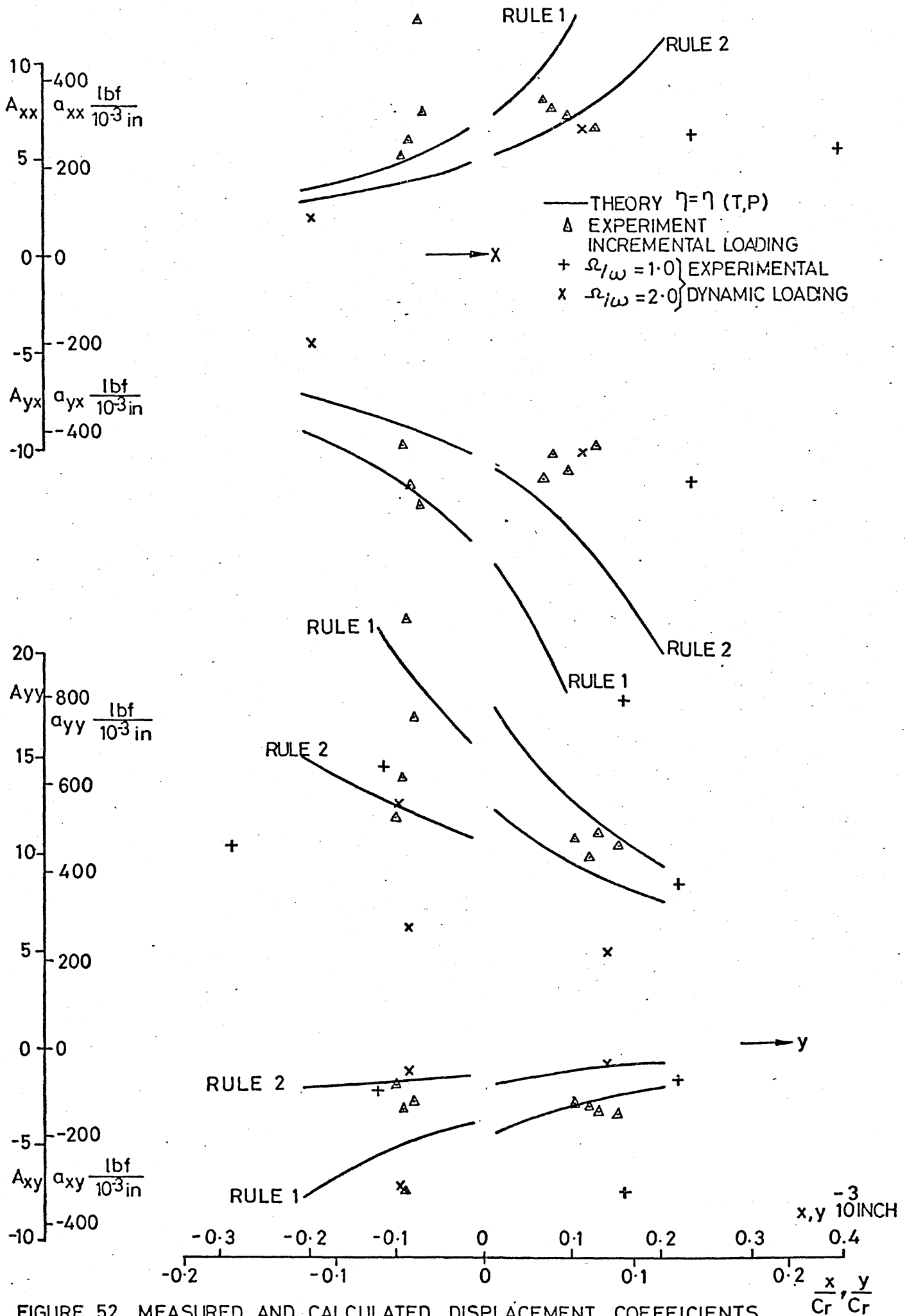


FIGURE 52 MEASURED AND CALCULATED DISPLACEMENT COEFFICIENTS
 $N = 2200 \text{ rpm}$, $W_y = 150 \text{ lbf}$, $PS = 15 \text{ lbf/in}^2$

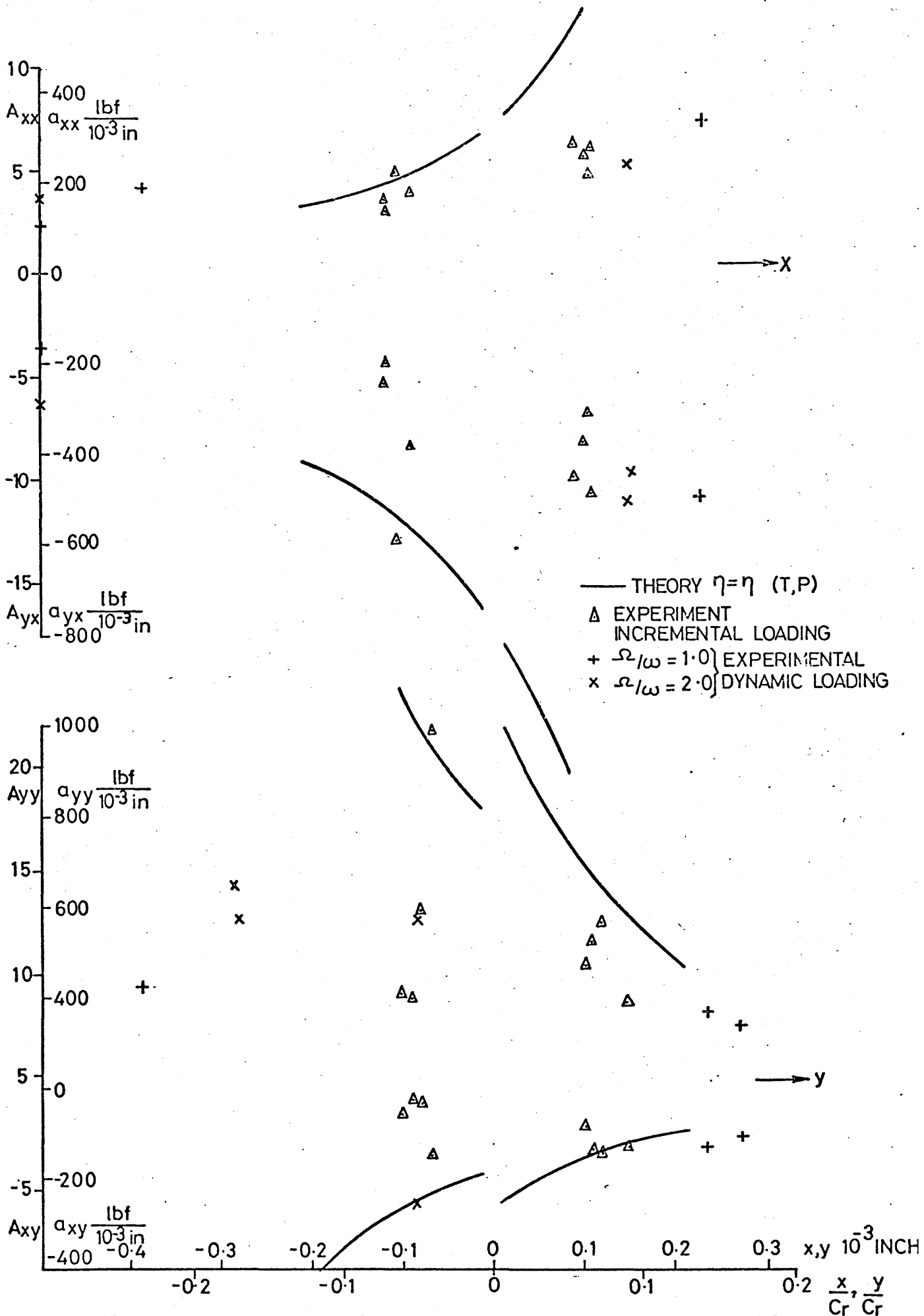


FIGURE 53 MEASURED AND CALCULATED DISPLACEMENT COEFFICIENTS
 $N = 1180 \text{ rpm}$, $W_y = 150 \text{ lbf}$, $PS = 7.5 \text{ lbf/in}^2$

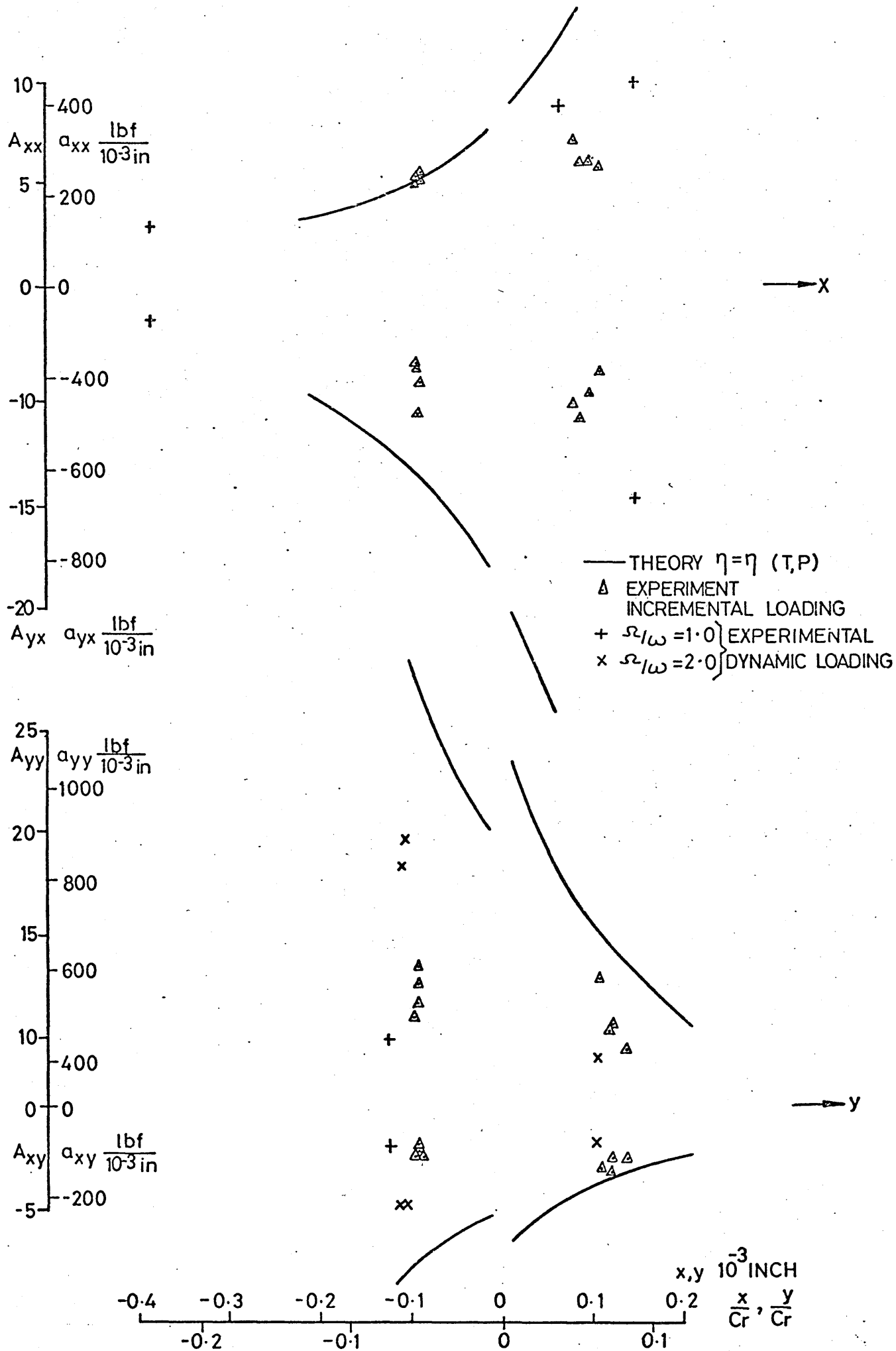


FIGURE 54 MEASURED AND CALCULATED DISPLACEMENT COEFFICIENTS
 $N = 1500 \text{ rpm}$, $W_y = 150 \text{ lb f}$, $PS = 7.5 \text{ lb f/in}^2$

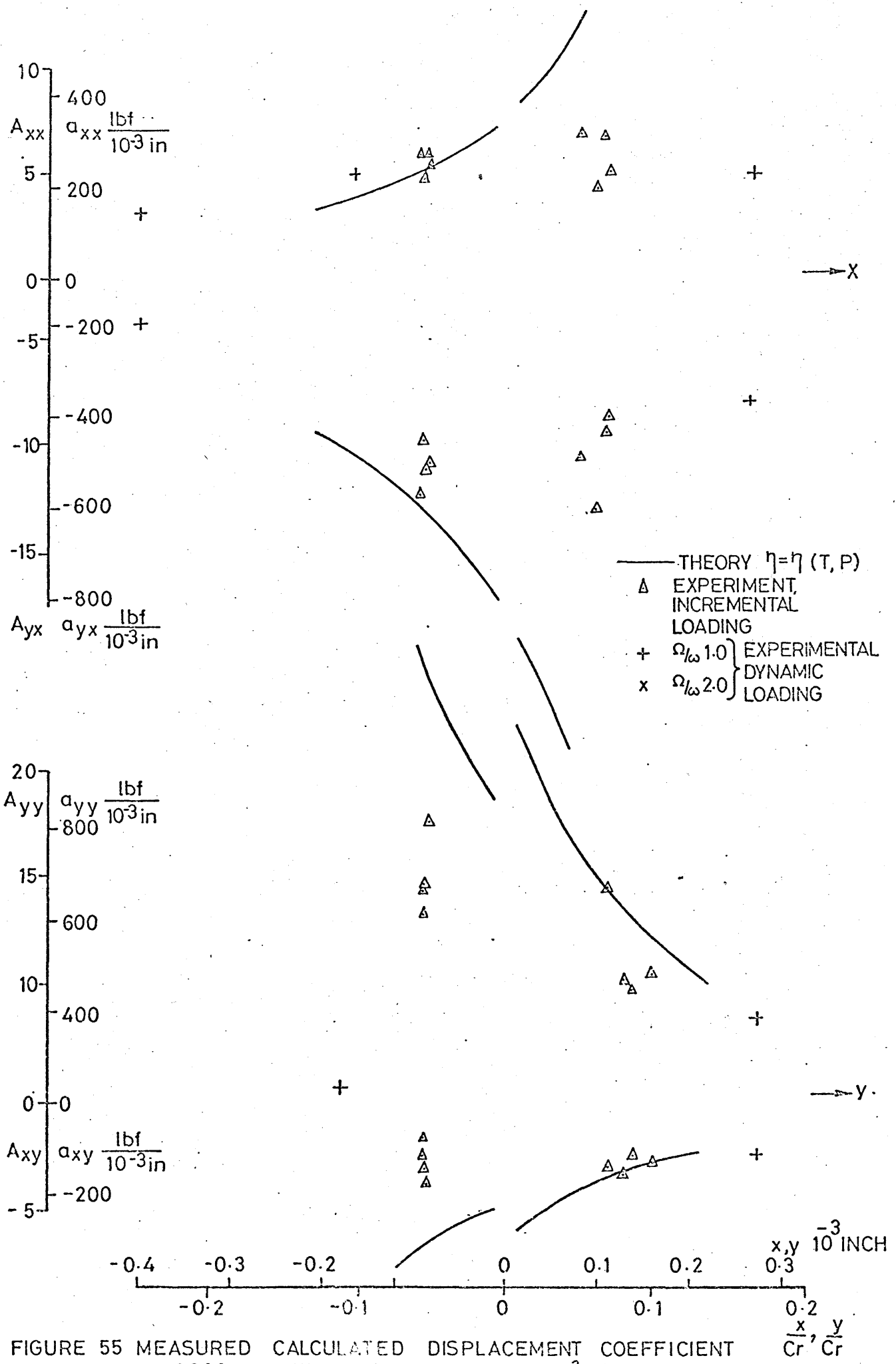


FIGURE 55 MEASURED CALCULATED DISPLACEMENT COEFFICIENT
 $N = 2200 \text{ rpm}$, $W_y = 150 \text{ lbf}$, $PS = 7.5 \text{ lbf/in}^2$

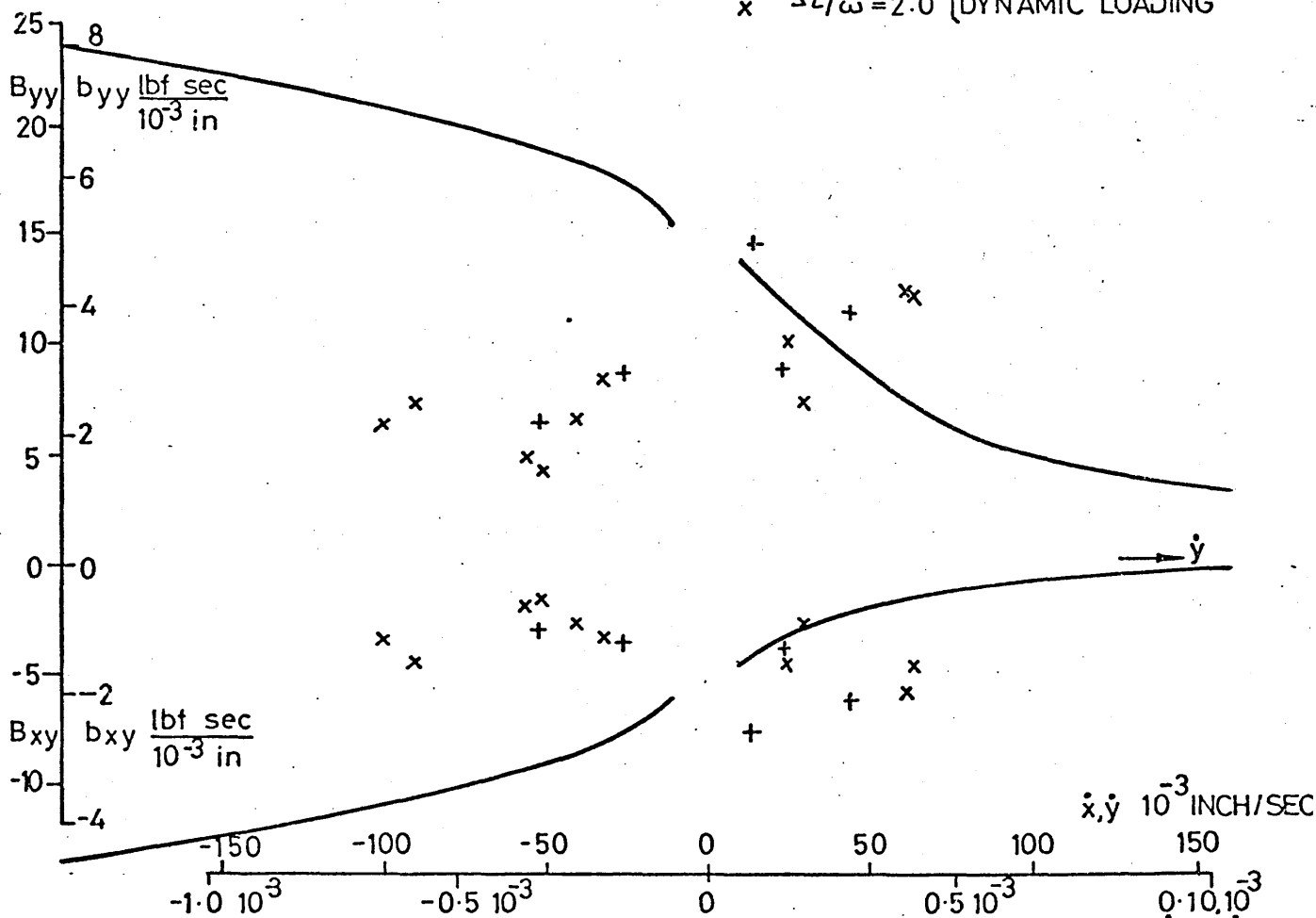
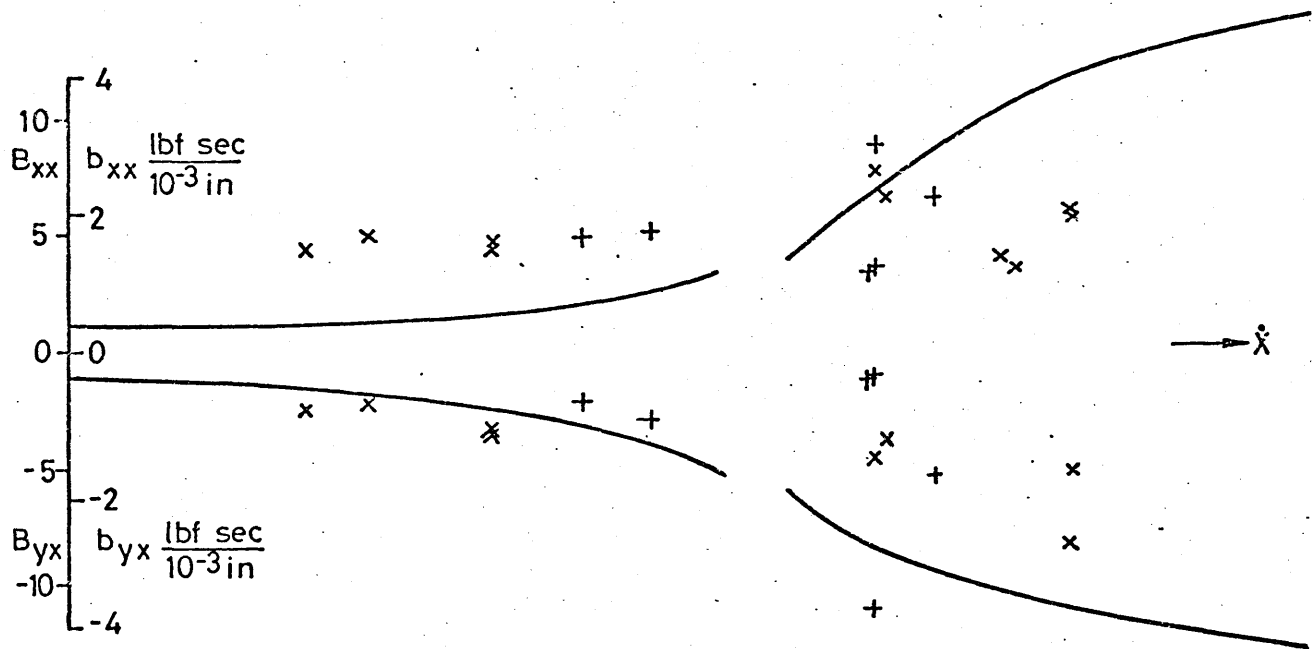


FIGURE 56 MEASURED AND CALCULATED VELOCITY COEFFICIENTS
 $N = 1180 \text{ rpm}$, $W_y = 150 \text{ lbf}$, $PS = 30 \text{ lbf/in}^2$

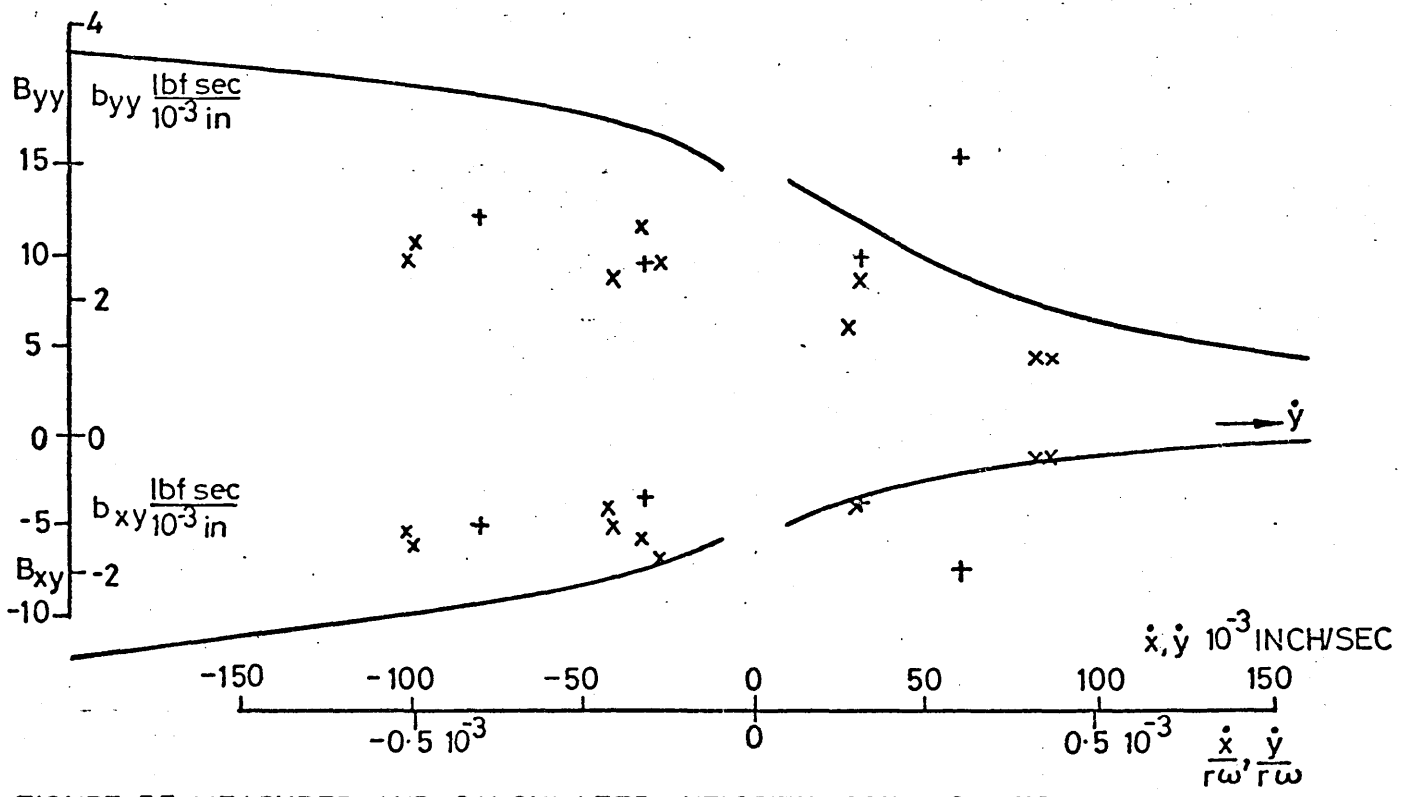
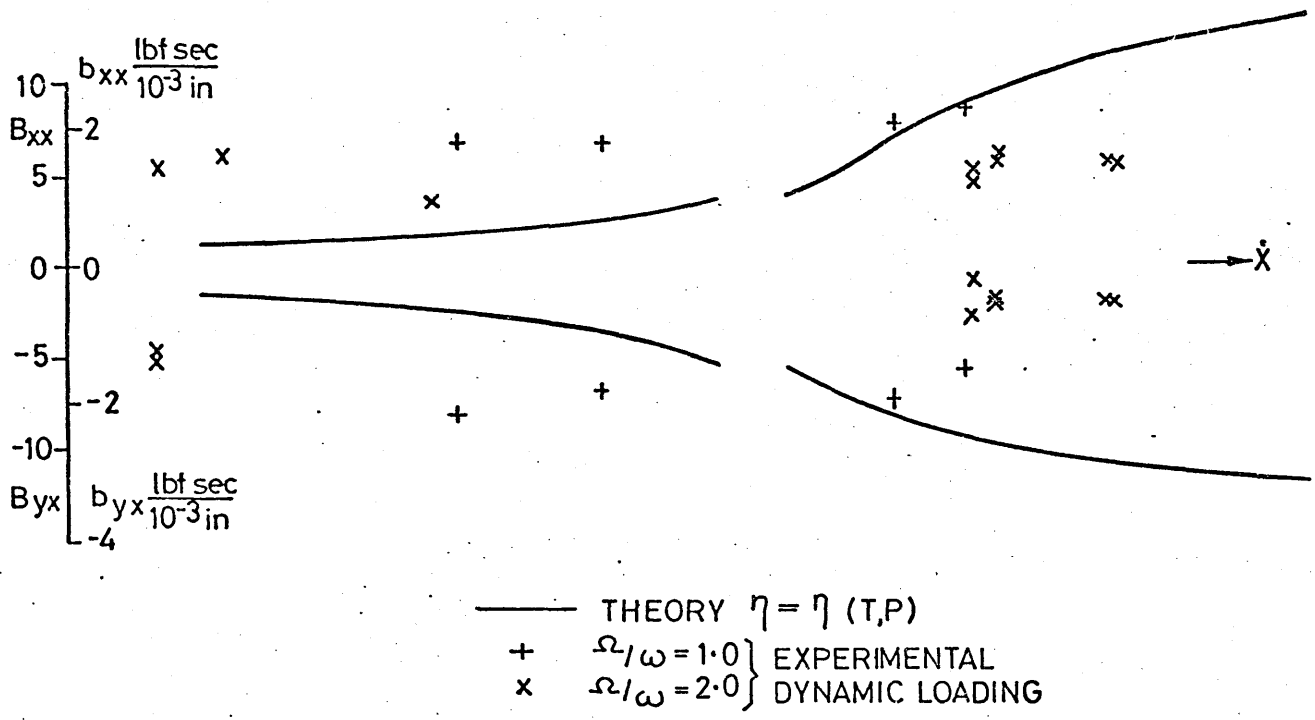
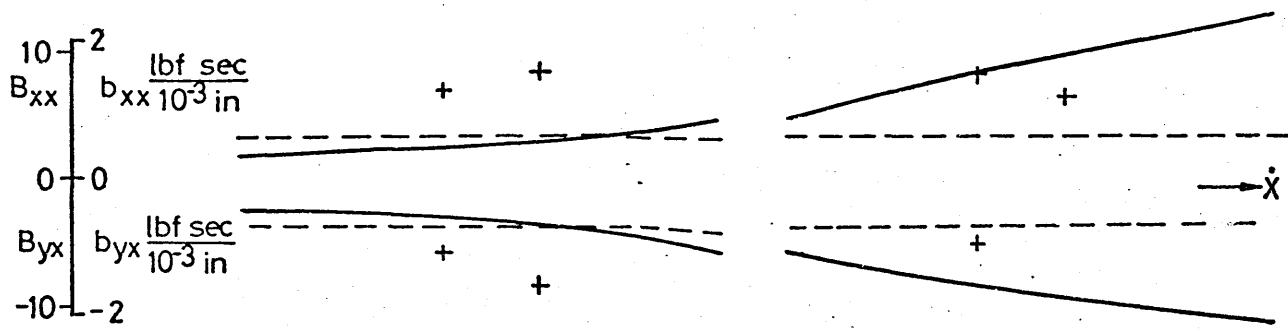


FIGURE 57 MEASURED AND CALCULATED VELOCITY COEFFICIENTS
 $N = 1500 \text{ rpm}$, $W_y = 150 \text{ lbf}$ $PS = 30 \text{ lbf/in}^2$



- - - - - SHORT BEARING APPROXIMATION
 ——— THEORY $\eta = \eta(T, P)$
 + $\Omega/\omega = 1.0$ } EXPERIMENTAL
 x $\Omega/\omega = 2.0$ } DYNAMIC LOADING

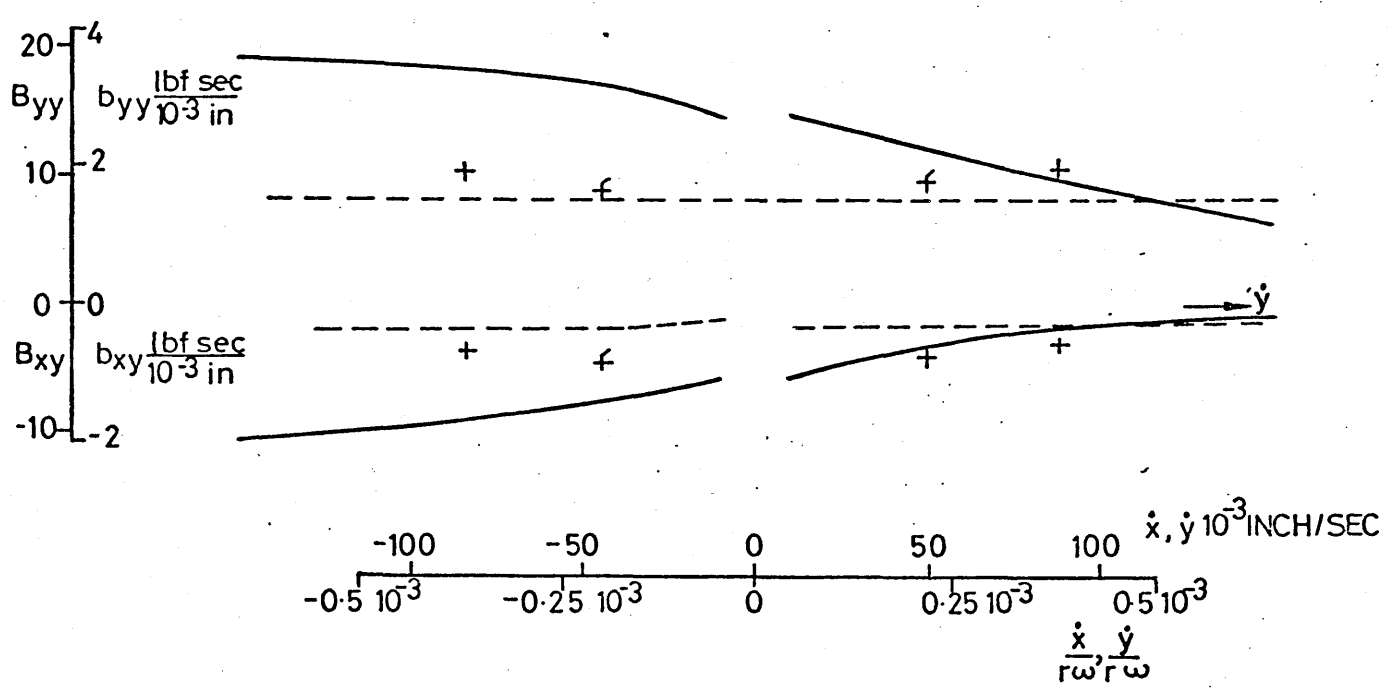


FIGURE 58 MEASURED AND CALCULATED VELOCITY COEFFICIENTS
 $N = 2200 \text{ rpm}$, $W_y = 150 \text{ lbf}$, $PS = 30 \text{ lbf/in}^2$

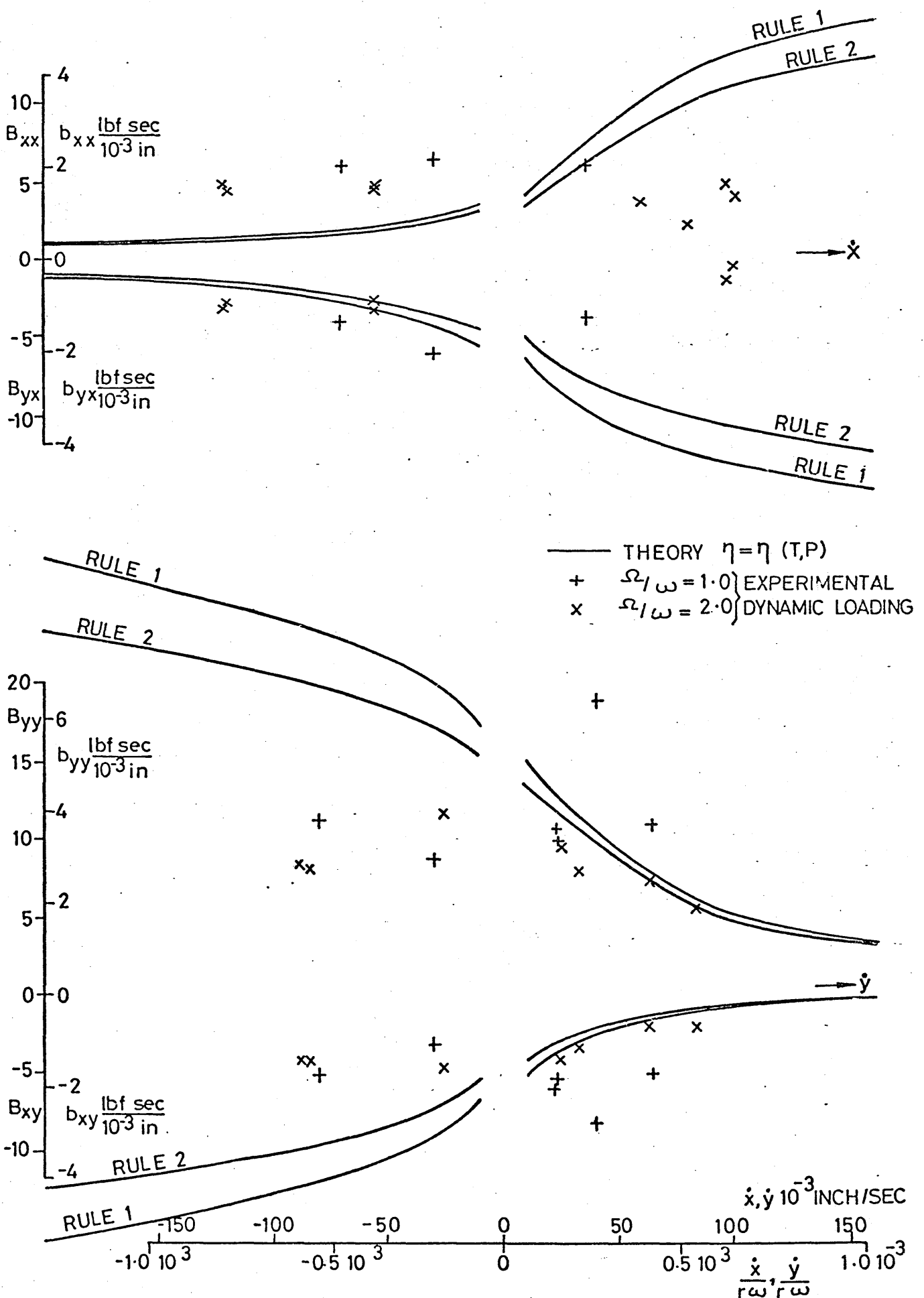
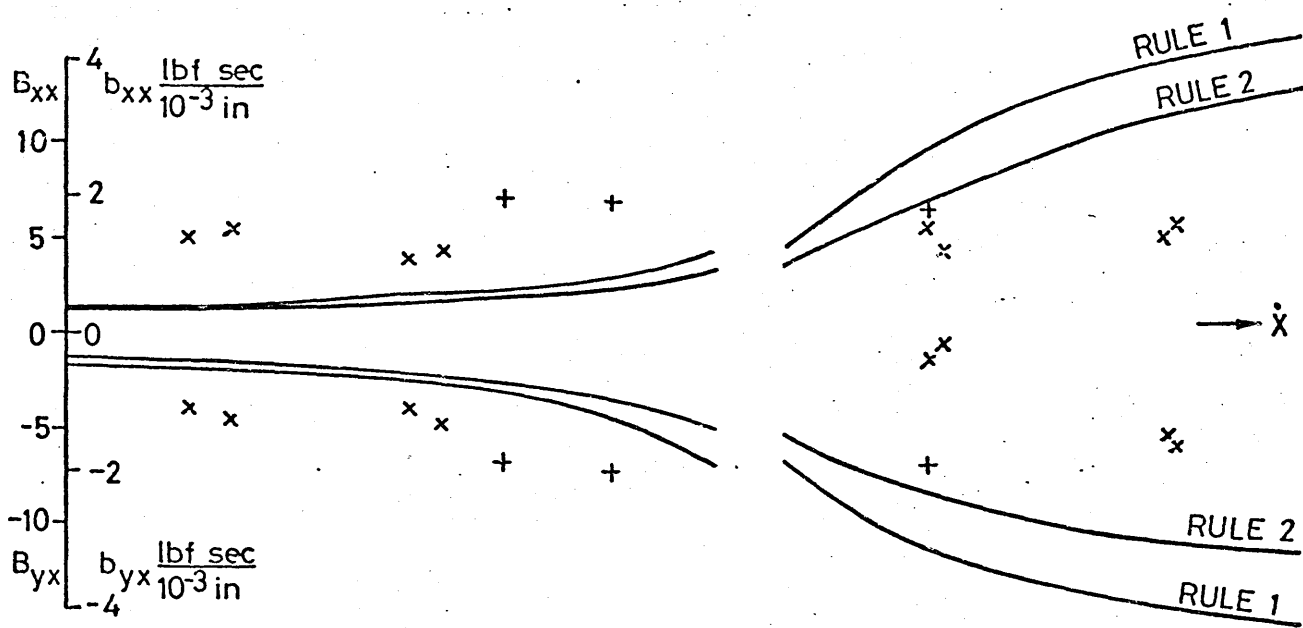


FIGURE 59 MEASURED AND CALCULATED VELOCITY COEFFICIENTS
 $N = 1180 \text{ rpm}$, $W_y = 150 \text{ lbf}$, $PS = 15 \text{ lbf/in}^2$



— THEORY $\eta = \eta(T, P)$
 + $\Omega/\omega = 1.0$ } EXPERIMENTAL
 x $\Omega/\omega = 2.0$ } DYNAMIC LOADING

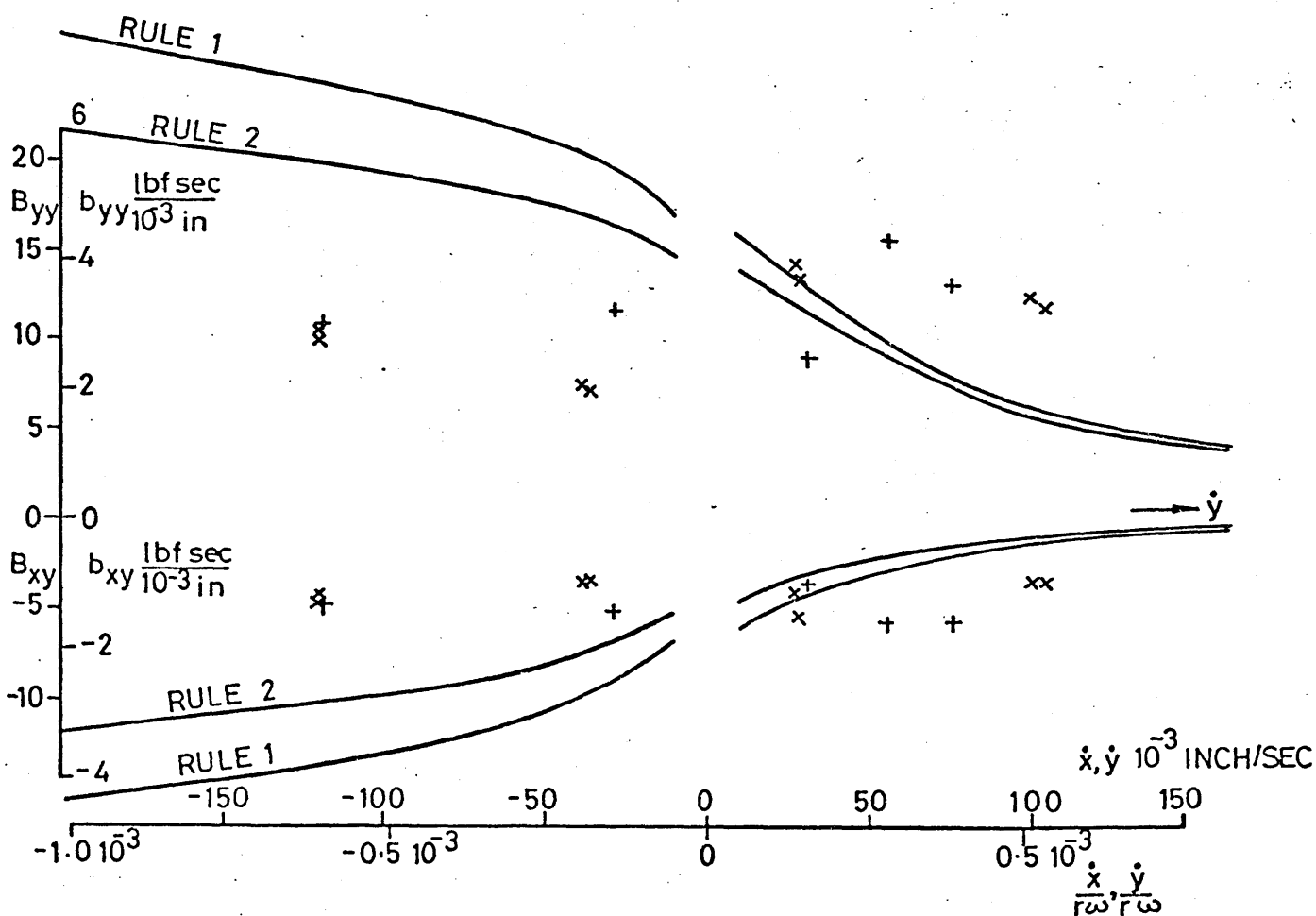
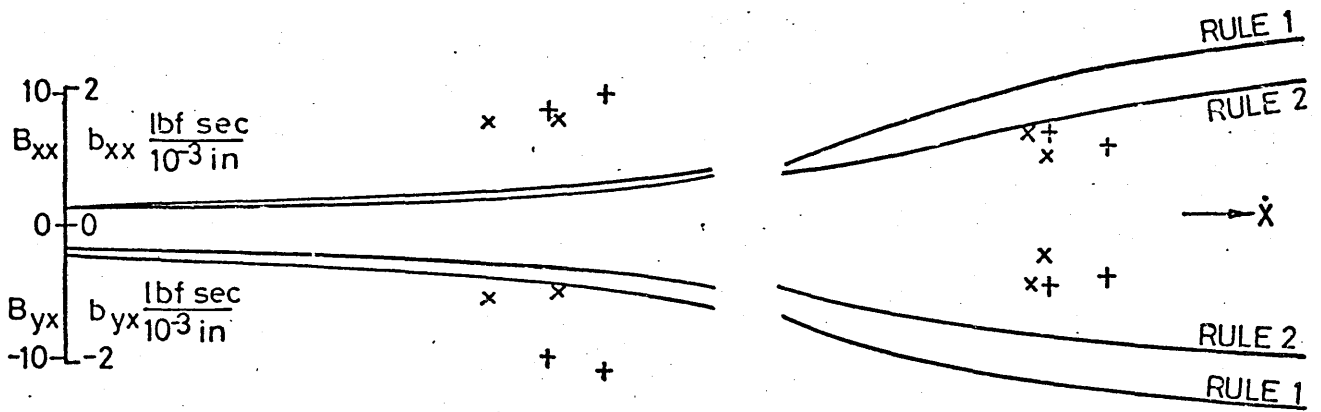


FIGURE 60 MEASURED AND CALCULATED VELOCITY COEFFICIENTS
 $N = 1500 \text{ rpm}$, $W_y = 150 \text{ lbf}$, $PS = 15 \text{ lbf/in}^2$



— THEORY $\eta = \eta(T, P)$
 + $\Omega/\omega = 1.0$ } EXPERIMENTAL
 x $\Omega/\omega = 2.0$ } DYNAMIC LOADING

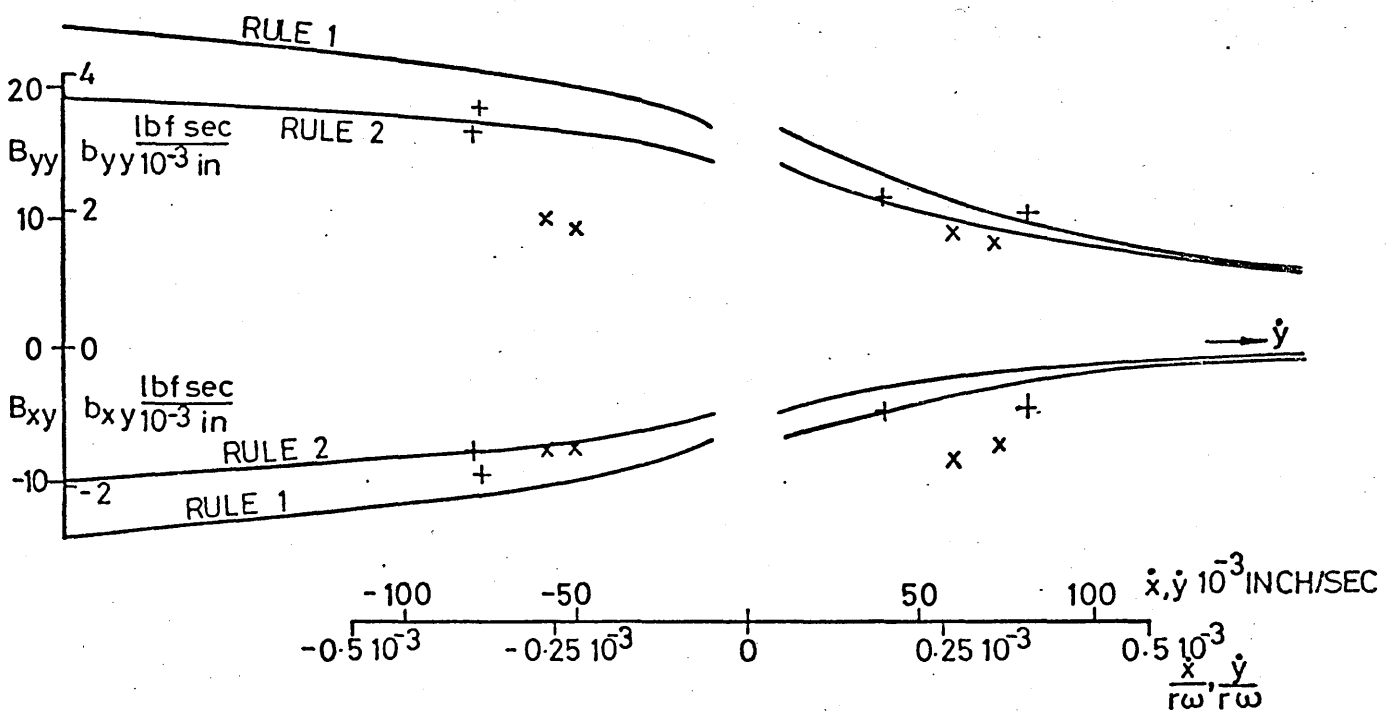


FIGURE 61 MEASURED AND CALCULATED VELOCITY COEFFICIENTS
 $N = 2200 \text{ rpm}$, $W_y = 150 \text{ lbf}$, $PS = 15 \text{ lbf/in}^2$

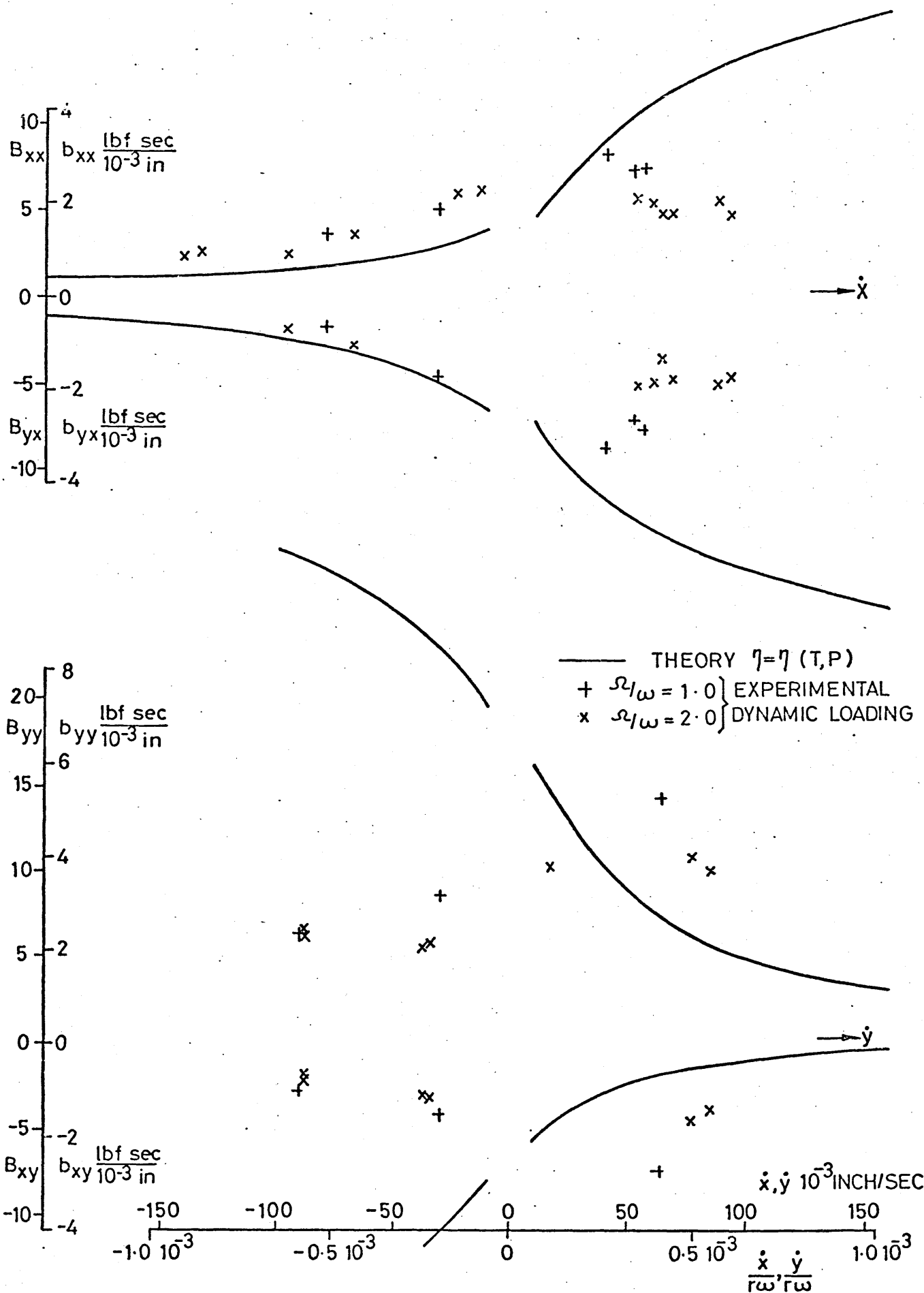


FIGURE 62 MEASURED AND CALCULATED VELOCITY COEFFICIENTS
 N=1180rpm, $W_y=150\text{lbf}$, $PS=7.5\text{lbf/in}^2$

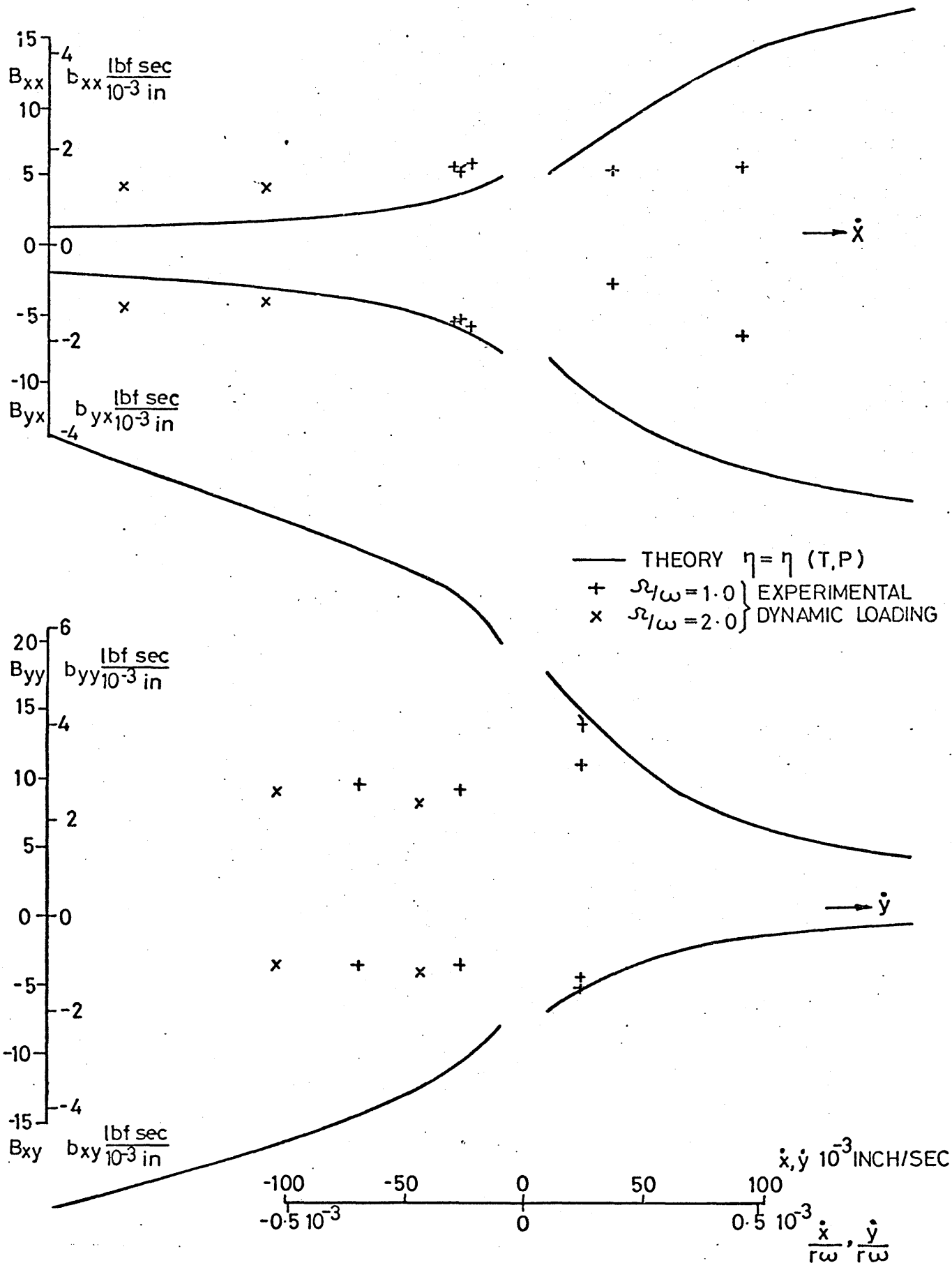


FIGURE 63 MEASURED AND CALCULATED VELOCITY COEFFICIENTS
 $N = 1500 \text{rpm}$, $W_y = 150 \text{ lbf}$, $PS = 7.5 \text{ lbf/in}^2$

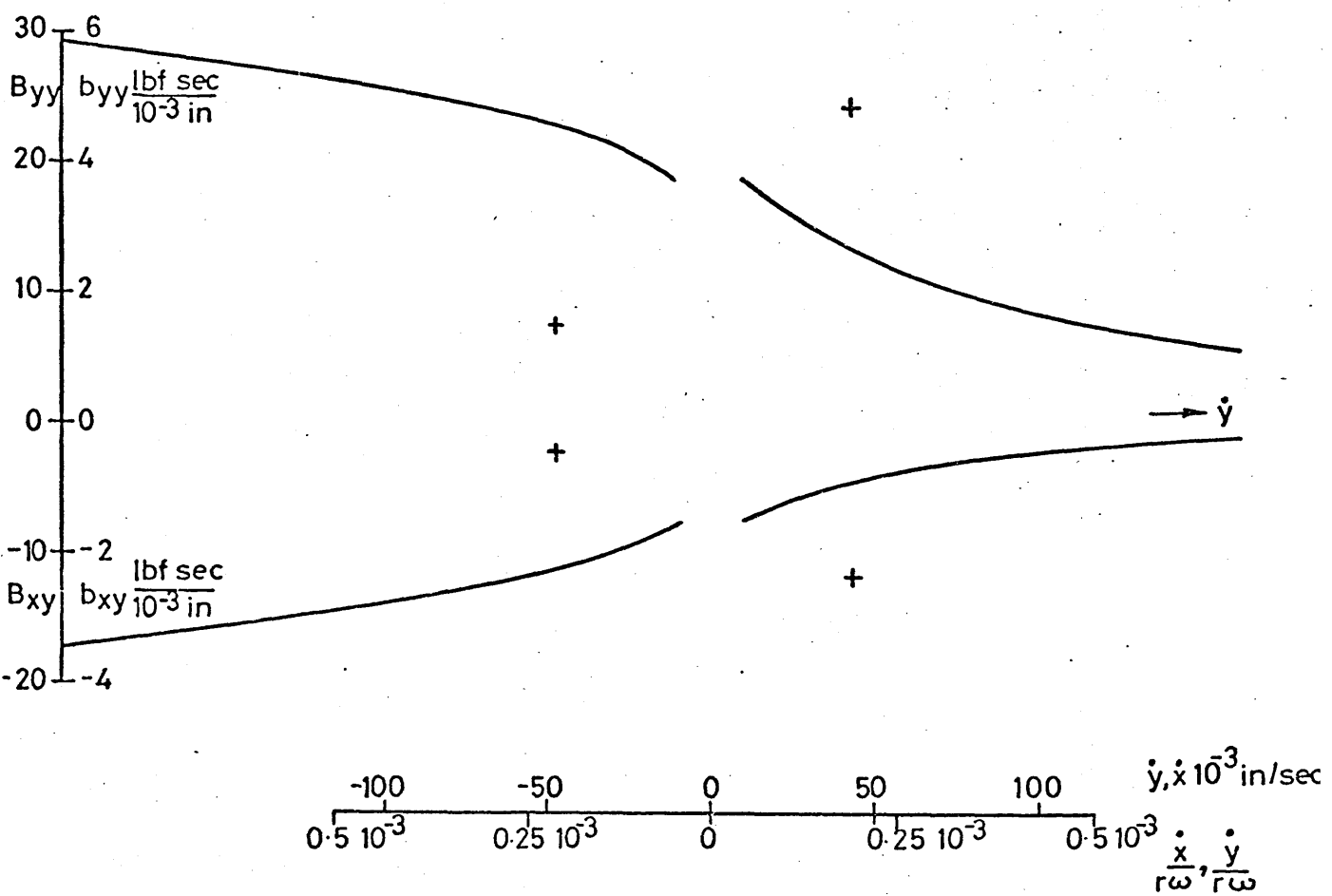
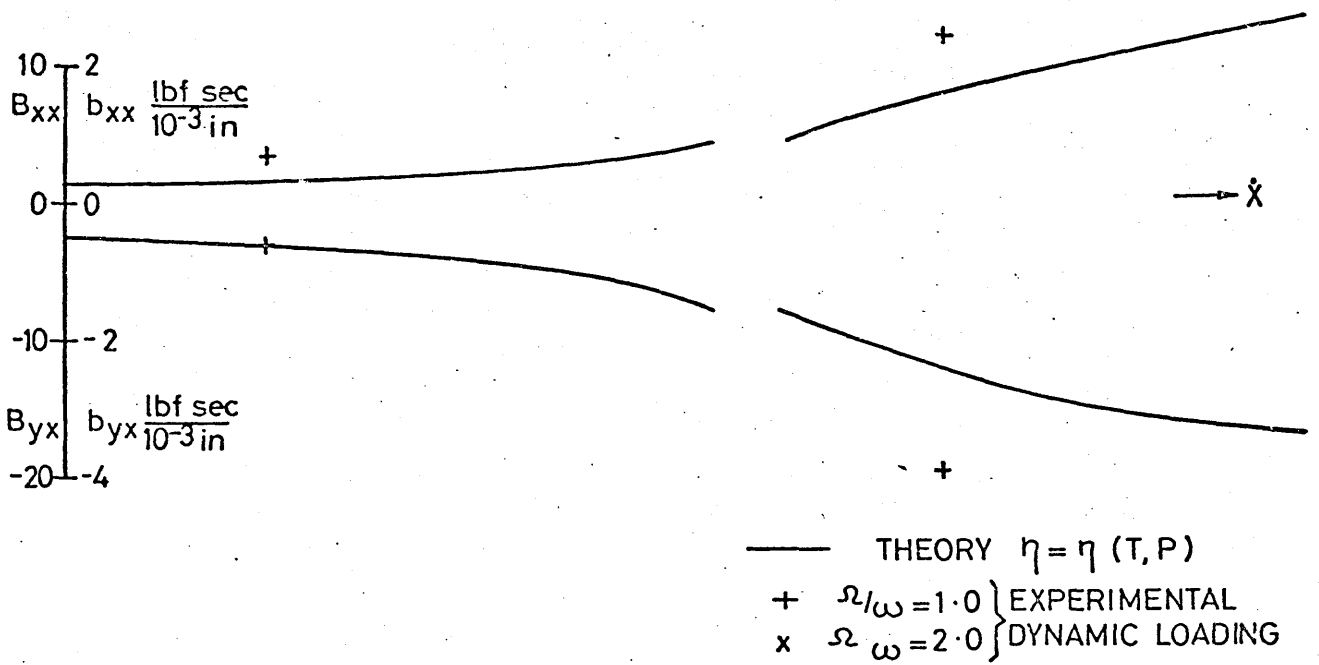


FIGURE 64 MEASURED AND CALCULATED VELOCITY COEFFICIENTS
 $N = 2200 \text{ rpm}$, $W_y = 150 \text{ lbf}$, $PS = 7.5 \text{ lbf/in}^2$

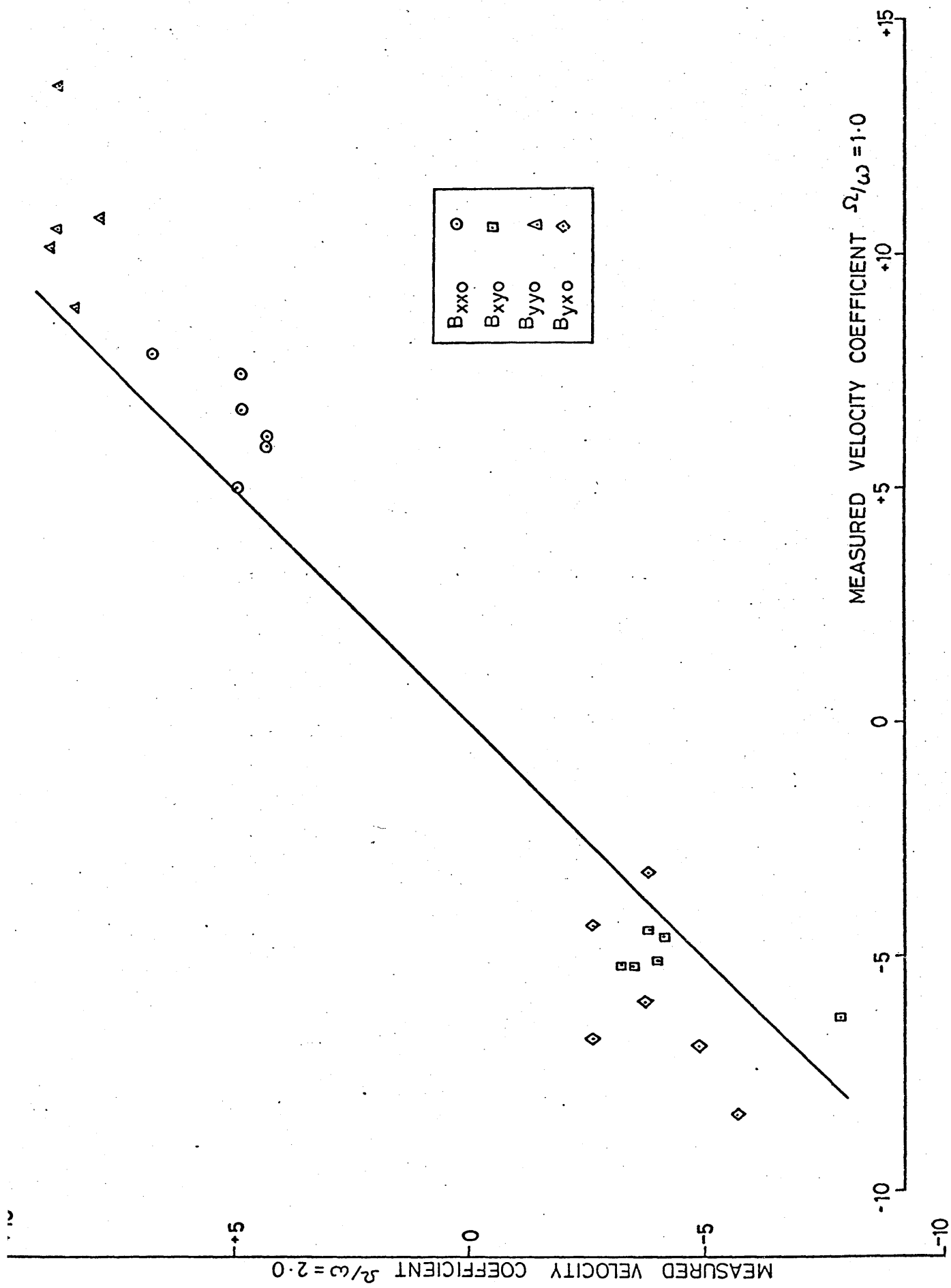
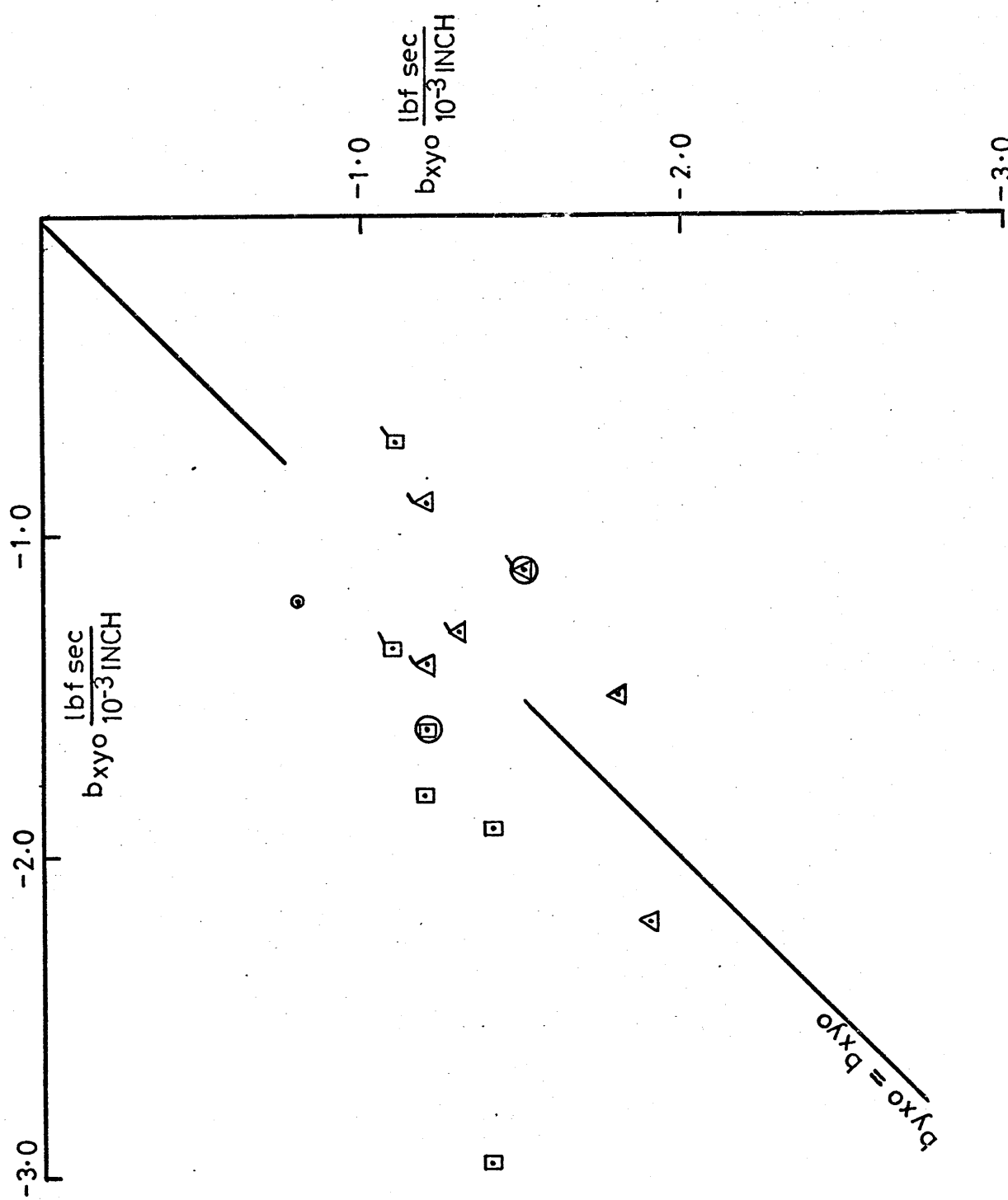


FIGURE 65 INFLUENCE OF VIBRATION ~ ROTATIONAL FREQUENCY RATIO Ω/ω



EXPERIMENTAL	
N	Ω / ω
1180	1.0
1500	2.0
2200	

FIGURE 66 MEASURED INDIRECT VELOCITY COEFFICIENTS

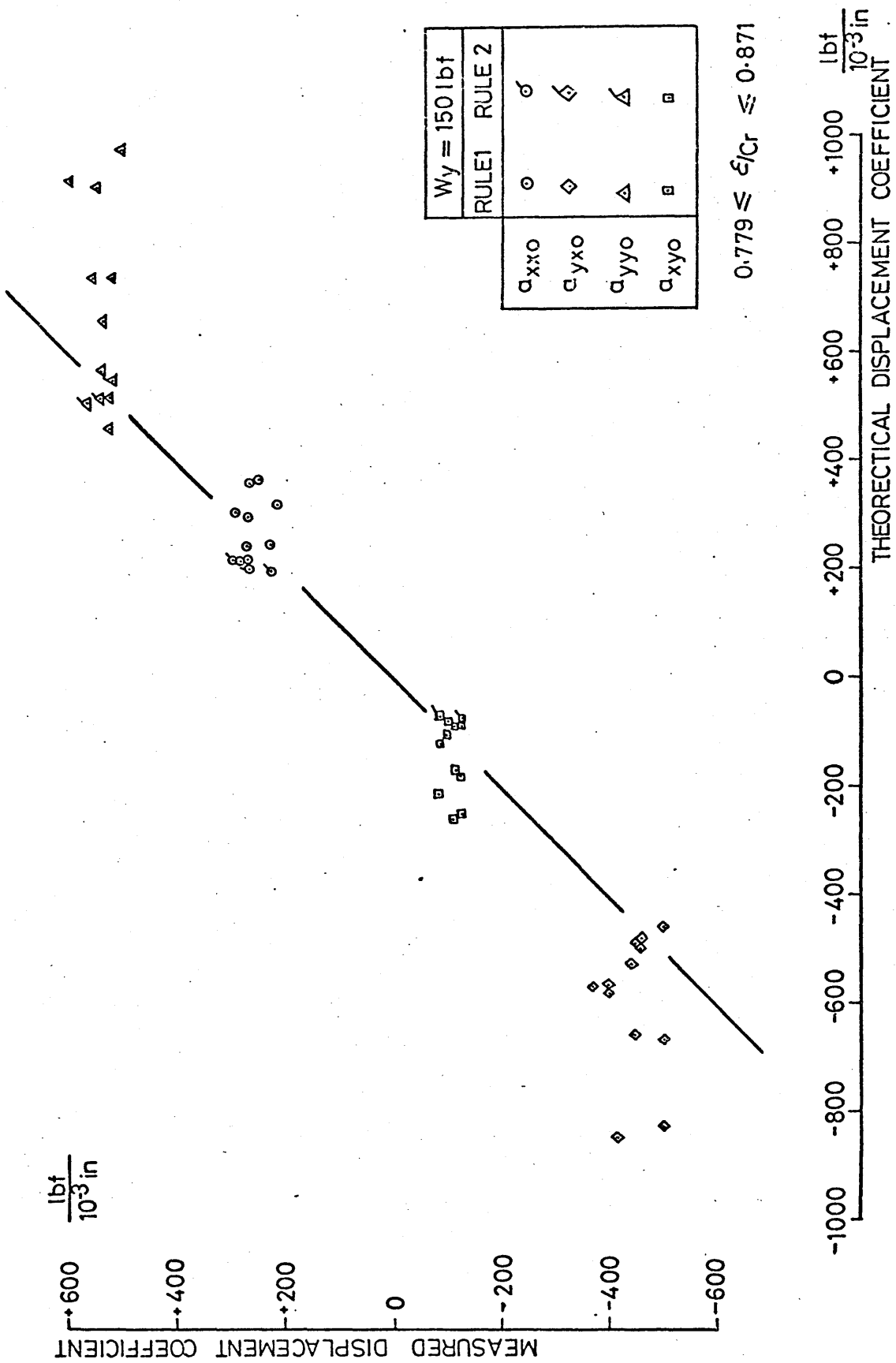


FIGURE 67 COMPARISON OF MEASURED AND CALCULATED DISPLACEMENT COEFFICIENTS

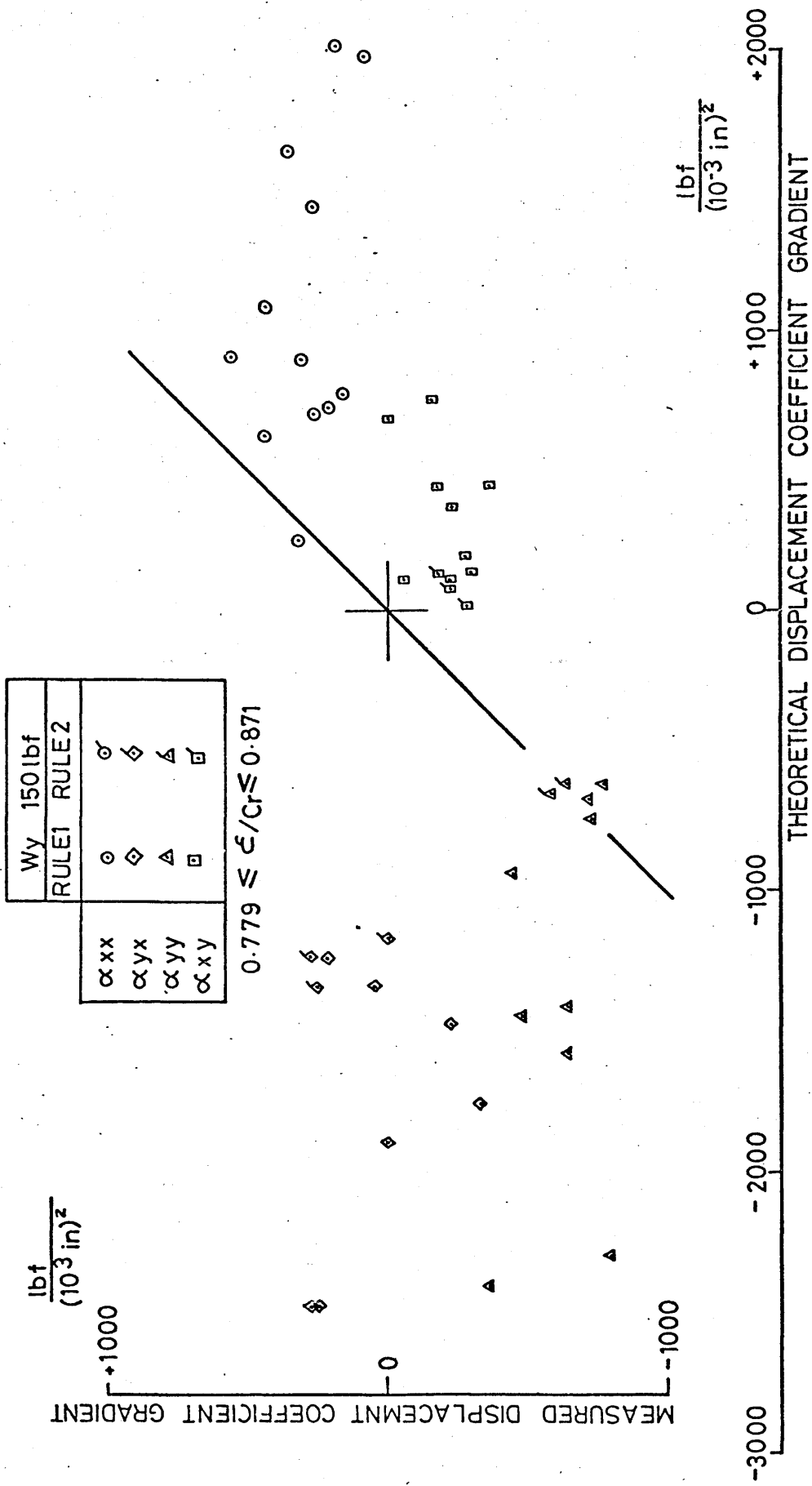


FIGURE 68 COMPARISON OF MEASURED & CALCULATED DISPLACEMENT COEFFICIENT GRADIENT.

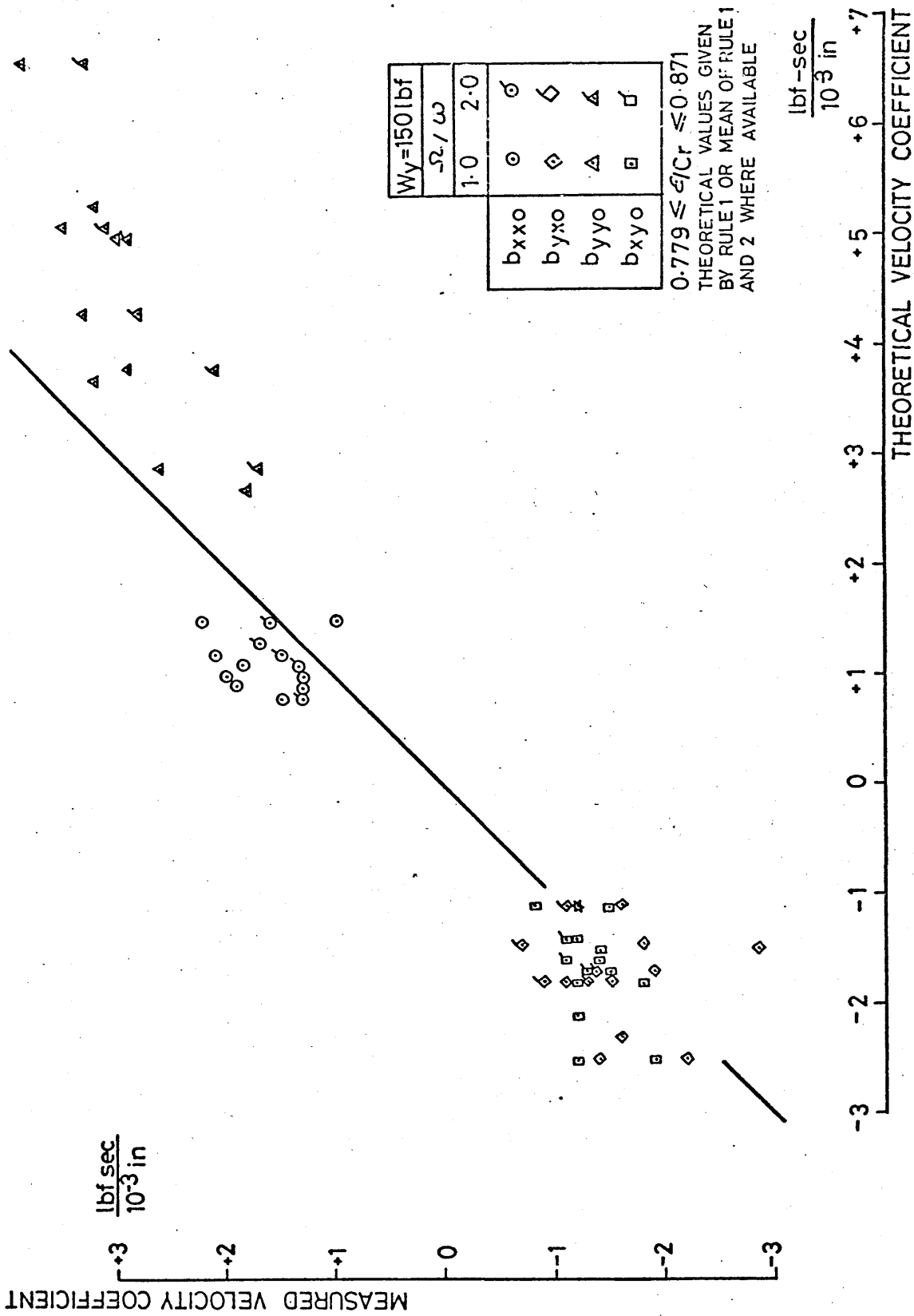


FIGURE 69 COMPARISON OF MEASURED & CALCULATED VELOCITY COEFFICIENT

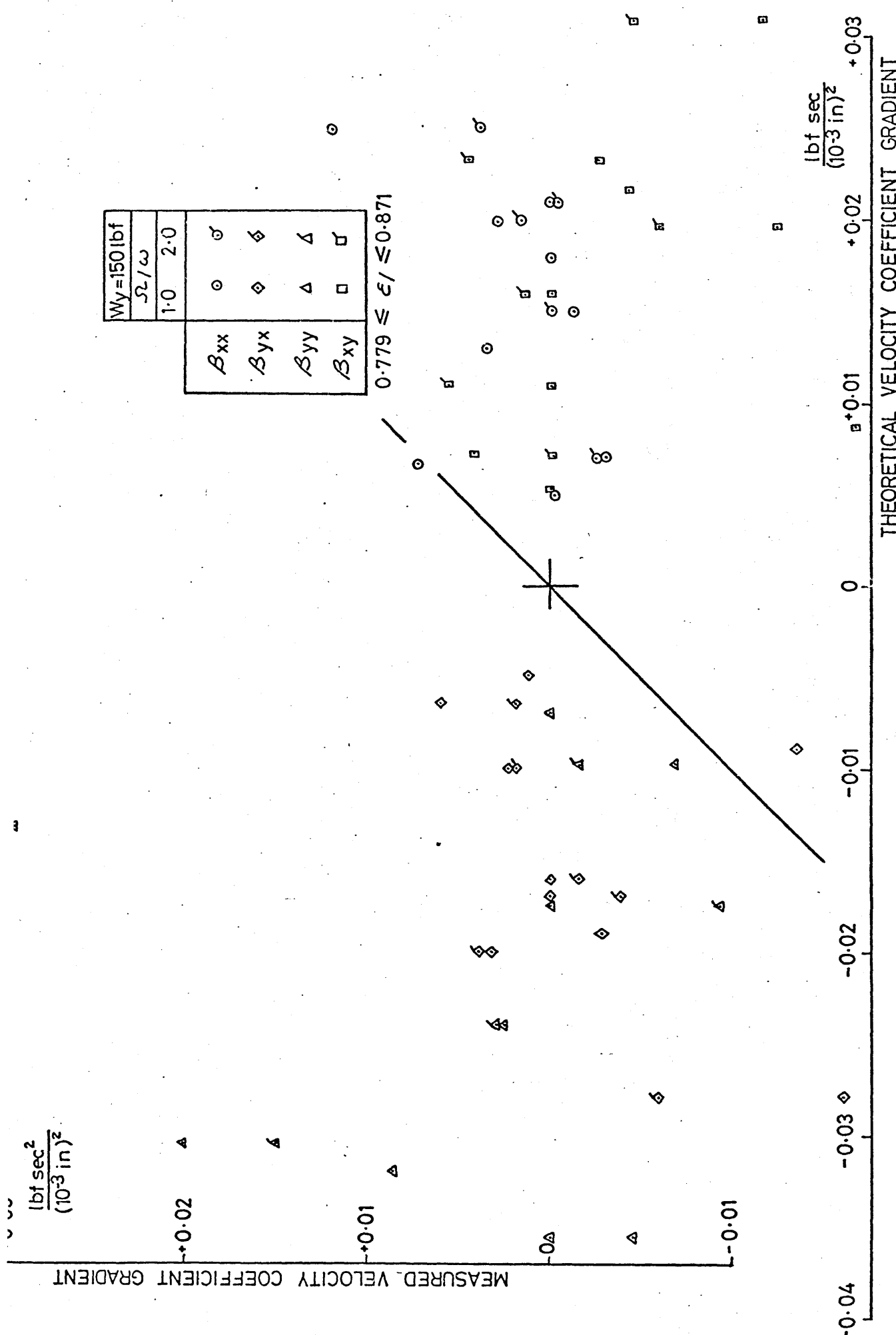


FIGURE 70 COMPARISON OF MEASURED & CALCULATED VELOCITY COEFFICIENT GRADIENT (RULE 1)

THEORETICAL DISPLACEMENT COEFFICIENT GRADIENT ($\frac{\alpha}{C_r} = \pm 0.03$)

-10 000 0 +10,000 +20000

$\frac{\text{lbf}}{(10^{-3}\text{in})^2}$

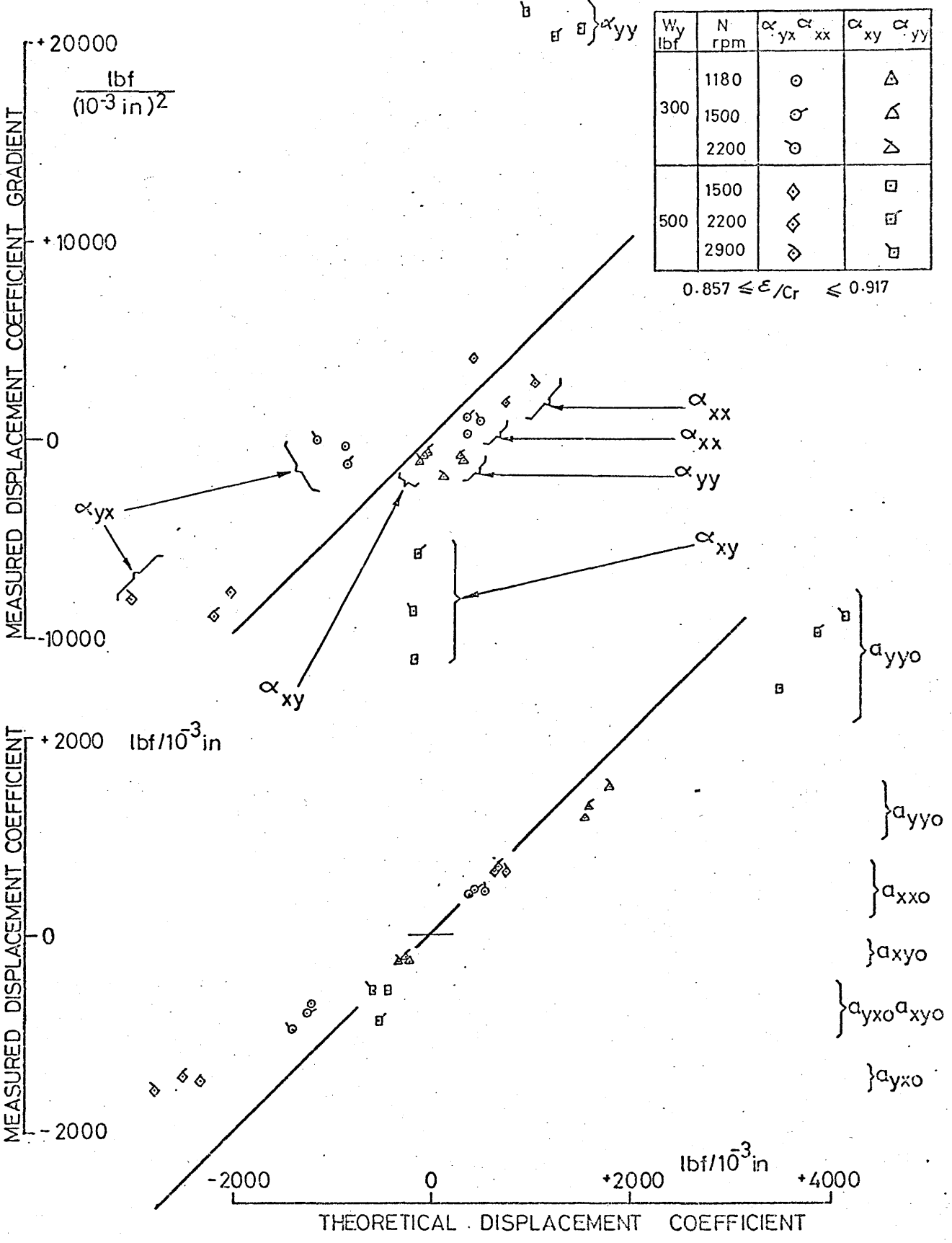


FIGURE 71 COMPARISON OF MEASURED & CALCULATED DISPLACEMENT COEFFICIENT & GRADIENT $W_y = 300$ & 500 lbf

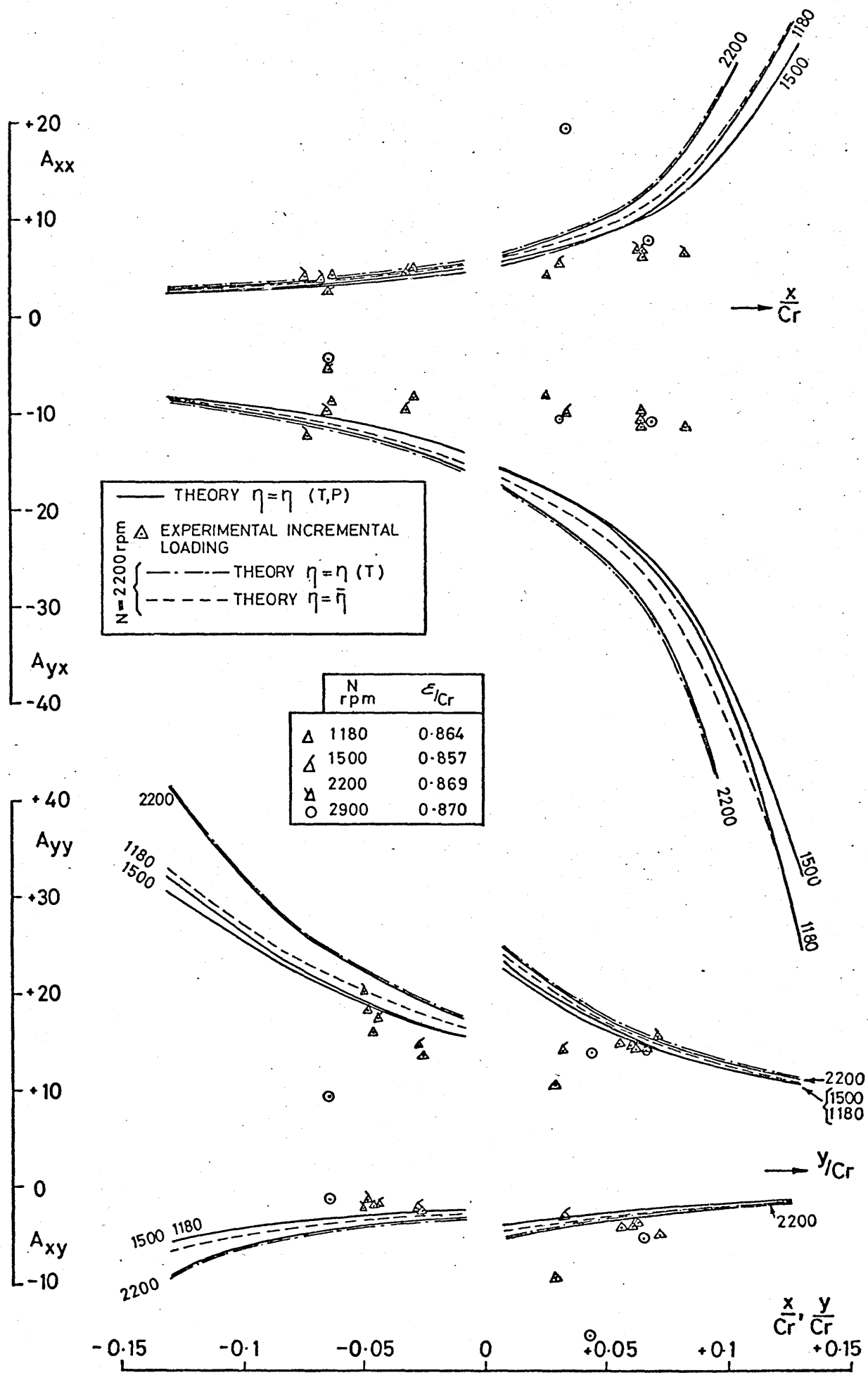
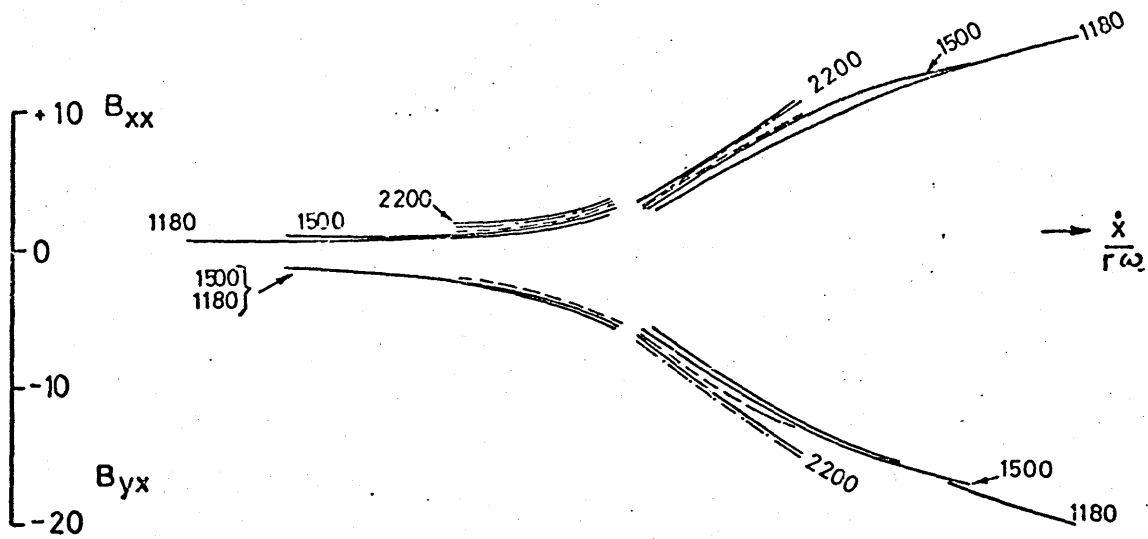
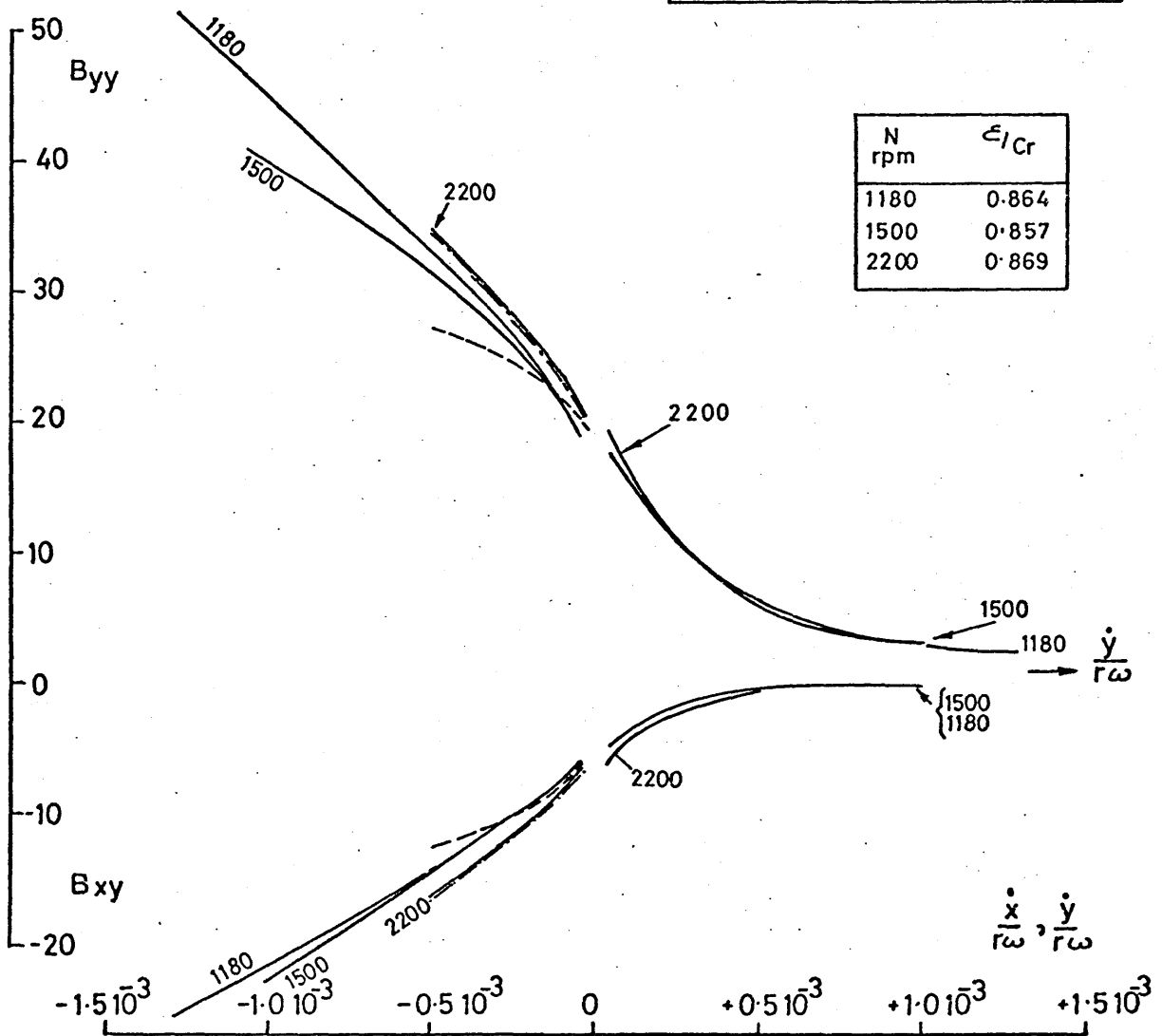


FIGURE 72 DISPLACEMENT COEFFICIENTS $W_y = 300 \text{ lbf}$ $PS = 30 \text{ lbf/in}^2$
 $N = 1180, 1500 \text{ \& } 2200 \text{ rpm}$



— THEORY $\eta = \eta(T, P)$
 N=2200rpm { - · · · · THEORY $\eta = \eta(T)$
 - - - - THEORY $\eta = \bar{\eta}$



N rpm	ϵ/Cr
1180	0.864
1500	0.857
2200	0.869

FIGURE 73 VELOCITY COEFFICIENTS $W_y=300 \text{ lbf}$ $PS=30 \frac{\text{lbf}}{\text{in}^2}$ $N=1180, 1500 \text{ \& } 2200 \text{ rpm}$

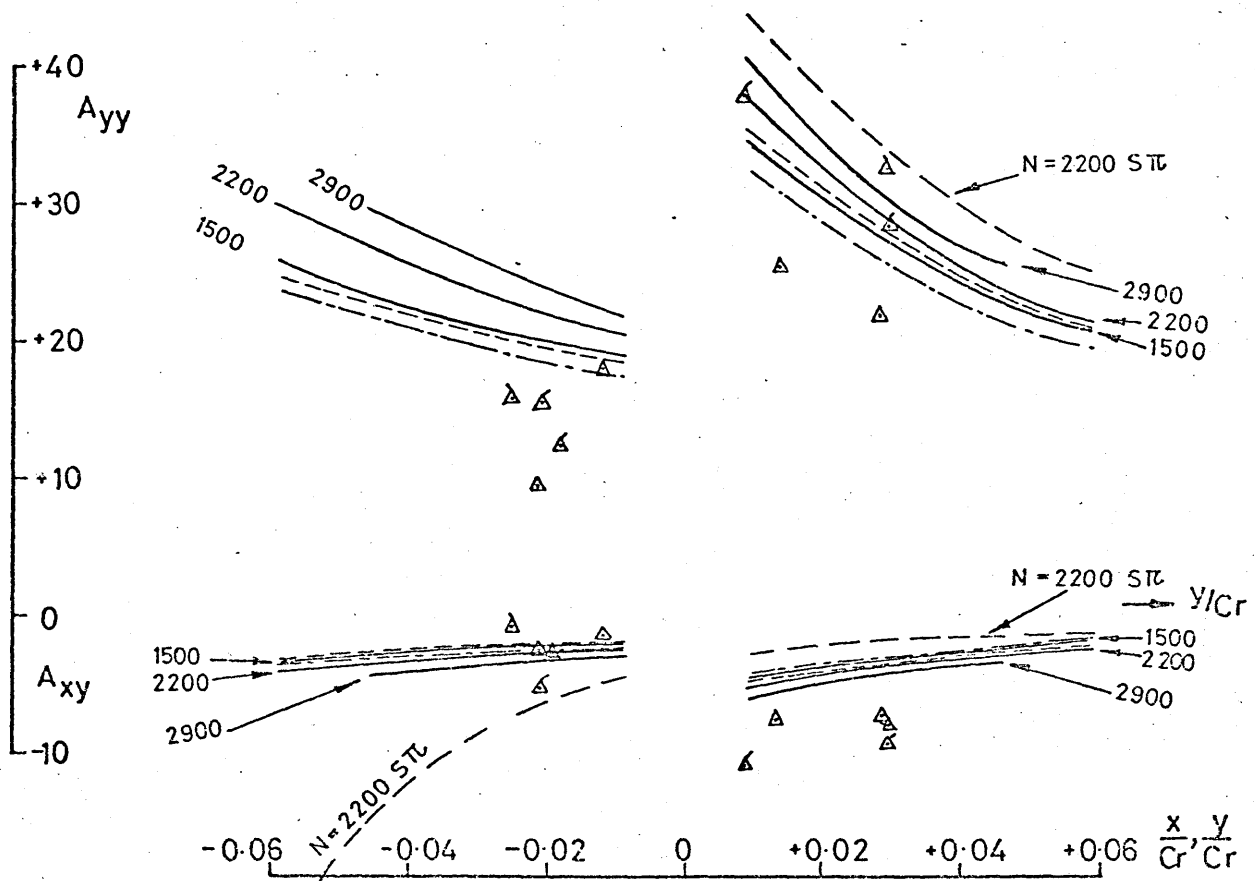
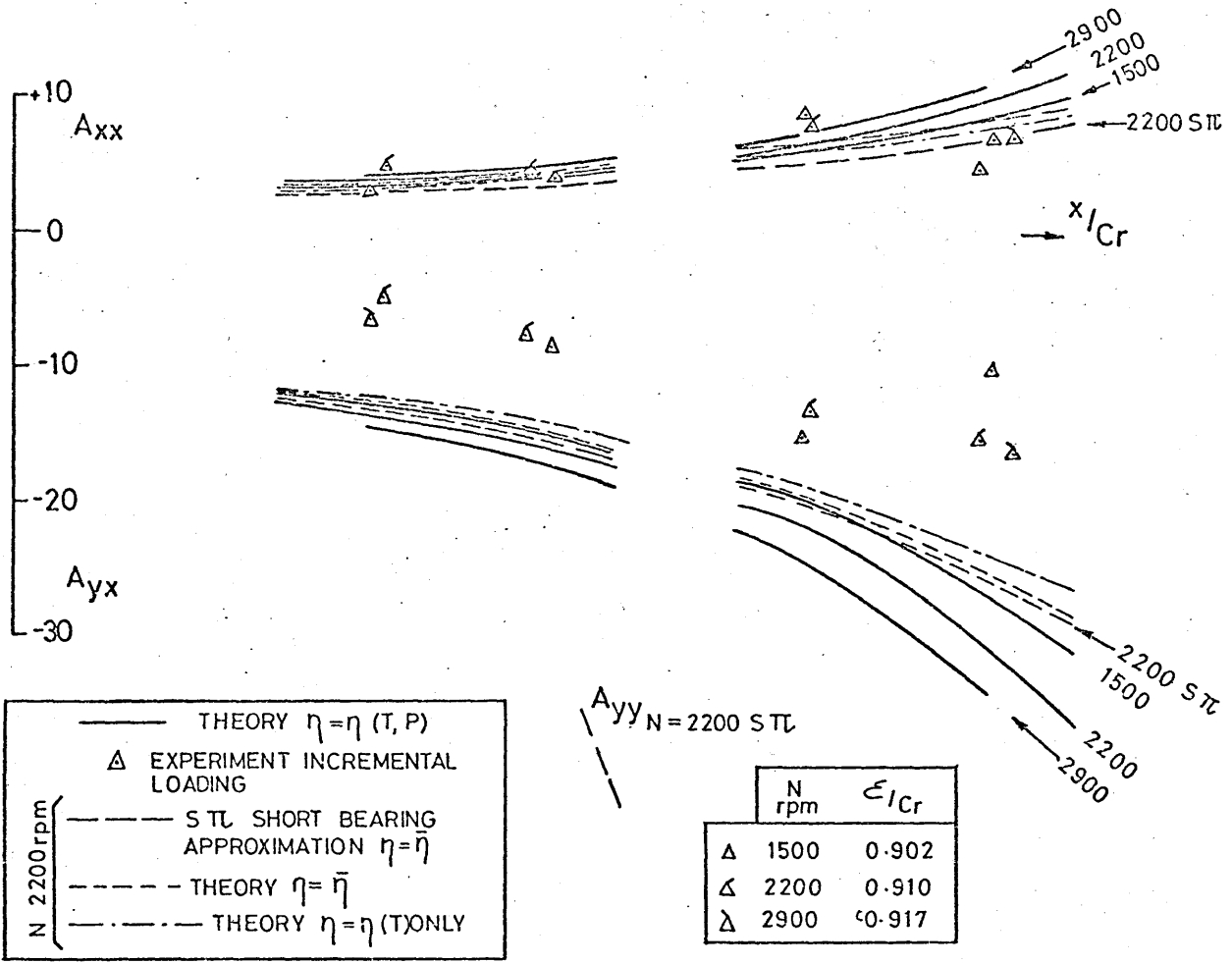


FIGURE 74 DISPLACEMENT COEFFICIENTS $W_y = 500 \text{ lbf}$, $PS = 30 \frac{\text{lbf}}{\text{in}^2}$ $N = 1500 \text{ } 2200 \text{ \& } 2900 \text{ rpm}$

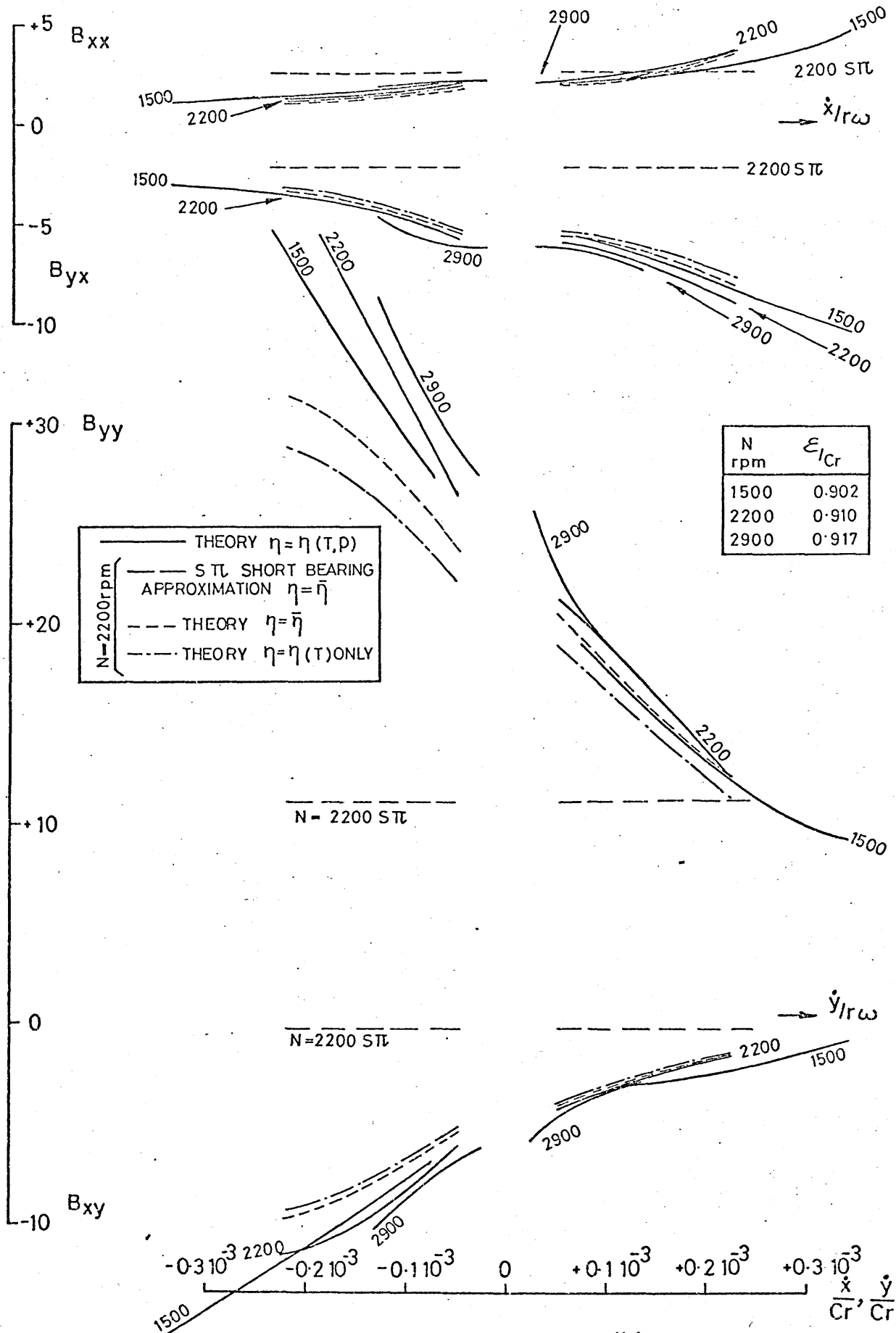


FIGURE 75 VELOCITY COEFFICIENTS $W_y = 500 \text{ lbf}$ $PS = 30 \frac{\text{lbf}}{\text{in}^2}$ $N = 1500, 2200 \text{ \& } 2900 \text{ rpm}$

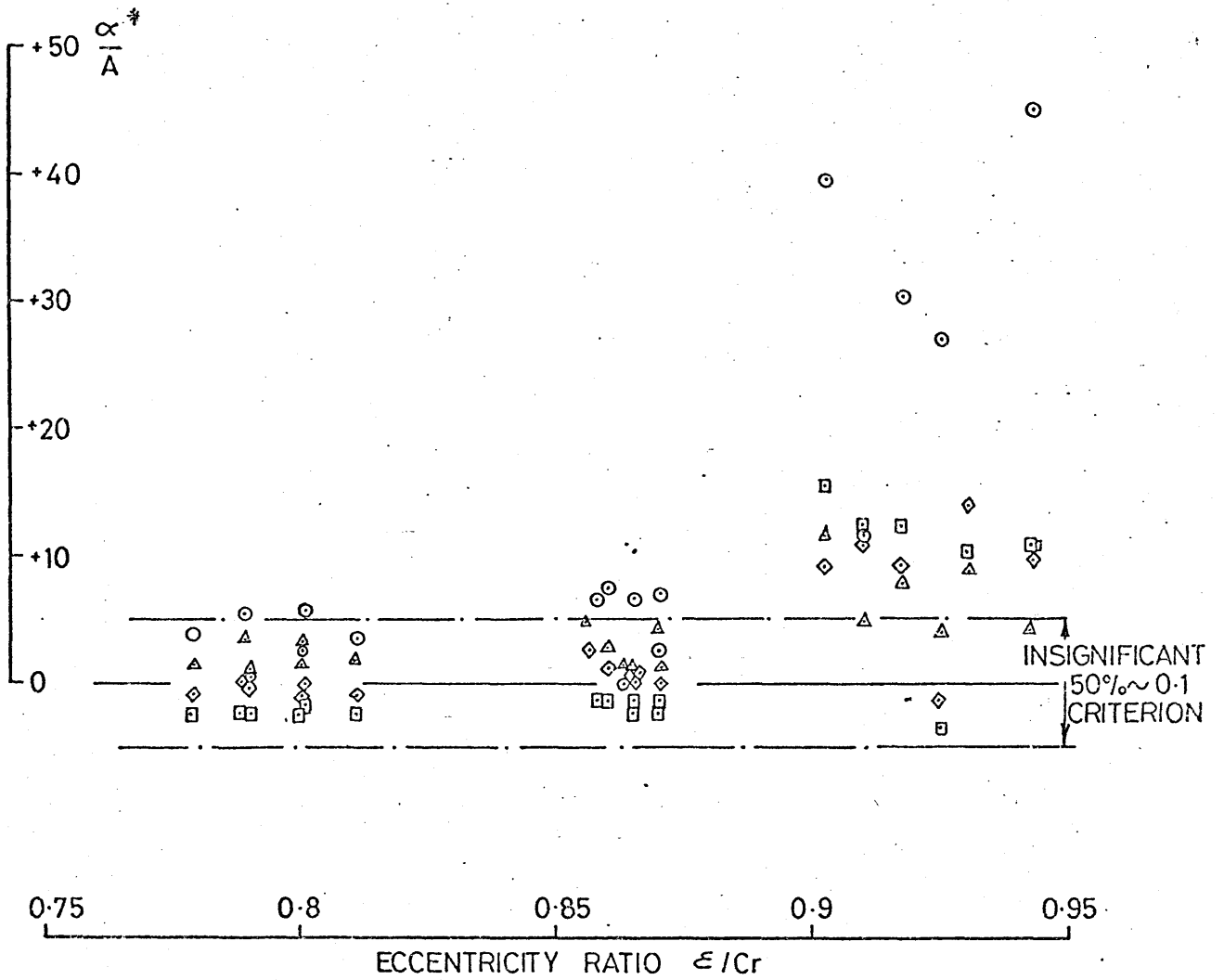
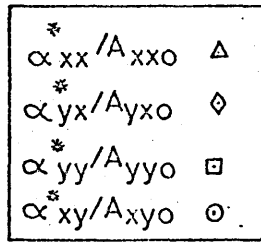


FIGURE 76 SIGNIFICANCE OF DISPLACEMENT COEFFICIENT GRADIENT

	Ω/ω	
	1.0	2.0
β_{xx}^* / B_{xx0}	Δ	\triangleleft
β_{yx}^* / B_{yx0}	\diamond	\diamondleftarrow
β_{yy}^* / B_{yy0}	\square	\squareleftarrow
β_{xy}^* / B_{xy}	\circ	\circleftarrow

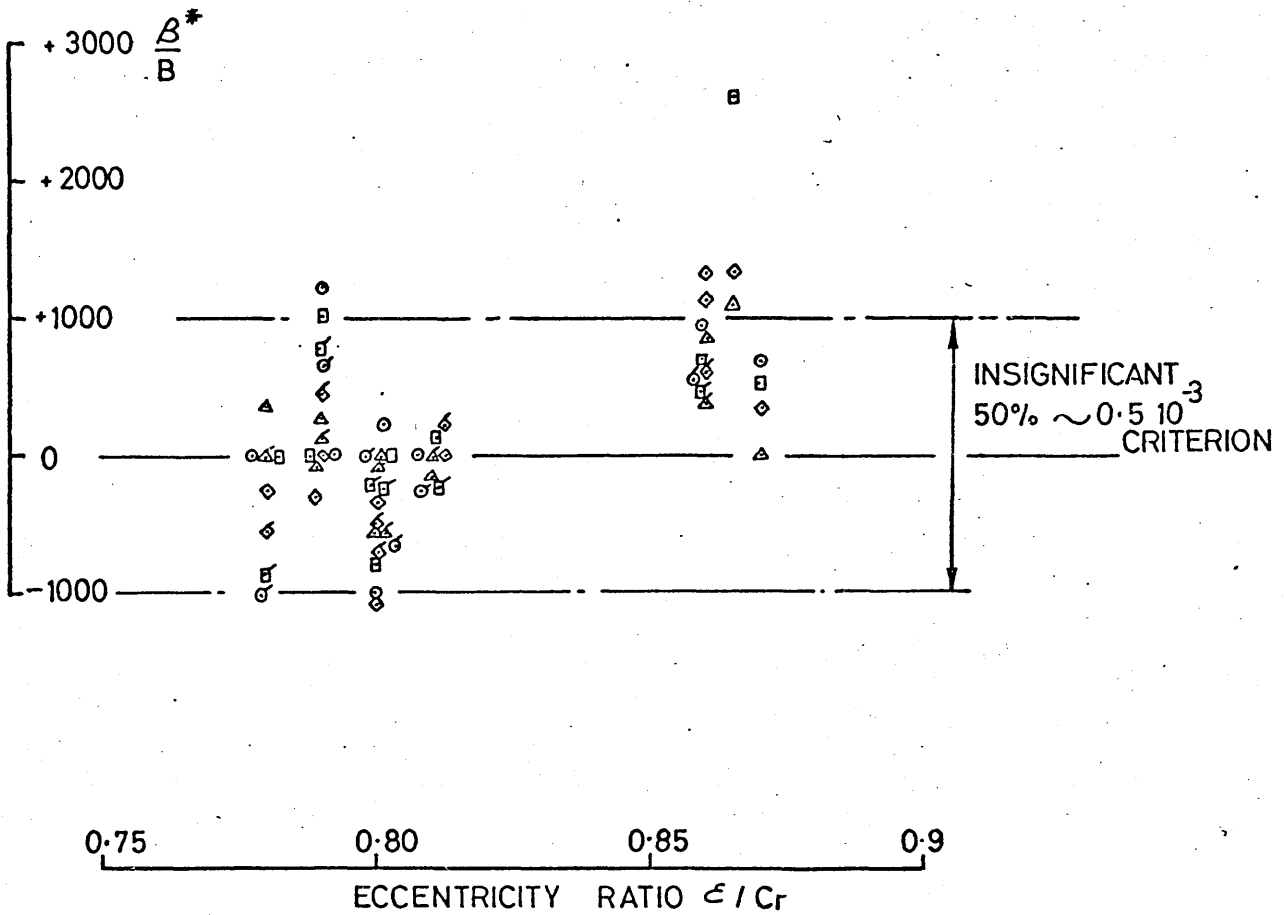


FIGURE 77 SIGNIFICANCE OF VELOCITY COEFFICIENT GRADIENT

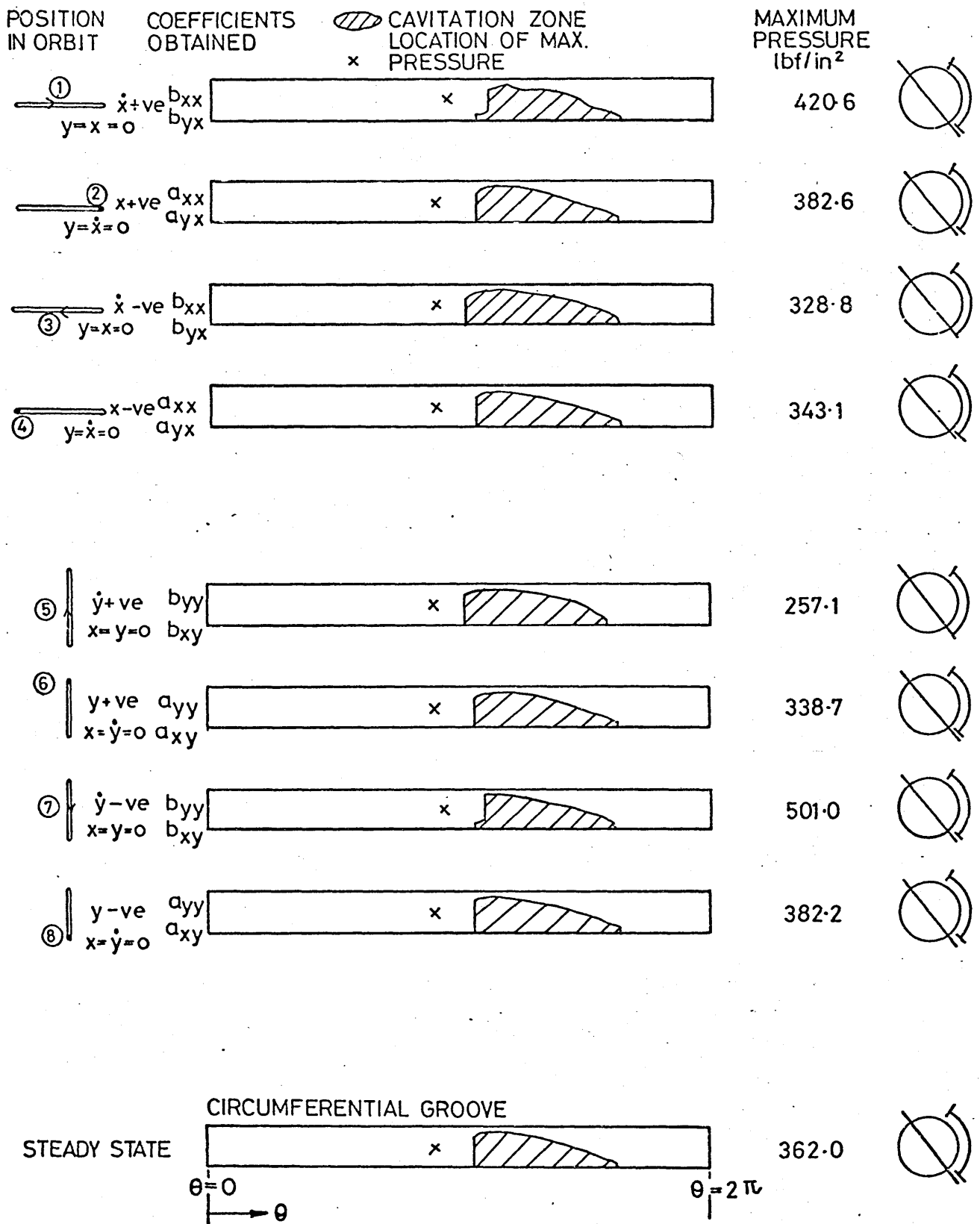


FIGURE 78 THEORETICAL LOCATION OF CAVITATION ZONE & PEAK PRESSURE—SMALL DISPLACEMENT & VELOCITY INCREMENTS

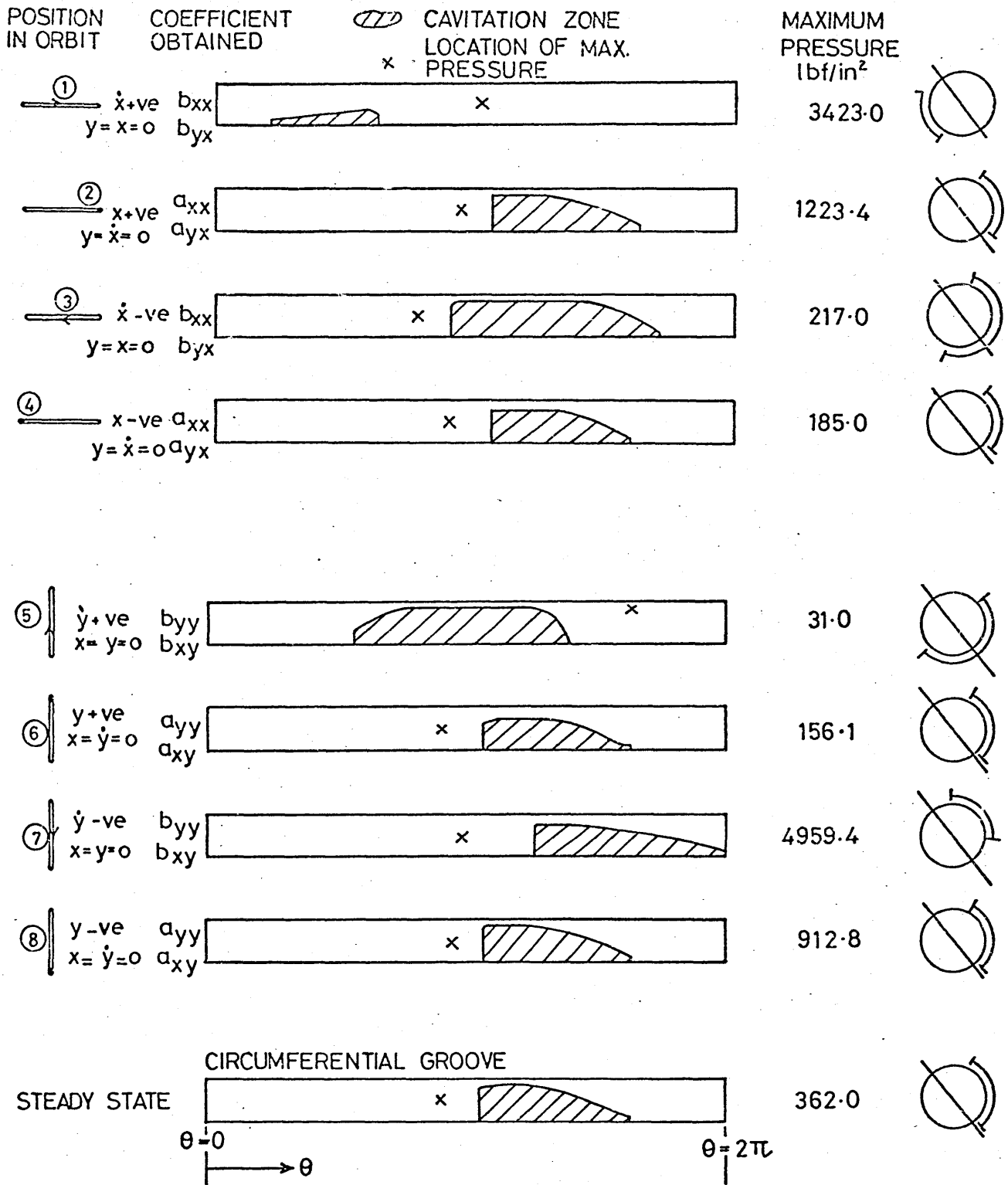


FIGURE 79 THEORETICAL LOCATION OF CAVITATION ZONE & PEAK PRESSURE—LARGE DISPLACEMENT & VELOCITY INCREMENTS.